

The Dalles Dam, Columbia River: Spillway Improvement CFD Study



C.B. Cook
M.C. Richmond
J.A. Serkowski

Final Report

June 2006

Prepared for the U.S. Army Corps of Engineers
Portland District, Portland, Oregon
Under a Related Services Agreement
with the U.S. Department of Energy
Contract DE-AC05-76RL01830

**Pacific Northwest
National Laboratory**

Operated by Battelle for the
U.S. Department of Energy

DISCLAIMER

This report was prepared as an account of work sponsored by an agency of the United States Government. Neither the United States Government nor any agency thereof, nor Battelle Memorial Institute, nor any of their employees, makes **any warranty, express or implied, or assumes any legal liability or responsibility for the accuracy, completeness, or usefulness of any information, apparatus, product, or process disclosed, or represents that its use would not infringe privately owned rights.** Reference herein to any specific commercial product, process, or service by trade name, trademark, manufacturer, or otherwise does not necessarily constitute or imply its endorsement, recommendation, or favoring by the United States Government or any agency thereof, or Battelle Memorial Institute. The views and opinions of authors expressed herein do not necessarily state or reflect those of the United States Government or any agency thereof.

PACIFIC NORTHWEST NATIONAL LABORATORY

operated by

BATTELLE

for the

UNITED STATES DEPARTMENT OF ENERGY

under Contract DE-AC05-76RL01830

Printed in the United States of America

Available to DOE and DOE contactors from the
Office of Scientific and Technical Information,
P.O. Box 62, Oak Ridge, TN 37831-0062;
ph: (865) 576-8401
fax: (865) 576-5728
email: reports@adonis.osti.gov

Available to the public from the National Technical Information Service,
U.S. Department of Commerce, 5285 Port Royal Rd., Springfield, VA 22161
ph: (800) 553-6847
fax: (703) 605-6900
email: orders@ntis.fedworld.gov
online ordering: <http://www.ntis.gov/ordering.htm>



This document was printed on recycled paper.
(9/2003)

The Dalles Dam, Columbia River: Spillway Improvement CFD Study

C.B. Cook
M.C. Richmond
J.A. Serkowski

Final Report

June 2006

Prepared for the U.S. Army Corps of Engineers
Portland District, Portland, Oregon
Under a Related Services Agreement
with the U.S. Department of Energy
Contract DE-AC05-76RL01830

Pacific Northwest National Laboratory
Richland, Washington 99352

Summary

This report documents development of computational fluid dynamics (CFD) models that were applied to The Dalles Dam spillway for the U. S. Army Corps of Engineers, Portland District. The models have been successfully validated against physical models and prototype data, and are suitable to support biological research and project operations. The CFD models have been proven to provide reliable information in the turbulent high-velocity flow field downstream of the spillway face that is typically difficult to monitor in the prototype. Although the CFD model is not an exact replica of the prototype, differences between simulations with and without the modification do indicate trends in hydraulic conditions. CFD model results can produce index metrics that were found to be useful for both concept testing, design parameters (e.g., velocity near the basalt river bed), and biological research. In addition, CFD data provides hydraulic information throughout the solution domain that can be easily extracted from archived simulations for later use.

This project is part of an ongoing program at the Portland District to improve spillway survival conditions for juvenile salmon at The Dalles. Biological data collected at The Dalles spillway have shown that for the original spillway configuration, juvenile salmon passage survival is lower than desired. Therefore, the Portland District is seeking to identify operational and/or structural changes that might be implemented to improve fish passage survival. In addition to the spillway improvement study (SIS), the Portland District is also conducting biological tests of spill at The Dalles. Sensor fish devices and CFD simulations are being used in a related project to investigate exposure conditions fish experience during spill passage. During biological tests of spill, sensor fish device releases are integrated into releases of live test fish. CFD simulations and inertial particle tracking can then be used to obtain statistical estimates of exposure history and to extend the analysis to conditions not tested because structures do not exist or because flow conditions could not be realized.

Pacific Northwest National Laboratory (PNNL) went through a sequence of steps to develop a CFD model of The Dalles spillway and tailrace. The first step was to identify a preferred CFD modeling package. Several packages are commercially supported, peer-reviewed, and well validated (basic requirements that were considered), but each package has different strengths and weaknesses. In the case of The Dalles spillway, Flow-3D was selected because of its ability to simulate the turbulent free-surface flows that occur downstream of each spilling bay.

The second step in development of The Dalles CFD model was to assemble bathymetric datasets and structural drawings sufficient to describe the dam (powerhouse, nonoverflow dam, spillway, fish ladder entrances) and tailrace. These datasets are documented in this report as are various 3-D graphical representations of The Dalles spillway and tailrace.

CFD models of the stilling basin and downstream tailrace were validated using data collected in physical models of The Dalles Dam. A CFD model was constructed to represent the 1950s Bonneville Hydraulics Laboratory 1:36 scale physical model that was originally used to design the prototype stilling basin. CFD simulated pressure heads were compared to observed physical model pressure heads, and differences between the two datasets were minor (0.51 ft over the baffle block and 0.40 ft over the end sill). A more recently developed 1:40 scale physical model of the spillway has been built at the Engineer Research and Development Center (ERDC) located in

Vicksburg, Mississippi. A CFD model was developed at the same scale as the physical model, and results from the two models were compared. Water velocity magnitude differences, compared at four locations both within and downstream of the stilling basin, were acceptable with 73% of the CFD measurements falling within one standard deviation of the physical model mean value.

The domain of the CFD model was subsequently increased to include the entire stilling basin and tailrace, and was then verified against data collected in the ERDC 1:80 general physical model of The Dalles Project. In general, differences between the two datasets were acceptable. Some differences in horizontal flow direction were observed.

At the conclusion of these validation exercises, the CFD model was considered tested and appropriate to simulate spillway, stilling basin, and tailrace flows at The Dalles Dam. The validated model was then applied to address specific SIS design questions. Specifically, the 1-bay, 3-bay, and bank-to-bank tailrace CFD models were used to evaluate flow deflectors, baffle block removal, and the effects of spillwalls. The CFD models were also used to evaluate downstream differences at other locations, such as at the Highway 197 bridge piers and Oregon shore islands, due to changes in spill pattern. CFD model results provided hydraulic insight into how different structural alternatives would affect the downstream flow field. Because the CFD model produces results at every cell within the computational domain, an extensive dataset of information around the tailrace can be mined for variations in velocity magnitude and direction (including gradient values, such as strain), static and dynamic pressure, water surface elevation, and turbulence intensity.

CFD model results were analyzed to compare impacts of the spillwall that has subsequently been constructed between bays 6 and 7. CFD model results provided detailed information about how the spillwall would impact downstream flow patterns that complemented results from the 1:80 scale physical model. The CFD model was also used to examine relative differences between the juvenile spill pattern used in previous years and the anticipated spill pattern that will be applied once the wall is complete. In addition, the CFD model examined velocity magnitudes over the downstream basalt shelf to investigate potential for erosion under high flow conditions (e.g., 21 kcfs/bay for bays 1 through 6) with the spillwall in place.

Acknowledgments

We sincerely acknowledge the cooperation, assistance, and dedication of the following persons:

- U. S. Army Corps of Engineers, Portland District
 - Robert Buchholz
 - Laurie Ebner
 - Michael Langeslay
 - Natalie Richards
 - Paul Williams
- U. S. Army Corps of Engineers, ERDC
 - Winston Glenn Davis
 - William Preslan
 - Steve Wilhelms
- Pacific Northwest National Laboratory
 - Tom Carlson
 - Mark Weiland

Glossary

Block A collection of mesh cells. Within a block the mesh cells can be uniformly or non-uniformly spaced. With a uniform mesh, the block edge coordinates and the total number of cells are specified, which uniquely defines the cell size. With a nonuniform mesh, the size of each cell can be varied in any coordinate direction. Although blocks can be either uniform or nonuniform, Flow3-D requires that mesh be orthogonal and defined in terms of either Cartesian or cylindrical coordinates.

CENWP Portland District, USACE.

CFD modeling Computational Fluid Dynamics modeling. The use of computers to analyze problems in fluid dynamics. The usual method is to discretize the fluid domain into small mesh cells and then to apply iterative methods to solve the Navier-Stokes equations.

FAVORTM Fractional Area/Volume Obstacle Representation method, outlined in Hirt and Sicilian (1985) and Savage and Johnson (2001), is a porosity technique used by Flow-3D to define complex geometric regions. Grid porosity is zero within cells completely filled with a solid obstacle and one for mesh cells that are without any solid obstacles (i.e., completely open). Mesh cells partially filled with a solid obstacle have a grid porosity between zero and one, based on the percent volume that is solid.

m.s.l. mean sea level.

Mesh cell Flow-3D numerically solves the equations of motion using finite-volume approximations. The flow region is subdivided into a mesh of fixed hexahedral cells. Within each cell, the Navier-Stokes equations are numerically solved resulting in local average values for each state variable. A mesh cell is therefore the smallest unit within the computational domain and is defined by two fixed points in each coordinate direction.

Multi-block In the multi-block gridding technique, the computational domain is decomposed into several mesh blocks each containing numerous mesh cells. These blocks can be nested for achieving higher local resolution, or linked face-to-face to cover a large or complex three-dimensional region. Information in linked blocks are communicated to adjoining blocks across interblock boundaries.

Sensor fish An autonomous sensor package that can be deployed in harsh hydraulic environments.

SIS Spillway Improvement Study.

STL StereoLithography. A method of describing three-dimensional geometry using triangles. STL files were used to describe the solid objects (e.g., tainter gates, bathymetry, spillway, etc) that were then imported into Flow-3D.

TDA The Dalles Lock and Dam.

USACE U. S. Army Corps of Engineers.

Contents

Summary	iii
Acknowledgments	v
Glossary	vii
1.0 Introduction	1.1
1.1 General Objectives	1.1
1.2 Modeled Site	1.1
1.3 Report Organization	1.4
2.0 Methods	2.1
2.1 Computational Fluid Dynamics Model	2.1
2.1.1 Model Selection	2.1
2.1.2 Model Formulation	2.1
2.2 Model application to The Dalles Dam	2.4
2.2.1 Bathymetry and Engineered Structures	2.4
2.2.2 Grid Domain and Boundary Conditions	2.9
2.3 Computational Fluid Dynamics Model Domains	2.11
2.3.1 One and Two Bay Spillway Simulations	2.11
2.3.2 Twelve, Fifteen, and Nineteen Bay Spillway Simulations	2.14
2.3.3 Bank-to-Bank Spillway Tailrace Simulations	2.18
3.0 Model Validation	3.1
3.1 Tainter Gate Simulations	3.1
3.1.1 Grid and Boundary Condition Sensitivity	3.4
3.2 Simulating the 1:36 Scale Sectional Model	3.6

3.3	Simulating the 1:40 Scale Sectional Model	3.13
3.4	Simulating the 1:80 Scale General Model	3.17
3.4.1	Flow Condition 1 Results	3.18
3.4.2	Flow Condition 2 Results	3.22
4.0	Computational Fluid Dynamics Simulations of The Dalles Spillway Tailrace	4.1
4.1	Washington Shore Weighted Spill Patterns	4.1
4.2	Spillwalls	4.2
4.3	Baffle Blocks: Influence and Partial Removal Scenarios	4.7
4.4	Flow Deflectors	4.9
4.5	Smooth Downstream Basalt Shelf	4.12
5.0	Conclusions and Recommendations	5.1
5.1	Conclusions	5.1
5.2	Recommendations	5.1
6.0	References	6.1
	Appendix A – Overview of CFD Simulations	A.1
	Appendix B – Tainter Gate Simulations	B.1
	Appendix C – 1-Bay Simulations	C.1
	Appendix D – 2-Bay Simulations	D.1
	Appendix E – 12-Bay Simulations	E.1
	Appendix F – 15-Bay Simulations	F.1
	Appendix G – 19-Bay Simulations	G.1
	Appendix H – Bank-to-Bank 8-Block Simulations	H.1
	Appendix I – Bank-to-Bank 4-Block Simulations	I.1

Appendix J – Bank-to-Bank 1-Block Simulations	J.1
Appendix K – Powerhouse Tailrace Simulations	K.1
Appendix L – 1:80 scale Powerhouse and Spillway Tailrace Simulations	L.1
Appendix M – 1:36 and 1:40 scale Simulations	M.1

Figures

1.1	Plan view of The Dalles Dam showing the primary structures, including the powerhouse, navigation lock, and spillway	1.2
1.2	Aerial view of The Dalles Lock and Dam with all spillway bays operating	1.2
1.3	Geometry of The Dalles spillway, stilling basin, and end sill.	1.3
2.1	Spatial distribution of bathymetry data	2.6
2.2	Anomalous bathymetry features between the powerhouse and tailrace bathymetry	2.7
2.3	Three-dimensional representation of the bathymetry	2.7
2.4	Extent of The Dalles CFD model STL file	2.8
2.5	Boundary conditions for the 2-D tainter gate model	2.10
2.6	Boundary conditions for one of the multi-block models (bank-to-bank 4-block)	2.10
2.7	Extent of the one-bay spillbay domain.	2.13
2.8	Extent of the two-bay spillway domain.	2.13
2.9	Plan view of the 12-bay spillway domain	2.15
2.10	Plan view of the 19-bay spillway domain	2.16
2.11	Plan view of the 19-bay May02T2 simulation	2.17
2.12	Plan view of the multi-block full spillway tailrace domain	2.19
3.1	ADV measurement locations in front of a TDA spillbay	3.2
3.2	Tainter gate validation	3.3
3.3	Free-surface TDA CFD domain	3.5
3.4	The Dalles tainter gate simulation for a 3-ft gate opening	3.5
3.5	Contours of the rigid lid and free-surface tainter gate simulations	3.6
3.6	Plan view: baffle block details and piezometer locations	3.7

3.7	Side view: baffle block details and piezometer locations	3.9
3.8	End sill and elevation 68-ft shelf piezometer locations	3.9
3.9	Water surface elevation and velocity vectors from the 5 kcfs per bay physical model simulation	3.10
3.10	Velocity magnitude shaded cross section generated by the CFD model for the 5 kcfs simulation	3.10
3.11	Comparison of physical model versus CFD model pressures around the baffle block	3.10
3.12	Comparison of physical model versus CFD model pressures around the end sill . .	3.11
3.13	Sketch of water surface elevation and velocity vectors from the 20 kcfs per bay physical model simulation	3.11
3.14	Velocity magnitude shaded cross section generated by the CFD model for the 20 kcfs simulation	3.11
3.15	Comparison of physical model versus CFD model pressures around the baffle block	3.12
3.16	Comparison of physical model versus CFD model pressures around the end sill . .	3.12
3.17	1:40 scale physical model of The Dalles Spillway at ERDC	3.13
3.18	3-D perspective of the CFD 1:40 scale flume	3.14
3.19	Plan view of the physical model flume and measurement sites	3.14
3.20	1:40 scale physical model versus CFD model comparison	3.16
3.21	1:80 scale CFD models: powerhouse and spillway tailrace	3.19
3.22	CFD model solution (Flow Condition 1) from the 1:80 scale spillway tailrace model at elevation 50 ft.	3.20
3.23	CFD model solution (Flow Condition 1) from the 1:80 scale spillway tailrace model at elevation 72 ft.	3.20
3.24	Plan view comparison of the CFD and physical model results (Flow Condition 1) at 1:80 scale	3.21
3.25	Oblique view comparison of the CFD and physical model results (Flow Condition 1) at 1:80 scale	3.21

3.26	Summary of results for Flow Condition 1 between the 1:80 scale physical and CFD spillway tailrace models	3.22
3.27	CFD model solution (Flow Condition 2) from the 1:80 scale spillway tailrace model at elevation 50 ft.	3.23
3.28	CFD model solution (Flow Condition 2) from the 1:80 scale spillway tailrace model at elevation 72 ft.	3.23
3.29	Plan view comparison of the CFD and physical model results (Flow Condition 2) at 1:80 scale	3.24
3.30	Oblique view comparison of the CFD and physical model results at 1:80 scale	3.24
3.31	Summary of results for Flow Condition 2 between the 1:80 scale physical and CFD spillway tailrace models	3.25
4.1	Oct02-T1 water surface elevation solution surface.	4.3
4.2	Highway 197 Bridge piers at which velocities were sampled and compared for Test 11 wall/no wall test case.	4.5
4.3	Test-11Wall solution	4.6
4.4	Test11A solution	4.7
4.5	Test11-NoBaffles solution	4.8
4.6	Deflector simulation.	4.11
4.7	Smooth downstream shelf results	4.13

Tables

2.1	Document sources for TDA structures	2.4
2.2	Document sources for bathymetry data	2.5
2.3	CENWP Rating Curve for TDA at Forebay Elevation 160 ft.	2.12
3.1	Summary of velocity magnitude error statistics for the tainter gate validation simulation cases	3.2
3.2	Comparison of computed discharge and discharge obtained from CENWP rating curve	3.2
3.3	Model parameters for the 1:36 model simulations	3.7
3.4	Comparison of horizontal velocity data for the 1:40 scale TDA model.	3.17
3.5	1:80 scale model flow boundary conditions	3.18

1.0 Introduction

1.1 General Objectives

Physical and numerical models of The Dalles Dam are used to design and test modifications to the existing structure and to investigate hydraulic characteristics to improve fish passage, navigation, and power generation. These models are representative of the prototype and involve approximations that must be tested against data collected in the field. In addition, these models can be compared against each other to better understand the approximations inherent in representing the prototype either at reduced scale or with non-exact solutions to the governing fluid dynamics equations.

The main objective of this work was to use computational fluid dynamics (CFD) modeling of The Dalles spillway and stilling basin, to investigate the performance of several combinations of structural modifications and flow conditions. Some of these structural modifications have been or are planned to be constructed, while others have been shown to create conditions that are not ideal for either structural integrity or improved fish passage survival. In a related study, the CFD simulations are being used in conjunction with field-tests using sensor fish devices (Carlson and Duncan 2003) and live fish (Normandeau Associates 2004) to investigate exposure conditions fish experience during spillway passage through the dam.

A second objective was to document validation of the numerical model against various physical model datasets. Validation of the model occurred before management scenarios were performed, and these tests demonstrate how the numerical model behaves under a wide variety of hydraulic scenarios and boundary conditions. Because both physical and numerical models are only representations of the prototype, the numerical model was also compared to prototype data, albeit limited, collected upstream of a single tainter gate.

1.2 Modeled Site

The Dalles Lock and Dam (TDA) was constructed at the head of Lake Bonneville, approximately 192 miles upstream of the mouth of the Columbia River (see Figure 1.1). Construction of TDA began in 1952, and water was first impounded in 1957 (USACE 2000). As shown in Figure 1.2, the spillway contains 23 spillway bays. Each 50 ft wide bay is controlled with a tainter gate (47 ft radius) and is separated from adjoining bays with a 10 ft wide pier. The overall length of the spillway is 1447 ft, with its crest elevation at 121 ft m.s.l. and top deck elevation at 185 ft m.s.l. The bottom of the stilling basin is at 55 ft m.s.l. and the downstream shelf rises up to 68 ft m.s.l. (Figure 1.3). Downstream of Bays 1 through 15, the basalt shelf extends for approximately 700 ft before a shear drop-off leading to the thalweg is reached. Downstream of Bays 15 through 23, the basalt shelf tapers back towards the spillway, and the length of the basalt shelf is much less (approximately 200 feet downstream of Bay 23).

Baffle blocks were constructed approximately 197 ft downstream of the crest to dissipate energy and force a hydraulic jump in the stilling basin. These 9 ft high by 10.5 ft wide sloping blocks are uniformly separated with a gap of 6.2 ft. A 13 ft high vertical wall (end sill) marks the downstream end of the stilling basin. A concrete apron then extends 52 ft downstream from the end sill.

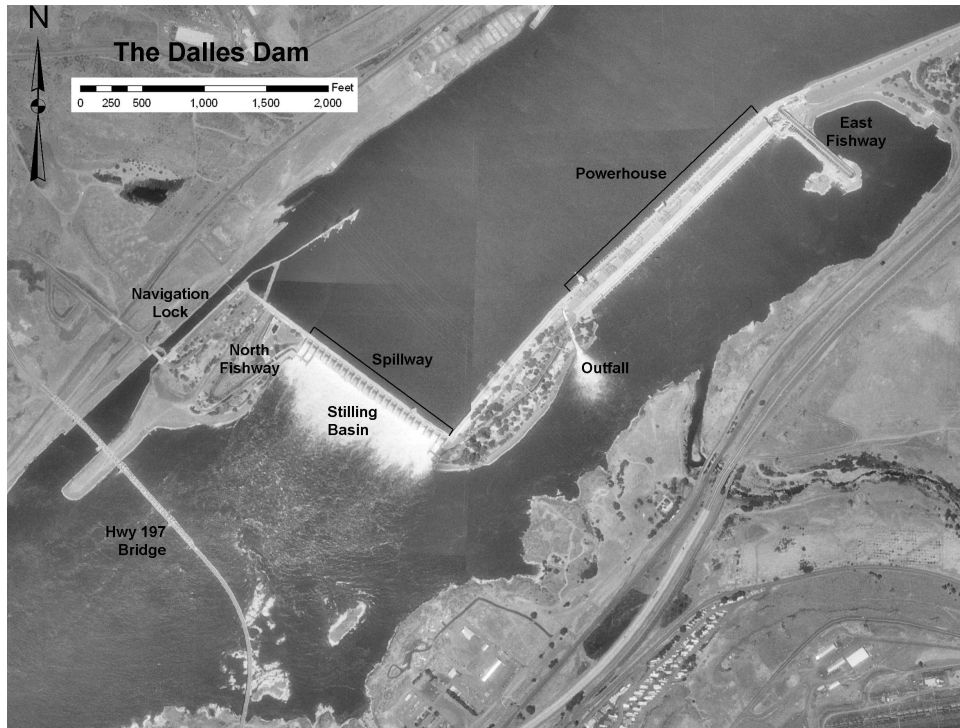


Figure 1.1. Plan view of The Dalles Dam showing the primary structures, including the powerhouse, navigation lock, and spillway

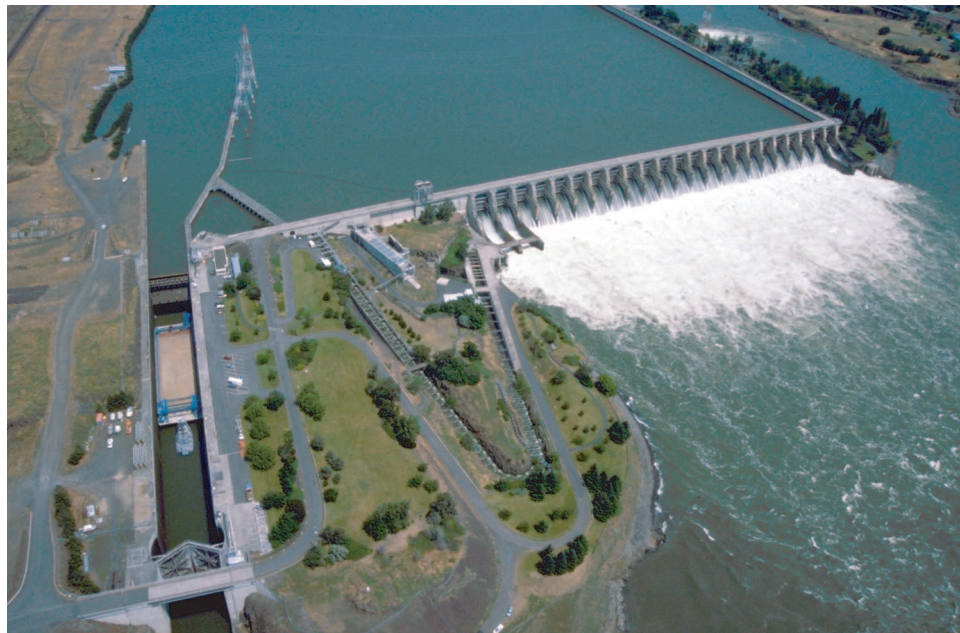


Figure 1.2. Aerial view of The Dalles Lock and Dam with all spillway bays operating

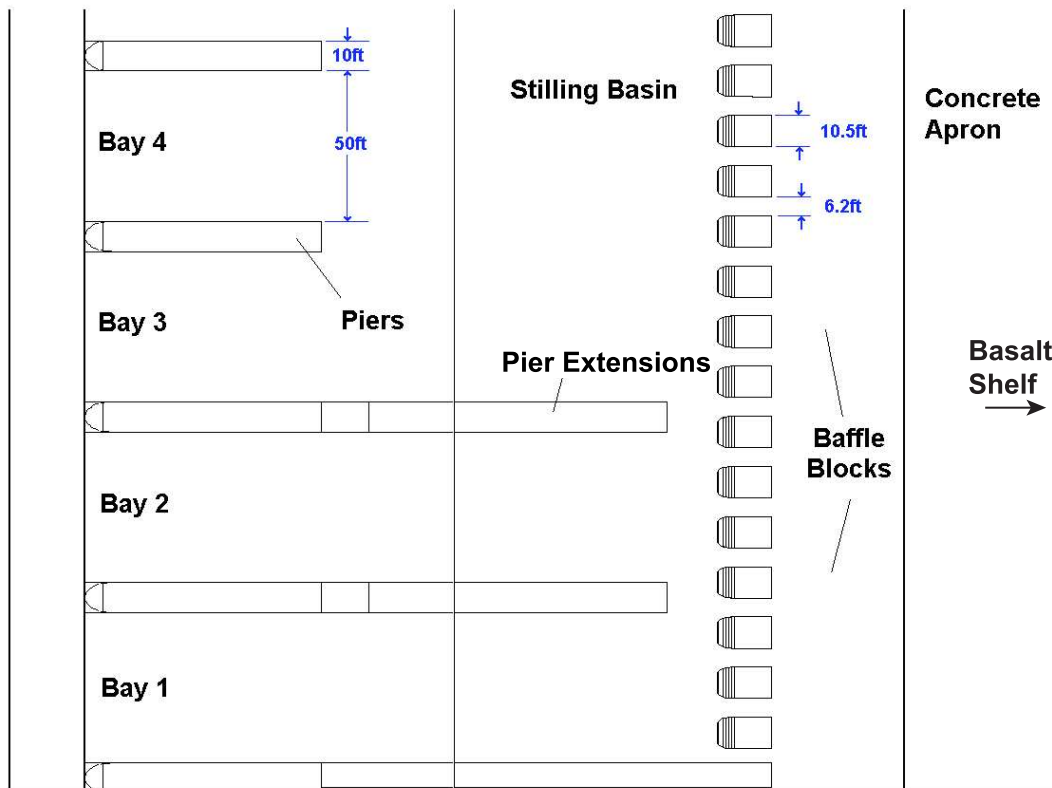
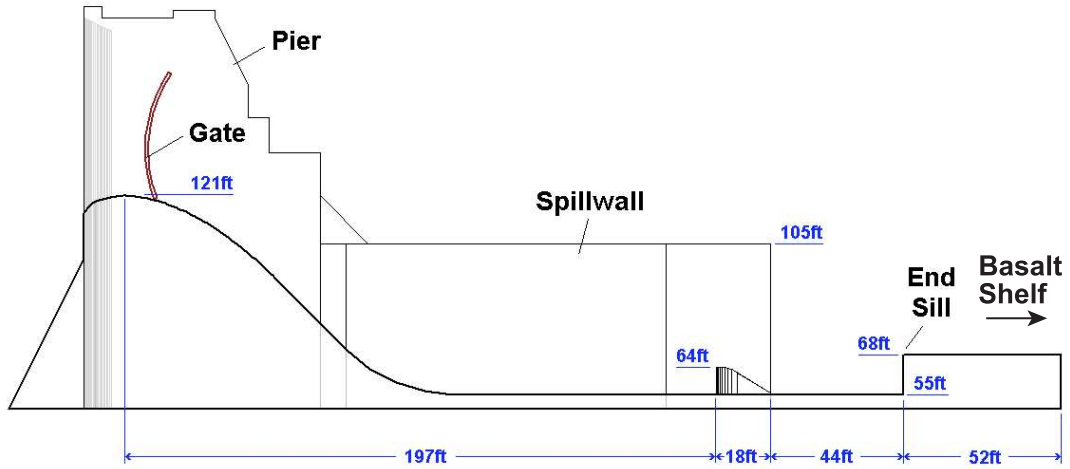


Figure 1.3. Geometry of The Dalles spillway, stilling basin, and end sill.

Discharge through each bay is governed by forebay elevation and gate opening. Unless otherwise noted, all simulations in this report assumed a level forebay elevation of 160 ft m.s.l. Discharge was specified in the model using a rating curve provided by the Portland District, US Army Corps of Engineers (P. Williams, personal communication), although the CFD model was also used to verify these values (see section 3.1).

1.3 Report Organization

The numerical model and methods used to generate the input files are described in Chapter 2. This chapter also describes the extent of the various CFD model domains simulated during the project. Chapter 3 describes validation of the numerical model against several scaled physical models and limited prototype data upstream of a single tainter gate. Chapter 4 describes simulations of structural alternatives to the existing spillway and/or stilling basin. Conclusions and recommendations are presented in Chapter 5.

Several appendices follow the results and discussion section of the report. These appendices document the large number of CFD simulations that have been performed by PNNL; both SIS and those performed for related biological tests.

Appendix A summarizes all CFD simulations performed during this project. For each simulation, boundary conditions, including tailwater height and spillway discharge, when appropriate, are presented. Table captions in Appendix A state which subsequent appendix (B through M) contains a graphical summary of the simulations described in each Appendix A table. The subsequent appendices provide at least one summary graphic for each simulation performed during the study. These graphics have been grouped by the size of the domain simulated by the CFD model.

In addition to the report document, all input files and simulation results have been archived at PNNL. As future questions evolve, this database of information can be queried to answer these questions in a rapid fashion as long as the hydraulic conditions (number of spillbays operating, spillwall present or not, tailwater height, etc.) are similar to those that were simulated. Additional simulations of new hydraulic conditions can, as the need arises, be started again from where any particular existing solutions stopped. This allows for the CFD solution of the new hydraulic conditions to be efficiently attained in a shorter period of time.

2.0 Methods

2.1 Computational Fluid Dynamics Model

2.1.1 Model Selection

Prior to the start of this project, several computational fluid dynamics (CFD) models were considered to simulate The Dalles spillway and stilling basin. The necessary requirements of these models were 1) that they numerically solve the three-dimensional Navier-Stokes equations without using the hydrostatic approximation and 2) were capable of simulating flow conditions in the “frothy” and transient stilling basin. A review paper by Freitas (1995) summarizes results from several CFD models that simulated various laboratory tests, which were then compared both to the laboratory results and to each other. This paper documents several models that satisfactorily meet the first requirement above, however this paper did not test the capability of these models to simulate a free-surface. It should be noted that at the time the Freitas (1995) tests were performed (1993-94), free-surface CFD was only implemented in Flow-3D, one of the pioneers in this area of CFD modeling. Based upon this peer-reviewed paper, PNNL reviewed several of the CFD models presented in Freitas (1995) that had subsequently incorporated free-surface modeling by 2001 (see Cook and Richmond (2001)). At the time Cook and Richmond (2001) was published, Flow-3D was found to produce superior results in highly turbulent zones with large amounts of free-surface breakup (i.e. “frothy” areas). Based upon these findings, Flow-3D was selected as the CFD model best suited to simulate The Dalles stilling basin.

Flow-3D is a commercial software package that is supported through Flow Science, Inc. The model has a large user base and has been previously tested under a wide range of applications. Several recent applications published in peer-reviewed journals include Bradford (2000), Bombardelli et al. (2001), and Savage and Johnson (2001).

2.1.2 Model Formulation

Flow-3D uses the finite volume method to discretize the Reynolds-averaged Navier-Stokes (RANS) equations. The physical domain to be simulated must be decomposed into Cartesian or cylindrical coordinate system blocks composed of variable-sized hexahedral cells. The domain can either be contained within a single block or several blocks, generally called “multi-blocks”. If several blocks are used, each block must either be completely contained within a larger block (“nested”) or be adjacent to another block and/or a domain boundary.

For each cell, average values for the fluid variables (pressure, velocity, turbulent kinetic energy, dissipation rate of turbulent kinetic energy) are computed at discrete times using a staggered grid technique (FSI 2003). The staggered grid technique places all dependent variables at the center of each cell except for velocities, which are located at cell faces. This prevents the “checkerboard” solution that can result in incompressible flow simulations when velocity and pressure become unlinked at adjacent computational nodes when velocities and pressure are defined at the same location (Patankar 1980). Most terms in the equations are evaluated explicitly using the current time-level values of the location variables. Although this explicit procedure is generally efficient and well suited for free-surface wave propagation, it requires that the time-step size be limited to

maintain numerical stability requirements. Time steps for most of The Dalles simulations were on the order of 0.001 seconds.

The general numerical formulation of Flow-3D has a formal accuracy that is first order with respect to both time and space increments. Second order accurate methods are also available in the model, and were used on several occasions in The Dalles simulations. Unless otherwise noted however, the simulations were performed using the first order accurate formulation.

Free-surface movement is computed using an Eulerian approach that involves tracking fluid movement into and out of stationary cells. This method was first developed by Hirt and Nichols (1981) and is commonly referred to as the volume-of-fluid (VOF) method. The VOF method implemented in Flow-3D applies a free-surface boundary condition and for The Dalles application involves the computation of only a single fluid (i.e. cells are either filled with solid, fluid, or void). This method can be contrasted with the free-surface technique used in other CFD programs, such as STAR-CD, that have been referred to as a partial VOF (PVOF) technique (Bombardelli et al. 2001). In the PVOF method, multiple fluids (usually water and air) are tracked. Variable density and viscosity functions are then defined throughout the domain by a weighting of the concentration of the two fluids in each computational cell. Unfortunately, the PVOF technique does not always work well, possibly due to rapid tangential velocity changes at surfaces separating fluids with large density differences (Bombardelli et al. 2001), such as the air-water interface at The Dalles. Simulations of “frothy” flows using the PVOF technique were also found to be problematic (Cook and Richmond 2001). To maintain a sharp interface for the free-surface function in a PVOF model, a very small grid size is required near the interface. During a transient solution the interface moves spatially, hence a fine mesh size is required in all areas where the interface might be expected during the solution. Since computation time is proportional to the number of mesh cells, simulation times for even simple free-surface problems using the PVOF technique can become very large.

The governing equations for incompressible flow, using the VOF methodology, are shown in equations (2.1) and (2.2):

Mass Continuity:

$$\frac{\partial}{\partial x}(uA_x) + \frac{\partial}{\partial y}(vA_y) + \frac{\partial}{\partial z}(wA_z) = 0 \quad (2.1)$$

Momentum:

$$\begin{aligned} \frac{\partial u}{\partial t} + \frac{1}{V_F} \left(uA_x \frac{\partial u}{\partial x} + vA_y \frac{\partial u}{\partial y} + wA_z \frac{\partial u}{\partial z} \right) &= -\frac{1}{\rho} \frac{\partial P}{\partial x} + F_x \\ \frac{\partial v}{\partial t} + \frac{1}{V_F} \left(uA_x \frac{\partial v}{\partial x} + vA_y \frac{\partial v}{\partial y} + wA_z \frac{\partial v}{\partial z} \right) &= -\frac{1}{\rho} \frac{\partial P}{\partial y} + F_y \\ \frac{\partial w}{\partial t} + \frac{1}{V_F} \left(uA_x \frac{\partial w}{\partial x} + vA_y \frac{\partial w}{\partial y} + wA_z \frac{\partial w}{\partial z} \right) &= -\frac{1}{\rho} \frac{\partial P}{\partial z} + G_z + F_z \end{aligned} \quad (2.2)$$

where V_F represents the fractional volume open to flow, ρ represents the fluid density, and the velocity components (u, v, w) are in the coordinate directions (x, y, z), respectively. A_x represents

the fractional area open to flow in the x direction, while A_y and A_z represent similar area fractions in the other two directions. Likewise, P represents the pressure, G_z represents the gravitational acceleration (the Z axis is defined as upward in The Dalles model), and (F_x, F_y, F_z) represent the viscous accelerations.

The governing equations are not complete without the specification of an equation of state, which relates fluid density to pressure, temperature, dissolved solids concentrations, etc. Flow-3D allows density to be non-uniform over the domain, however for The Dalles simulations density was specified as a uniform constant (isothermal, incompressible fluid with a uniform dissolved solids concentration).

The viscous accelerations are defined in the model using an eddy viscosity approach to the so called Reynolds stress terms. This results in the following suite of equations:

$$\begin{aligned}
 F_x &= -\frac{1}{\rho V_F} \left(\frac{\partial}{\partial x} (A_x \tau_{xx}) + \frac{\partial}{\partial y} (A_y \tau_{xy}) + \frac{\partial}{\partial z} (A_z \tau_{xz}) \right) \\
 F_y &= -\frac{1}{\rho V_F} \left(\frac{\partial}{\partial x} (A_x \tau_{yx}) + \frac{\partial}{\partial y} (A_y \tau_{yy}) + \frac{\partial}{\partial z} (A_z \tau_{yz}) \right) \\
 F_z &= -\frac{1}{\rho V_F} \left(\frac{\partial}{\partial x} (A_x \tau_{zx}) + \frac{\partial}{\partial y} (A_y \tau_{zy}) + \frac{\partial}{\partial z} (A_z \tau_{zz}) \right)
 \end{aligned} \tag{2.3}$$

where the Reynolds stress tensor is:

$$\begin{aligned}
 \tau_{xx} &= -2\mu \frac{\partial u}{\partial x} & \tau_{yy} &= -2\mu \frac{\partial v}{\partial y} & \tau_{zz} &= -2\mu \frac{\partial w}{\partial z} \\
 \tau_{xy} &= \tau_{yx} & &= -\mu \left(\frac{\partial u}{\partial y} + \frac{\partial v}{\partial x} \right) \\
 \tau_{xz} &= \tau_{zx} & &= -\mu \left(\frac{\partial u}{\partial z} + \frac{\partial w}{\partial x} \right) \\
 \tau_{yz} &= \tau_{zy} & &= -\mu \left(\frac{\partial v}{\partial z} + \frac{\partial w}{\partial y} \right)
 \end{aligned} \tag{2.4}$$

The coefficient of dynamic viscosity, μ , is assumed to be the sum of the molecular (ν) and turbulent kinematic viscosities (ν_t):

$$\mu = \rho(\nu_t + \nu) \tag{2.5}$$

Flow-3D has several models for calculating the turbulent viscosity: Prandtl mixing length, one-equation, two-equation $\kappa - \epsilon$ and ‘‘Renormalization Group’’ (RNG) $\kappa - \epsilon$, and Large Eddy Simulation (LES). These turbulence models have been well tested and documented in the relevant technical literatures. Based upon prior experience with Flow-3D, the size of the domain, and the turbulence complexity of the stilling basin, the RNG model was selected for all TDA simulations.

The RNG model applies statistical methods for a derivation of the averaged equations for turbulence quantities, such as turbulent kinetic energy and dissipation rate. The RNG model also relies less on empirical constants versus the standard $\kappa - \epsilon$ model. Details on the turbulence model can be found in Yakhot and A.Orszag (1986), Yakhot and M.Smith (1992) and Yakhot et al. (1992).

2.2 Model application to The Dalles Dam

The domain for the CFD model of The Dalles tailrace was constructed by using multiple sources of information. The information provided by these sources can be broken down into two categories: a) description of general engineered structures and b) description of the above and below water surface topography.

2.2.1 Bathymetry and Engineered Structures

Engineered structures include the spillway, powerhouse, non-overflow dam, existing ice-and-trash outfall, and several proposed relocated outfall chutes. Engineering drawings and other documents obtained from the U.S. Army Corps of Engineers (USACE) were used to create three-dimensional representations of these structures (Table 2.1). These structures were initially modeled using three-dimensional computer aided design (CAD) software using a spillway oriented horizontal coordinate system in English units, which can be directly converted to Oregon North State Plane units by applying the following transformation: 1) rotate 126.5° clockwise about the vertical axis, and 2) add 1,837,668.96 and 710,923.24 to the easting and northing coordinates, respectively. This was done to facilitate simulation of the spillway using Flow-3D. The vertical datum was mean sea level (NGVD29).

Table 2.1. Document sources for TDA structures

<i>Structure</i>	<i>Document</i>
Spillway	USACE drawings: DDD-1-4-1/1 DDD-1-4-2/1 DDD-1-4-4/1 DDD-1-4-8-9i
Powerhouse	USACE drawings: DDP-1-0-0/2 DDP-1-0-0/7 DDP-8-0-0/7
Non-Spill Dam	USACE drawings: DDD-1-4-3.1/1
Sluiceway	USACE drawings: DDD-1-4-3.1/25 DDD-1-4-3.1/29
Proposed outfalls	USACE spreadsheet: OUTFALL-EXIT-Cond.xls

River bathymetry and shoreline topography were combined to create a single continuous land elevation surface. This surface was generated by interpolation from point elevations obtained from sources listed in Table 2.2 and shown in Figure 2.1.

All elevation datasets were first loaded into a geographic information system for spatial manipu-

Table 2.2. Document sources for bathymetry data

<i>Dataset</i>	<i>Source</i>	<i>Description</i>
PTS-DEM	USGS	10 meter digital elevation model used for topography.
PTS-MAY2000	USACE Arc-Info cover: addsurvey	Additional points from the May 24, 2000 hydrographic survey.
PTS-99222FORE-TAIL	USACE file: 99222Dal-points.dgn	Detailed bathymetry survey conducted in September 1999 by Minister-Glaeser Surveying, Inc covering areas above and below dam. Some anomalous points removed.
PTS-OUTFALL	USACE file: Hydro2001.dgn	Detailed bathymetry survey covering the plunge pool of the ice and trash sluiceway outfall.
PTS-FORE160 PTS-TAIL74	USGS DOQQ	Columbia River shoreline points developed from digital orthoquad image.
PTS-JASCONT	PNNL	Manually generated points to force interpolation near engineered structures and where data were absent.
PTS-2FTCONT	USACE file: Dalles-1999A.dwg	Points extracted from 2-ft contour lines used for island topography only.

lation. In regions where datasets overlapped, one dataset was chosen to prevail to the exclusion of the others. For example, the detailed bathymetric data collected in September 1999 (PTS-99222FORE and PTS-99222TAIL) superseded overlapping points in the PTS-MAY2000 datasets. Similarly, the digital elevation model dataset (PTS-DEM) was not used when other datasets were available.

Three special datasets were created to improve surface interpolation. The PTS-TAIL74 and PTS-FORE160 datasets represent the river shorelines at an elevation of 74 ft and 160 ft, respectively. These points were obtained by digitizing the shoreline from a US Geological Survey aerial photograph set, where the forebay and tailrace elevations were known from historic records. Minor adjustments were made to the digitized points to accommodate surveyed information. These datasets were constructed to help smooth the interpolation where relatively dense bathymetric data adjoin more sparse topographic data.

A third dataset, PTS-JASCONT, was created to force the interpolated surface beneath engineered structures and also to smooth out areas in the lower tailrace where bathymetric data is absent. In the latter case, sparse PTS-MAY2000 data points collected in a meandering pattern across the river resulted in an interpolation with an unnaturally undulating channel bottom. To correct this sampling artifact, manually drawn contours were added to force the bathymetry to align in the direc-

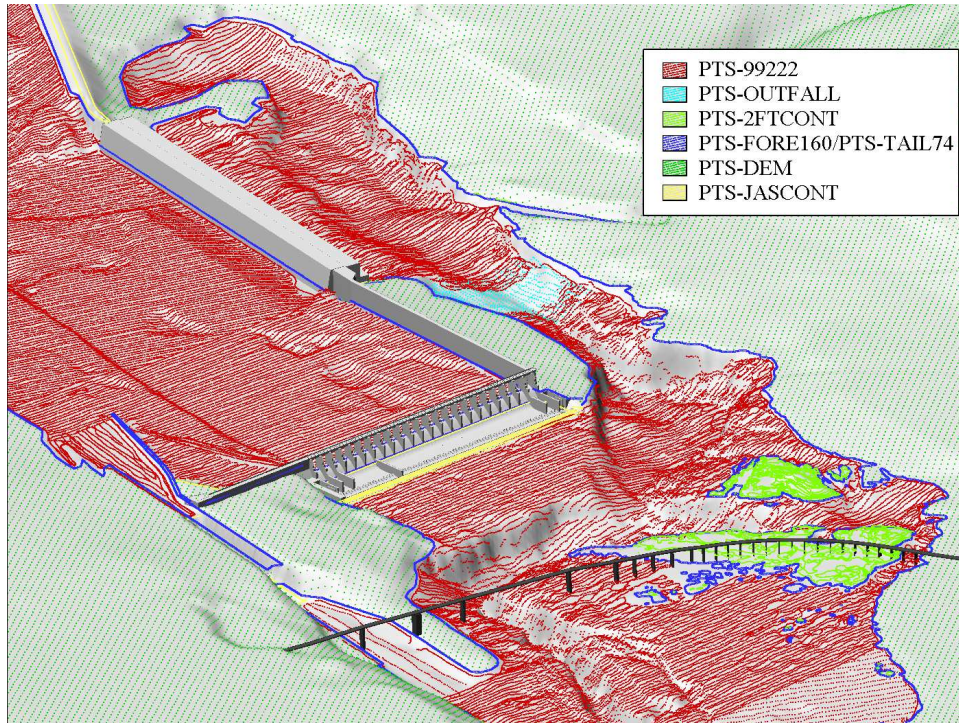


Figure 2.1. Spatial distribution of point elevation data

tion of the river channel. Points extracted from these contours were added to the PTS-JASCONT dataset.

The engineered structure models were then combined with the topographic grid for visual examination. Unintended gaps between the topographic and engineered structures required minor adjustments to prevent simulated fluid from passing through these gaps. The topographic surface was also adjusted to prevent unintended blockage (overlap) of engineered structures. These problems were corrected by iteratively modifying the PTS-JASCONT dataset.

The topographic surface was inspected for unnatural features that resulted from dataset errors. One such feature was discovered in the narrow channel at the lower end of the powerhouse tailrace, just south of the spillway (see Figure 2.2). This narrow fin extends halfway across the deepest part of the channel. Based on a reconnaissance survey, CENWP agreed to exclude the fin from the model. Several smaller anomalous features, involving only a few survey points, were also excluded from the model.

The completed datasets were exported in a format compatible with the CFD model (STL format) and could be combined with numerical representations of the engineered structures (see Figure 2.3). The final extent of the STL domain included the entire tailrace downstream of the powerhouse (see Figure 2.4). The STL continued downstream past the spillway and Highway 197 bridge for more than two miles. The CFD model interpolated the STL to the input specified domain limits for each simulation, so a larger STL extent allowed for expansions of the model domain without a need to recreate the underlying STL.

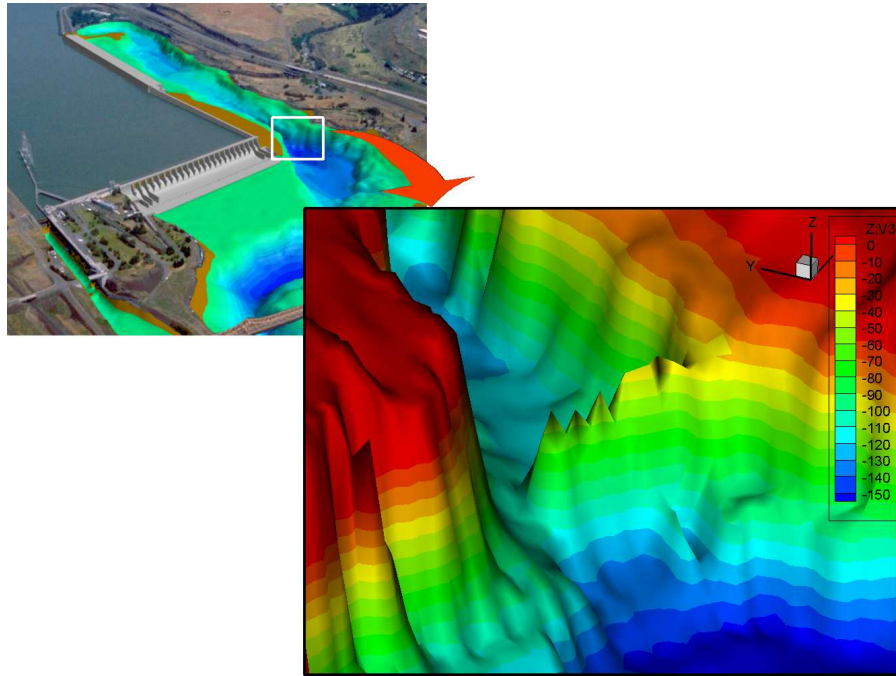


Figure 2.2. Anomalous bathymetry features between the powerhouse and tailrace bathymetry

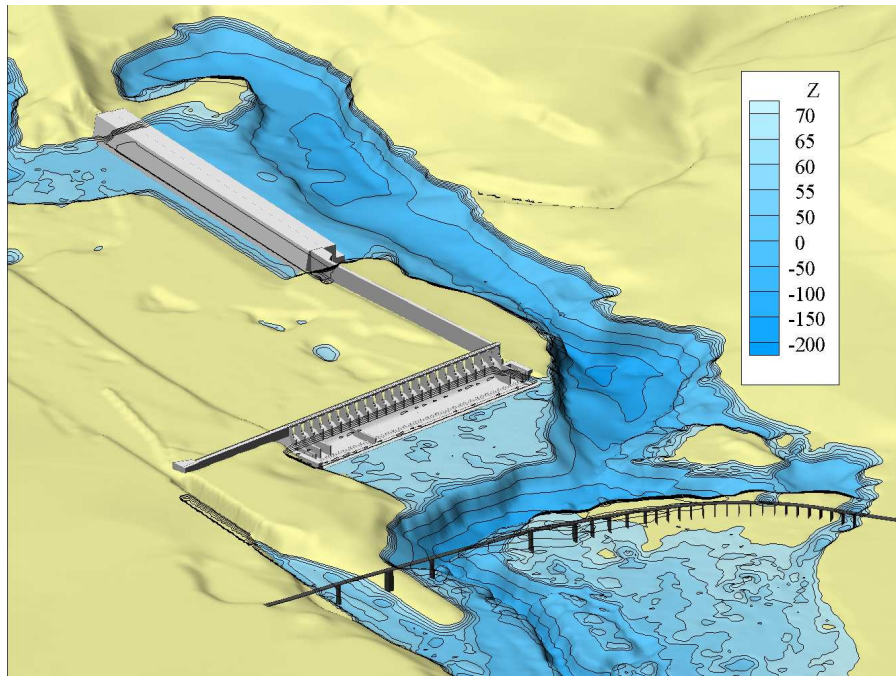


Figure 2.3. Three-dimensional representation of the modeled bathymetry and engineering structures. Bathymetry has been shaded by elevation.

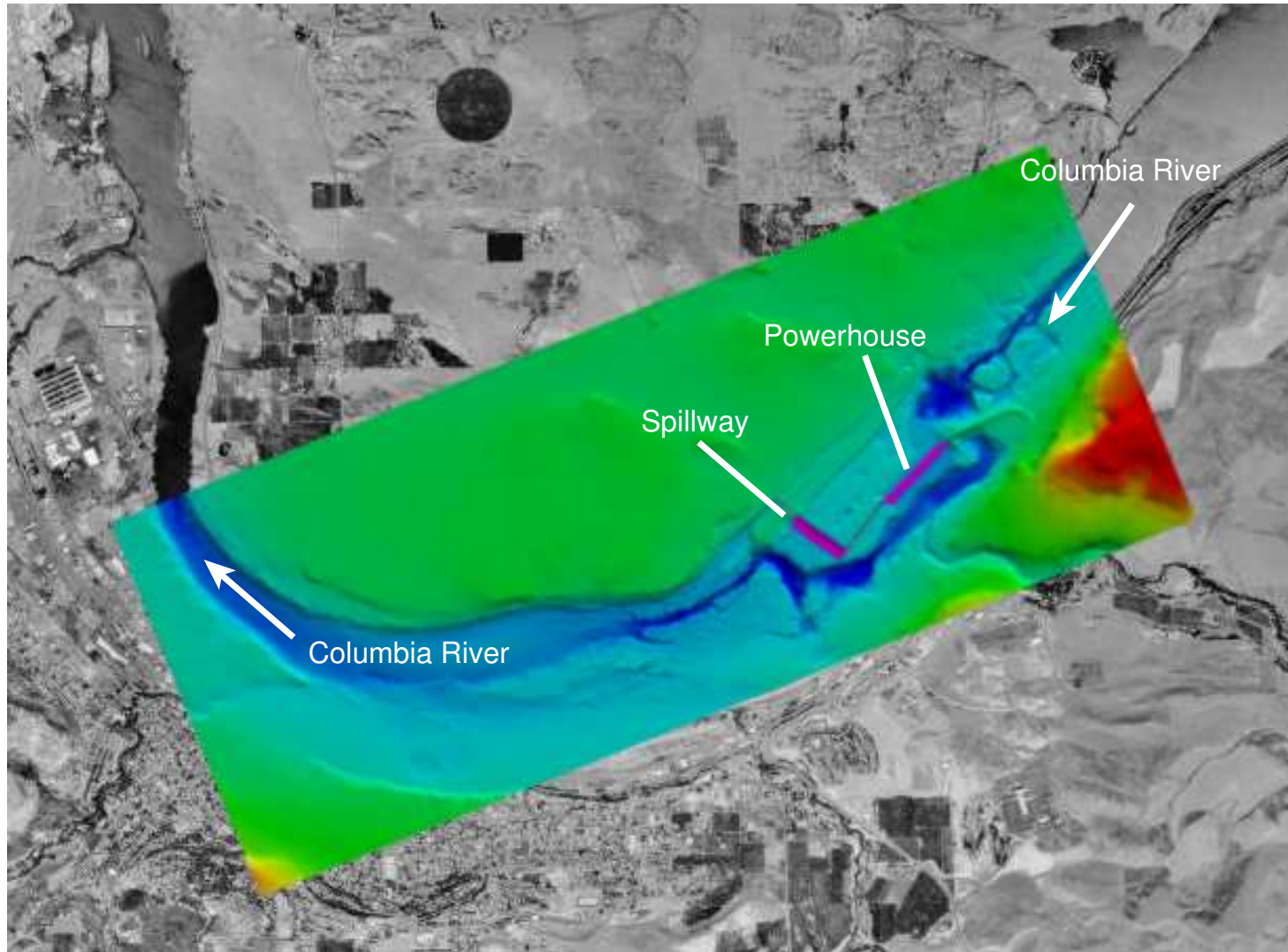


Figure 2.4. Extent of The Dalles CFD model STL file. The STL has been placed on top of a black and white overflight of the The Dalles area. The STL has been shaded by elevation, with dark blue representing the deepest portions of the river thalweg (-200 ft).

2.2.2 Grid Domain and Boundary Conditions

Flow-3D uses a technique called the Fractional Area/Volume Obstacle Representation (FAVORTM) technique to define solids within the model domain (FSI 2003). Unlike the finite element or other types of boundary fitted CFD models, the FAVORTM technique requires the user to first define a bounding hexahedron. Inside of this hexahedron, the user can define the coordinates of basic shapes, such as spheres or cubes, or import STL shapes to define solid objects. The model determines at the onset of each simulation which cells within the hexahedron are fully “blocked” and does not solve the equations of motion within these cells. Therefore, although the domain of the various TDA CFD models varied in spatial extent and grid resolution throughout the project, the same underlying STLs were used for all simulations. Separate STLs that defined the deflectors, pier extensions, and spillwalls were later added into the existing TDA models to simulate these structures. Likewise, baffle blocks were removed from the original spillway STL during these simulations.

Boundary conditions must be specified at all edges of the hexahedron domain. For The Dalles model, six types of boundaries were used: wall, symmetry, velocity, pressure, outflow, and multi-block. Examples of where these boundary types were used are shown in Figures 2.5 and 2.6. The first figure displays a slice of velocity contours through a 2-D model of the forebay, tainter gate, and spillway face. For this simulation the velocities and pressures along the spillway and crest were of primary concern, hence the tailwater was not controlled and an outflow boundary (sometimes called a radiation boundary condition) was used. An outflow boundary condition allows waves to leave the domain with minimal upstream impact. Along the upstream boundary of the model, a uniform velocity vector and stage height were specified, which defined the discharge through the model. Along the top edge of the model, a symmetry boundary conditions was defined, which forces velocities to be normal to the boundary. This is analogous to placing a rigid lid on top of the forebay. This was done to remove spurious wave that formed along the water surface. Along the bottom edge of the domain the STL blocked all cells, which is analogous to a wall boundary.

The second boundary condition figure displays the domain of a four block bank-to-bank model of The Dalles tailrace. Block 1 contains the actively spilling bays and a velocity boundary condition has been applied at the upstream boundary. A similar boundary condition was usually applied to the upstream end of Block 2, unless restarting from a simulation where the powerhouse tailrace was simulated. In these cases, the velocities calculated in the powerhouse tailrace were applied. The downstream boundary conditions for blocks 2, 3, and 4 were pressure boundaries with a specified stage height. This type of boundary set the downstream tailwater elevation for the simulation. Lastly, between the blocks, a “multi-block” linking boundary was used that communicates solution information between blocks during transient simulations.

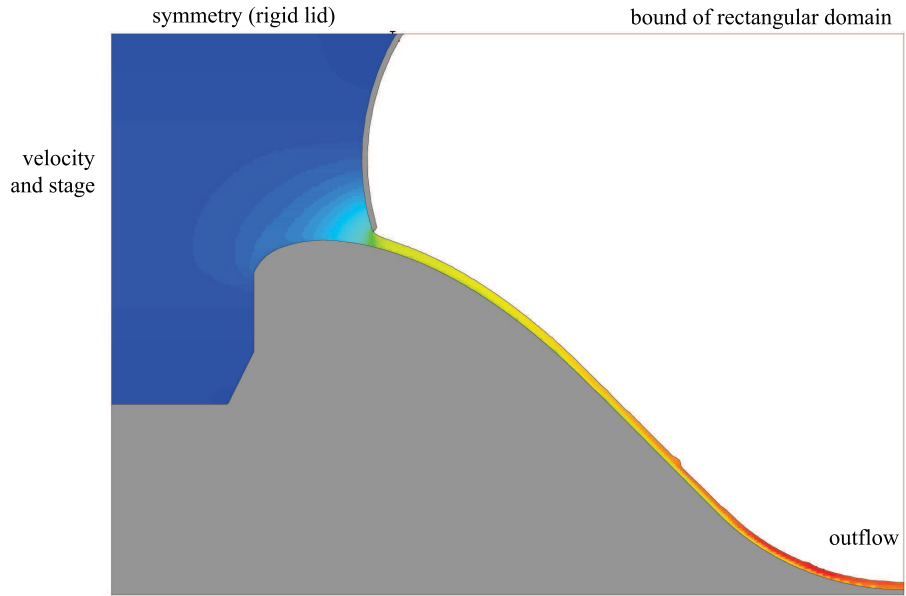


Figure 2.5. Boundary conditions for the 2-D tainter gate model

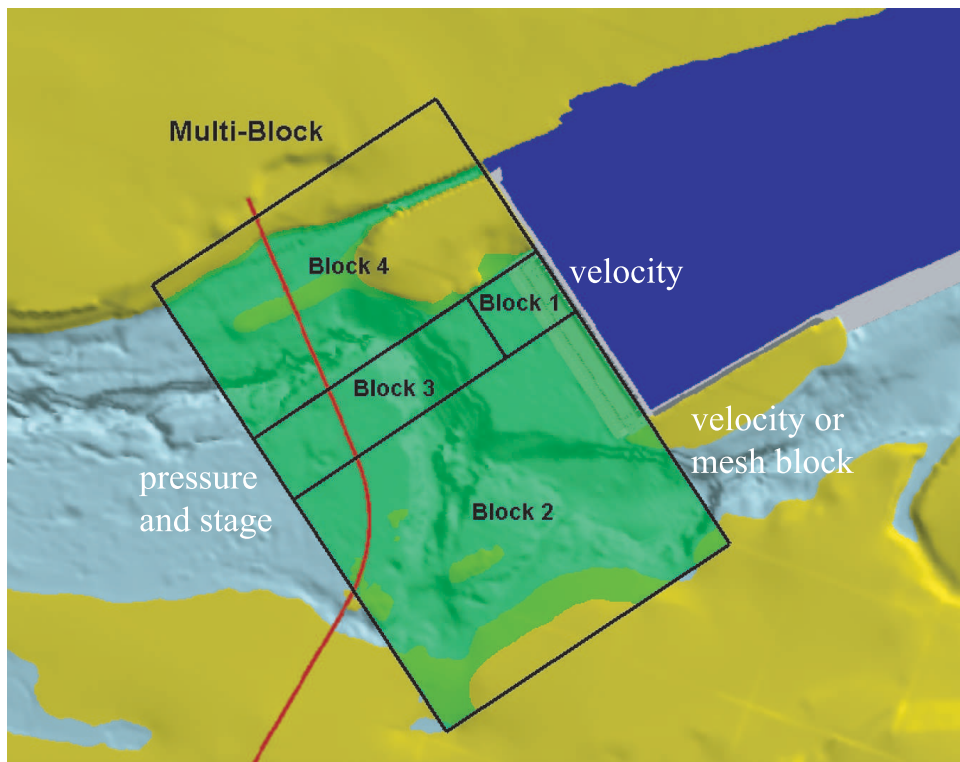


Figure 2.6. Boundary conditions for one of the multi-block models (bank-to-bank 4-block)

2.3 Computational Fluid Dynamics Model Domains

Simulations discussed in this section of the report differ only by the geographic extent of the CFD model domain. The same underlying dam structure and bathymetry (i.e. STL files) were used for all simulations. The separating factor between simulations discussed in this section is the overall extent of the modeled domain. As a general rule the maximum number of grid cells that can be simulated by Flow-3D on available desktop computers with 4Gb of RAM is approximately 7 million cells. Therefore, as the size of the domain increased, the mean cell spacing decreased. Multi-block techniques allow for cell refinement in areas of interest, but the general principle still holds true. As a consequence, the reduced domain simulations generally provided greater detail in the stilling basin and around the baffle blocks, while the bank-to-bank CFD models provided coarser information over a larger tailrace extent.

The reduced domain simulations discussed in this section span anywhere from one to 19 spillway bays. The reasons behind selecting one of the four reduced domain meshes depended upon the necessary grid size for the problem at hand and the length of time required for the simulation to warm-up and reach a dynamic equilibrium.

2.3.1 One and Two Bay Spillway Simulations

The 1- and 2-bay CFD domains are shown in Figures 2.7 and 2.8. Since The Dalles spillway bays are identical, except for those adjoining pier extensions, these CFD domains could represent any bay. These CFD domains are analogous to the sectional physical models, and the 2-bay domain model was always operated with a uniform flow discharging from all bays. It should be noted that the 2-bay model actually involves three bays; two half bays on either side of one full bay.

The upstream limit of the 1- and 2-bay domains began 50 ft downstream of the spillway crest. The upstream boundary condition for these models was determined by performing numerous tainter gate simulations with domains similar to that shown in Figure 2.5 and applying the CENWP rating curve with a forebay elevation at 160 ft (see Table 2.3). It was noted that over a wide range of gate openings that spillway jet velocities a set distance downstream from the gate were approximately constant. At 50 ft downstream of the crest, the average velocities were $u=41.4$ ft/s and $w=-40.8$ ft/s, where u is the longitudinal/downstream velocity component and w is the vertical component (positive upwards). Between a discharge of 4 and 18 kcfs, u and w varied by a maximum of 7% (max deviation from the mean was 2.8 ft/s in u and 2.5 ft/s in w). The impacts of this simplifying assumption was considered negligible after taking into consideration the accuracy of the spillway rating curve and the lack of air entrained by the CFD model as the water flows down the spillway face.

The domain of the models extended a hundred feet or more downstream of the end wall. The 1- and 2-bay models terminated 350 ft from the spillway crest (approximately 100 ft downstream of the end sill) and this domain was applied only for cases with small discharges (e.g. gate opening of 5 ft or less) (see Figure 2.7). The downstream boundary was extended by an additional 100 ft when large discharges were simulated to capture the hydraulic jump that would occur near the end sill (see Figure 2.8). For either domain length, the downstream boundary for the 1- and 2-bay models was a set fluid height (i.e. pressure boundary).

The lateral side boundaries for the 1- and 2-bay models were defined as symmetry conditions, which forces the velocity vectors to flow parallel to the boundary (i.e. zero normal component). The bottom domain boundary was the STL obstacle, which is equivalent to a wall boundary and a law-of-the-wall type profile was assigned. The resulting shear stresses were computed using a $\frac{1}{7}$ power-law approximation to the logarithmic expression. The top domain boundary was set to atmospheric pressure with zero fluid fraction, implying that the boundary should be dry.

Twenty-seven simulations were performed using either the 1- or 2-bay models. Nine of the 1-bay models involved testing deflectors, and will be discussed later in this report. All simulation results, including a graphical distillation of the each simulation, can be found in the appendices.

Table 2.3. CENWP Rating Curve for TDA at Forebay Elevation 160 ft. Single bay tainter gate opening in feet and the corresponding discharge values are in cfs.

opening discharge									
0.0	-	7.5	11,183	15.0	22,077	22.5	32,420	30.0	42,124
0.5	711	8.0	11,913	15.5	22,761	23.0	33,175	30.5	42,834
1.0	1,464	8.5	12,658	16.0	23,508	23.5	33,880	31.0	43,361
1.5	2,215	9.0	13,402	16.5	24,219	24.0	34,485	Full Open	46,199
2.0	2,969	9.5	14,145	17.0	24,891	24.5	35,184		
2.5	3,720	10.0	14,864	17.5	25,631	25.0	35,778		
3.0	4,475	10.5	15,580	18.0	26,370	25.5	36,469		
3.5	5,223	11.0	16,316	18.5	27,029	26.0	37,156		
4.0	5,970	11.5	17,050	19.0	27,722	26.5	37,735		
4.5	6,725	12.0	17,782	19.5	28,412	27.0	38,468		
5.0	7,469	12.5	18,484	20.0	29,056	27.5	39,036		
5.5	8,210	13.0	19,211	20.5	29,780	28.0	39,707		
6.0	8,962	13.5	19,935	21.0	30,501	28.5	40,263		
6.5	9,700	14.0	20,633	21.5	31,131	29.0	40,926		
7.0	10,450	14.5	21,357	22.0	31,801	29.5	41,586		

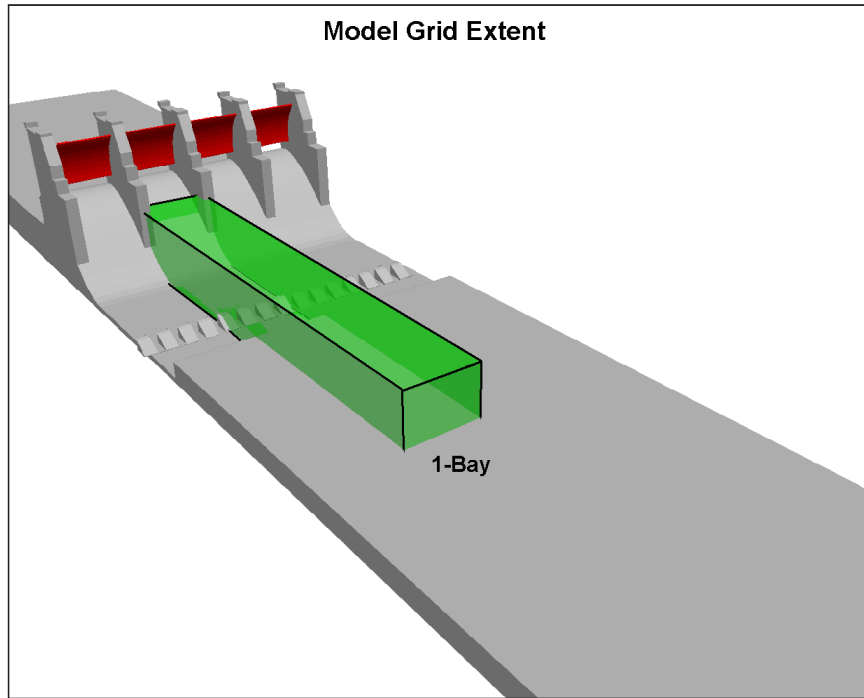


Figure 2.7. Extent of the one-bay spillbay domain.

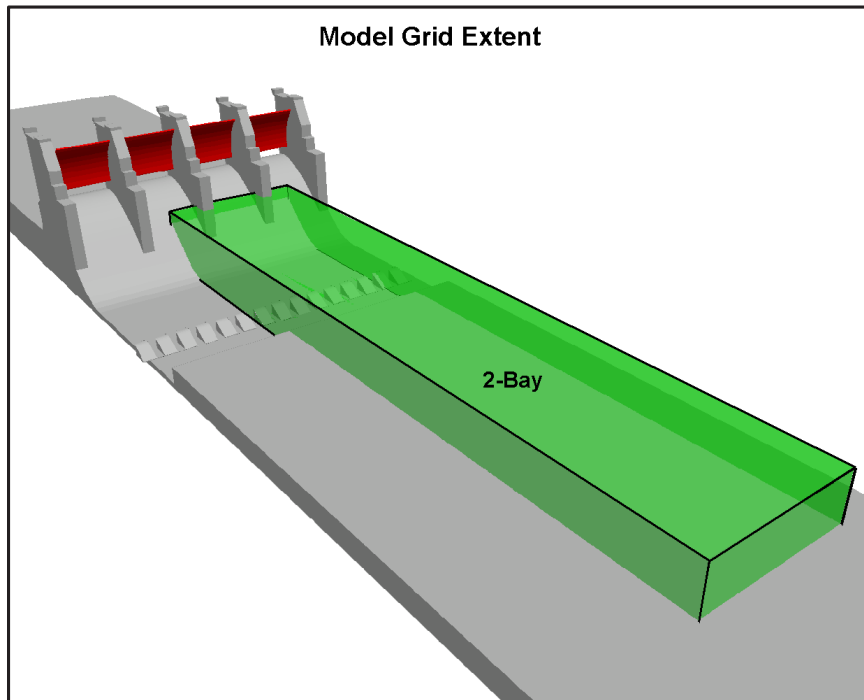


Figure 2.8. Extent of the two-bay spillway domain.

2.3.2 Twelve, Fifteen, and Nineteen Bay Spillway Simulations

The 12-, 15-, and 19-bay spillway models incorporated a much larger portion of the stilling basin. Because multiple bays were simulated, the model was able to capture laterally entrained flow that enters along the south (river left) boundary of the domain as illustrated with arrows in Figures 2.9 and 2.10. This phenomenon has been observed in the prototype, and is driven primarily by changes in water surface elevation in the stilling basin downstream of each spilling bay. The depressed water surface elevation induces lateral flow (i.e. flow parallel to the dam face) to occur in front of the non-spilling bays adjacent to the spilling bays. This phenomenon is shown by the direction of the short particle tracks downstream of any non-spilling bays (bays 14-19) and the first spilling bays (bays 12 through and 14) in Figure 2.11.

To capture this phenomenon in the numerical model, a side velocity boundary was applied based upon the full spillway tailrace CFD model results. Although both the magnitude and direction of the lateral flow was observed to change along the boundary, the flow could be approximated over most discharge conditions simulated with the 12- and 19-bay models with $u = -1.0$ ft/s and $v = -3.0$ ft/s, where u is the longitudinal velocity (negative upstream) and v is the lateral velocity (negative northward or into the domain). The 15-bay model improved slightly upon this approximation by varying the lateral flow for each block (see Figure A.5). From upstream (nearest spillway - block 4) to downstream (block 1) the boundary velocities were: 50 to 153 ft from crest $u = -0.5$ ft/s $v = -1.0$ ft/s; 153 to 365 ft from crest $u = -0.5$ ft/s and $v = -2.0$ ft/s; 365 to 500 ft from crest $u = -0.5$ ft/s and $v = -3.0$ ft/s; 500 to 850 ft from crest $u = 0.0$ $v = -3.5$ ft/s.

The remaining domain boundaries for the 12-, 15-, and 19-bay models were identical to the 1- and 2-bay models. Internal boundaries between blocks in the 15-bay model were specified as “mesh block” boundaries and required no additional information (see FSI 2003 for details).

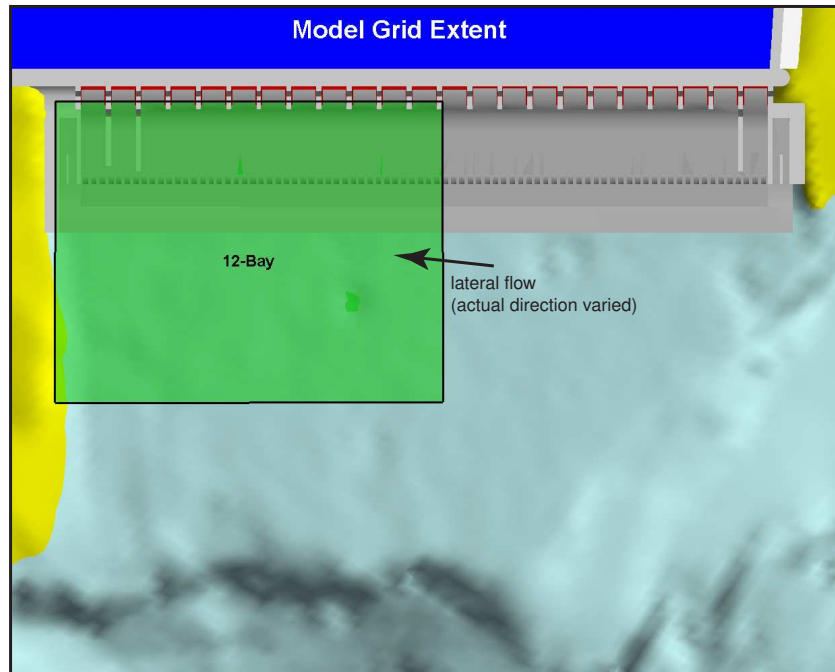


Figure 2.9. Plan view of the 12-bay spillway domain (green rectangle). Gray represents the spillway, light blue represents the bathymetry (note the deep trough is partially visible at the bottom of the figure), tainter gates are shown in red, dry land has been shaded in gold, and dark blue represents the forebay (not simulated).

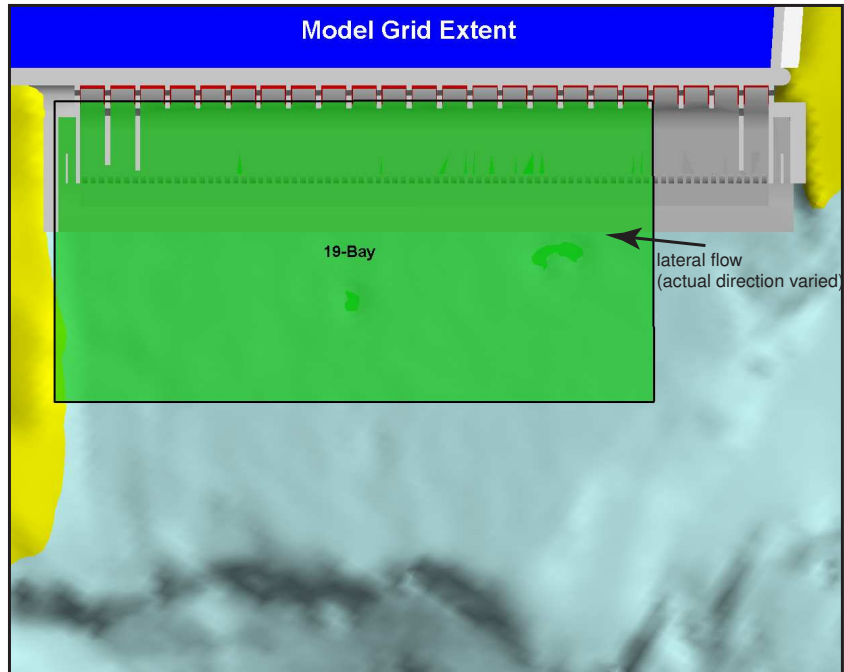


Figure 2.10. Plan view of the 19-bay spillway domain. Gray represents the spillway, light blue represents the bathymetry (note the deep trough is partially visible at the bottom of the figure), tainter gates are shown in red, dry land has been shaded in gold, and dark blue represents the forebay (not simulated).



Figure 2.11. Plan view of the 19-bay May02T2 simulation. Solution surface at elevation 70 ft. Spillway discharge was 63 kcfs and tailwater was 81.8 ft. Particle tracks of equal duration have been added to illustrate the direction of flow. The circles indicate the starting position for each track and the track length is proportional to the velocity magnitude.

2.3.3 Bank-to-Bank Spillway Tailrace Simulations

The bank-to-bank spillway tailrace domain extended laterally across the entire river and longitudinally from several hundred feet upstream of the spillway crest and extending downstream past the Highway-197 bridge. The first bank-to-bank spillway models were developed without the use of multi-block grid techniques, and the entire domain was contained with a single grid block. Because of this limitation, necessary refinement along the spillway face was not possible and mass source blocks were used to inject the flow from the spillway into the stilling basin. Using a new release of Flow-3D, the input files were reconstructed using multi-block techniques that simulated the spillway face and no longer required the use of mass blocks. Spillway boundary conditions for each bay in the multi-block models were identical to those described earlier for 1-, 2-, 12-, 15-, and 19-bay models.

The upstream thalweg boundary of the bank-to-bank spillway tailrace model was determined in the older models using a separate powerhouse tailrace CFD model. This model, which simulated the entire powerhouse tailrace including the draft tubes exits, took several “wall-clock” days to reach a dynamic equilibrium for a given discharge and tailrace condition. The downstream extent of the powerhouse model overlapped with the upstream thalweg portion of the spillway tailrace model. Along the boundary of the spillway model, the powerhouse model solution was “overlaid” and state variables were held constant during the spillway simulation as the upstream thalweg boundary condition. Although this method worked well, the process was time consuming. It was noted after several powerhouse simulations were complete that the velocity distribution laterally and vertically near the spillway boundary was relatively uniform and could be approximated with a constant velocity. In addition, the thalweg boundary is upstream of a constriction in the bathymetry, which also helped to remove any downstream influences of this simplifying assumption. This assumption was used for all multi-block simulations.

The multi-block model was generally composed of eight discrete blocks (see Figure 2.12). Each block had a variable number of cells and non-uniform cell spacing, ranging from a maximum of 20 ft cell spacing near the bottom of the thalweg to 1 ft cell spacing near the spillway face. Cell size ratios at the boundary between mesh blocks was controlled for numerical accuracy so that a maximum of three cells on one side of a mesh boundary matched with a single cell on the other side of the boundary.

Top and bottom boundary conditions were specified for each mesh block. The top boundary was a atmospheric pressure boundary for all blocks, implying that the boundary should be without fluid. The bottom boundary for each mesh block was the STL obstacle (spillway, bathymetry, etc.) except for a small portion of the thalweg below elevation -200 ft m.s.l. This small deep portion of the river was not simulated and the model placed a wall boundary at this elevation.

A total of thirteen full spillway tailrace scenarios were simulated. In addition, six powerhouse tailrace scenarios were modeled and used to construct boundary condition files for the full spillway tailrace. Of the thirteen full spillway tailrace scenarios that were simulated, six were implemented with the newer multi-block technique. Complete documentation of the flow conditions and a graphical summary of each scenario can be found in the appendices.

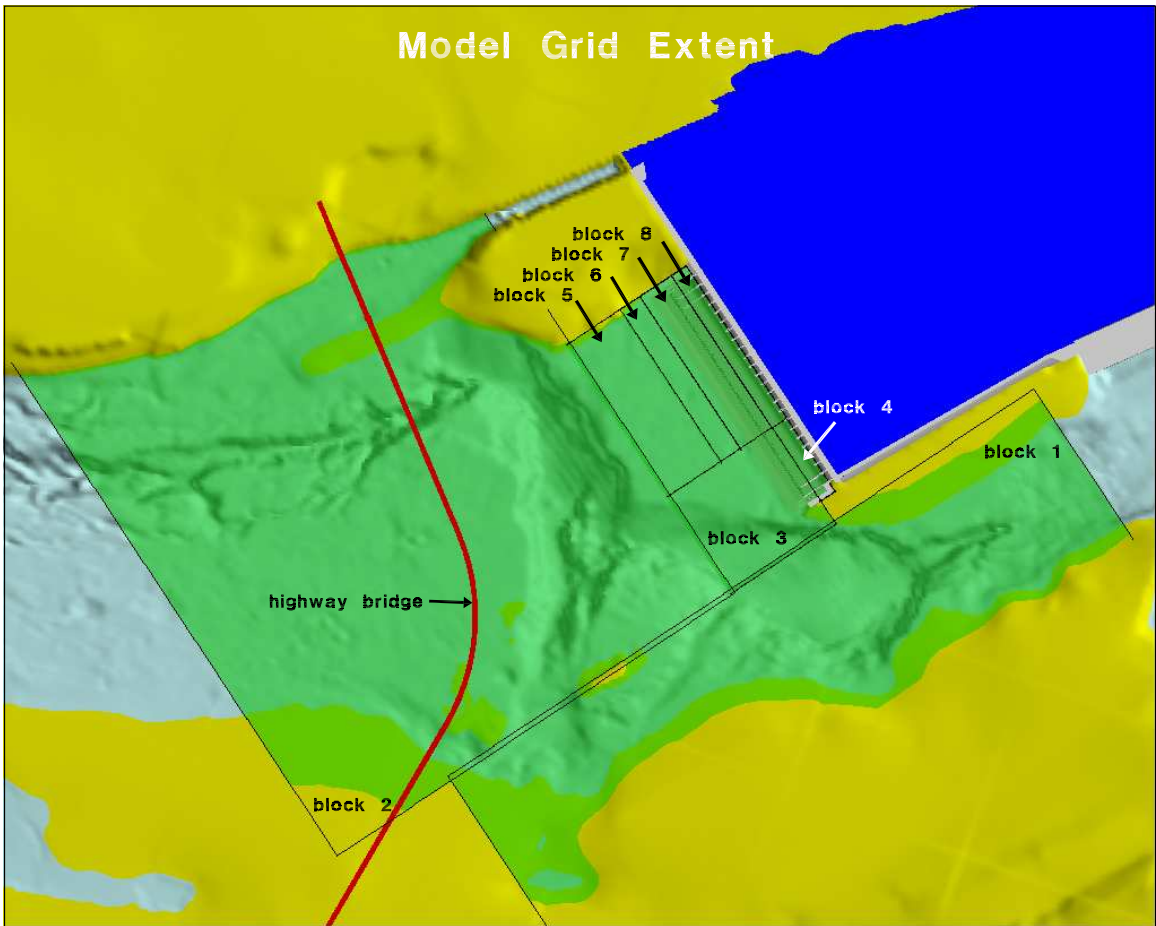


Figure 2.12. Plan view of the multi-block full spillway tailrace domain

3.0 Model Validation

Before Flow-3D was applied to TDA to support structural design activities, biological research, and spill management, the model was rigorously tested to understand how it would perform under a range of hydraulic conditions. Simulation results were then developed that replicated specific physical model and prototype datasets where hydraulic conditions were *a priori* known. Comparison of results between simulated and observed databases reveals that the model is capable of providing reliable information both upstream of the tainter gates and downstream in the turbulent high-velocity flow field downstream of the spillway face. These validation test cases, and the supporting comparisons of results, are presented in this chapter.

3.1 Tainter Gate Simulations

A CFD model of a single TDA spillway bay was constructed to compute the velocity field upstream and immediately downstream of the tainter gates along the spillway face. Spillway face velocities were later used to determine upstream boundary conditions for the multiple-bay and bank-to-bank CFD simulations. CFD results upstream of the tainter gates were also later used by fish biologists to determine placement of live and sensor fish release pipes and optimum aiming orientations for hydroacoustic instruments.

To reduce the computational effort required to operate the CFD model, the model domain was reduced to a single 2-D plane that passes through the centerline of a spillway bay. This approximation is appropriate for understanding hydraulic phenomenon in close proximity to the tainter gate centerline, however differences between the CFD model and prototype would be expected near the piers. Several 3-D phenomena occur near these piers, including vortices, which will not be captured by this 2-D model. Air-core vortices have been observed upstream of the tainter gates for some operational conditions. In addition, far upstream of the gate there will be a lateral component to the approach flow, the strength of which depends upon powerhouse and spillway conditions. If results far upstream of the gate are required, a 3-D model (Rakowski et al. 2006) of the forebay which incorporates these lateral flows should be applied because these conditions are not represented by the 2-D model.

Water velocities were measured upstream of an open tainter gate at The Dalles using a Sontek acoustic Doppler velocimeter (ADV)^(a). Cables were strung along Lines A and B (see Figure 3.1), which were then used to lower the ADV to different depths. At each of these depths, the ADV collected multiple individual velocity readings that were later averaged into ensemble means to form a validation dataset for a 2-D Flow-3D model of The Dalles spillway.

The CFD model domain extended approximately 100 ft upstream of the tainter gate. The gate was fixed at a set opening (1 ft, 3 ft, or 5 ft) and a uniform upstream forebay elevation of 158.6 ft was applied.

Measured versus simulated velocity magnitudes are compared in Figure 3.2. Due to the harsh flow conditions (shedding vortices and high velocities) along Line B, the ADV was not stable at

(a) M. A. Weiland, unpublished data.

many of the depths along that line. Therefore, a complete velocity profile along the entire line was not collected. A partial data set, collected when the spillway gate was open 5 ft, was also compared to CFD model results (Figure 3.2). Table 3.1 summarizes the error statistics comparing the measured and simulated velocity magnitudes. Mean absolute error (MAE) was less than 0.25 ft/s for all cases simulated. The simulated discharge, discharge from the CENWP rating curve^(b), and their difference is listed in Table 3.2.

Table 3.1. Summary of velocity magnitude error statistics for the tainter gate validation simulation cases

Gate Opening (ft)	Meas. Line	Bias (ft/s)	MAE (ft/s)	RMS (ft/s)
1	A	0.02	0.11	0.14
3	A	0.06	0.15	0.25
5	A	0.09	0.25	0.30
5	B	0.04	0.19	0.25

Table 3.2. Comparison of computed discharge and discharge obtained from CENWP rating curve

Forebay Elev. (ft)	Gate Opening (ft)	Simulated (cfs)	Rating Curve (cfs)	Difference
158.6	1	1621	1438	12%
158.6	3	4514	4394	3%
158.6	5	7434	7329	1%

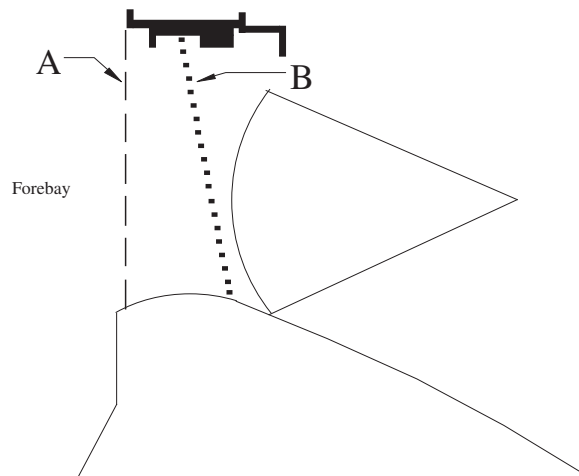


Figure 3.1. Cross-sectional view of the spillway bay where ADV measurements were performed. Line A is near the pier nose and Line B is near midpoint of the bay at bridge deck to near the opening.

(b) P. Williams, personal communication.

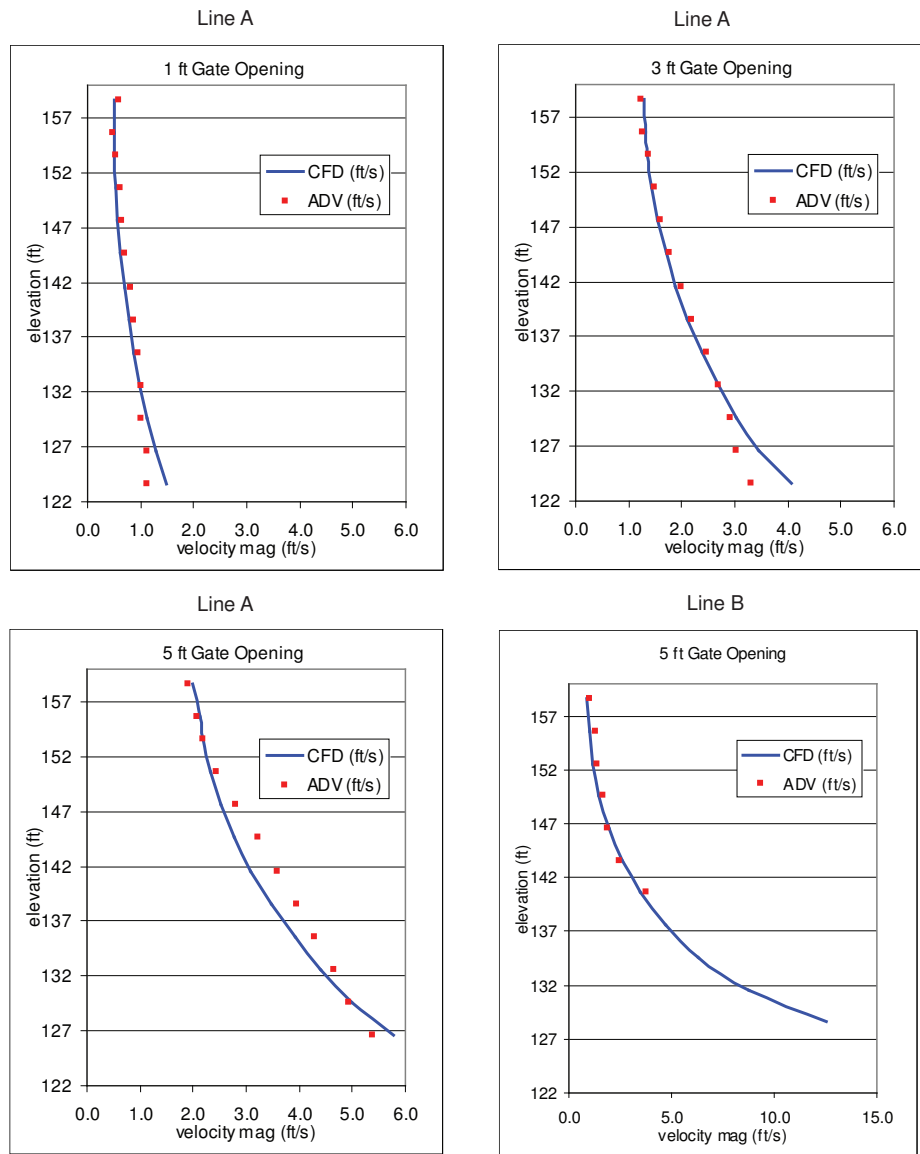


Figure 3.2. Comparison of measured and computed velocity magnitude profiles upstream of a tainter gate at The Dalles. All profiles were measured along Line A (see Figure 3.1) except for one partial profile along Line B at a 5 ft. gate opening.

3.1.1 Grid and Boundary Condition Sensitivity

The 2-D CFD model domain was tested for sensitivity to grid resolution and forebay boundary conditions. Since Flow-3D was chosen for this project because of its ability to simulate transient free-surface flows, the first version of the tainter gate model had a free-surface top boundary and pressure upstream boundary. This is in contrast to the boundary conditions displayed in Figure 2.5, which has a rigid lid top surface and a fixed velocity upstream boundary condition.

In the free-surface version, gravity waves formed along the free-surface as the model converged towards the correct forebay velocity field. These gravity waves would oscillate between the tainter gate and upstream boundary, resulting in surges of flow down the spillway face in response to the change in hydrostatic pressure above the gate. Since the objective of these simulations was to simulate a dynamic equilibrium between inflows and outflows, a wall was placed over the top of the forebay domain to quickly dampen these surface waves. A free-surface gap of several feet along the forebay water surface ensured that water pressures at the surface were atmospheric. A graphic illustrating this version of the model domain is shown in Figure 3.3.

The upstream pressure boundary did not constrain the quantity of flow entering the domain. As expected, the accuracy of the model to correctly calculate contraction losses and boundary-layer friction under the tainter gate, as compared to the CENWP rating curve, improved with increasing grid resolution. Grid resolution was increased (see Figure 3.4) until discharge differences between simulations were small. For the 3 ft gate opening and a grid resolution of 0.10 ft or less, computed discharges were within 7% of the CENWP rating curve discharge.

To reduce the warm-up gravity waves two assumptions were applied: 1) the forebay free-surface boundary was replaced with a rigid lid (symmetry plane) and, 2) the upstream forebay boundary was replaced with a velocity boundary condition (reverting to the boundary conditions shown in Figure 2.5). The impacts of these assumptions were tested against free-surface top boundary solutions by comparing velocity contours in the forebay, and were found to be negligible. The largest impact on the forebay water velocities was found to be associated with the discharge passing through the model. Figure 3.5 illustrates the impact in velocity contour location between the free-surface calculated discharge and the CENWP discharge (approximately 7%). It should be noted however that although a difference in contour location is detectable, even the largest distance between the 2 ft/s isovel (isovel farthest from the gate opening) are on the order of 3 ft. The benefit in using these two approximations was that simulations could be completed in approximately 3 hrs of “wall-clock” time.

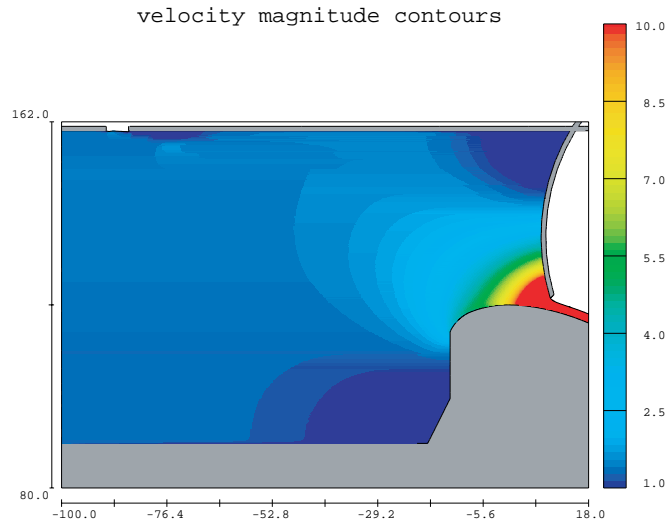


Figure 3.3. Free-surface CFD domain with a gate opening of 3 ft and uniform mesh of 0.1 ft. Velocities greater than or equal to 10 ft/s are shown in red.

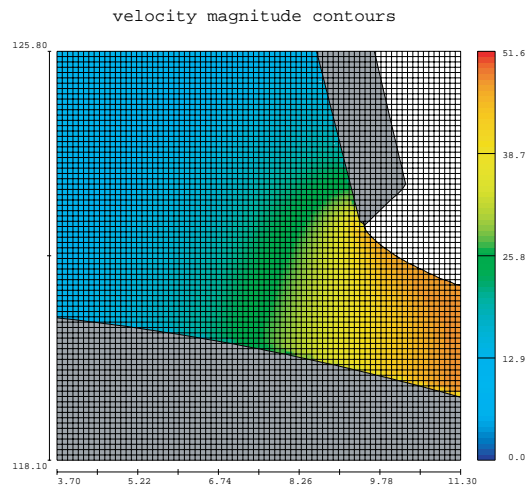


Figure 3.4. Close-up of the tainter gate lip for the uniform 0.10 ft mesh, 3 ft gate opening, free-surface simulation. Contours are in ft/s.

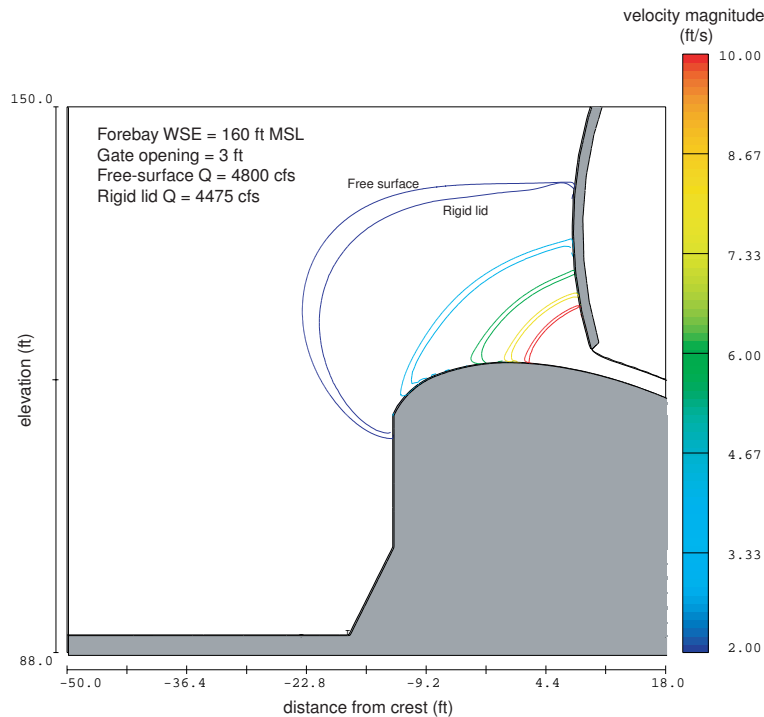


Figure 3.5. Contours of the rigid lid and free-surface tainter gate simulations. Discharge for the free-surface simulation is 7% larger than the rigid lid simulation (difference between the CENWP and computed rating curve with a 3 ft gate opening).

3.2 Simulating the 1:36 Scale Sectional Model

The Bonneville Hydraulic Laboratory, US Army Corps of Engineers, constructed a 1:36 scale sectional model of The Dalles Dam spillway before the prototype was constructed in the mid-1950s. This physical model was used for a wide variety of engineering design tests, including determining the discharge capacities of the final design spillway crest, minimum limits for excavation in the stilling basin, and other information pertinent to design of the dam. Data preserved in the Bonneville Hydraulics Laboratory report germane to this study are pressures on the baffle blocks and end sill measured by means of piezometers installed in the model and connected to a manometer board. Prototype flow rates through the physical model ranged from a total river discharge of 100 kcfs to a maximum flood discharge of 2,290 kcfs.

Memorandum Report 1-7 (Bonneville Hydraulic Laboratory (1952)) and the summary Technical Report No 55-1 (Bonneville Hydraulic Laboratory (1964)) describe the model tests and present summaries of the collected data. Figures 3.6 through 3.12 have been duplicated from these reports to describe the various piezometer locations. All reported piezometer values were rounded in the reports to the nearest foot of water. Neither report discussed the typical range of water variation in the manometer board measurements nor the accuracy of the reported pressure measurements.

Two of the 1:36 scale physical model tests using the final (as built) spillway design were replicated using the numerical CFD model Flow-3D. It should be noted that the physical model released flows uniformly from all three spillway bays. Because of the lateral symmetry in hydraulic conditions,

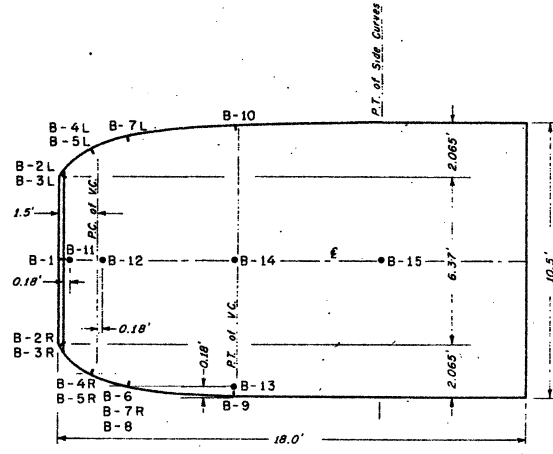


Figure 3.6. Plan view of the instrumented 1:36 scale baffle block with piezometer locations. Dimensions are in prototype units of feet, and the B prefix signifies piezometers were located on the baffle block. Source: Bonneville Hydraulic Laboratory (1952).

piezometers in the stilling basin were placed (approximately) along the center line of the physical model (note: because of the size and spacing of the baffle blocks, the centerline of the model was approximately in line with piezometers B-2L and B-3L instead of B-1). To minimize computational effort, the CFD model took advantage of this symmetry about the model centerline and only the center spillway bay was simulated. As with the physical model, the CFD model domain and boundary inputs were reduced to 1:36 scale for the simulation and then scaled back to prototype equivalents at the end of the simulation. Both test conditions used identical finite volume cell sizes and boundary conditions. Table 3.3 summarizes the simulation parameters.

Table 3.3. Model parameters for the 1:36 model simulations

Finite volume grid mesh	Uniform size of 0.0278 ft in all dimensions. At prototype scale, this grid size spacing is approximate 1 ft.
Model width extent	One bay plus end piers
Turbulence model	Renormalized group (RNG) $k - \epsilon$ model
Upstream boundary	Specified velocity at approximately half-way down the spillway face
Downstream boundary	Tailrace water surface elevation

The first of the two test conditions were: discharge of 5000 kcfs per bay, forebay pool elevation at 160 ft, and tailwater elevation at 76.8 ft. These conditions are identified in the 1:36 physical model report as the 200,000 cfs river discharge and 100,000 cfs spillway discharge test case.

A sketch of the physical model flow pattern for this discharge condition is shown in Figure 3.9. A

comparable slice from the CFD model is shown in Figure 3.10. Both the profiles of water surface elevation and water velocity magnitudes over the end shelf are similar between the two figures. Both models show a distinct shear layer (zone of small magnitude between two layers going in different directions) between the end of the spillway face and the baffle block. The location and extent of the shear layer is approximately the same between the two model results.

Pressures computed by the CFD model were sampled at locations corresponding to the piezometer locations in the physical model. The results generated by both models are shown for the baffle block (Figure 3.11) and for the end sill/downstream shelf (Figure 3.12). The average bias in pressure between the CFD and physical model data were -0.1 ft over the baffle block and -0.2 ft over the end sill/shelf. It should be noted that these errors were computed at prototype scale; however, both the CFD and physical model results were computed at 1:36 scale. Mean average error (MAE) and root-mean-square (RMS) errors were 0.4 ft and 0.5 ft, respectively. A difference of 0.5 feet at prototype scale is 0.014 ft at 1:36 scale. Although the Memorandum Reports do not comment on expected instrument error or measurement accuracy, differences in pressure on the order 0.01 ft are expected to be within the accuracy of the measurement device.

The second of the two test conditions were: discharge of 20,000 kcfs per bay, forebay pool elevation at 160 ft, and tailwater elevation at 94.0 ft. These conditions are identified in the 1:36 physical model report as the 600,000 cfs river discharge and 400,000 cfs spillway discharge test case.

A sketch of the physical model results for the second discharge condition is shown in Figure 3.13, and the CFD model result slice is shown in Figure 3.14. Both the profile of water surface elevation and water velocity magnitude over the end shelf are similar between the two figures. As with the 5 kcfs simulation, the location and extent of the shear layer appear to be of approximately the same size and extent. Also, just downstream of the stilling basin and near the end sill wall, a small back roller was drawn in the sketch. The same hydraulic phenomenon was identified by the CFD model, and can be seen as the low velocity (blue) zone just past the leading edge of the end sill. The increase in velocity magnitude as the flow exits the stilling basin (accelerating from approximately 10 ft/s to upwards of 14 ft/s) shown in the physical model was also captured by the CFD model, as can be seen by noting the shift in colors from green (10 ft/s) to yellow (15 ft/s) along the end shelf.

Pressures computed by the CFD model were sampled at locations corresponding to the piezometer locations in the physical model. The results generated by both models are shown for the baffle block (Figure 3.15) and for the end sill/downstream shelf (Figure 3.16). The average bias in pressure between the CFD and physical model data was 2.7 ft over the baffle block. Although the bias is much larger for the baffle block zone at 20 kcfs than for the 5 kcfs test, we feel the results are reasonable considering the turbulent fluctuations occurring around the baffle block at this relatively large discharge. Perhaps more important than the absolute pressure magnitudes are the general rise and fall trends in pressure at the various piezometer locations, which were captured correctly by the CFD model. Therefore, although CFD computed pressures are higher than the physical model values, the overall trends in pressure fluctuation near the baffle block are similar. Downstream of the baffle block and near the end shelf, pressure values computed by the CFD model fall back inline with those reported by the physical model. CFD model pressure bias in this zone is, on average, only 0.4 ft/s and the MAE and RMS errors are 0.9 ft and 1.0 ft, respectively.

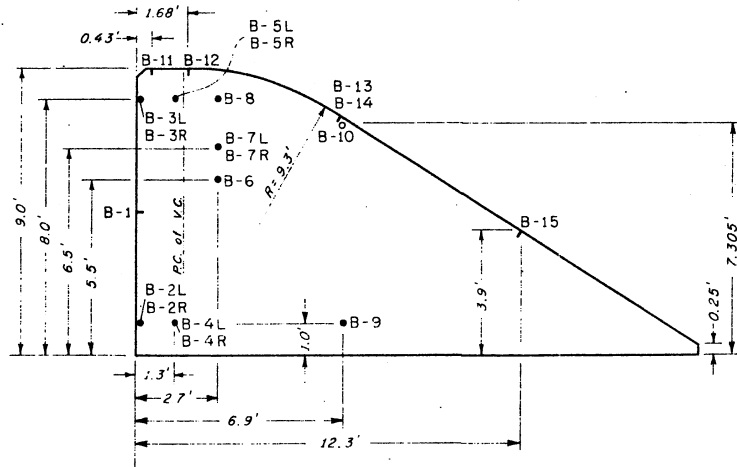


Figure 3.7. Side view of the instrumented 1:36 scale baffle block with piezometer locations. Dimensions are in prototype units of feet, and the B prefix signifies piezometers were located on the baffle block. Source: Bonneville Hydraulic Laboratory (1952)

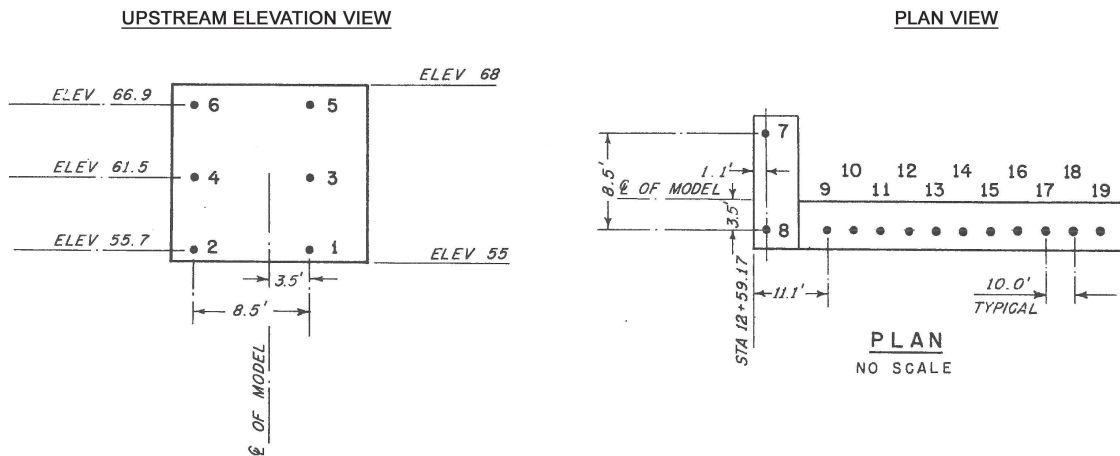


Figure 3.8. Upstream elevation view (left; at Station 12+59.17) of the end sill piezometers and plan view (right) of the elevation 68 ft shelf piezometers located downstream of the stilling basin. Piezometers E-8 through E-19 are inline and directly downstream of test baffle block, and piezometer E-19 is located the farthest downstream from the spillway. Dimensions are in prototype units of feet. Piezometer numbers are shown without the prefix "E" in the figure, which denotes end sill/shelf. Source: Bonneville Hydraulic Laboratory (1952)

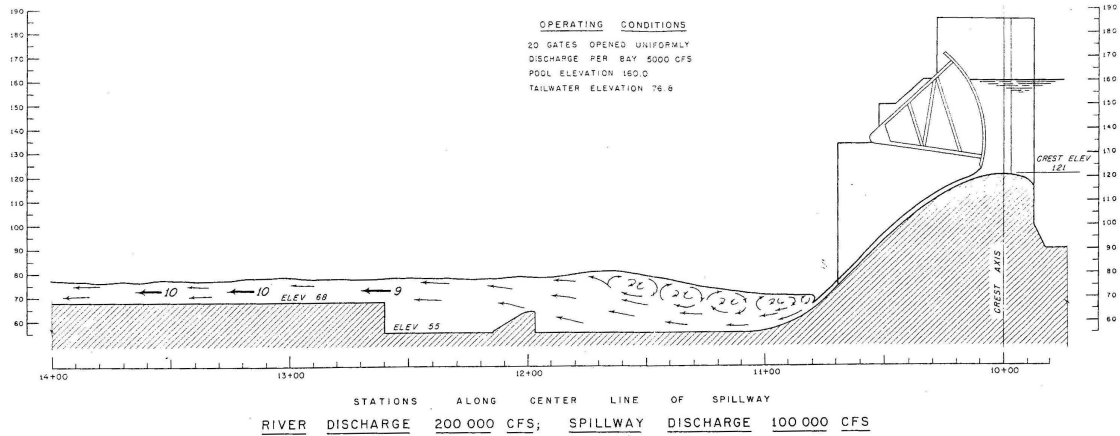


Figure 3.9. Water surface elevation and velocity vectors from the 5 kcfs per bay physical model simulation. Source: Bonneville Hydraulic Laboratory (1964).

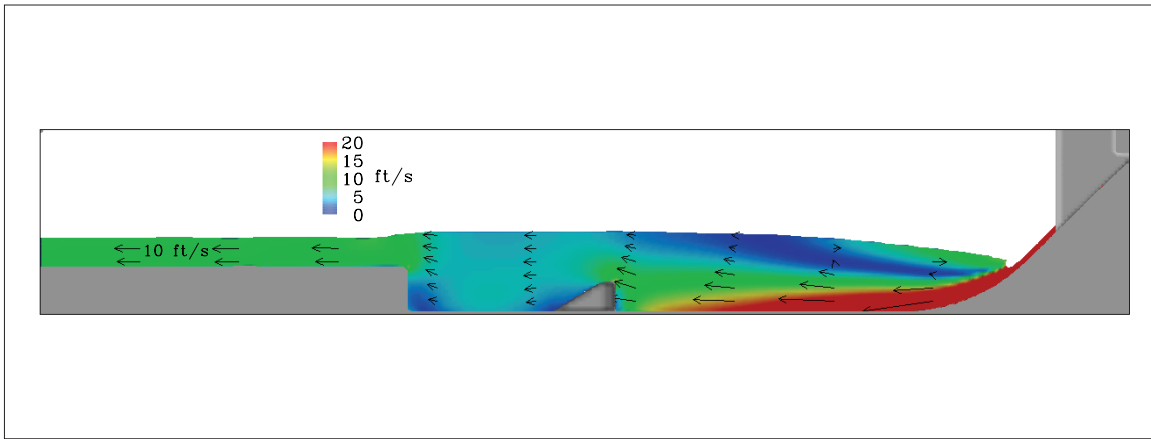


Figure 3.10. Velocity magnitude shaded cross section generated by the CFD model for the 5 kcfs simulation. The cross section passes through the model centerline baffle.

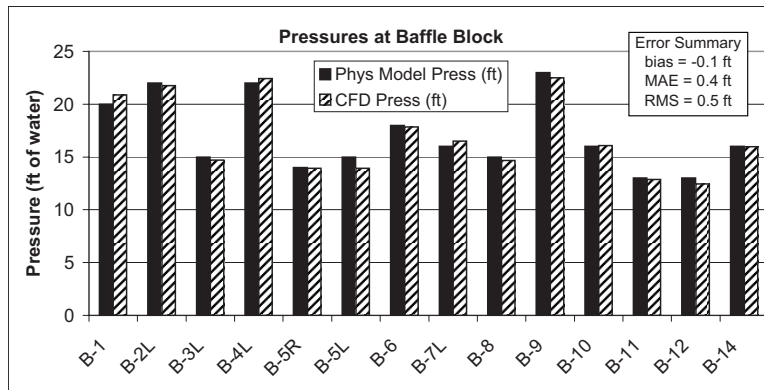


Figure 3.11. Comparison of physical model versus CFD model pressures around the baffle block

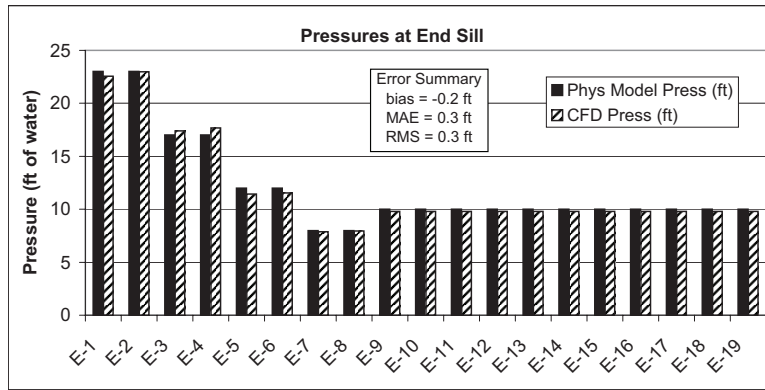


Figure 3.12. Comparison of physical model versus CFD model pressures around the end sill

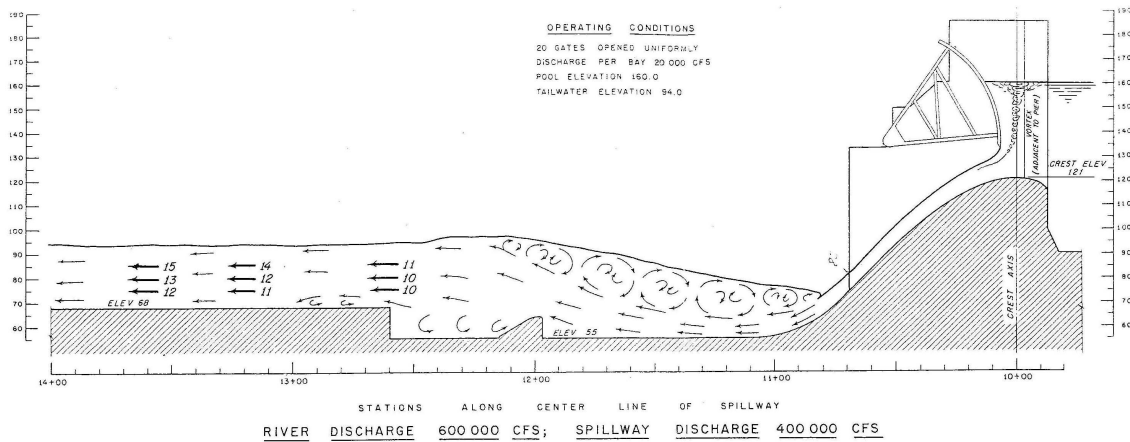


Figure 3.13. Sketch of water surface elevation and velocity vectors from the 20 kcfs per bay physical model simulation. Source: Bonneville Hydraulic Laboratory (1964).

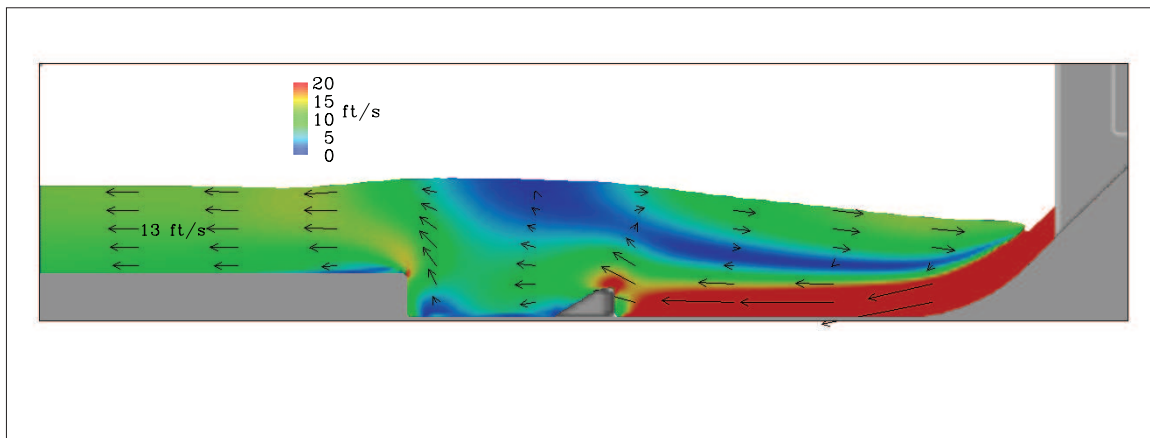


Figure 3.14. Velocity magnitude shaded cross section generated by the CFD model for the 20 kcfs simulation. The cross section passes through the model centerline baffle.

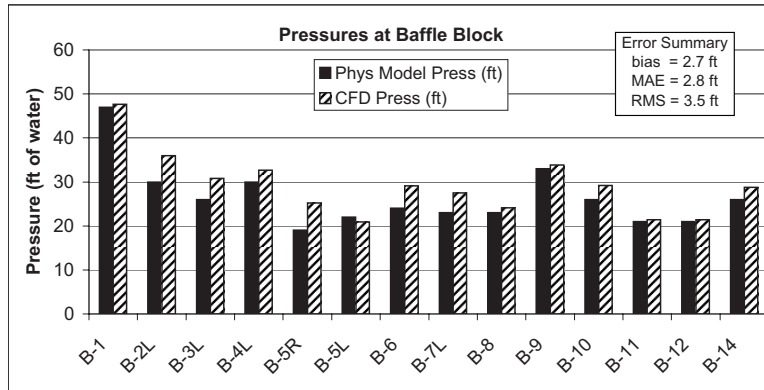


Figure 3.15. Comparison of physical model versus CFD model pressures around the baffle block

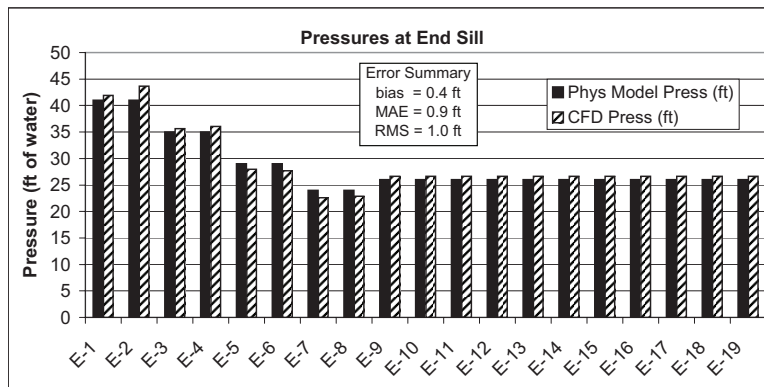


Figure 3.16. Comparison of physical model versus CFD model pressures around the end sill

3.3 Simulating the 1:40 Scale Sectional Model

A 1:40 scale sectional physical model of The Dalles Spillway (see Figure 3.17) was constructed at the Engineer Research and Development Center (ERDC), USACE Preslan and Wilhelms (2001). Conditions in the physical model were then recreated using Flow-3D (see Figure 3.18). Water velocity data were collected in the physical model at the set shown in Figure 3.19.

Since the 3.5 bays of the physical model were symmetric, it was assumed that flow patterns were symmetric from one bay to the next. Therefore, to decrease the “wall-clock” time required for each simulation, the CFD model only simulated a single center bay (see the gray rectangular section in Figure 3.19).

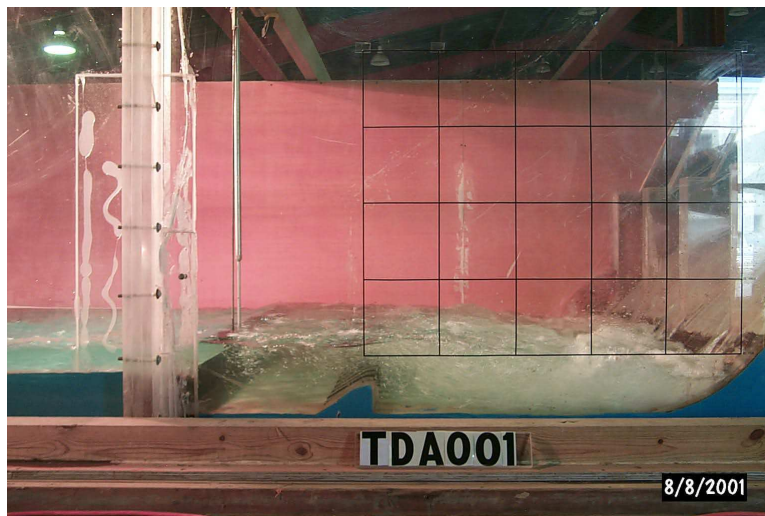


Figure 3.17. 1:40 scale physical model of The Dalles Spillway at ERDC

Comparisons were developed between the ERDC Dalles metrics feasibility study data (Preslan and Wilhelms 2001) and CFD results for the “no deflector with baffle test case”. Results were compared at four locations: 7 ft in front of the baffles, 9 ft in front of the end sill, 51 ft past the end sill, and 111 ft past the end sill. For this test case, the CFD model was set up with the following boundary conditions (note: the CFD model, like the physical model, was actually at 1:40 scale, however all results have been scaled up to prototype using Froude number similarity): forebay was set at 160 ft, radial gates were opened 3 ft, the tailwater was set at 78 ft, and the flow rate was set at 5850 cfs. The flow rate set in the CFD model was derived by integrating the physical model vertical velocity profile at 370 ft.

Graphical and numerical comparisons of horizontal velocity component results are presented in Figure 3.20 and Tables 3.4. Since the CFD model boundary conditions were steady, only the mean CFD velocity results are presented. Water velocity magnitude differences, compared at four locations both within and downstream of the stilling basin, were minor with 73% of the CFD measurements falling within one standard deviation of the physical model mean value.

At 190 ft, CFD and physical model profiles roughly agree in shape, although the CFD model profile

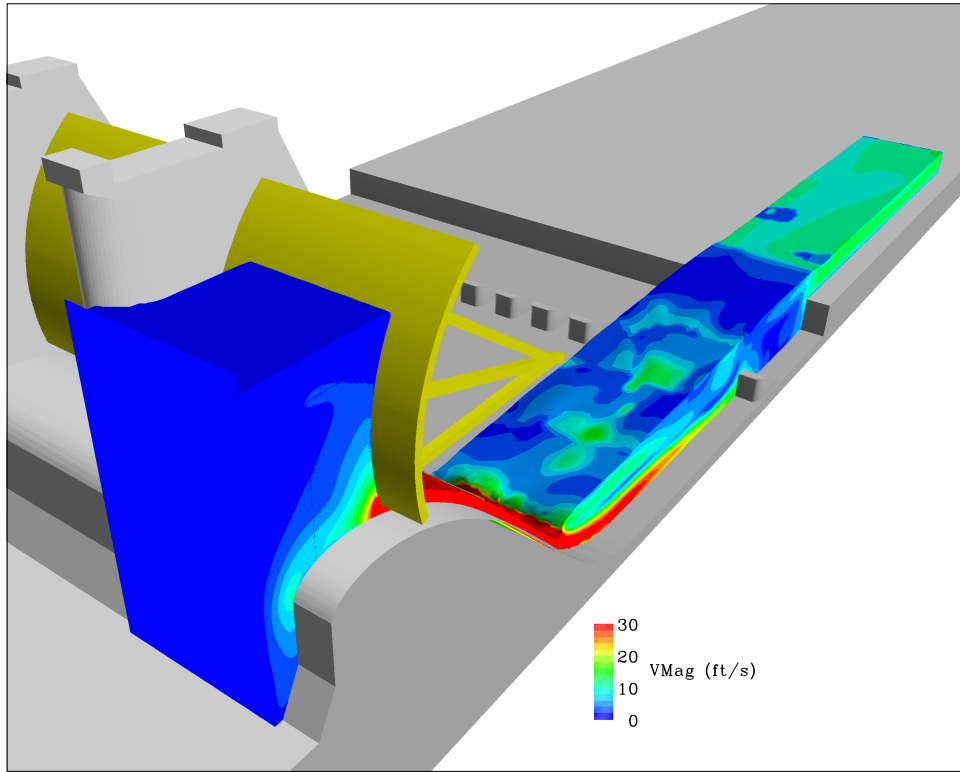


Figure 3.18. 3-D perspective of the CFD 1:40 scale flume

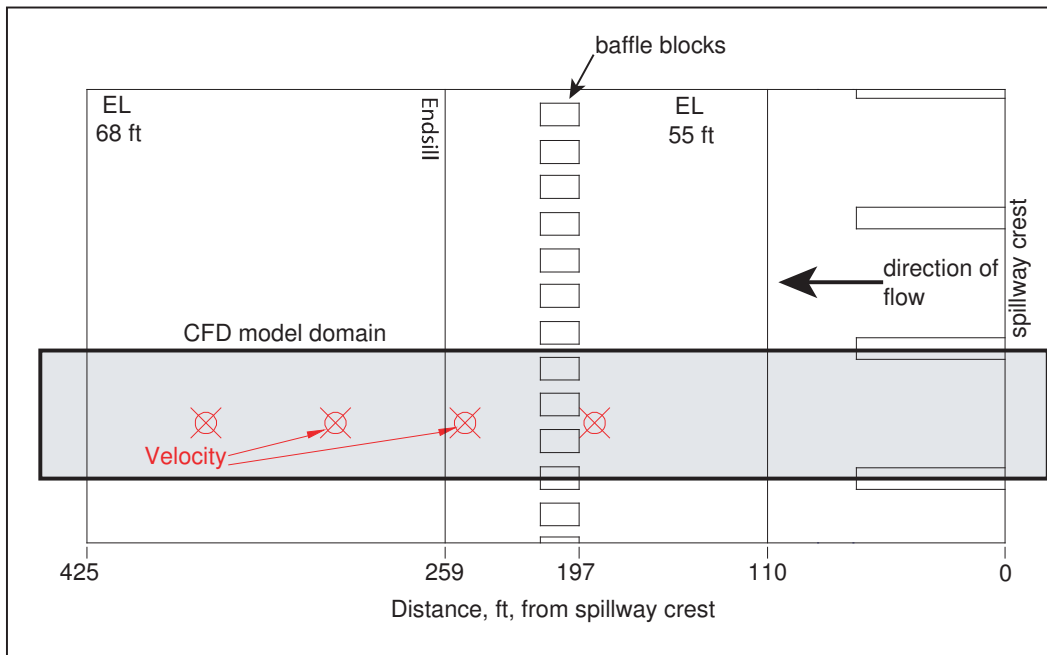


Figure 3.19. Plan view of the physical model flume and measurement sites. CFD model domain was simplified to a single bay (shown in gray). Both model domains extend farther into the forebay and tailrace than shown.

appears to be slightly less than the physical model means. The CFD model results all fall within one standard deviation, so differences may be due to the transient nature of the flow field (both the physical and CFD models). Differences would also result if the flow rates or gate openings between the physical and CFD models were different.

At 310 and 370 ft the velocity distribution observed in the physical model displays a more uniform trend over the depth than the CFD model. The largest differences between the CFD and physical model lie at 370 ft. The bottom reading at these locations is at elevation 68.5 ft, or 0.5 ft off the bottom. At 1:40 scale, 0.5 ft is less than $1/6^{th}$ of an inch. Differences between the two models this close to the bottom may be due to a number of factors including: boundary layer influences caused by the velocity probe in the physical model, insufficient grid refinement in the CFD model, and/or turbulence and boundary wall functions used to approximate the boundary layer in the CFD model. If the errors are due to the CFD model's approximation of the boundary layer, this impact will be diminished when the CFD model is applied at prototype scale due to (a) reduced size of the boundary layer relative to the overall water column thickness and (b) the Reynolds number is higher in the prototype, which also diminishes the influence of the boundary layer on the overall water column.

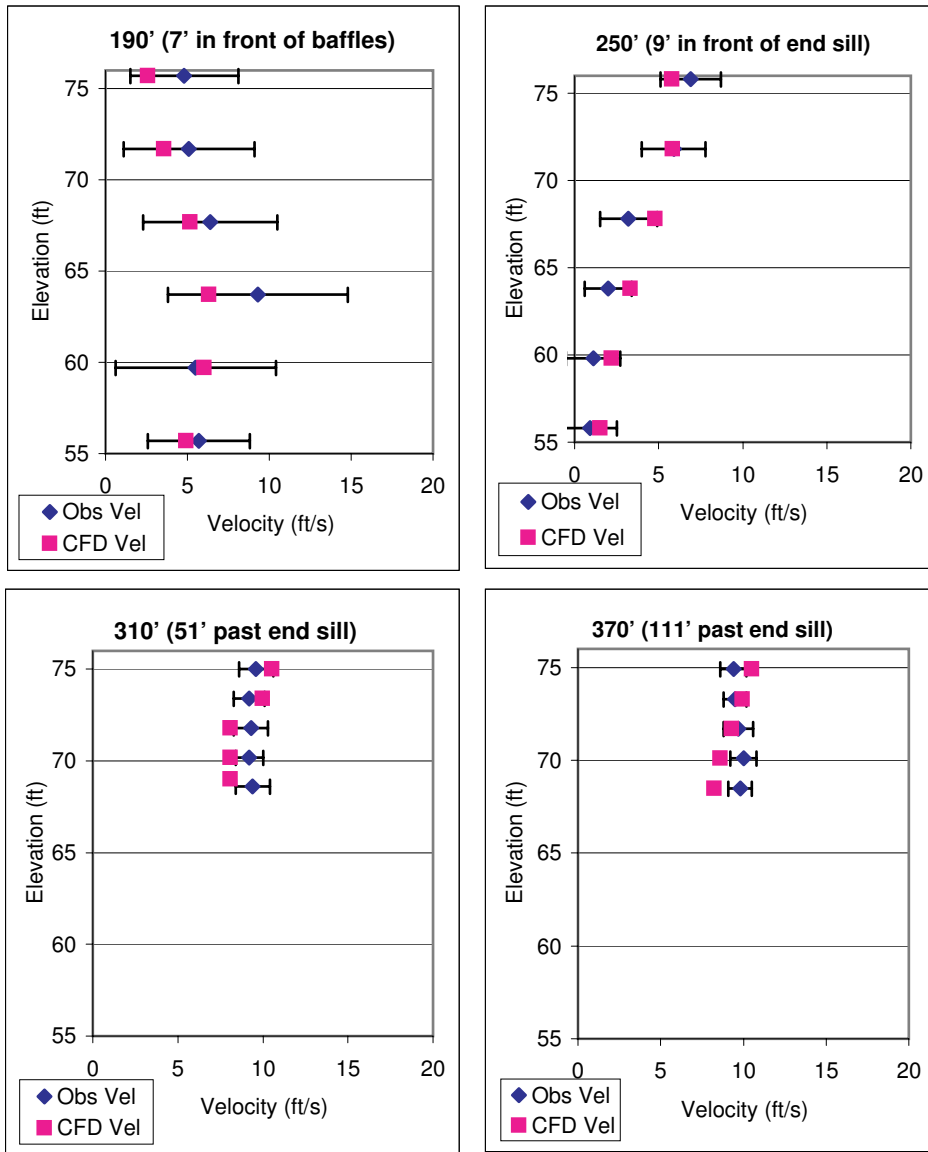


Figure 3.20. Horizontal velocity component comparison between the 1:40 scale physical model and CFD model. Observed mean data have been plotted with blue squares with bars representing one standard deviation from the mean

Table 3.4. Comparison of horizontal velocity data for the 1:40 scale TDA model.

<i>At 190' (7' in front of baffles)</i>				<i>At 250' (9' in front of end sill)</i>			
Elevation	Obs Vel	Obs σ	CFD Vel	Elevation	Obs Vel	Obs σ	CFD Vel
55.7	5.7	3.1	4.9	55.8	0.9	1.6	1.5
59.7	5.5	4.9	6.0	59.8	1.1	1.6	2.2
63.7	9.3	5.5	6.3	63.8	2.0	1.4	3.3
67.7	6.4	4.1	5.2	67.8	3.2	1.7	4.8
71.7	5.1	4.0	3.6	71.8	5.9	1.9	5.8
75.7	4.8	3.3	2.6	75.8	6.9	1.8	5.8

<i>At 310' (51' downstream of end sill)</i>				<i>At 370' (111' downstream of end sill)</i>			
Elevation	Obs Vel	Obs σ	CFD Vel	Elevation	Obs Vel	Obs σ	CFD Vel
68.6	9.4	1.0	8.1	68.5	9.8	0.7	8.2
70.2	9.2	0.8	8.1	70.1	10.0	0.8	8.6
71.8	9.3	1.0	8.1	71.7	9.7	0.9	9.3
73.4	9.2	0.9	10.0	73.3	9.5	0.7	9.9
75.0	9.6	1.0	10.5	74.9	9.4	0.8	10.5

3.4 Simulating the 1:80 Scale General Model

The CFD model was validated against data collected in the 1:80 scale general physical model of The Dalles Project (see Davis (2001b) and Davis (2001a)) that is located at the Engineer Research and Development Center (ERDC), US Army Corps of Engineers, Vicksburg, Mississippi.

Operational conditions for the physical model were derived from historical TDA Project operations between May 21-25, 2001. These operations were distilled into two scenarios labeled Flow 1 and Flow 2 in Davis (2001b) and summarized in Table 3.5. Miscellaneous flows (labeled other in the table) total 7.1 cfs for both conditions and represent north fish ladder/WASCO discharge of 1.4 kcfs, east fish ladder discharge of 0.1 kcfs, fish turbine bay 1 discharge of 2.5 kcfs, fish turbine bay 2 discharge of 2.5 kcfs, and service station bay discharge of 0.6 kcfs. The ice and trash sluiceway was off.

The CFD modeled tailrace model domain was approximately 4600 ft long (east-west), and terminates approximately 2100 ft downstream of the Highway 197 Bridge. The domain was approximately 4200 ft wide (north-south) and extends vertically from above the free-surface to elevation -195 ft m.s.l. The tailrace domain was subdivided into eight blocks of variable cell size, as shown in Figure 3.21.

All CFD simulations were performed at reduced (1:80) scale although all dimensions and results have been transformed to prototype scale. The model blocks with the greatest number of cells were blocks 7 and 8. Near the spillway face (block 8), cells were 1 ft x 3 ft x 1 ft in the X (downstream and perpendicular to the spillway face), Y (parallel to the spillway face), and Z (vertical)

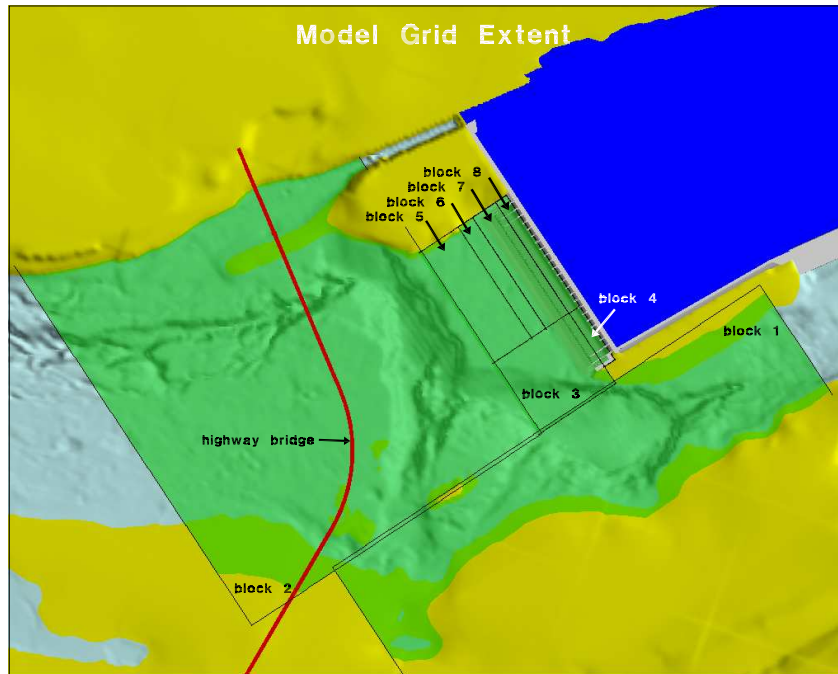


Figure 3.21. 1:80 scale CFD models: powerhouse and spillway tailrace

The circles indicate the starting position for each track and the track length is proportional to the velocity magnitude.

Velocities were observed in the physical model using a Nixon meter (a miniature propeller velocity meter) along three transects downstream of the spillway (Davis 2001b). The first transect extended longitudinally downstream from the first non-spilling bay. The other two transects were lateral, extending from Bay 1 to the intersection with the longitudinal transect. Measurements were typically 30 to 40 ft apart. Velocity results from both the physical and CFD model are shown in plan (Figure 3.24) and oblique views (Figure 3.25). The greatest differences in both velocity magnitudes and directions occurs along longitudinal transect extending downstream from the first non-spilling bay. This zone is highly non-uniform and large differences in velocity direction occur within a relatively short distance. A counter-clockwise gyre was noted to form, and this gyre impacts the spillway jet. Although the CFD model captured this gyre, the location was slightly different from that observed in the physical model. Hence the CFD spillway jet flows were not as constricted towards the lower numbered bays as in downstream. This also caused the velocity magnitudes immediately downstream of bays 5 through 9 to be less than those observed in the physical model. Away from the influence of this gyre, the direction and magnitude of the two model results are increasingly similar.

The table and Figure 3.26 presents a statistical summary of the differences between physical and CFD model horizontal velocity components for Flow Condition 1. Included are the MAE (mean absolute error is defined as the mean of the absolute values of the differences) and RMS (root mean square) differences. The right side of the figure presents a graphical comparison between physical and CFD model data. If both datasets were in perfect agreement, all points would lie along the 45-deg black line.

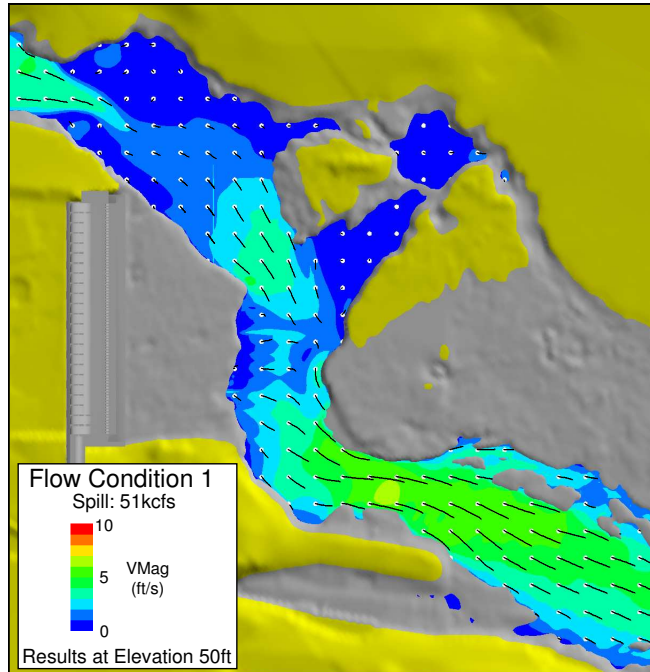


Figure 3.22. CFD model solution (Flow Condition 1) from the 1:80 scale spillway tailrace model at elevation 50 ft.

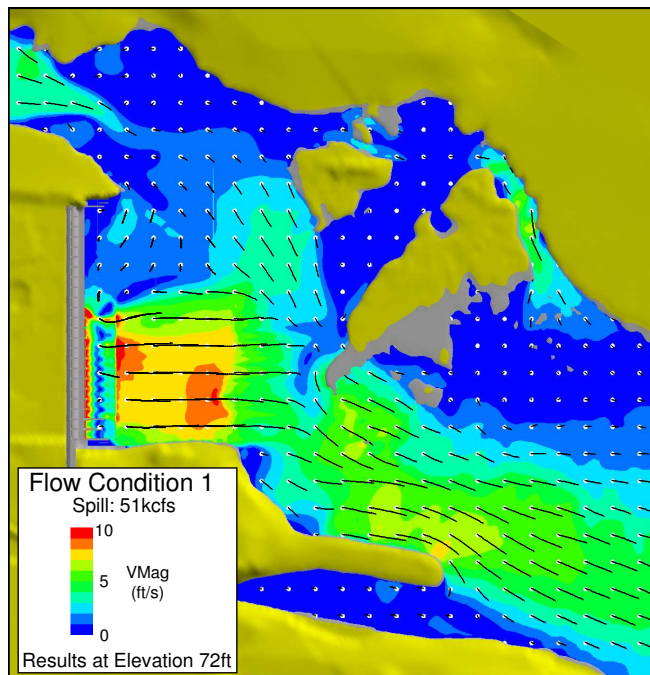


Figure 3.23. CFD model solution (Flow Condition 1) from the 1:80 scale spillway tailrace model at elevation 72 ft.

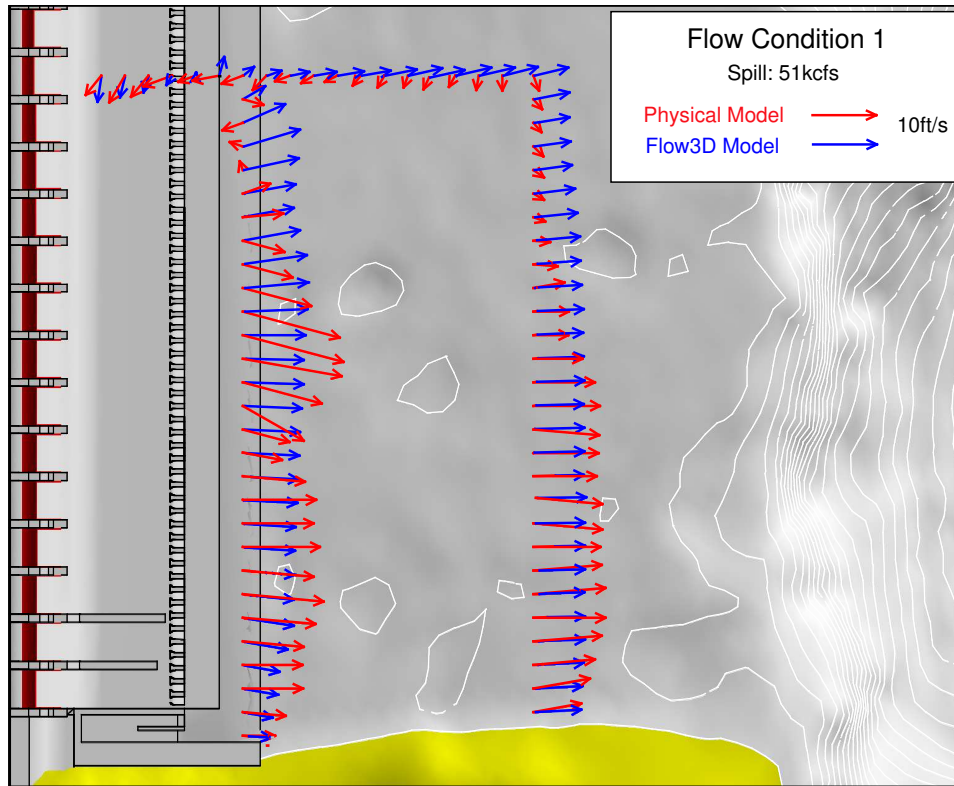


Figure 3.24. Plan view comparison of the CFD and physical model results (Flow Condition 1) at 1:80 scale

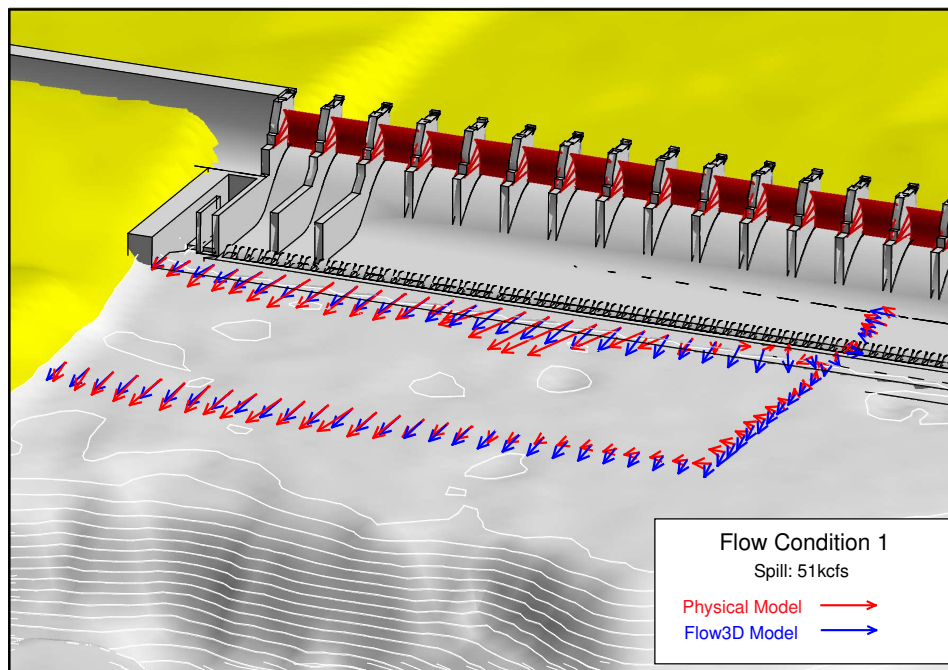


Figure 3.25. Oblique view comparison of the CFD and physical model results (Flow Condition 1) at 1:80 scale

Flow Cond 1			
Horizontal magnitude			
N	Mean	MAE	RMS diff
74	6.57	2.70	3.14
U velocity component			
N	Mean	MAE	RMS diff
74	5.11	3.46	4.06
V velocity component			
N	Mean	MAE	RMS diff
74	-0.94	1.27	1.70

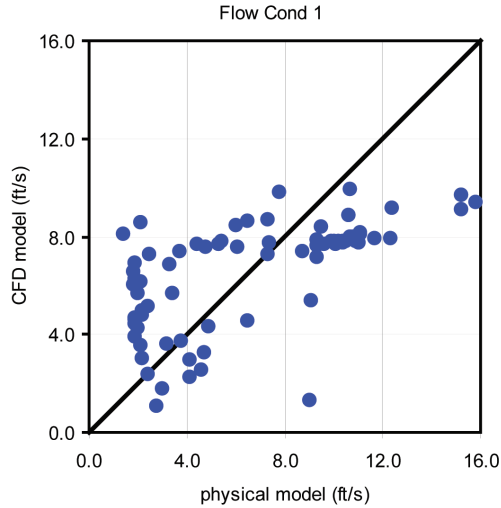


Figure 3.26. Summary of results for Flow Condition 1 between the 1:80 scale physical and CFD spillway tailrace models

3.4.2 Flow Condition 2 Results

Flow Condition 2 boundary conditions were specified along the appropriate boundary faces of the CFD model following the values in Table 3.5. As with Flow Condition 1, the initial tailrace condition was a quiescent fluid with a level water surface and the CFD model was run for approximately 15 minutes to allow time for the initial waves to dissipate.

Figures 3.27 and 3.28 display velocity magnitude contours of the solution at 50 ft (deeper than the elevation 68 ft shelf that extends away from the spillway) and 72 ft (just below the free-surface).

As with Flow Condition 1, velocities were observed in the physical model along three transects downstream of the spillway (Davis 2001b). Velocity results from both the physical and CFD model are shown in plan (Figure 3.29) and oblique views (Figure 3.30). The greatest differences in both velocity magnitudes and directions occurs along longitudinal transect extending downstream from the first non-spilling bay. This zone is highly non-uniform and large differences in velocity direction occur within a relatively short distance. A counter-clockwise gyre was noted to form, and this gyre impacted the spillway jet. Although the CFD model captured this gyre, the location was slightly different from that observed in the physical model. Hence the CFD spillway jet flows were not as constricted towards the lower numbered bays as in downstream. This also caused the velocity magnitudes immediately downstream of bays 5 through 9 to be less than those observed in the physical model. Away from the influence of this gyre, the direction and magnitude of the two model results are progressively more similar.

The table and Figure 3.31 presents a statistical summary of the differences between physical and CFD model horizontal velocity components for Flow Condition 2. Included are the MAE (mean absolute error is defined as the mean of the absolute values of the differences) and RMS (root mean square) differences. The right side of the figure presents a graphical comparison between physical

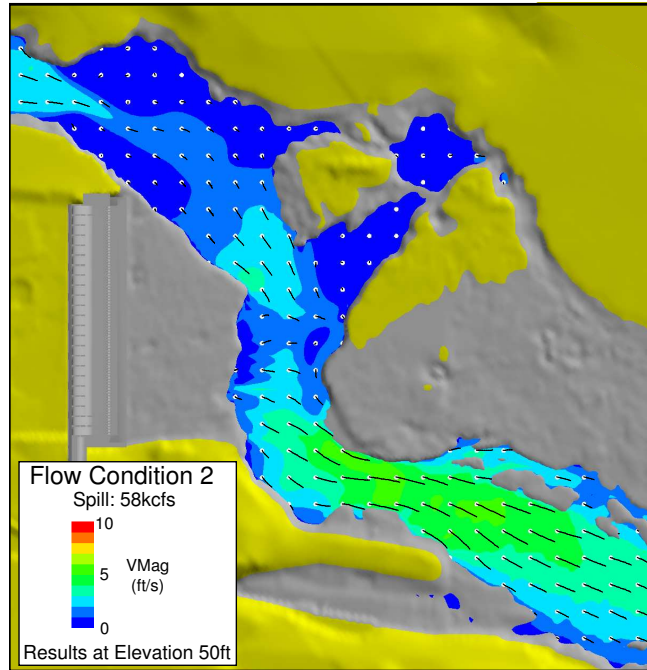


Figure 3.27. CFD model solution (Flow Condition 2) from the 1:80 scale spillway tailrace model at elevation 50 ft.

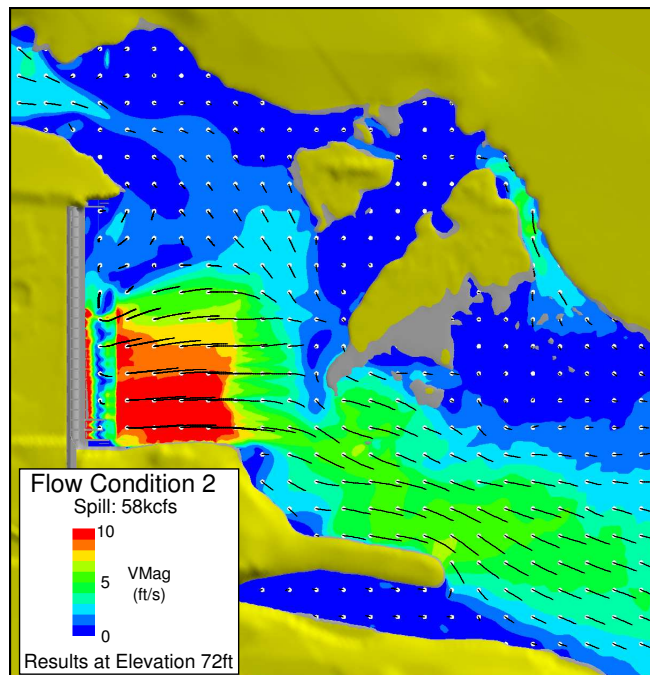


Figure 3.28. CFD model solution (Flow Condition 2) from the 1:80 scale spillway tailrace model at elevation 72 ft.

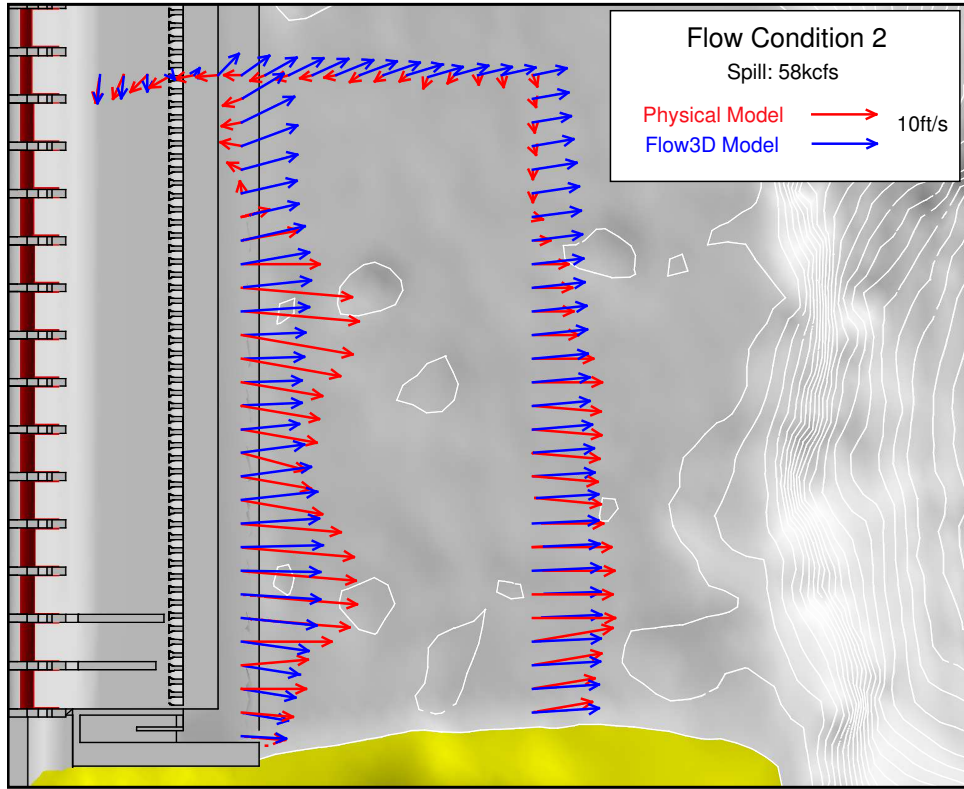


Figure 3.29. Plan view comparison of the CFD and physical model results (Flow Condition 2) at 1:80 scale

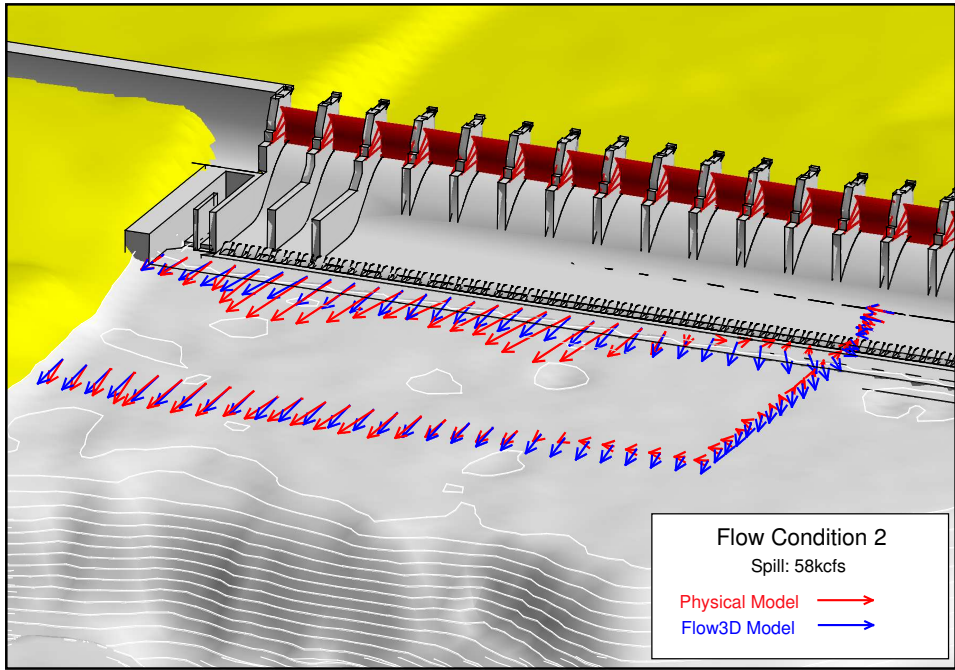


Figure 3.30. Oblique view comparison of the CFD and physical model results at 1:80 scale

and CFD model data. If both datasets were in perfect agreement, all points would lie along the 45-deg black line.

Flow Cond 2

Horizontal magnitude

N	Mean	MAE	RMS diff
74	7.52	3.05	3.66

U velocity component

N	Mean	MAE	RMS diff
74	6.03	4.02	5.03

V velocity component

N	Mean	MAE	RMS diff
74	-0.74	1.85	2.19

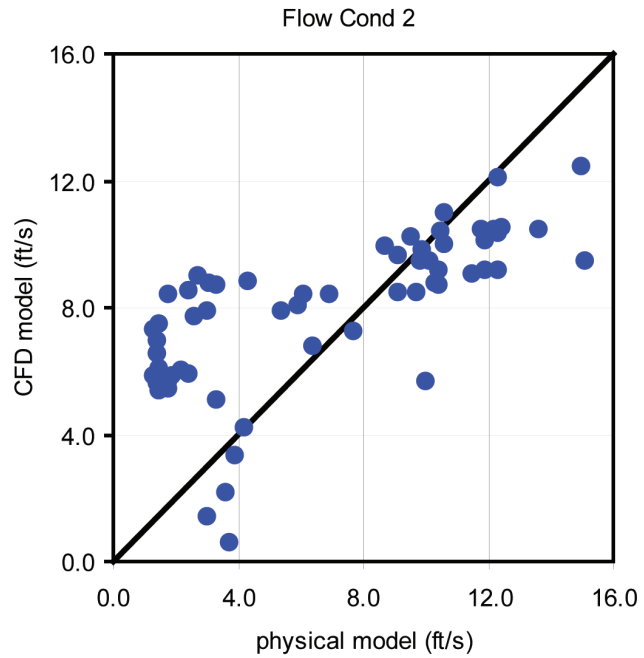


Figure 3.31. Summary of results for Flow Condition 2 between the 1:80 scale physical and CFD spillway tailrace models

4.0 Computational Fluid Dynamics Simulations of The Dalles Spillway Tailrace

Following the completion of the validation tests the performance of the CFD models were judged to be acceptable for the purposes of this study. In this chapter, the CFD models are applied to investigate a wide range of structural and operational conditions at the spillway and tailrace.

The CFD models of TDA were used to evaluate and compare various spill patterns and structural modifications. Modifications included adding spillwalls, removing baffle blocks, adding flow deflectors, and smoothing the downstream basalt shelf. Structural evaluations were generally performed by simulating comparable hydraulic conditions in an unmodified version of the prototype, and then evaluating changes in index metrics (velocity magnitude, velocity gradients, inertial particle tracking statistics, etc). Although the CFD model is not an exact replica of the prototype, differences between simulations with and without the modification do indicate trends in hydraulic conditions, and CFD model produced index metrics that were found to be a useful for both idea testing (“is it feasible?”), design parameters (e.g., hydraulic loads, egress issues, velocity near the basalt river bed, etc.), and biological research (e.g., location of live fish and sensor fish release pipes).

4.1 Washington Shore Weighted Spill Patterns

The Washington, or North Shore, weighted spill patterns involved a variable number of bays that were actively spilling. The number of bays that were spilling generally determined the size of the CFD domain. Domain sizes ranged from 12-bay to full spillway tailrace.

A typical domain and solution is shown in Figure 4.1, which is a 12-bay model. For this simulation, the tailwater was at 77ft and the spillway discharge was 72 kcfs and was distributed as follows: Bay 1 = 9 kcfs, Bays 2 through 5 = 12 kcfs, and Bay 6 = 15 kcfs. Particle tracks of equal duration have been added to illustrate the direction of flow. The circles indicate the starting position for each track and the track length is proportional to the velocity magnitude. The dramatic rise in water above elevation 80 feet occurs at and downstream of the end sill. Downstream of the end sill, the flow downstream of Bays 2 through 5 is supercritical, and a hydraulic jump occurs downstream as the flow transitions back through critical depth. Surface water patterns such as the ones displayed here are useful in determining downstream flow characteristics and have been confirmed by visual observation of similar hydraulic conditions in the prototype and physical model.

Solutions (denoted by the simulation code name) that investigated differences in tailrace hydraulic conditions between various Washington Shore spill patterns are:

- May02-T1, May02-T2, May02-T3, May02-T4, Sp01-T1, Sp01-T2, Sp01-T3, Ps01-T4, P-Sensor7, SpIllprn
 - Domain size: 19-bay multi-block domain
 - Objective: evaluate hydraulic conditions in the stilling basin and within several hundred feet of the end sill.

- Spillway discharge: Various, spillway discharge ranged between 52.4 kcfs and 110.9 kcfs
- Ambient-S, SF-HighQ, SF-LowQ, SVS3, SVS4
 - Domain size: full spillway tailrace model. (note: these simulations were performed before the multi-block version of the model was available. Grid resolution, especially near the spillway, is very coarse and the spillway discharge was approximated using the procedure described for simulating the 1:80 scale general model. These simulation were performed at prototype scale.)
 - Objective: evaluate hydraulic conditions throughout the spillway tailrace and downstream to approximately the Highway 197 bridge.
 - Spillway discharge: Various, spillway discharge ranged between 26.4 kcfs and 100 kcfs
- Oct02-T1, Oct02-T2, Oct02-T3, Oct02-T4
 - Domain size: 12-bay model.
 - Objective: evaluate hydraulic conditions in the stilling basin and within several hundred feet of the end sill.
 - Spillway discharge: Various, spillway discharge ranged between 4.5 kcfs and 72 kcfs.
- Spr04-17K and Spr03-20K
 - Domain size: 15-bay model.
 - Objective: evaluate hydraulic conditions in the stilling basin and within several hundred feet of the end sill. Refined the grid downstream of Bay 2 using multi-block.
 - Spillway discharge: 17 or 20 kcfs.
- Oct02-T1-MB, Oct02-T2-MB, Test11-NoWall, Test11-Wall,
 - Domain size: full spillway multi-block tailrace model. (note: multi-block simulations were performed with a higher level of grid refinement near the spillway.)
 - Objective: evaluate hydraulic conditions throughout the spillway tailrace and past the Highway 197 bridge.
 - Spillway discharge: Various, spillway discharge ranged between 51.0 kcfs and 106.5 kcfs

4.2 Spillwalls

A spillwall was proposed and constructed in the prototype between Bays 6 and 7. Design of this spillwall was similar to the pier extensions originally constructed between Bays 1 and 2 and Bays 2

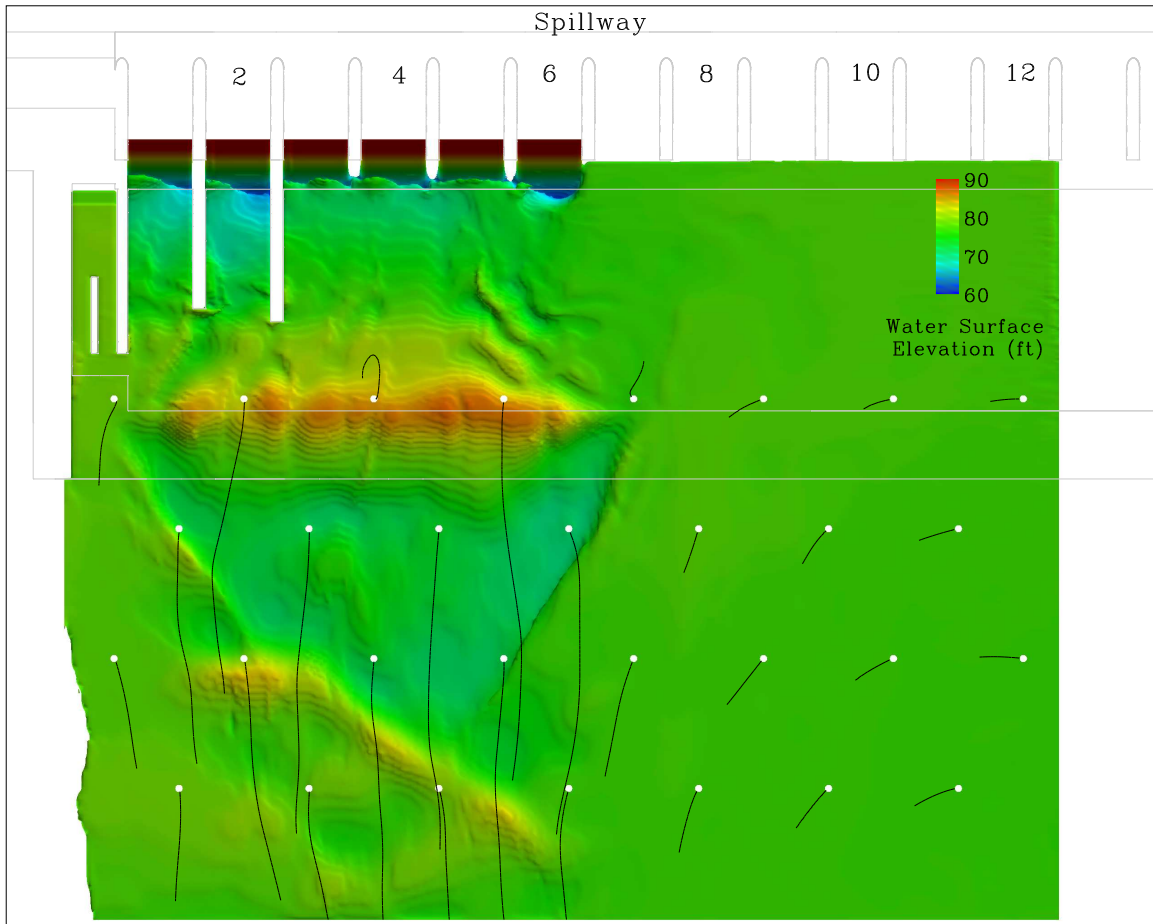


Figure 4.1. Oct02-T1 water surface elevation solution surface.

and 3 (see Figure 1.3) except that the spillwall extends downstream to the end sill (see Figure 1.3).

CFD simulations associated with the spillwalls investigated hydraulic performance under a variety of situations. Several simulations were also performed that examined the hydraulic characteristics of a “hydraulic spillwall”; formed by releasing a large discharge through the last (closest to the Oregon Shore) actively spilling bay.

Four combinations of wall/no wall pairs were simulated and evaluated during the project. An example pair, labeled Test 11-Wall and Test 11-A, evaluated velocity increases at the Highway 197 Bridge piers (see Figure 4.2) and used the multi-block full spillway tailrace model domain (see Figure 2.12). Boundary conditions for the model were as follows: powerhouse discharge was 183 kcfs with a water surface at elevation 81.5 ft, downstream tailwater at elevation 80.5 ft, the total spillway discharge was 126 kcfs, and the fishways were discharging 1.4 kcfs. Test-11Wall operated with a uniform discharge through Bays 1 through 6 of 21 kcfs, while Test11A had a distributed spill weighted toward the Washington Shore (typical juvenile spill pattern). The velocity magnitudes near the water surface are displayed in Figures 4.3 and 4.4.

As expected, by confining the total spillway discharge between Bays 1 through 6, the velocities

downstream of Bays 1 through 6 were higher than with the more distributed spill pattern. In addition, lateral flow was reduced due to the presence of the spillwall. Velocity magnitudes at the bridge piers were computed by averaging over the entire water column, and were larger with the spillwall in place. Generally, velocity magnitudes ranged between 21 to 27 ft/s at the piers for the spillwall test case, while for distributed test case velocity magnitudes ranged between 8 and 15 ft/s.

As mentioned above, a series of simulations investigated the hydraulic impacts of spillwalls, both hydraulic and solid, on stilling basin and tailrace conditions. The details of these simulations are discussed in the appendices, however the simulations of note for this section are:

- Test-11A versus Test11-Wall
 - Domain size: multi-block full spillway tailrace
 - Objective: evaluate differences between the distributed 30% juvenile spill pattern and the same discharge with a spillwall in place between Bays 6 and 7.
 - Spillway discharge: 126 kcfs
- Test-11A versus Test11-No23 Wall
 - Domain size: multi-block full spillway tailrace
 - Objective: evaluate removal of wall between Bays 2 and 3
 - Spillway discharge: 126 kcfs
- SIS-NoWall versus SIS-Wall
 - Domain size: 12 bay
 - Objective: evaluate differences between a spillwall between Bays 6 and 7 and a hydraulic wall.
 - Spillway discharge: Wall = 108 kcfs. No wall = 102 kcfs (hydraulic wall bay 6).
- SVS3 versus SVS3-Wall
 - Domain size: 12 bay
 - Objective: evaluate differences between a spillwall between Bays 6 and 7 and a hydraulic wall.
 - Spillway discharge: Wall = 24 kcfs. No wall = 26 kcfs (hydraulic wall bay 6).
- SVS4 versus SVS4-Wall
 - Domain size: 12 bay
 - Objective: evaluate differences between a spillwall between Bays 6 and 7 and a hydraulic wall.

- Spillway discharge: Wall = 72 kcfs. No wall = 64 kcfs (hydraulic wall bay 6).

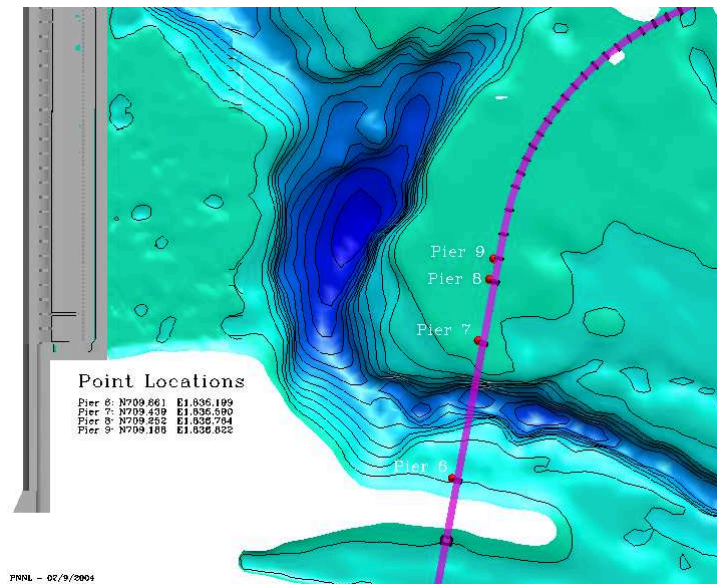


Figure 4.2. Highway 197 Bridge piers at which velocities were sampled and compared for Test 11 wall/no wall test case.

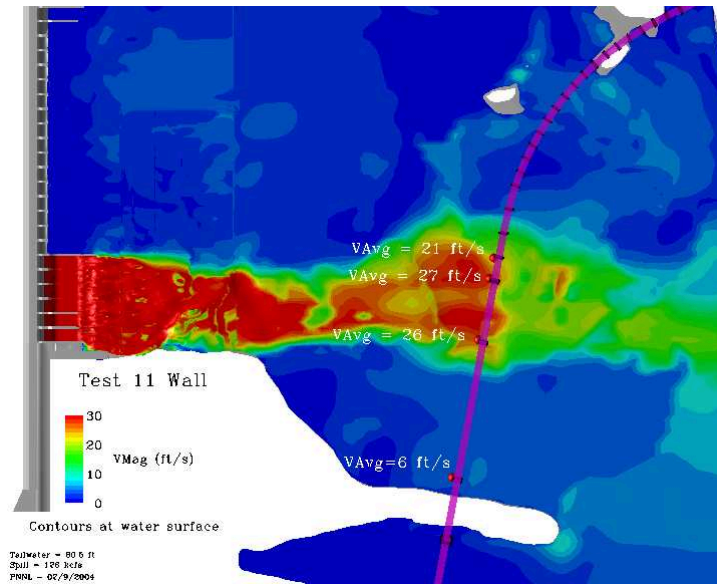


Figure 4.3. Test 11-Wall solution. Discharge through the spillway gates are: Bays 1 through 6 = 21 kcfs, all other bays off. Pier velocities reported in the figure are depth averaged.

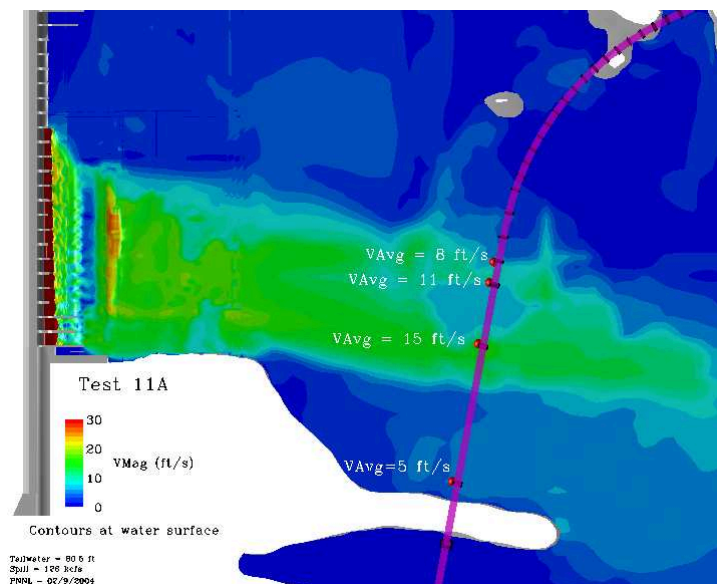


Figure 4.4. Test-11A solution. Discharge through Bays 1 through 15, respectively, were: 9, 9, 10.5, 12, 10.5, 10.5, 9, 9, 9, 9, 7.5, 7.5, 6, 4.5, 3 kcfs. Pier velocities reported in the figure are depth averaged.

4.3 Baffle Blocks: Influence and Partial Removal Scenarios

Baffle blocks were constructed in the prototype stilling basin to dissipate kinetic energy before the spillway jet reached the unprotected basalt shelf. By attenuating the spillway jet velocity, the downstream shelf is safeguarded against erosion that may occur during high flow events. Unfortunately the baffle blocks may also injure fish if they impact these blocks at high speeds.

As shown in Figure 1.3, the baffle blocks are uniformly spaced 6.2 ft apart. The blocks themselves are 10.5 ft wide and 9 ft tall at the leading edge.

To better understand the effects baffle blocks have on stilling bay hydraulics and how those hydraulics change when they are removed, Test11-Wall (see previous section and Figure 4.3) was simulated with the baffle blocks removed from downstream of Bay 2 only. Note that all other simulations had a complete set of baffle blocks. The boundary conditions for the model were as follows: powerhouse discharge was 183 kcfs with a water surface elevation of 81.5 ft, downstream tailwater surface at elevation 80.5 ft, total spillway discharge was 126 kcfs, and the fishways were discharging 1.4 kcfs. The spill was uniformly distributed through Bays 1 through 6 (21 kcfs each), and the spillwall was in place between Bays 6 and 7.

Figure 4.5 displays CFD model results from a side view (elevation) perspective. The upper graphic displays a slice through the centerline of Bay 2. The impact of removing the baffles from downstream of this bay can be seen by comparing this graphic with the two graphics below it through Bay 4.

A significant difference in the solution downstream of Bays 2 and 4 is the velocity of the spillway jet at the start of the end sill. Downstream of Bay 2, the velocities are close to 45 ft/s just upstream of the end sill, and once this jet impacts the end sill the flow is forced upward above elevation 100 ft. A check of energy conservation supports the CFD result; with a speed of 45 ft/s the equivalent potential energy height is elevation 112 ft (80.5 ft + 31.5 ft). Downstream of Bay 4 however, the spillway jet speed has been attenuated, and velocities near the start of the end sill velocities are below 30 ft/s. Hence, downstream of Bay 4 a large hump in the water surface elevation does not form just after the end sill.

It should also be noted that simulation results presented in this figure are from a single time step of the solution. Although the boundary conditions to the model were constant throughout the simulation, slight differences in velocities did occur even after the model had reached a dynamic equilibrium.

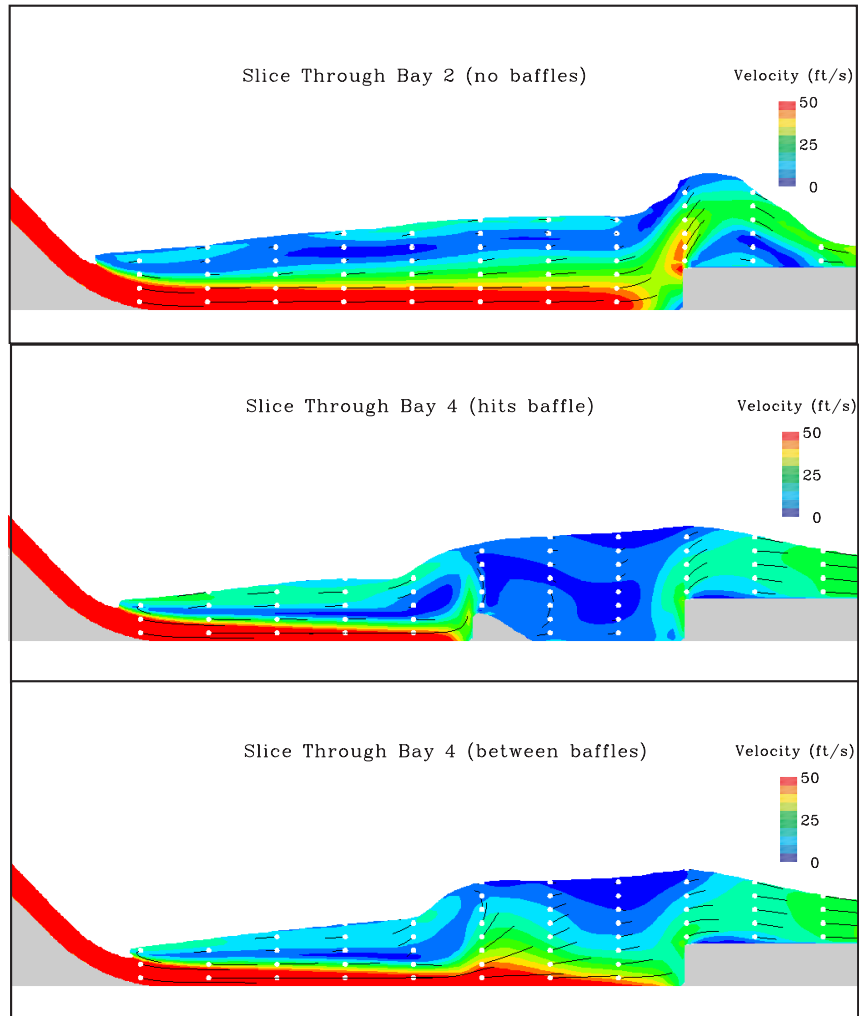


Figure 4.5. Test11-NoBaffles solution. Discharge through the spillway gates are: Bays 1 through 6 = 21 kcfs, all other bays off (same as Figure 4.3). Conditions are the same as Test11-Wall except baffle blocks downstream of Bay 2 have been removed. Note that velocities equal to and greater than 50 ft/s are shaded red.

Several simulations of note that investigated removal of baffle blocks from the stilling basin are listed below. Outside of this list, all other simulations that were performed mimicked the prototype and had a full contingent of baffle blocks in the stilling basin.

- Test-11A versus Test11-NoBaffles
 - Domain size: multi-block full spillway tailrace
 - Objective: evaluate hydraulic conditions when baffle blocks downstream of Bay 2 only are removed and the spillwall between Bays 6 and 7 is in place.
 - Spillway discharge: 126 kcfs
- Deflector-NoBaf versus Deflector-WithBaf
 - Domain size: Single bay at 1:40 scale.
 - Objective: evaluate hydraulic impacts of removing baffle blocks when a deflector at elevation 70 ft is in place.
 - Spillway discharge: 5.8 kcfs/bay
- 30 kcfs NoBafs
 - Domain size: 12 bay
 - Objective: evaluate hydraulic conditions at large spillway discharges with the baffle blocks removed.
 - Spillway discharge: 180 kcfs (30 kcfs/bay for Bays 1-6)

4.4 Flow Deflectors

Spillway deflectors were evaluated using the CFD model. Ideally, deflectors would produce a more horizontal spill flow and limit the plunge depth of water over the dam spillway, reducing the amount of entrained gas, during small discharge summer spill. Skimming horizontal flow patterns may reduce the potential for fish injury and/or mortality by reducing the potential for fish to impact the baffle blocks. Moreover, at higher discharges, the deflectors would be overwhelmed (i.e., resulting in a plunging flow condition) and energy dissipation in the baffle block region would proceed as designed in the stilling basin (see baffle block section above).

Figure 4.6 displays results from three related CFD simulations. All three simulation were performed at 1:40 scale (matching the ERDC physical model flume) and were one bay wide (see Figure 3.18). Discharge through the spillway bay was 5808 cfs and the deflector, when present, was placed so that the top horizontal shelf was at elevation 70 ft. The downstream boundary was a stage elevation of 78 ft.

The top graphic in the figure displays the existing geometry solution, while the middle and bottom graphics display the solution with the deflector in place. For this particular case, a skimming

flow develops so that the spillway jet rides along near the water surface in the spillway. For this particular case and when the deflectors are in place, removal of the baffle blocks has little impact on the flows in the stilling basin. At larger flows however, the deflectors would be overwhelmed and the spillway jet would plunge and impact the baffle blocks.

Several simulations of note that investigated flow deflectors are listed below. Most of these simulations were performed at 1:40 scale, mimicking the 1:40 scale physical model at ERDC.

- D68T76G3
 - Domain size: 2-bay model
 - Objective: evaluate hydraulic conditions when a deflector is placed at elevation 68 and the tailwater is at 76 ft.
 - Spillway discharge: 4.5 kcfs/bay
- D68T76G5, D68T70G3, D68T82G3, D68T92G21, D68T91G21, D70T76G3, D70T76G5, D73T76G3, D73T76G5
 - Domain size: 1-bay model at prototype scale
 - Objective: This suite of simulations examine deflectors (D) at heights of 68 or 70 ft. Tailwater (T) range from 76 to 92 feet.
 - Spillway discharge: varies (G = gate opening). G5 = 7.2 kcfs/bay, G3 = 4.5 kcfs/bay, G21 = 30 kcfs/bay.
- 3Dpartial-Defl-NoBaf-5808cfs, 3Dpartial-Defl-WBaf-5808cfs
 - Domain size: 1-bay of the 1:40 scale physical model
 - Objective: evaluate hydraulic conditions with deflectors at 70. These cases examine the flow regime with and with baffle blocks (see Figure 4.6)
 - Spillway discharge: 5.8 kcfs/bay

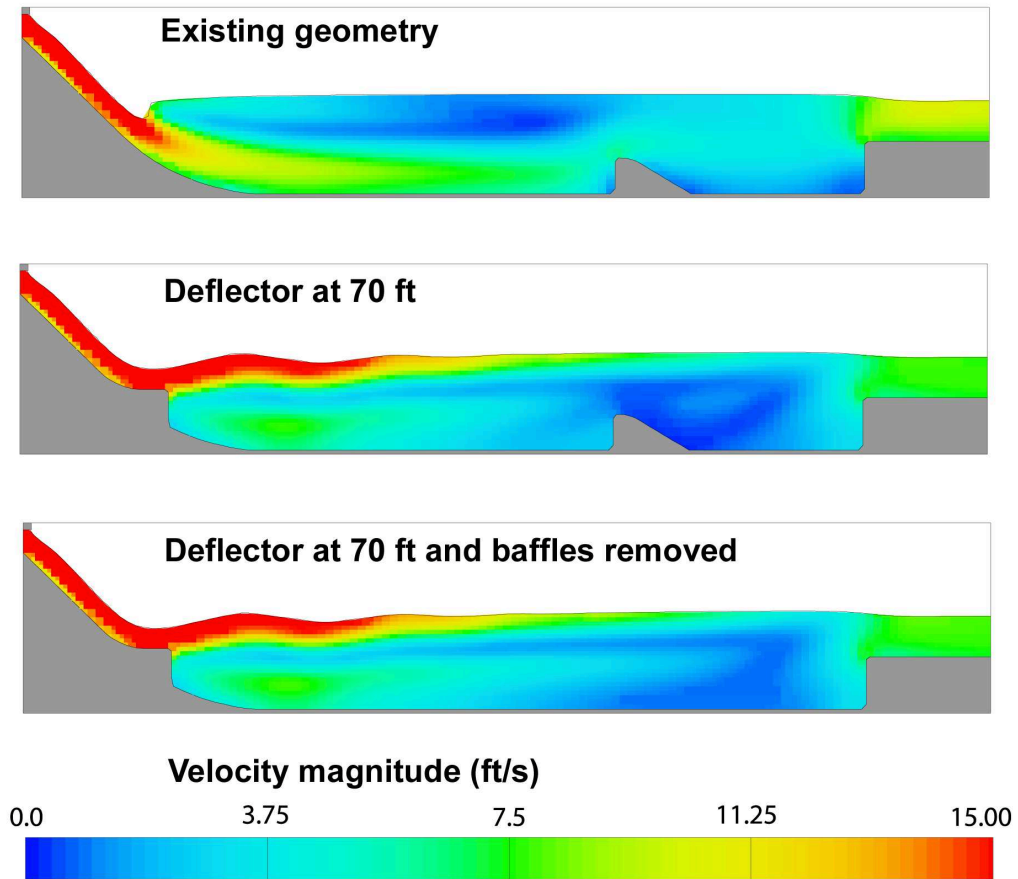


Figure 4.6. Example of CFD simulations simulating the hydraulic impacts of flow deflectors. Deflector was placed at elevation 70 ft.

4.5 Smooth Downstream Basalt Shelf

Downstream of the stilling basin and concrete end sill, several large depressions exist in the unprotected basalt shelf (see Figure 1.3 and Figure 2.3). The majority of these holes are relatively shallow, although downstream of Bays 9 and 16 the most recent bathymetric survey indicates bottom elevations below 55 ft m.s.l. Since the average elevation of the downstream basalt shelf is at approximately 68 ft, the deeper holes are more than 10 ft deep (see Figure 2.3).

To better understand how these depressions impact hydraulic conditions of the tailrace, a CFD simulation was performed that duplicated the 1:80 scale Flow Case 1 simulation (see Section 3.4 and Table 3.5); tailwater was at elevation 76.8 ft, total spill discharge was 51.0 kcfs, and total river flow was 162.9 kcfs. The basalt shelf, which was previously simulated using the surveyed bathymetric data, was replaced with a smooth horizontal plane at elevation 68 ft.

Results shown in Figure 4.7 display the solution surface at elevation 70.6 (approximately 6 ft beneath the water surface). The primary difference between the two sets of results are in direction; the velocity magnitudes are generally the same. Differences in direction were largest over the basalt shelf and the thalweg (i.e., canyon) downstream of Bays 3 through 9. As expected, differences in velocity vectors were primarily surface phenomenon (i.e., results between elevation 68 (basalt shelf) and the surface). Below elevation 64 ft, velocity direction differences in the thalweg zone were much less.

The solutions of note that investigated differences in hydraulic conditions when the basalt shelf was smoothed out are:

- FlowCon1 versus FlowCon1-SmoothShelf
 - Domain size: 1:80 scale full tailrace model
 - Objective: evaluate hydraulic conditions that develop when the basalt shelf is smoothed out at elevation 68 ft.
 - Spillway discharge: Flow Condition 1 (see Table 3.5).

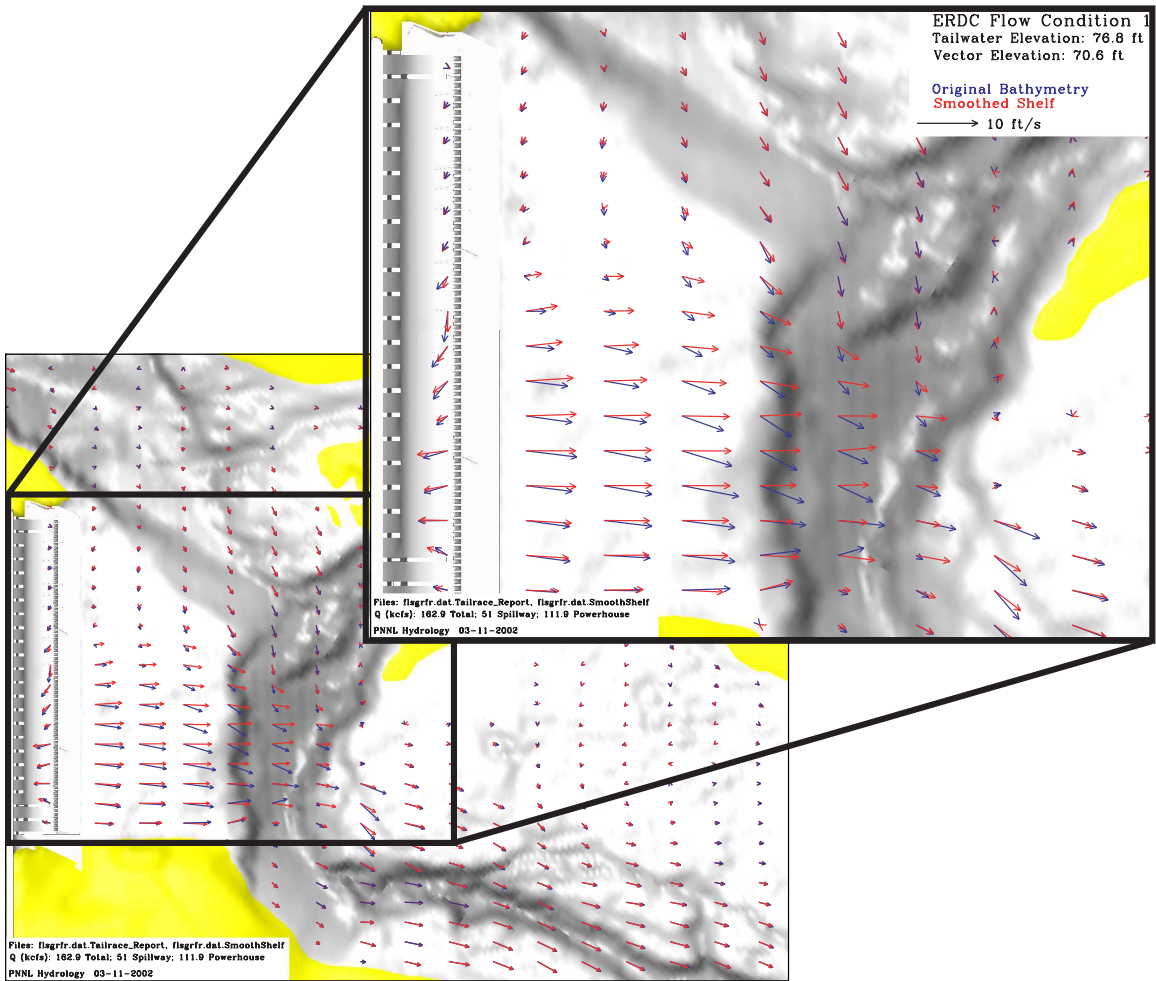


Figure 4.7. Smooth downstream basalt shelf results. Comparison is between a solution with a smooth basalt shelf at elevation 68 ft versus an end shelf constructed using the observed bathymetry, including scour holes. Solution surface shown in the surface is at elevation 70.6 ft.

5.0 Conclusions and Recommendations

5.1 Conclusions

This report documents development of CFD models that were applied to The Dalles spillway tailrace. These models have been successfully validated against physical models and prototype data, and are suitable to support structural design activities, biological research, and spill management.

The CFD models was validated for a wide range of hydraulic conditions. The first validation case was to simulate flow passage, starting in the forebay, passing under a tainter gate, and then down the face of the ogee spillway. Simulation results were compared to both prototype and 1:25 scale physical model data collected upstream of the tainter gate. Additional validation cases examined the ability of the CFD model to simulate the turbulent and highly transient stilling basin flows and the transition to the less turbulent downstream tailrace flows. CFD model results were compared to physical model data collected in three different physical models of The Dalles tailrace. In all validation cases, and for a wide range hydraulic conditions, CFD model results compared favorably to observed physical model pressures and water velocities, as well as to limited prototype data.

After the CFD model was successfully validated, it was used to provide hydraulic information to USACE hydraulic design engineers and fisheries researchers. The first application was to help biological researchers determine the best locations to place acoustic fish detection instruments and pipes from which both live and “sensor” fish were released. Downstream of the spillway, the CFD model has been applied to address specific SIS design questions including removal of baffle blocks and the installation of Type II spillway deflectors. Although neither of these design actions have yet to be undertaken by USACE, the CFD model was used by researchers and staff to understand the potential consequences of these structural alterations.

The CFD models have been applied to calculate hydraulic conditions in the tailrace with the new spillwall in place between Bays 6 and 7. The spillwall was constructed and completed in 2004. The CFD model was applied to simulate differences in flow patterns caused by the wall, as well as changes in water velocity increases at the Highway 197 bridge. The CFD models were also applied to examine the potential for increased basalt erosion and the relative differences between juvenile spill patterns used in previous years and the anticipated spill pattern that will be applied once the wall is complete.

5.2 Recommendations

All input and simulation results completed during this project have been archived at PNNL. As future questions arise regarding the hydraulic performance of the tailrace under different spill patterns or structural alterations, this large database of information can be queried as long as the hydraulic conditions are similar to those that were previously simulated. If future simulations are different from those that were simulated during the project (e.g. the new Bay 6 and 7 spillwall), restart files from simulations close to the new condition can be used as an efficient restart file to “warm-start” the model.

Because sample sizes are small, Sensor Fish data cannot be used (at reasonable cost) to estimate the

frequency of occurrence of poor passage conditions during a particular spill operating condition for a particular structural configuration. The CFD model simulations and inertial particle tracking can be used to obtain such statistical estimates and to extend the analysis to conditions not tested because structures do not yet exist or because flow conditions could not be achieved in prototype tests.

Several specific applications of the CFD model that may help CENWP evaluate future structural modifications (see Sapere Consulting (2004)) are: 1) removal of the spillwall between Bays 2 and 3, 2) impacts of lengthening the stilling basin by 200 ft, and 3) lengthening the stilling basin to the thalweg, including shaping the cut out portions to improve egress. All of the above modifications can easily be performed using the validated CFD model through changes to the underlying bathymetric surfaces.

6.0 References

- Bombardelli FA, CW Hirt, and MH Garcia. 2001. "Discussion on 'Computations of Curved Free Surface Water Flow on Spiral Concentrators'." *Journal of Hydraulic Engineering* 127(7).
- Bonneville Hydraulic Laboratory. 1952. *Spillway and Stilling Basin for The Dalles Dam Columbia River, Oregon and Washington*. 1-6, Bonneville Hydraulic Laboratory, US Army Engineer District, Portland, OR.
- Bonneville Hydraulic Laboratory. 1964. *Spillway and Stilling Basin for The Dalles Dam Columbia River, Oregon and Washington, Hydraulic Model Investigation*. 55-1, Bonneville Hydraulic Laboratory, US Army Engineer District, Portland, OR.
- Bradford SF. 2000. "Numerical Simulation of Surf Zone Dynamics." *Journal of Waterway, Port, Coastal, and Ocean Engineering* 126(1).
- Carlson TJ and JP Duncan. 2003. *Evolution of the sensor fish device for measuring physical conditions in severe hydraulic environments*. DOE/ID-11079, US Department of Energy, Idaho Operations Office, Idaho Falls, ID.
- Cook CB and MC Richmond. 2001. *Simulation of Tailrace Hydrodynamics Using Computational Fluid Dynamics Models*. PNNL-13467, Pacific Northwest National Laboratory, Richland, WA.
- Davis WG. 2001a. *Data Report, Model Study of The Dalles Dam 1:80 scale General Model, Comparisons of model surveys with recent hydrographic surveys*. US Army Corps of Engineers, Engineer Research and Development Center, Vicksburg, MS.
- Davis WG. 2001b. *Data Report: Model Study of The Dalles Dam, 1:80-Scale General Model, Feasibility Work in Support of the Spillway Improvement Study*. US Army Corps of Engineers, Engineer Research and Development Center, Vicksburg, MS.
- Freitas CJ. 1995. "Perspective: Selected Benchmarks from Commercial CFD Codes." *Journal of Fluids Engineering* 117:208–218.
- FSI. 2003. *Flow3-D User's Manual*. Flow Science, Inc., Sante Fe, NM.
- Hirt CW and BW Nichols. 1981. "Volume of Fluid (VOF) Method for the Dynamics of Free Boundaries." *Journal of Computational Physics* 39:201–255.
- Hirt CW and JM Sicilian. 1985. "A porosity technique for the definition of obstacles in rectangular cell meshes." In *Proc., 4th Int. Conf. Ship Hydro.*, pp. 1–19. Washington, D.C. National Academy of Sciences.
- Normandeau Associates. 2004. *Direct Effects of Differential Spill Volumes on Mortality and Injury Rates of Juvenile Salmonids at The Dalles Dam Spillway, Columbia River in Fall 2002 and Spring 2003*. Report to the US Army Corps of Engineers, Portland District, Portland, OR.
- Patankar SV. 1980. *Numerical Heat Transfer and Fluid Flow*. Hemisphere, New York.
- Preslan W and S Wilhelms. 2001. *Dalles, Metrics Feasibility Study Draft submitted to Portland District, USACE*. ERDC.

Rakowski CL, MC Richmond, JA Serkowski, and GE Johnson. 2006. *Forebay Computational Fluid Dynamics Modeling for The Dalles Dam to Support Behavior Guidance System Siting Studies*. PNNL-15689, Pacific Northwest National Laboratory, Richland, WA.

Sapere Consulting. 2004. *The Dalles Dam Spillway Strategy, Prepared for the US Army Corps of Engineers Portland District*. Sapere Consulting, Portland, OR.

Savage BM and MC Johnson. 2001. “Flow over Ogee Spillway: Physical and Numerical Model Case Study.” *Journal of Hydraulic Engineering* 127(8).

USACE. 2000. *Water Resources Development in Oregon 2000*. US Army Corps of Engineers, Portland, Oregon.

Yakhot V and S A.Orszag. 1986. “Renormalization Group Analysis of Turbulence. I. Basic Theory.” *J. Scientific Computing* 1:1–51.

Yakhot V and L M.Smith. 1992. “The Renormalization Group, the ϵ -Expansion and Derivation of Turbulence Models.” *J. Scientific Computing* 7:35–61.

Yakhot V, SA Orszag, S Thangam, TB Gatski, and CG Speziale. 1992. “Development of turbulence models for shear flows by a double expansion technique.” *Phys. Fluids* A4(7):1510–1520.

Appendix A

Overview of CFD Simulations

Appendix A – Overview of CFD Simulations

The figures and tables in this appendix outline the simulations performed during this project. The simulations are organized according to the size of the modeled domain and are not grouped by the objective of the simulation. This is primarily because most simulations served to answer multiple questions about how the hydraulic conditions would change, given a set geometry and boundary condition. Simulation also were compared to each other to better understand how a specific alteration in either spill or engineered structure would affect tailrace conditions.

Chapters 3 and 4 discuss the various tasks covered during the project: model validation, variations with Washington Shore spill pattern, spillwall evaluation, hydraulic impact of the baffle blocks and baffle block removal, flow deflector evaluation, and smoothing of the downstream basalt shelf. Under each of the sections in these chapters, a list of the specific simulation names is provided. The reader is advised to consult these discussion lists and then use these appendixes to obtain exact simulation boundary conditions and a graphical representation of the results.

Appendixes B through M each describe a specific CFD model domain, ranging from the simple 2-D tainter gate models to the complex eight multi-block bank-to-bank simulations. For each domain size, a table that summarizes the boundary conditions for each simulation has been created in Appendix A. On the page opposite each table, a graphical sketch of the appropriate model domain also has been provided.

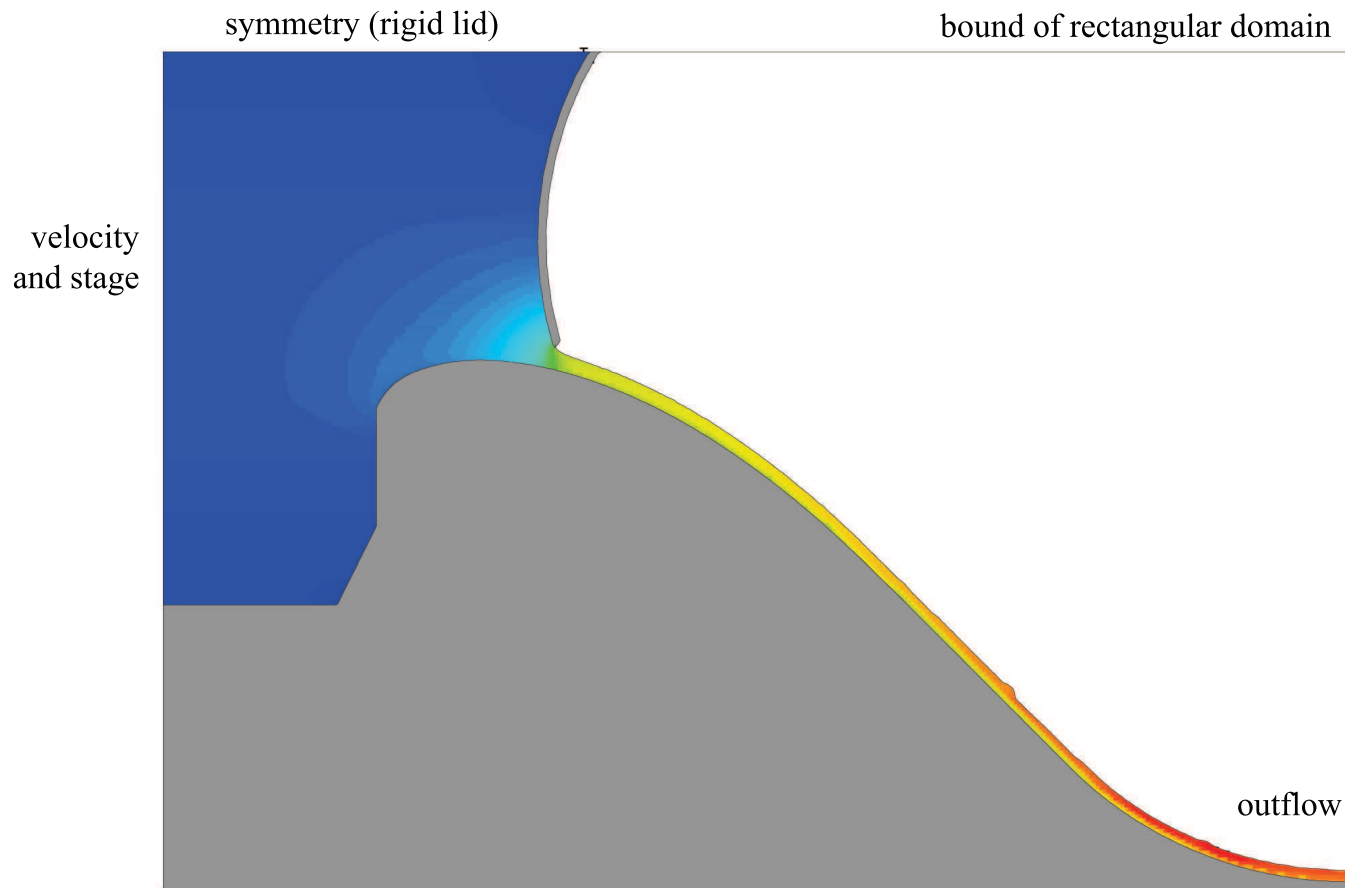


Figure A.1. Tainter Gate Model Domain (Appendix B).

PNNL run name		1.5kcfs	3.0kcfs	4.0kcfs	4.5kcfs	5.0kcfs	6.0kcfs
PNNL model type		tainter gate					
	UNIT						
Forebay Elevation	msl, ft	160	160	160	160	160	160
Spillway Operations							
Gate opening	ft	1.00	2.02	2.69	3.00	3.00	4.00
discharge	Kcfs	1.50	3.0	4.0	4.5	5.0	6.00
Total	Kcfs	1.50	3.0	4.0	4.5	5.0	6.00

PNNL run name		7.5kcfs	8.0 kcfs	9.0kcfs	10.0kcfs	12.0kcfs	16.0kcfs
PNNL model type		tainter gate					
	UNIT						
Forebay Elevation	msl, ft	160	160	160	160	160	160
Spillway Operations							
Gate opening	ft	5.00	5.36	6.00	6.70	8.06	10.79
discharge	Kcfs	7.5	8.0	9.00	10.0	12.0	16.0
Total	Kcfs	7.5	8.0	9.00	10.0	12.0	16.0

PNNL run name		18.0kcfs	20.0kcfs	30.0 kcfs
PNNL model type		tainter gate	tainter gate	tainter gate
	UNIT			
Forebay Elevation	msl, ft	160	160	160
Spillway Operations				
Gate opening	ft	12.16	13.55	20.65
discharge	Kcfs	18.0	20.0	30.0
Total	Kcfs	18.0	20.0	30.0

Table A.1. Scenarios Simulated with the Tainter Gate Domain. Results presented in Appendix B

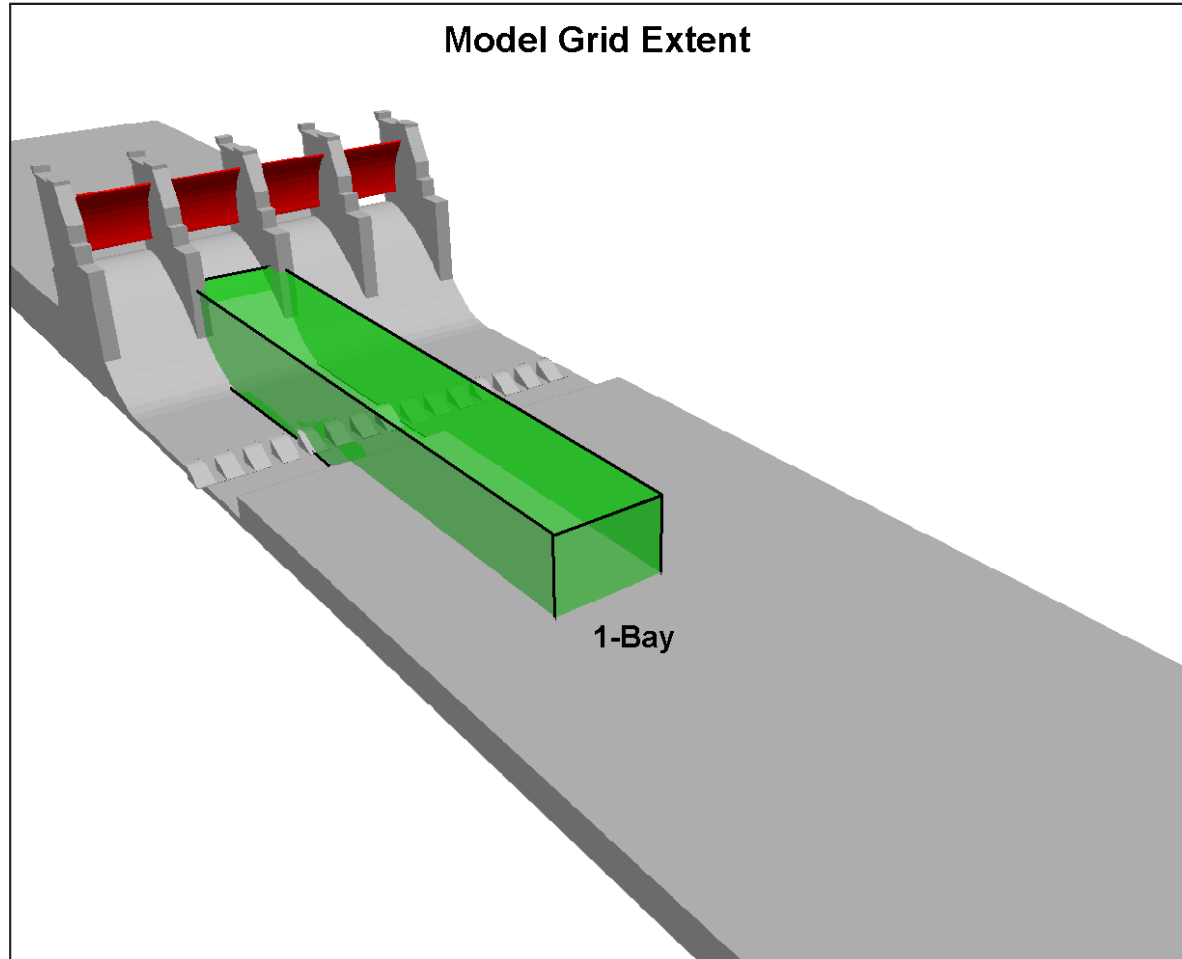


Figure A.2. 1-Bay Model Domain (Appendix C).

PNNL run name			4.5kcfs76Tail70Def		4.5kcfs76Tail73Def		4.5kcfs79Tail68Def		4.5kcfs82Tail68Def
PNNL model type			1-bay		1-bay		1-bay		1-bay
	UNIT		deflector at 70'		deflector at 73'		deflector at 68'		deflector at 68'
Tailwater Elevation									
Spillway Basalt	msl, ft		76.0		76.0		79.0		82.0
Spillway Operations									
Bay 6 w/ smooth end shelf	Kcfs		4.5		4.5		4.5		4.5
Total	Kcfs		4.5		4.5		4.5		4.5
PNNL run name			7.5kcfs76Tail68Def		7.5kcfs76Tail70Def		7.5kcfs76Tail73Def		30kcfs91Tail
PNNL model type			1-bay		1-bay		1-bay		1-bay
	UNIT		deflector at 68'		deflector at 70'		deflector at 73'		
Tailwater Elevation									
Spillway Basalt	msl, ft		76.0		76.0		76.0		91.0
Spillway Operations									
Bay 6 w/ smooth end shelf	Kcfs		7.5		7.5		7.5		30.0
Total	Kcfs		7.5		7.5		7.5		30.0
PNNL run name			30kcfs91Tail68Def		30kcfs91Tail68Def-NoBaf		30kcfs91Tail-Bay16Geom		30kcfs91Tail-NoBaf
PNNL model type			1-bay		1-bay		1-bay		1-bay
	UNIT		deflector at 68'		deflector at 68' - No baffles		Bay 16 end shelf (holes)		No baffles
Tailwater Elevation									
Spillway Basalt	msl, ft		91.0		91.0		91.0		91.0
Spillway Operations									
Bay 6 w/ smooth end shelf	Kcfs		30.0		30.0		30.0		30.0
Total	Kcfs		30.0		30.0		30.0		30.0

Table A.2. Scenarios Simulated with the 1-Bay Domain. Results presented in Appendix C

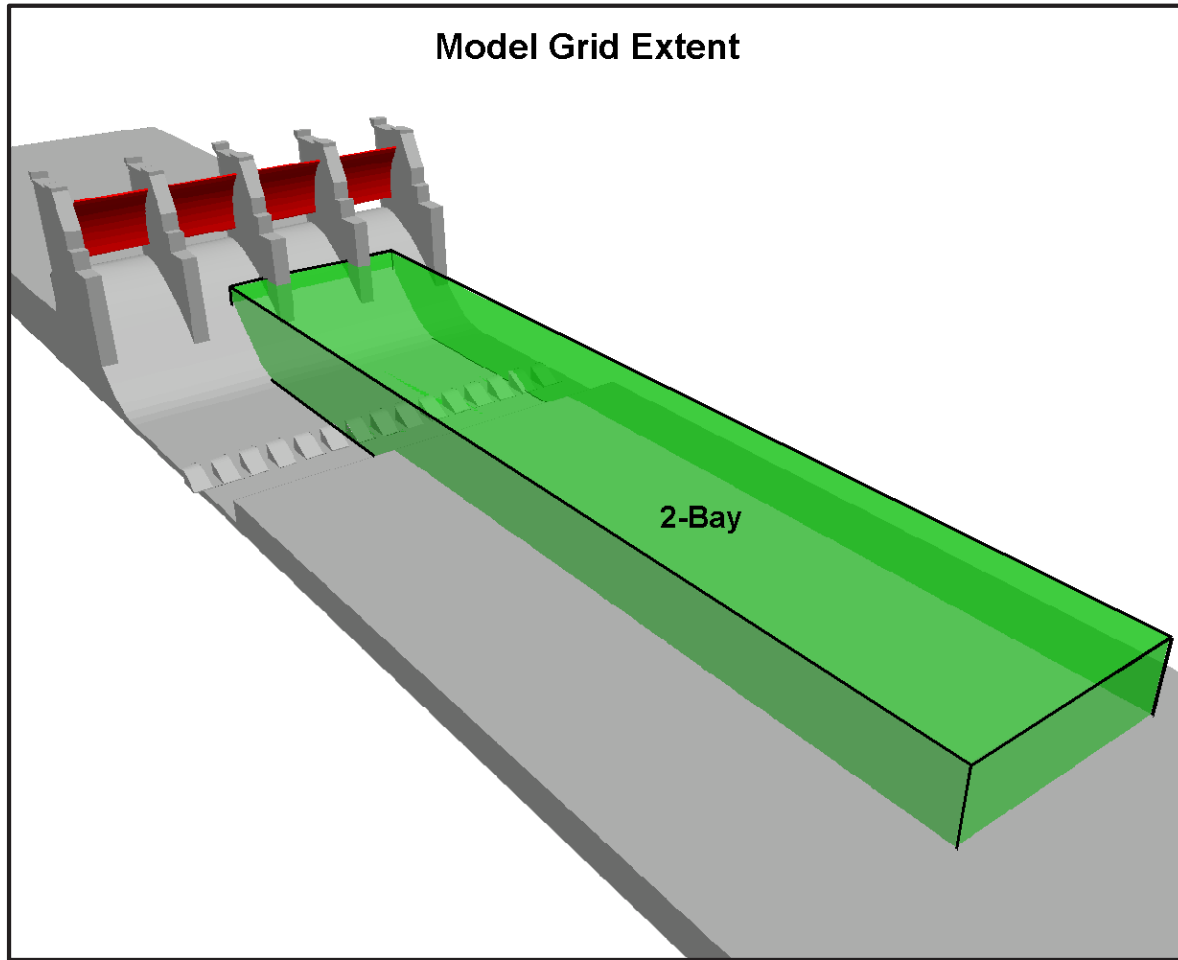


Figure A.3. 2-Bay Model Domain (Appendix D).

PNNL run name		03kcfs76Tail	03kcfs80Tail	04kcfs76Tail	08kcfs76Tail	08kcfs80Tail	08kcfs85Tail
PNNL model type		2-bay	2-bay	2-bay	2-bay	2-bay	2-bay
UNIT							
Tailwater Elevation							
Spillway Basalt	msl, ft	76.5	80.0	76.5	76.5	80.0	85.0
Spillway Operations							
Bay 5 w/ smooth end shelf	Kcfs	3.0	3.0	4.0	8.0	8.0	8.0
Bay 6 w/ smooth end shelf	Kcfs	3.0	3.0	4.0	8.0	8.0	8.0
Bay 7 w/ smooth end shelf	Kcfs	3.0	3.0	4.0	8.0	8.0	8.0
Total	Kcfs	9.0	9.0	12.0	24.0	24.0	24.0

PNNL run name		10kcfs80Tail	12kcfs76Tail	12kcfs80Tail	12kcfs85Tail	12kcfs90Tail	16kcfs76Tail
PNNL model type		2-bay	2-bay	2-bay	2-bay	2-bay	2-bay
UNIT							
Tailwater Elevation							
Spillway Basalt	msl, ft	80.0	76.5	80.0	85.0	90.0	76.5
Spillway Operations							
Bay 5 w/ smooth end shelf	Kcfs	10.0	12.0	12.0	12.0	12.0	16.0
Bay 6 w/ smooth end shelf	Kcfs	10.0	12.0	12.0	12.0	12.0	16.0
Bay 7 w/ smooth end shelf	Kcfs	10.0	12.0	12.0	12.0	12.0	16.0
Total	Kcfs	30.0	36.0	36.0	36.0	36.0	48.0

PNNL run name		16kcfs80Tail	16kcfs85Tail	20kcfs80Tail	20kcfs85Tail	4.5kcfs76Tail68def
PNNL model type		2-bay	2-bay	2-bay	2-bay	2-bay
						deflector at 68'
Tailwater Elevation						
Spillway Basalt	msl, ft	80.0	85.0	80.0	85.0	76.0
Spillway Operations						
Bay 5 w/ smooth end shelf	Kcfs	16.0	16.0	20.0	20.0	4.5
Bay 6 w/ smooth end shelf	Kcfs	16.0	16.0	20.0	20.0	4.5
Bay 7 w/ smooth end shelf	Kcfs	16.0	16.0	20.0	20.0	4.5
Total	Kcfs	48.0	48.0	60.0	60.0	13.5

Table A.3. Scenarios Simulated with the 2-Bay Domain. Results presented in Appendix D

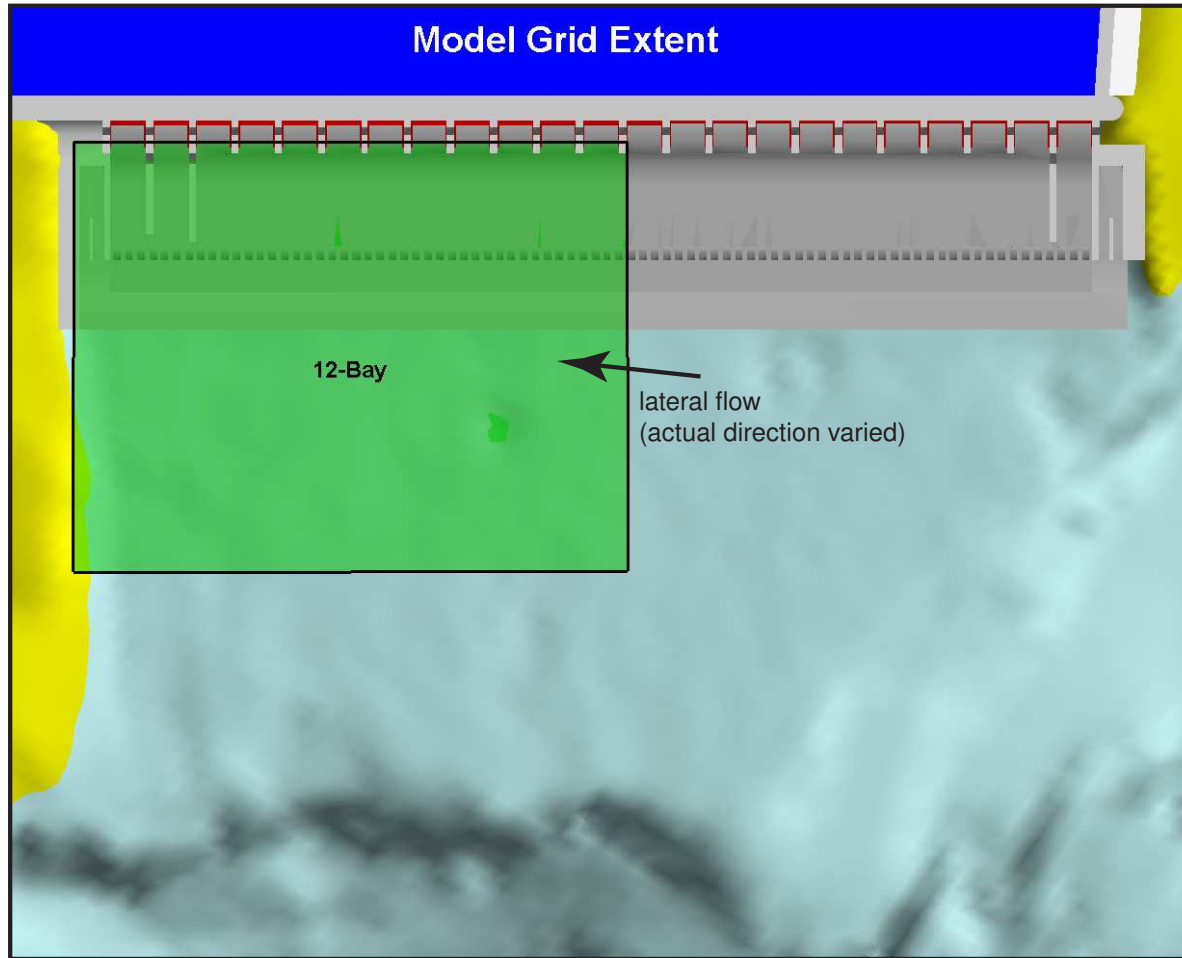


Figure A.4. 12-Bay Model Domain (Appendix E).

PNNL run name		30kcf91Tail-NoBaf	Oct02_T1	Oct02_T2	Oct02_T3	Oct02_T4	P-Sensor2
PNNL model type		12-bay	12-bay	12-bay	12-bay	12-bay	12-bay
	UNIT	No baffles					
Tailwater Elevation							
Spillway Basalt	msl, ft	91.0	77.0	77.0	77.0	77.0	78.9
Spillway Operations							
North Ladder	Kcfs	1.4	1.4	1.4	1.4	1.4	1.4
Bay 1	Kcfs	30.0	9.0				1.5
Bay 2	Kcfs	30.0	12.0	4.5	12.0	4.5	3.0
Bay 3	Kcfs	30.0	12.0	4.5			6.0
Bay 4	Kcfs	30.0	12.0	4.5			6.0
Bay 5	Kcfs	30.0	12.0	4.5			6.0
Bay 6	Kcfs	30.0	15.0	4.5			3.0
Bay 7	Kcfs			4.5			1.5
Bay 8	Kcfs			6.0			
Bay 9	Kcfs						
Bay 10	Kcfs						
Bay 11	Kcfs						
Bay 12	Kcfs						
Total	Kcfs	181.4	73.4	34.4	13.4	5.9	28.4
PNNL run name		SIS_NoWall	SIS_Wall	SVS3	SVS3wall	SVS4	SVS4wall
PNNL model type		12-bay	12-bay	12-bay	12-bay	12-bay	12-bay
	UNIT						
Tailwater Elevation							
Spillway Basalt	msl, ft	79.2	79.2	77.0	77.0	77.0	77.0
Spillway Operations							
North Ladder	Kcfs	1.4	1.4	1.4	1.4	1.4	1.4
Bay 1	Kcfs	9.0	18.0		4.0		12.0
Bay 2	Kcfs	18.0	18.0	4.0	4.0	10.0	12.0
Bay 3	Kcfs	18.0	18.0	4.0	4.0	12.0	12.0
Bay 4	Kcfs	18.0	18.0	4.0	4.0	12.0	12.0
Bay 5	Kcfs	18.0	18.0	4.0	4.0	12.0	12.0
Bay 6	Kcfs	21.0	18.0	10.0	4.0	18.0	12.0
Bay 7	Kcfs						
Bay 8	Kcfs						
Bay 9	Kcfs						
Bay 10	Kcfs						
Bay 11	Kcfs						
Bay 12	Kcfs						
Total	Kcfs	103.4	109.4	27.4	25.4	65.4	73.4

Table A.4. Scenarios Simulated with the 12-Bay Domain. Results presented in Appendix E

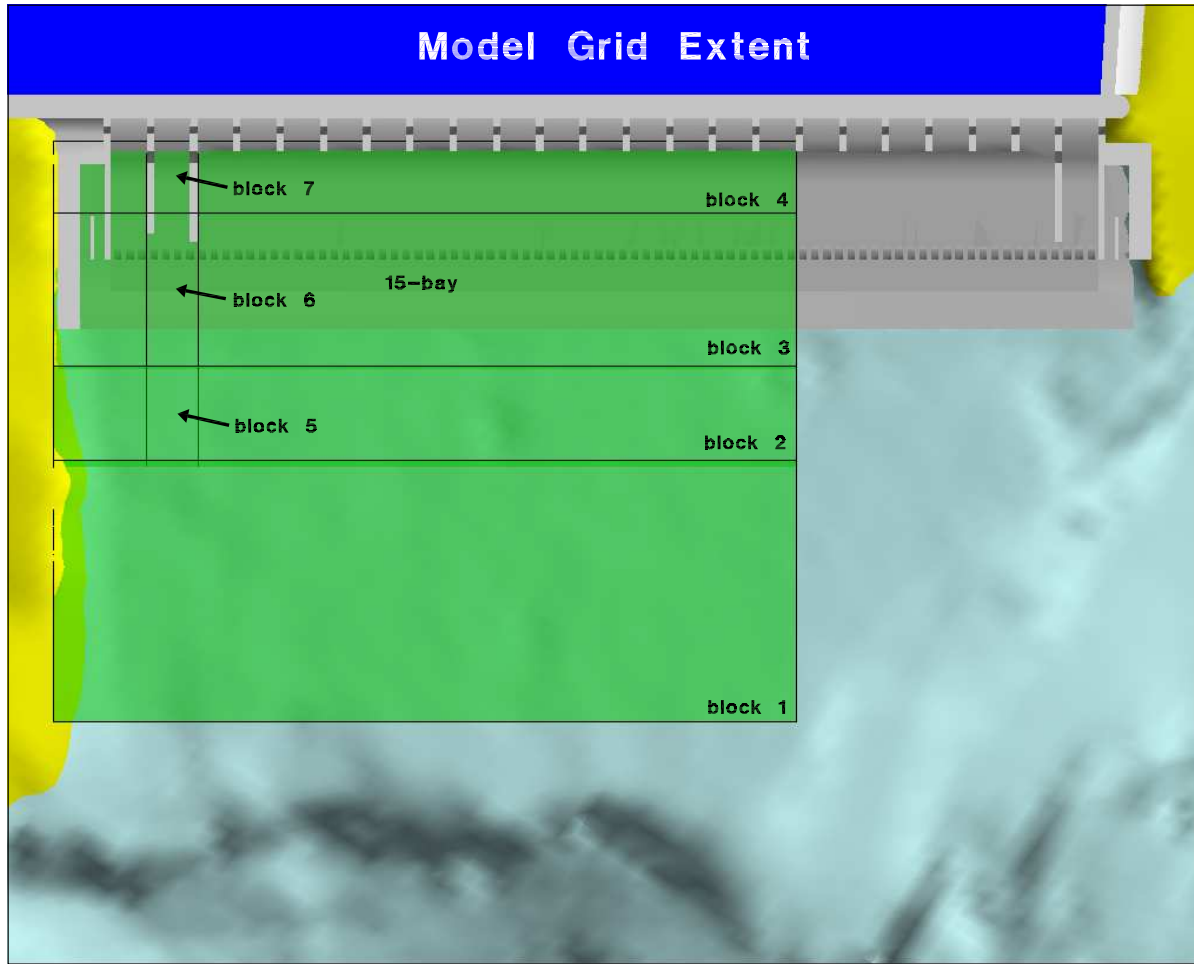


Figure A.5. 15-Bay Model Domain (Appendix F).

PNNL run name		Spr03_18k	Spr03_21k
PNNL model type		15-bay	15-bay
UNIT			
Tailwater Elevation			
Spillway Basalt	msl, ft	81.0	81
Spillway Operations			
North Ladder	Kcfs	1.4	1.4
Bay 1	Kcfs	9.0	4.5
Bay 2	Kcfs	18.0	21.0
Bay 3	Kcfs	18.0	6.0
Bay 4	Kcfs	18.0	6.0
Bay 5	Kcfs	18.0	6.0
Bay 6	Kcfs	21.0	6.0
Bay 7	Kcfs		6.0
Bay 8	Kcfs		6.0
Bay 9	Kcfs		6.0
Bay 10	Kcfs		12.0
Bay 11	Kcfs		10.0
Bay 12	Kcfs		9.0
Bay 13			
Bay 14			
Bay 15	Kcfs		
Total	Kcfs	103.4	99.9

Table A.5. Scenarios Simulated with the 15-Bay Domain. Results presented in Appendix F

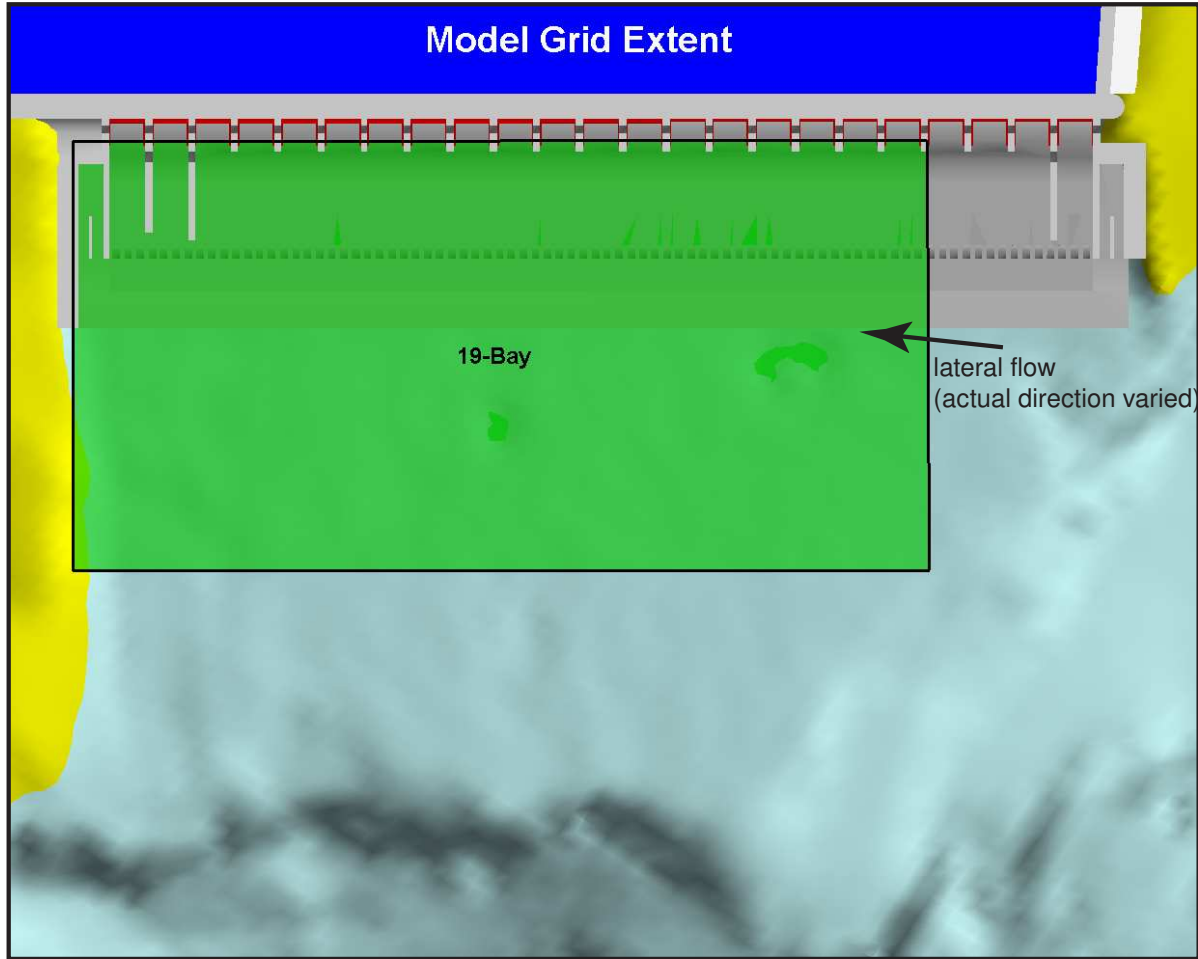


Figure A.6. 19-Bay Model Domain (Appendix G).

PNNL run name		4.5kcfs_SIS	May02_T1	May02_T2	May02_T3	May02_T4	P-Sensor7	Sp01_T1	Sp01_T2	Sp01_T3	Sp01_T4
PNNL model type		19-bay	19-bay	19-bay	19-bay	19-bay	19-bay	19-bay	19-bay	19-bay	19-bay
	UNIT										
Tailwater Elevation	msl, ft										
Spillway Basalt	msl, ft	77.0	81.8	80.2	82.2	81.0	79.4	78.0	78.5	77.5	76.5
Spillway Operations											
North Ladder	Kcfs	1.4	1.4	1.4	1.4	1.4	1.4	1.4	1.4	1.4	1.4
Bay 1	Kcfs	4.5	7.5	4.5	6.0	7.5	3.0	3.0	3.0	4.5	4.5
Bay 2	Kcfs	4.5	9.0	4.5	6.0	7.5	3.0	3.0	4.5	4.5	4.5
Bay 3	Kcfs	4.5	9.0	6.0	7.5	7.5	4.5	4.5	4.5	6.0	6.0
Bay 4	Kcfs	4.5	10.5	6.0	9.0	9.0	4.5	4.5	6.0	7.5	6.0
Bay 5	Kcfs	4.5	10.5	6.0	7.5	9.0	4.5	4.5	4.5	6.0	6.0
Bay 6	Kcfs	4.5	9.0	4.5	7.5	9.0	4.5	4.5	4.5	6.0	4.5
Bay 7	Kcfs	4.5	9.0	4.5	7.5	7.5	4.5	4.5	4.5	6.0	4.5
Bay 8	Kcfs	15.0	7.5	4.5	6.0	7.5	4.5	4.5	4.5	4.5	4.5
Bay 9	Kcfs	12.0	7.5	4.5	6.0	7.5	4.5	4.5	4.5	4.5	4.5
Bay 10	Kcfs	12.0	6.0	4.5	6.0	6.0	4.5	4.5	4.5	4.5	4.5
Bay 11	Kcfs	12.0	6.0	4.5	6.0	6.0	3.0	3.0	3.0	4.5	3.0
Bay 12	Kcfs	12.0	6.0	4.5	6.0	6.0	3.0	3.0	3.0	4.5	3.0
Bay 13	Kcfs	12.0	4.5	3.0	3.0	4.5	3.0	3.0	3.0	3.0	3.0
Bay 14	Kcfs		4.5	1.5	3.0	3.0				3.0	
Bay 15	Kcfs		3.0			3.0					
Bay 16	Kcfs										
Bay 17	Kcfs										
Bay 18	Kcfs										
Bay 19	Kcfs										
Total	Kcfs	107.9	110.9	64.4	88.4	101.9	52.4	52.4	55.4	70.4	59.9

Table A.6. Scenarios Simulated with the 19-Bay Domain. Results presented in Appendix G

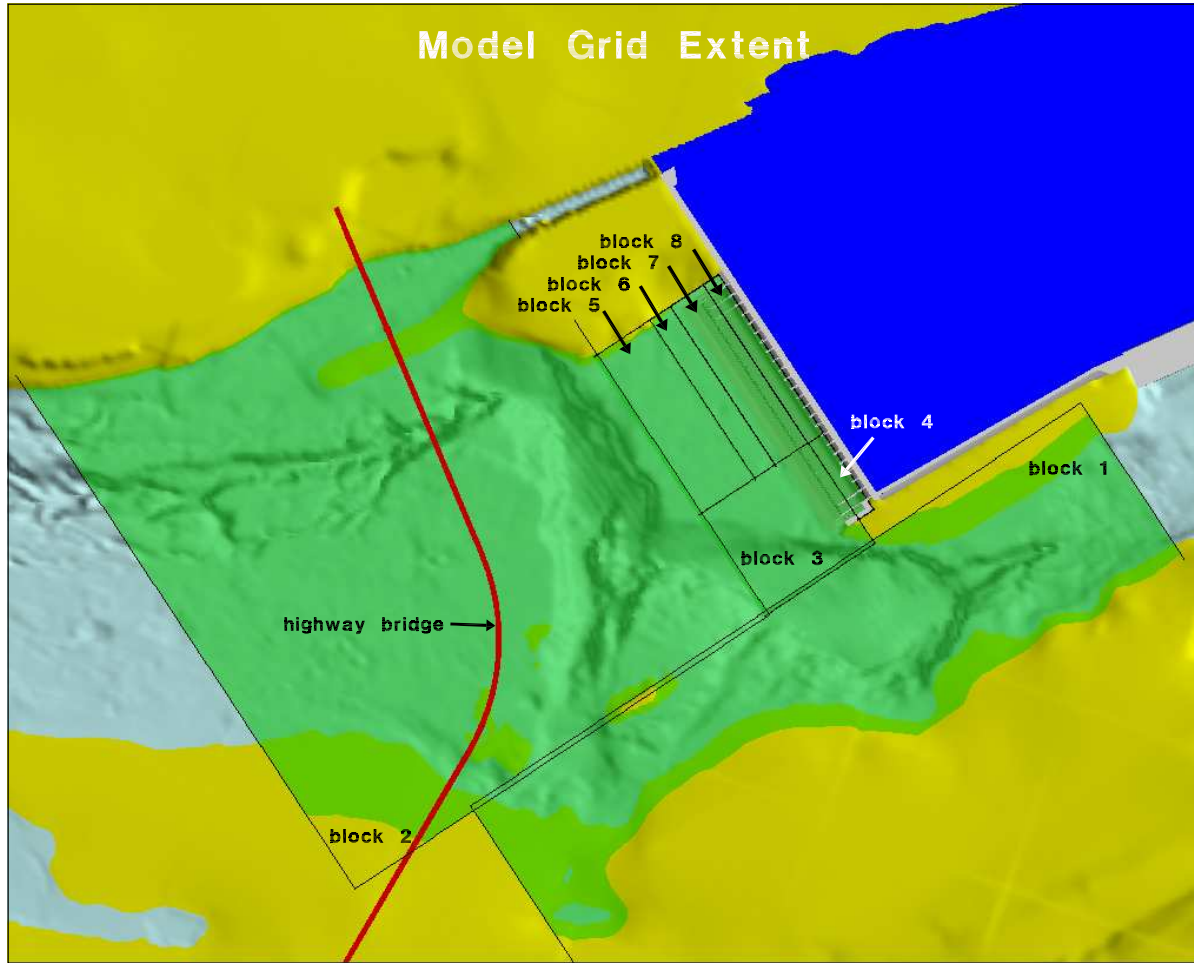


Figure A.7. Bank-to-Bank 8-block Model Domain (Appendix H).

Run Name		Test11_No23Wall	Test11_NoBaf	Test11_Wall	Test11_NoWall	Apr-04
PNNL model type		Bank to Bank - 8 blks	Bank to Bank - 8 blks	Bank to Bank - 8 blks	Bank to Bank - 8 blks	Bank to Bank - 8 blks
	UNIT	No Bay2-3 wall & with Bay6-7 wall	No Bay 2 baffles & with Bay6-7 wall	Bay 6-7 wall		Bay 6-7 wall
Total River Q	Kcfs	310.4	310.4	310.4	310.4	158.8
Spill Q	Kcfs	126.0	126.0	126.0	126.0	63.0
Powerhouse Q	Kcfs	183.0	183.0	183.0	183.0	94.4
Tailwater Elevation	msl, ft					
Powerhouse BC	msl, ft	81.5	81.5	81.5	81.5	78.0
Downstream	msl, ft	80.5	80.5	80.5	80.5	77.0
Spillway Operations						
North Ladder	Kcfs	1.4	1.4	1.4	1.4	1.4
Bay 1	Kcfs	21.0	21.0	21.0	9.0	10.5
Bay 2	Kcfs	21.0	21.0	21.0	9.0	10.5
Bay 3	Kcfs	21.0	21.0	21.0	10.5	10.5
Bay 4	Kcfs	21.0	21.0	21.0	12.0	10.5
Bay 5	Kcfs	21.0	21.0	21.0	10.5	10.5
Bay 6	Kcfs	21.0	21.0	21.0	10.5	10.5
Bay 7	Kcfs				9.0	
Bay 8	Kcfs				9.0	
Bay 9	Kcfs				9.0	
Bay 10	Kcfs				9.0	
Bay 11	Kcfs				7.5	
Bay 12	Kcfs				7.5	
Bay 13	Kcfs				6.0	
Bay 14	Kcfs				4.5	
Bay 15	Kcfs				3.0	
Bay 16	Kcfs					
Bay 17	Kcfs					
Bay 18	Kcfs					
Bay 19	Kcfs					
Bay 20	Kcfs					
Bay 21	Kcfs					
Bay 22	Kcfs					
Bay 23	Kcfs					
Total	Kcfs	127.4	127.4	127.4	127.4	64.4

Table A.7. Scenarios Simulated with the Bank-to-Bank 8-block Domain. Results presented in Appendix H

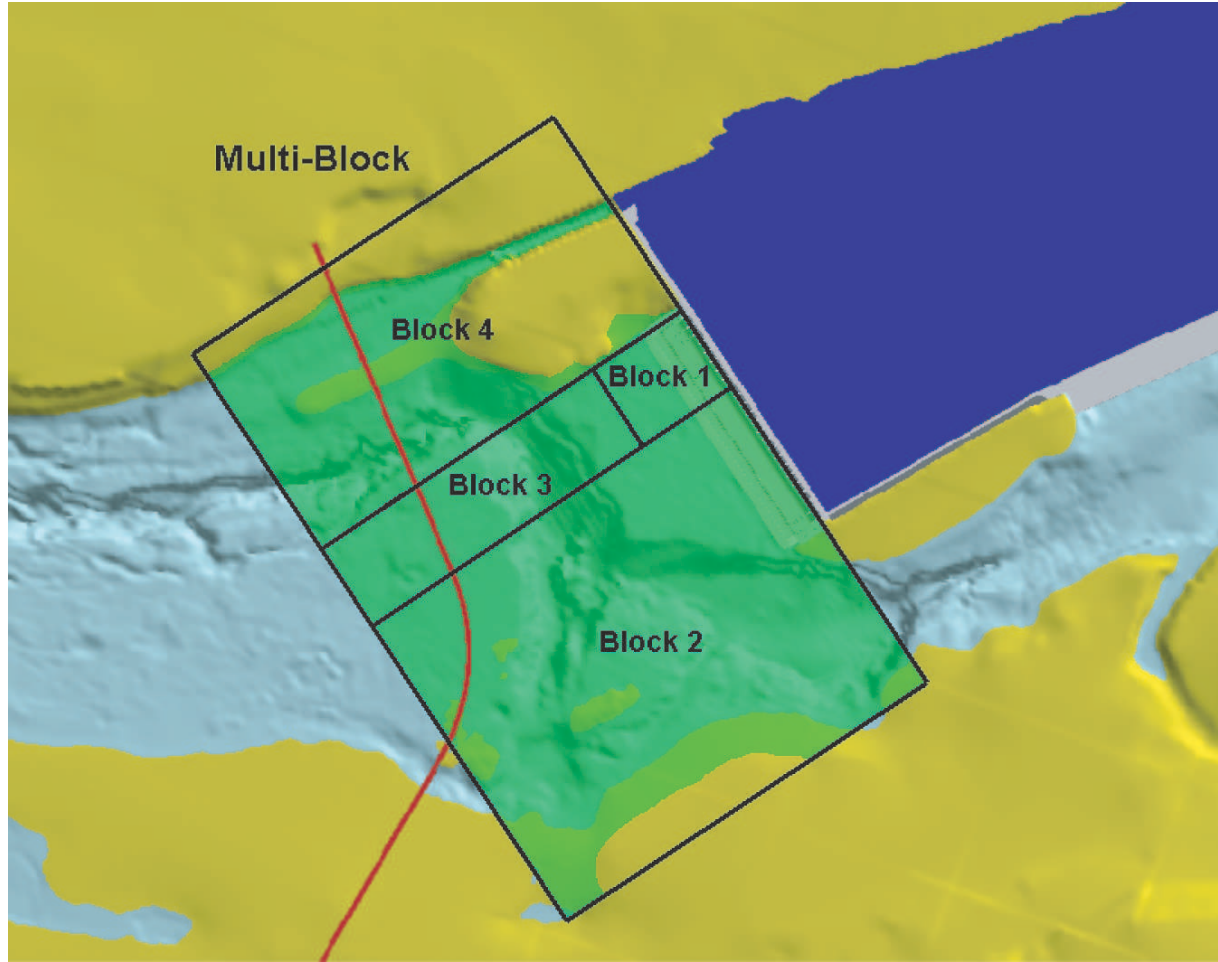


Figure A.8. Bank-to-Bank 4-block Model Domain (Appendix I).

Run Name		Oct02_T1_75tail	Oct02_T2_75tail
PNNL model type		Bank to Bank - 4 blocks	Bank to Bank - 4 blocks
	UNIT		
Total River Q	Kcfs	250.4	211.4
Spill Q	Kcfs	72.0	33.0
Powerhouse Q	Kcfs	177.0	177.0
Tailwater Elevation	msl, ft		
Powerhouse BC	msl, ft	77.0	77.0
Downstream	msl, ft	75.0	75.0
Spillway Operations			
North Ladder	Kcfs	1.4	1.4
Bay 1	Kcfs	9.0	4.5
Bay 2	Kcfs	12.0	4.5
Bay 3	Kcfs	12.0	4.5
Bay 4	Kcfs	12.0	4.5
Bay 5	Kcfs	12.0	4.5
Bay 6	Kcfs	15.0	4.5
Bay 7	Kcfs		6.0
Bay 8	Kcfs		
Bay 9	Kcfs		
Bay 10	Kcfs		
Bay 11	Kcfs		
Bay 12	Kcfs		
Bay 13	Kcfs		
Bay 14	Kcfs		
Bay 15	Kcfs		
Bay 16	Kcfs		
Bay 17	Kcfs		
Bay 18	Kcfs		
Bay 19	Kcfs		
Bay 20	Kcfs		
Bay 21	Kcfs		
Bay 22	Kcfs		
Bay 23	Kcfs		
Total	Kcfs	73.4	34.4

Table A.8. Scenarios Simulated with the Bank-to-Bank 4-block Domain. Results presented in Appendix I

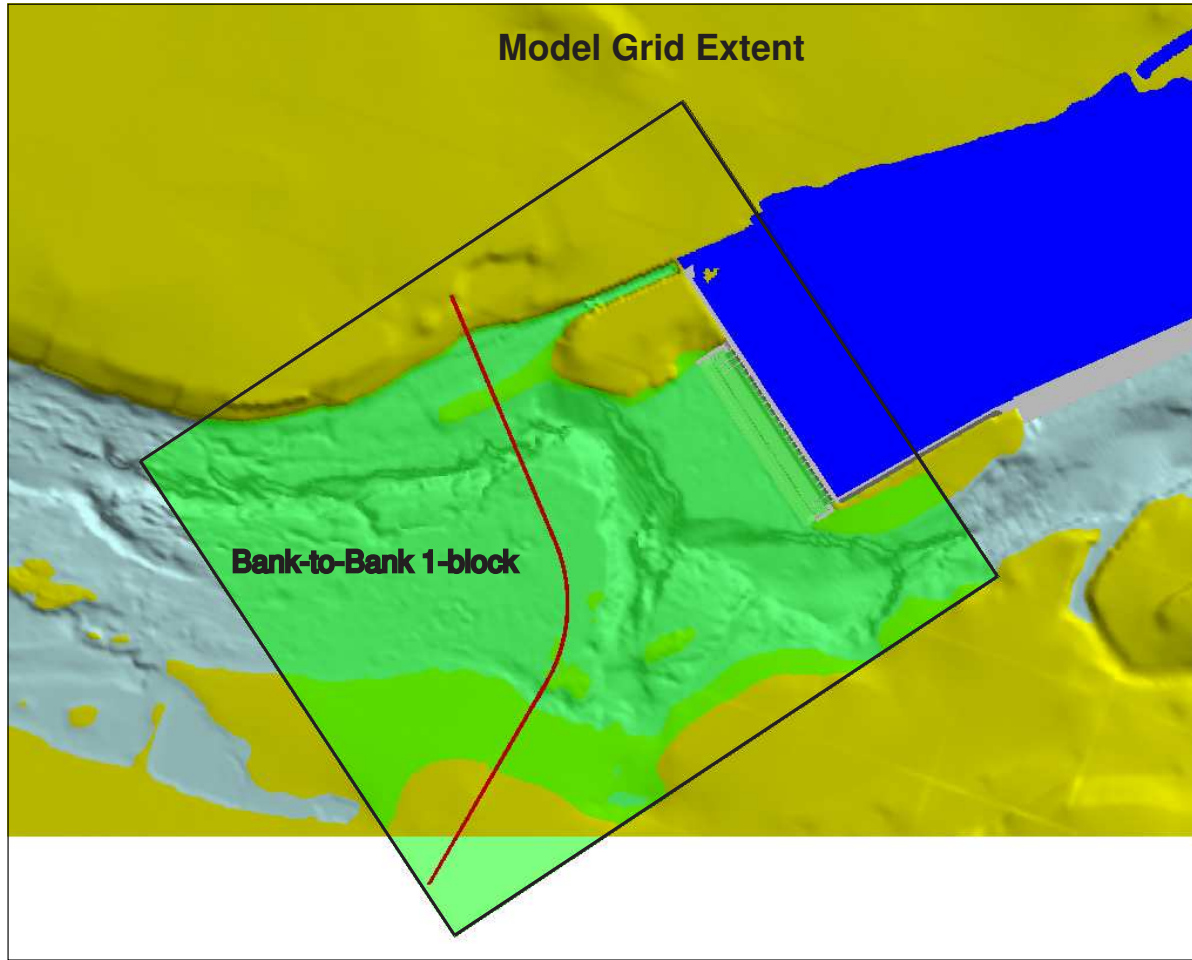


Figure A.9. Bank-to-Bank 1-block Model Domain (Appendix J).

Run Name		Ambient	SF_HighQ	SF_LowQ	SVS3	SVS3WALL	SVS4	SVS4WALL
PNNL model type		Bank to Bank - 1 blk						
	UNIT					Bay 6-7 wall		Bay 6-7 wall
Total River Q	Kcfs	235.0	193.2	154.2	126.2	124.2	124.2	132.2
Spill Q	Kcfs	100.0	72.0	33.0	26.0	24.0	64.0	72.0
Powerhouse Q	Kcfs	135.0	120.0	120.0	99.0	99.0	59.0	59.0
Tailwater Elevation	msl, ft							
Powerhouse BC	msl, ft	79.5	77.0	77.0	79.5	79.5	77.0	77.0
Downstream	msl, ft	78.5	77.0	77.0	76.0	76.0	76.0	76.0
Spillway Operations								
North Ladder	Kcfs		1.2	1.2	1.2	1.2	1.2	1.2
Bay 1	Kcfs	7.5	9.0			4.0		12.0
Bay 2	Kcfs	7.5	12.0	4.5	4.0	4.0	10.0	12.0
Bay 3	Kcfs	7.5	12.0	4.5	4.0	4.0	12.0	12.0
Bay 4	Kcfs	9.0	12.0	4.5	4.0	4.0	12.0	12.0
Bay 5	Kcfs	9.0	12.0	4.5	4.0	4.0	12.0	12.0
Bay 6	Kcfs	9.0	15.0	4.5	10.0	4.0	18.0	12.0
Bay 7	Kcfs	7.5		4.5				
Bay 8	Kcfs	7.5		6.0				
Bay 9	Kcfs	7.5						
Bay 10	Kcfs	6.0						
Bay 11	Kcfs	6.0						
Bay 12	Kcfs	6.0						
Bay 13	Kcfs	4.5						
Bay 14	Kcfs	3.0						
Bay 15	Kcfs	2.5						
Bay 16	Kcfs							
Bay 17	Kcfs							
Bay 18	Kcfs							
Bay 19	Kcfs							
Bay 20	Kcfs							
Bay 21	Kcfs							
Bay 22	Kcfs							
Bay 23	Kcfs							
Total	Kcfs	100.0	73.2	34.2	27.2	25.2	65.2	73.2

Table A.9. Scenarios Simulated with the Bank-to-Bank 1-block Domain. Results presented in Appendix J

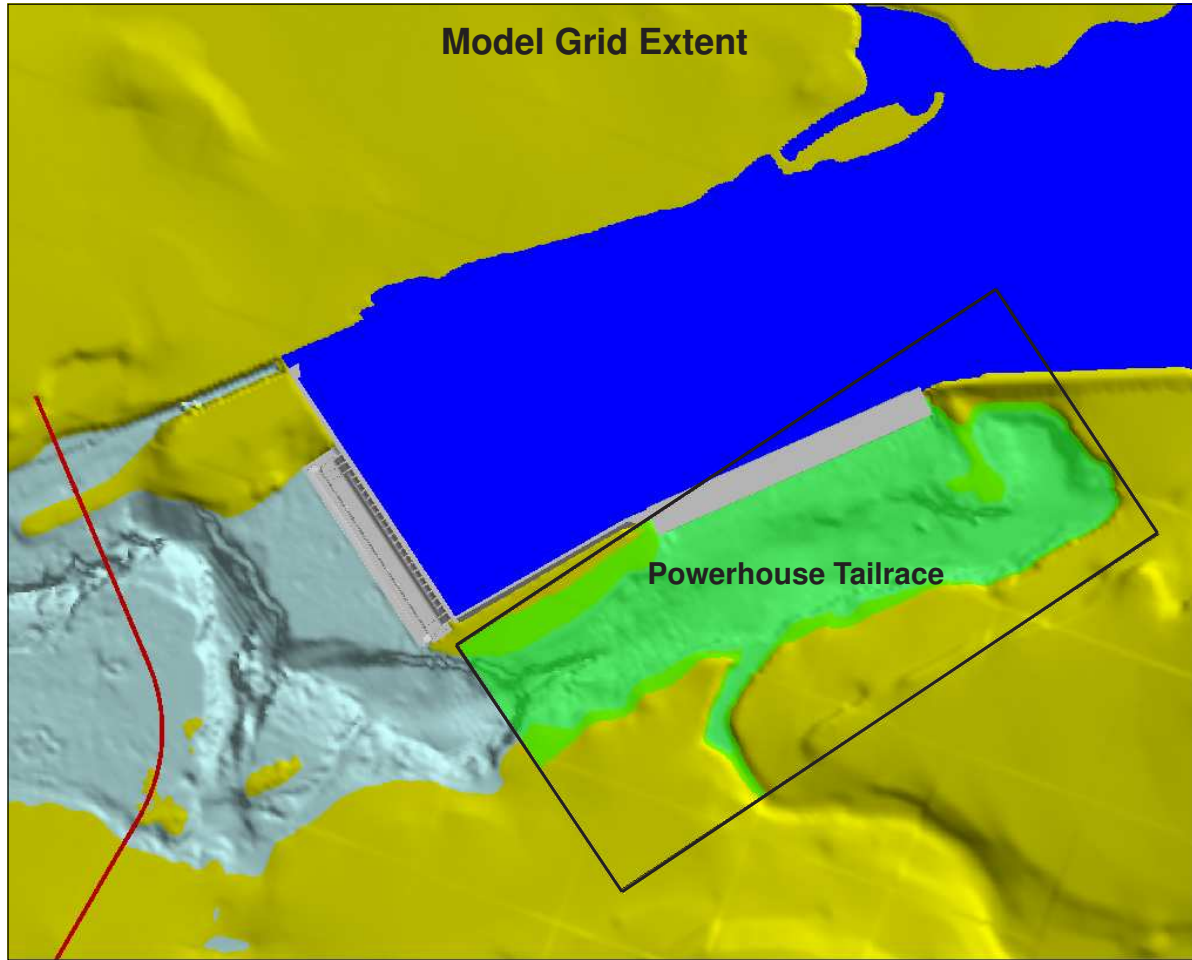


Figure A.10. Powerhouse Tailrace Model Domain (Appendix K).

PNNL run name PNNL model type			Ambient Powerhouse tailrace	SIS_High Powerhouse tailrace	SIS_Low Powerhouse tailrace	SVS1 Powerhouse tailrace	SVS3 Powerhouse tailrace	SVS4 Powerhouse tailrace
UNIT								
Tailwater Elevation	Powerhouse BC	msl, ft						
			79.5	81.5	79.5	77.0	77.0	77.0
Powerhouse	Unit 1	Kcfs	10.8	14.0	11.0	11.0	11.1	12.2
	Unit 2	Kcfs	10.8	14.0				
	Unit 3	Kcfs	10.8	14.0	11.0	11.0	11.1	12.2
	Unit 4	Kcfs	10.8	14.0				
	Unit 5	Kcfs	10.7	14.0	10.7	11.0	11.1	12.2
	Unit 6	Kcfs		14.0				
	Unit 7	Kcfs	10.7	14.0	10.5	11.0	11.1	12.2
	Unit 8	Kcfs						
	Unit 9	Kcfs	10.7	13.7	10.5	11.0	11.1	12.2
	Unit 10	Kcfs						
	Unit 11	Kcfs	10.7	13.5	10.5	11.0	11.1	
	Unit 12	Kcfs						
	Unit 13	Kcfs	10.7	13.5	10.5	11.0	11.1	
	Unit 14	Kcfs						
	Unit 15	Kcfs	10.7	15.5	14.0	11.0	11.1	
	Unit 16	Kcfs						
	Unit 17	Kcfs	10.7	15.5	14.0	11.0	11.1	
	Unit 18	Kcfs						
	Unit 19	Kcfs	10.7	15.5	14.0	11.0		
	Unit 20	Kcfs						
	Unit 21	Kcfs	10.7	15.5	14.0	11.0		
	Unit 22	Kcfs						
	East Fish	Kcfs	1.8	2.5	2.5			
	West Fish	Kcfs	1.8	2.5	2.5			
	Total	Kcfs	143.0	206.0	136.0	121.0	99.9	61.0

Table A.10. Scenarios Simulated with the Powerhouse Tailrace Domain. Results presented in Appendix K

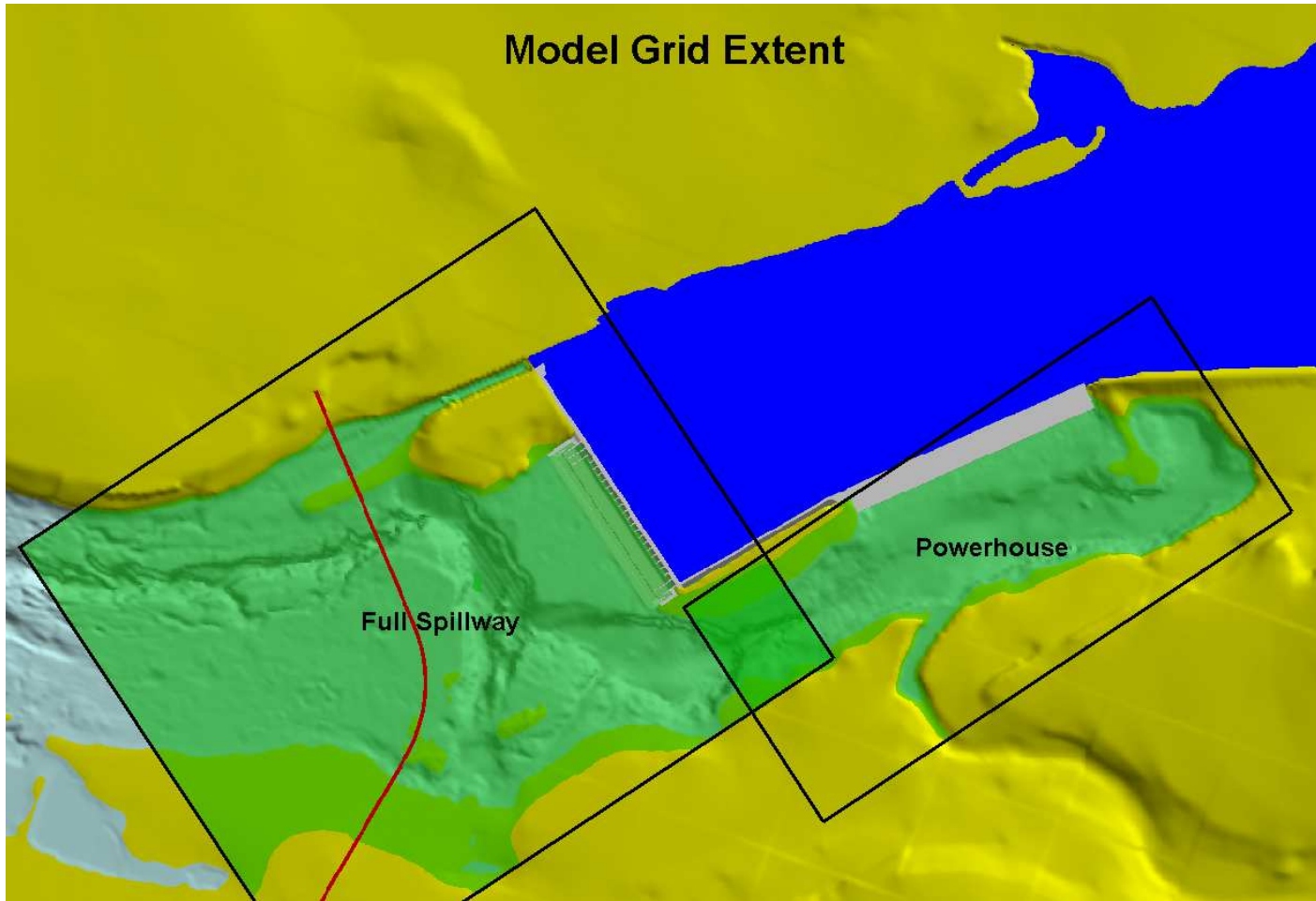


Figure A.11. 1:80 scale Powerhouse and Spillway Tailrace Model Domain (Appendix L).

			POWERHOUSE	
PNNL run name			Flow Condition 1	Flow Condition 2
PNNL model type			1:80 scale Powerhouse	1:80 scale Powerhouse
UNIT				
Tailwater Elevation				
Powerhouse BC msl, ft			76.8	76.8
Powerhouse				
Unit 1	Kcfs		13.0	11.5
Unit 2	Kcfs			
Unit 3	Kcfs		12.7	11.4
Unit 4	Kcfs			
Unit 5	Kcfs		12.4	11.3
Unit 6	Kcfs			
Unit 7	Kcfs		12.3	11.3
Unit 8	Kcfs			
Unit 9	Kcfs		12.3	11.3
Unit 10	Kcfs			
Unit 11	Kcfs		12.3	11.3
Unit 12	Kcfs			
Unit 13	Kcfs		12.3	11.3
Unit 14	Kcfs			
Unit 15	Kcfs		12.3	
Unit 16	Kcfs			
Unit 17	Kcfs		12.3	
Unit 18	Kcfs			
Unit 19	Kcfs			
Unit 20	Kcfs			
Unit 21	Kcfs			
Unit 22	Kcfs			
East Fish	Kcfs			
West Fish	Kcfs			
Total			111.9	79.4

			SPILLWAY	
Run Name			Flow Condition 1	Flow Condition 1
PNNL model type			1:80 scale Spillway	1:80 scale Spillway
UNIT				
			Smooth End Shelf	
Total River Q	Kcfs		162.9	162.9
Spill Q	Kcfs		51.0	51.0
Powerhouse Q	Kcfs		111.9	111.9
Tailwater Elevation				
Powerhouse BC			76.8	76.8
Downstream			76.8	76.8
Spillway Operations				
North Ladder				
Bay 1	Kcfs		3.0	3.0
Bay 2	Kcfs		3.0	3.0
Bay 3	Kcfs		4.5	4.5
Bay 4	Kcfs		4.5	4.5
Bay 5	Kcfs		4.5	4.5
Bay 6	Kcfs		4.5	4.5
Bay 7	Kcfs		4.5	4.5
Bay 8	Kcfs		4.5	4.5
Bay 9	Kcfs		4.5	4.5
Bay 10	Kcfs		4.5	4.5
Bay 11	Kcfs		3.0	3.0
Bay 12	Kcfs		3.0	3.0
Bay 13	Kcfs		3.0	3.0
Bay 14	Kcfs			
Bay 15	Kcfs			
Bay 16	Kcfs			
Bay 17	Kcfs			
Bay 18	Kcfs			
Bay 19	Kcfs			
Bay 20	Kcfs			
Bay 21	Kcfs			
Bay 22	Kcfs			
Bay 23	Kcfs			
Total			51.0	51.0

Table A.11. Scenarios Simulated with the 1:80 scale Powerhouse and Spillway Tailrace Domain. Results presented in Appendix L

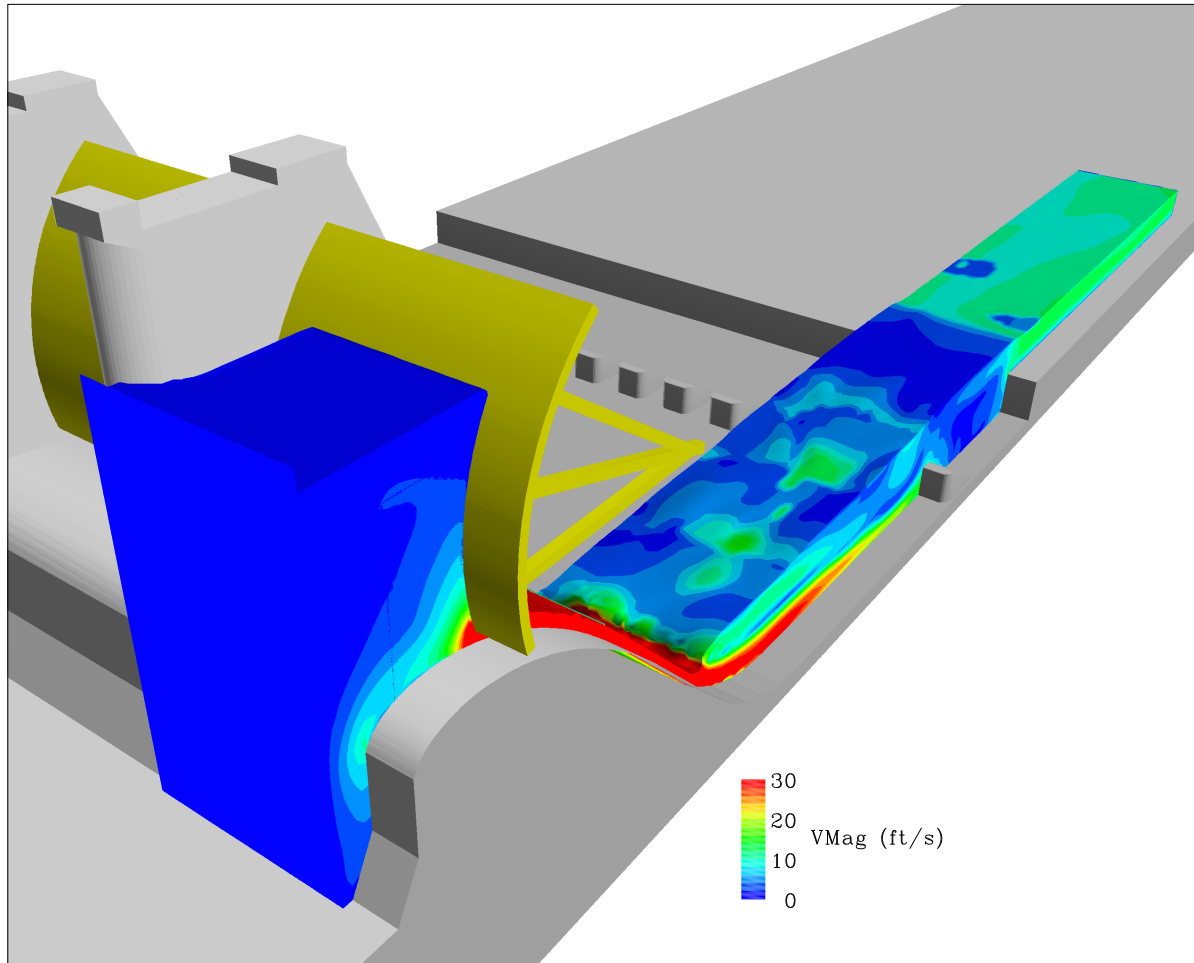


Figure A.12. Only one 1:40 scale model simulated the entire forebay to end shelf domain shown above. The remainder of the 1:40 scale and all of the 1:36 scale models simulated only the spillway face to end shelf portions. (Appendix M)

1:40 SCALE

PNNL run name		5.8kcfs78Tail	5.8kcfs78Tail70Def	5.8kcfs78Tail70Def-NoBaf	6.6kcfs78Tail-ForebayToEndsill
PNNL model type		1:40 scale 1-bay	1:40 scale 1-bay	1:40 scale 1-bay	1:40 scale 1-bay
	UNIT		deflector at 70'	deflector at 70'	forebay & gate
Tailwater Elevation					
Spillway Basalt	msl, ft	78.0	78.0	78.0	78.0
Spillway Operations					
Bay 6 w/ smooth end shelf	Kcfs	5.8	5.8	5.8	6.6
Total	Kcfs	5.8	5.8	5.8	6.6

1:36 SCALE

PNNL run name		5kcfs76.8Tail
PNNL model type		1:36 scale 1-bay
	UNIT	
Tailwater Elevation		
Spillway Basalt	msl, ft	76.8
Spillway Operations		
Bay 6 w/ smooth end shelf	Kcfs	5.0
Total	Kcfs	5.0

Table A.12. Scenarios Simulated with the 1:36 and 1:40 scale Domain. Results presented in Appendix M

Appendix B

Tainter Gate Simulations

Appendix B – Tainter Gate Simulations

The following appendix summarizes simulation results from the tainter gate simulations (Figure A.1 displays the domain extent). In all figures particle tracks of equal duration have been added to illustrate the direction of flow. The circles indicate the starting position for each track and the track length is proportional to the velocity magnitude.

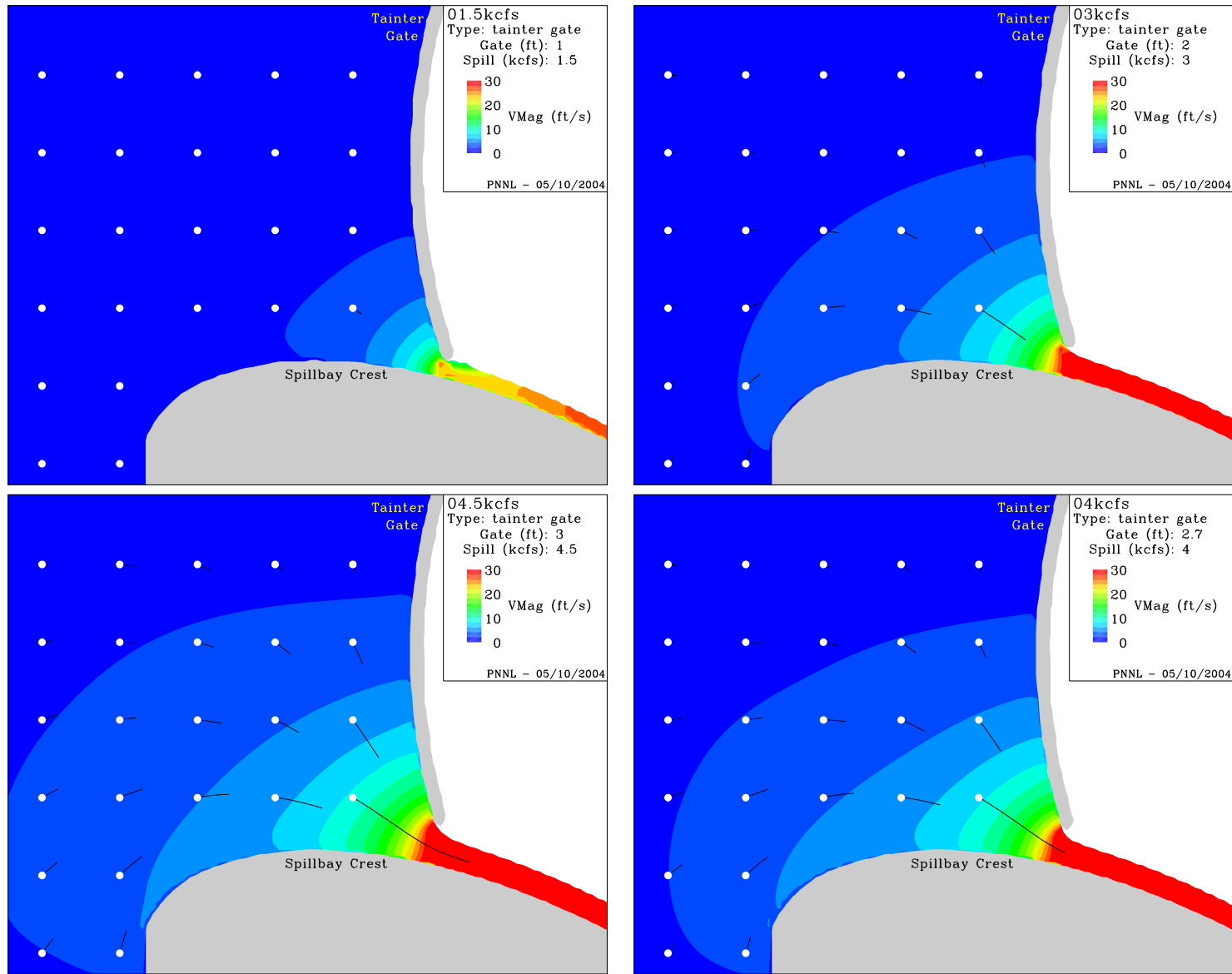


Figure B.1. Results for CFD model of The Dalles Dam tailrace (Gate3001.5kcfs.eps).

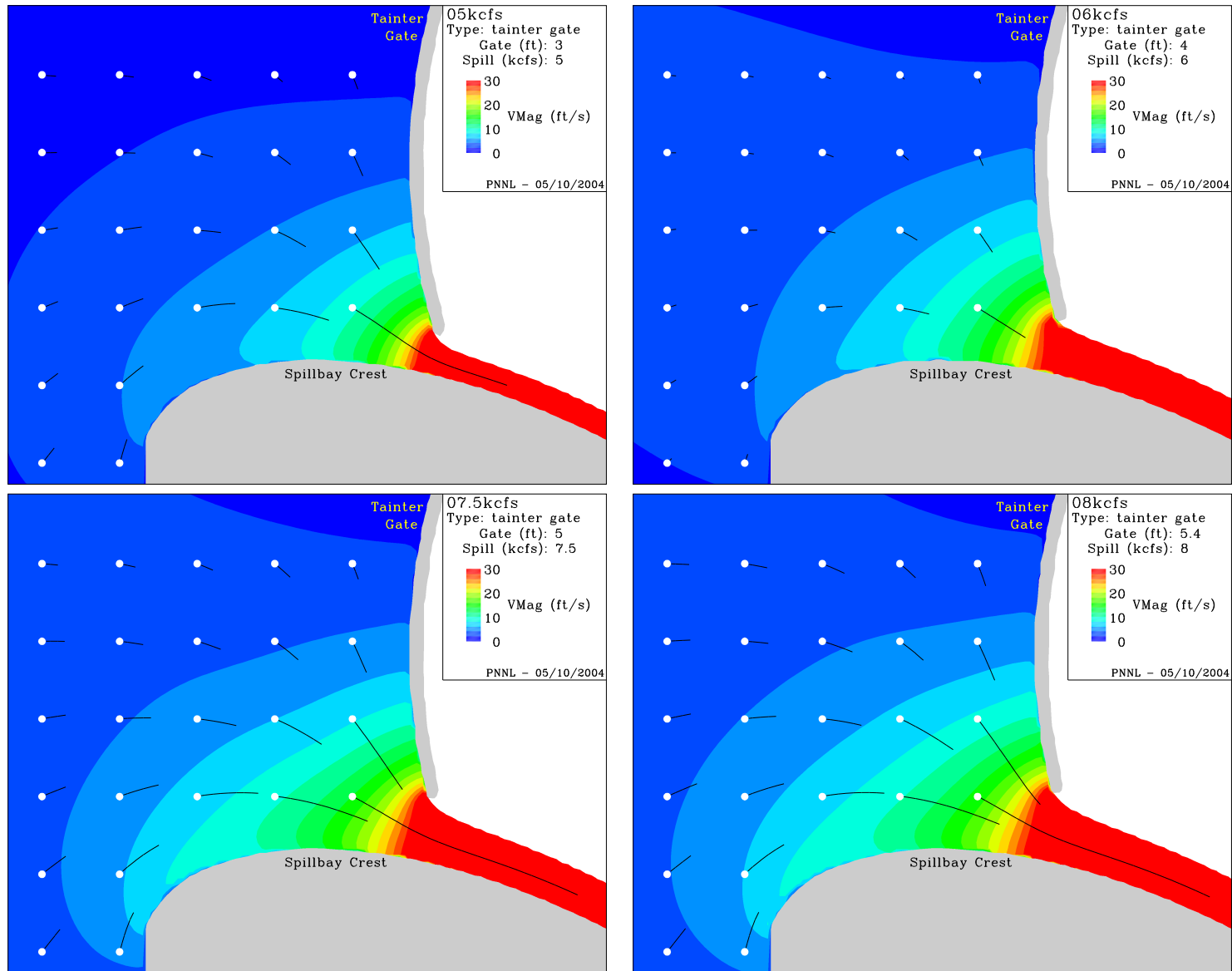


Figure B.2. Results for CFD model of The Dalles Dam tailrace (Gate05kcfs.eps).

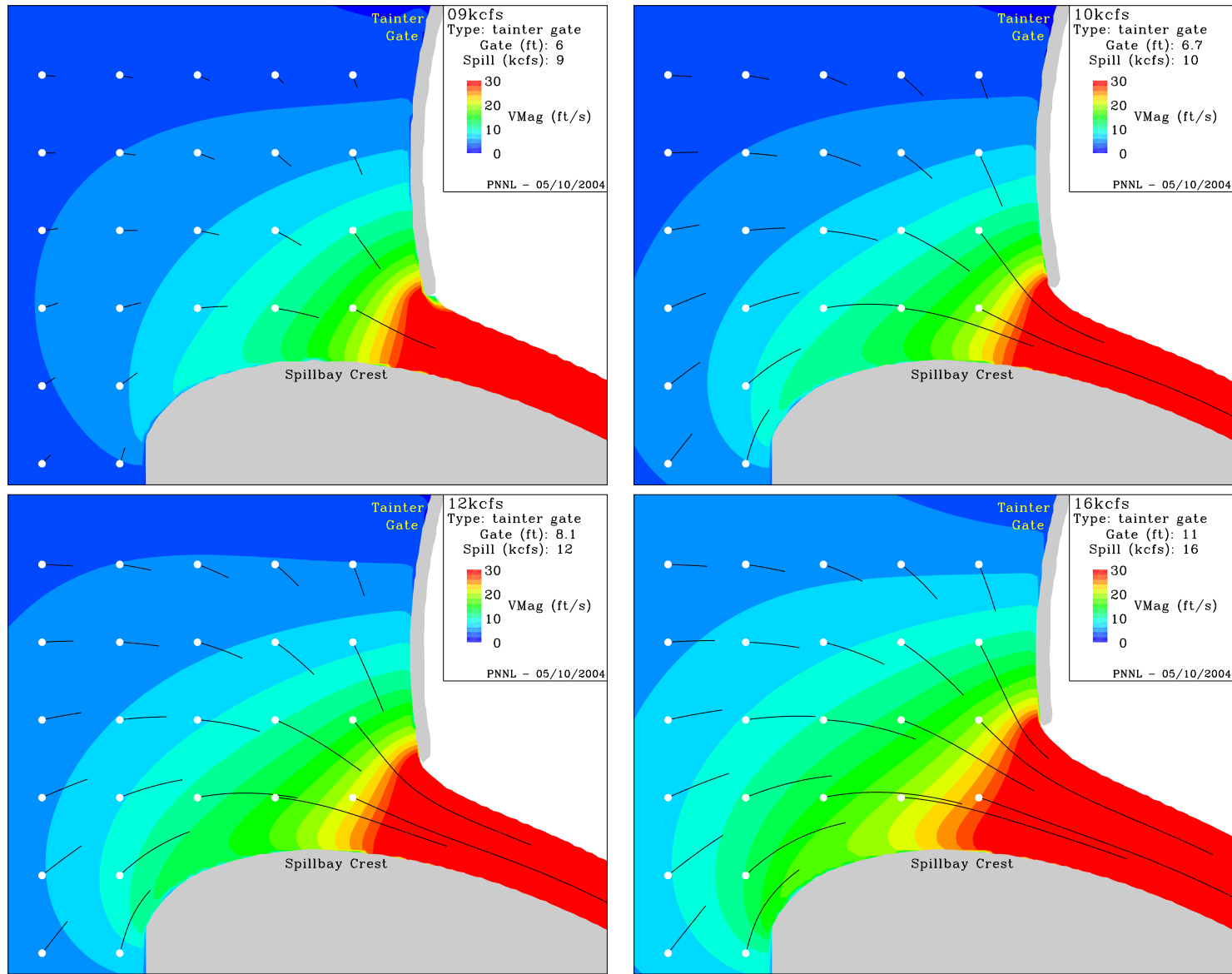


Figure B.3. Results for CFD model of The Dalles Dam tailrace (Gate3009kcfs.eps).

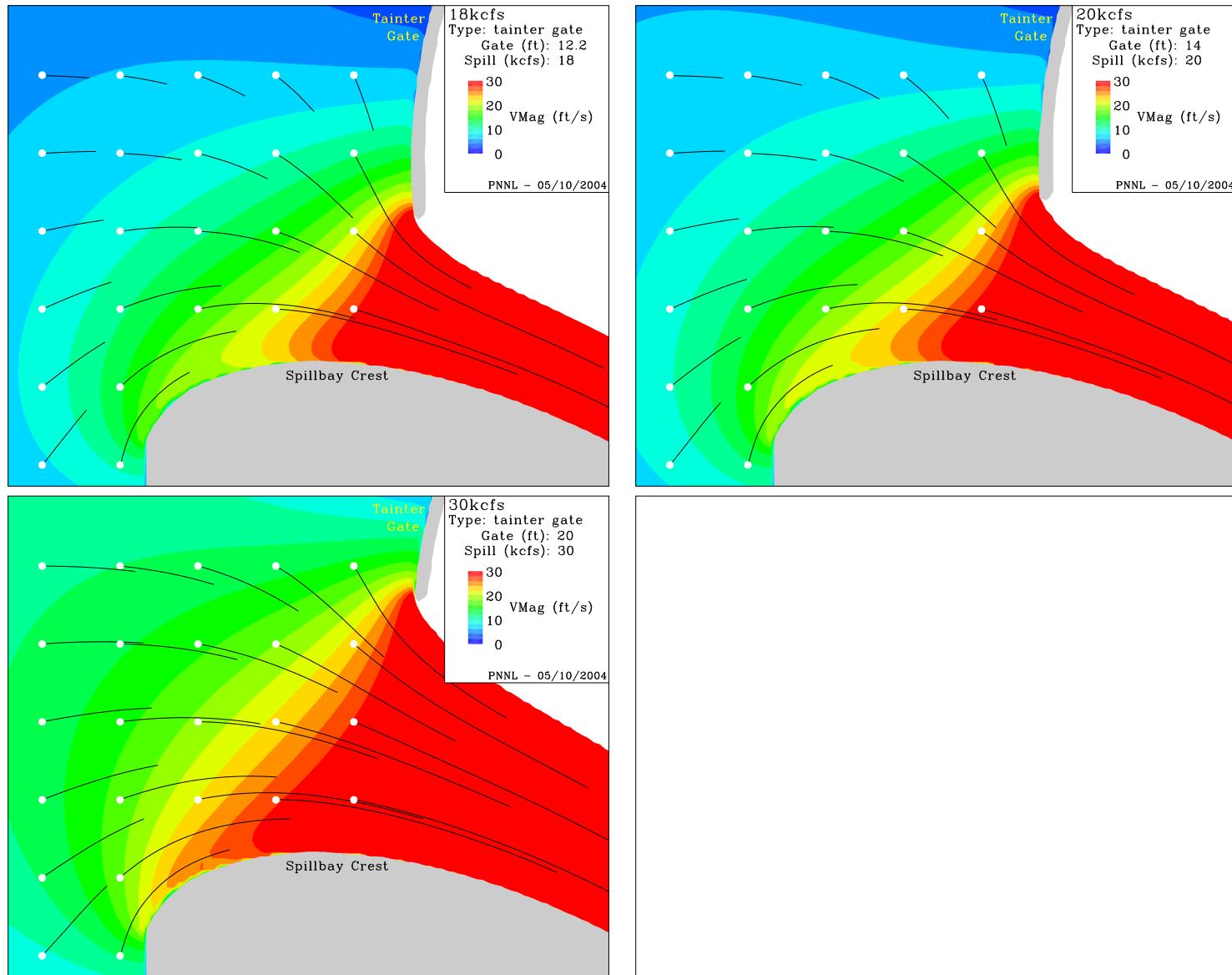


Figure B.4. Results for CFD model of The Dalles Dam tailrace (Gate18k cfs.eps).

Appendix C

1-Bay Simulations

Appendix C – 1-Bay Simulations

The following appendix summarizes simulation results from a single spillway bay (Figure A.2 displays the domain extent). In all figures particle tracks of equal duration have been added to illustrate the direction of flow. The circles indicate the starting position for each track and the track length is proportional to the velocity magnitude.

C.2

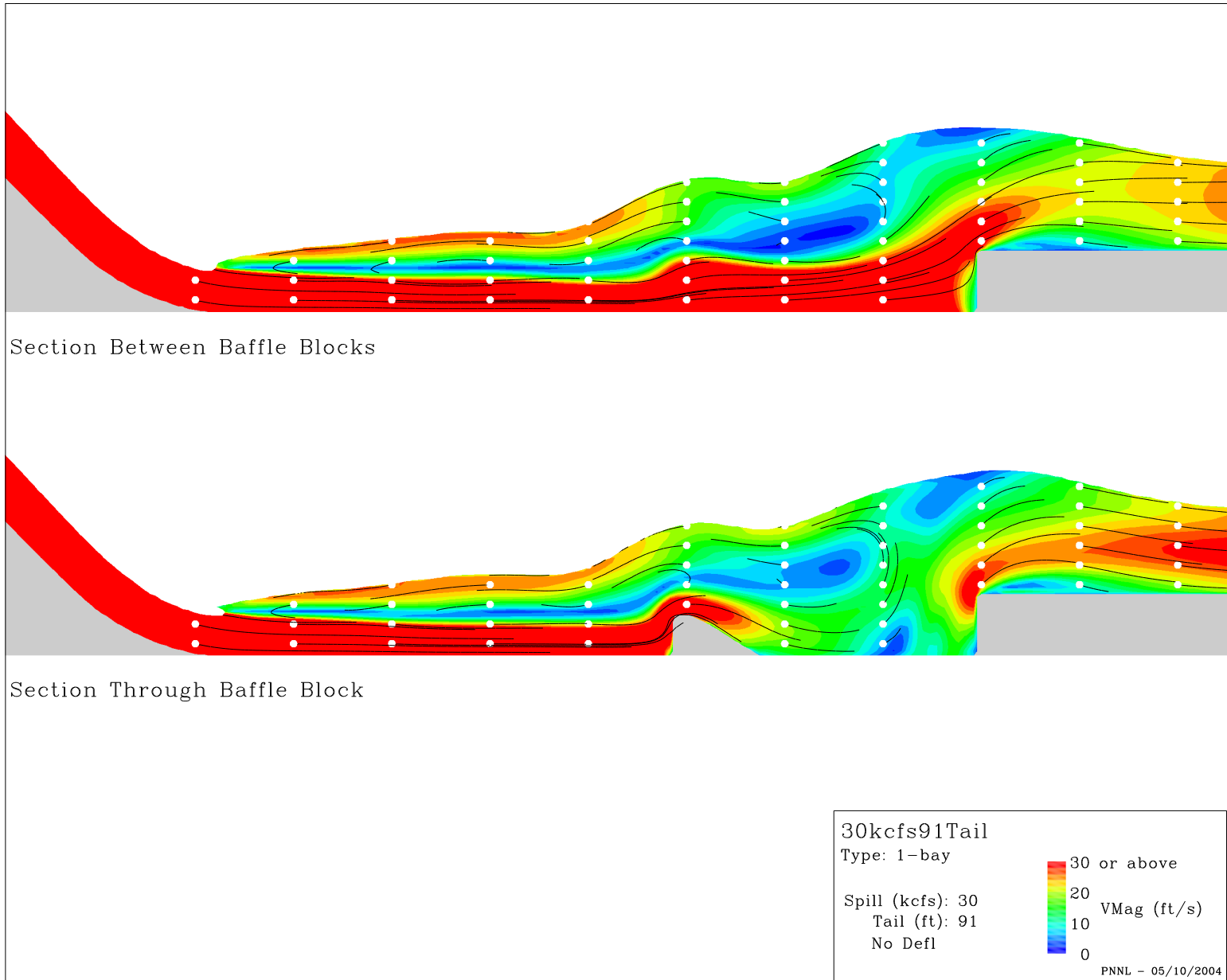


Figure C.1. Results for CFD model of The Dalles Dam tailrace (OneBay30kcs91Tail.eps).

C.3

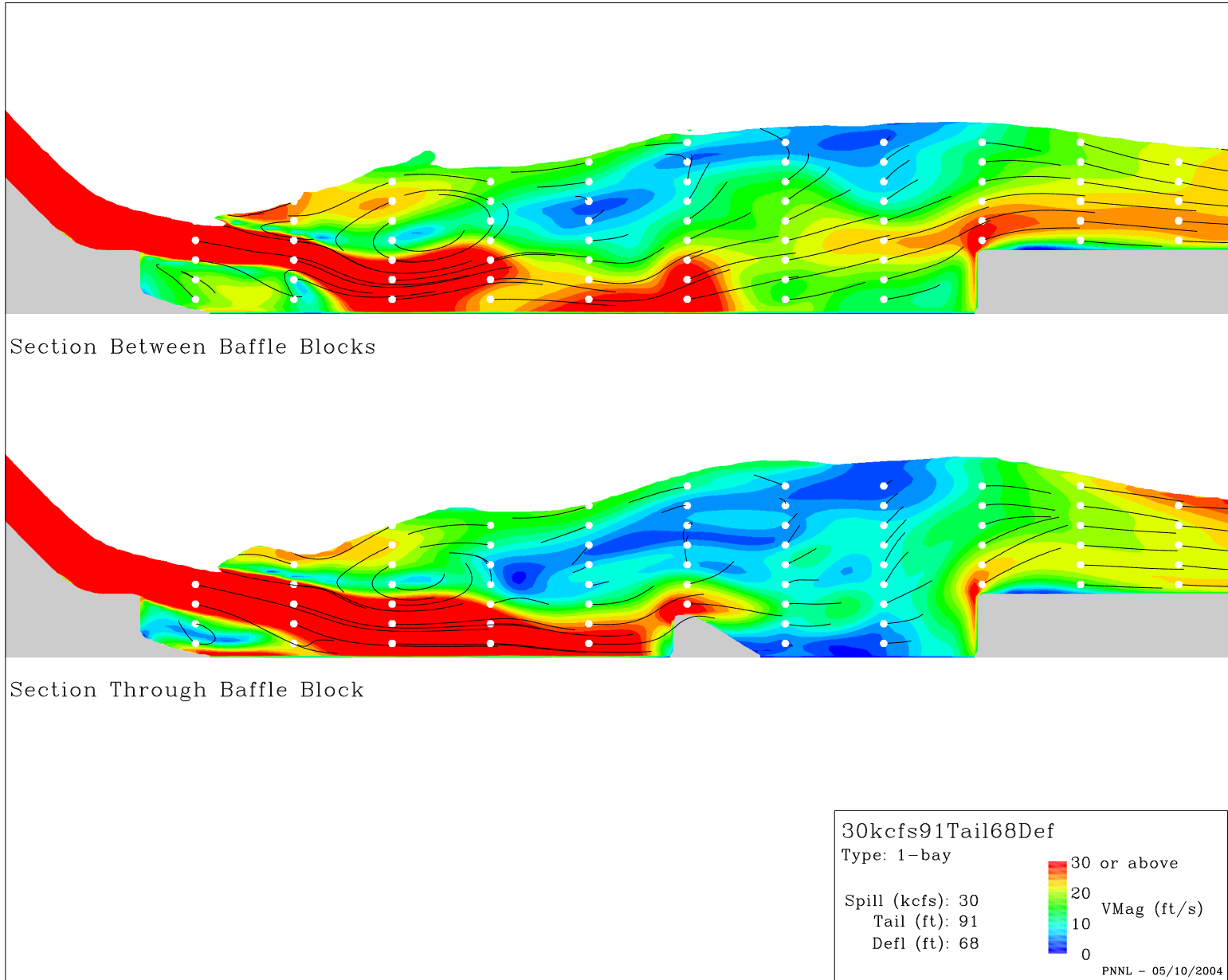


Figure C.2. Results for CFD model of The Dalles Dam tailrace (OneBay30kcfs91Tail68Def.eps).

C.4

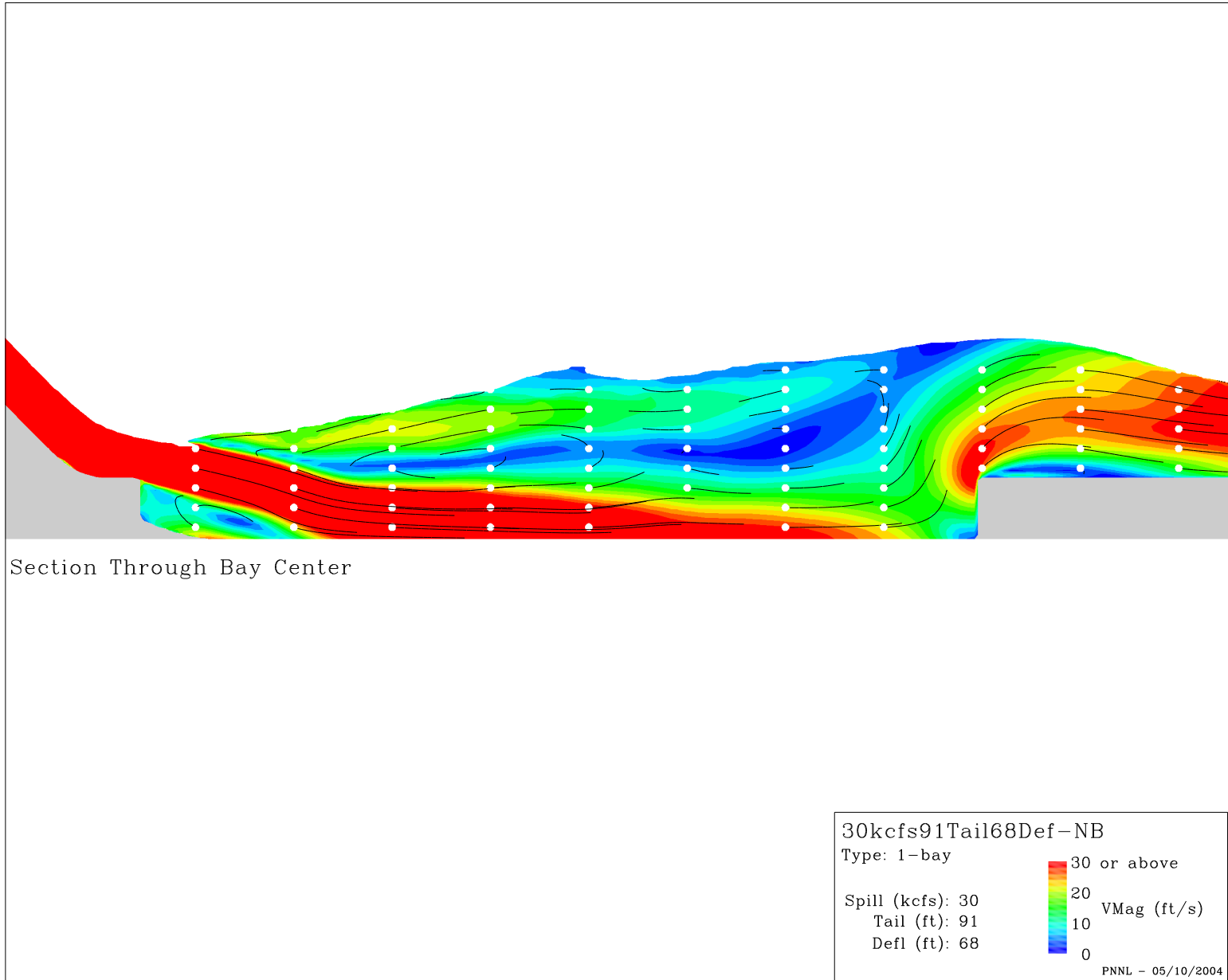


Figure C.3. Results for CFD model of The Dalles Dam tailrace (OneBayNB30kcfs91Tail68Def-NoBaf.eps).

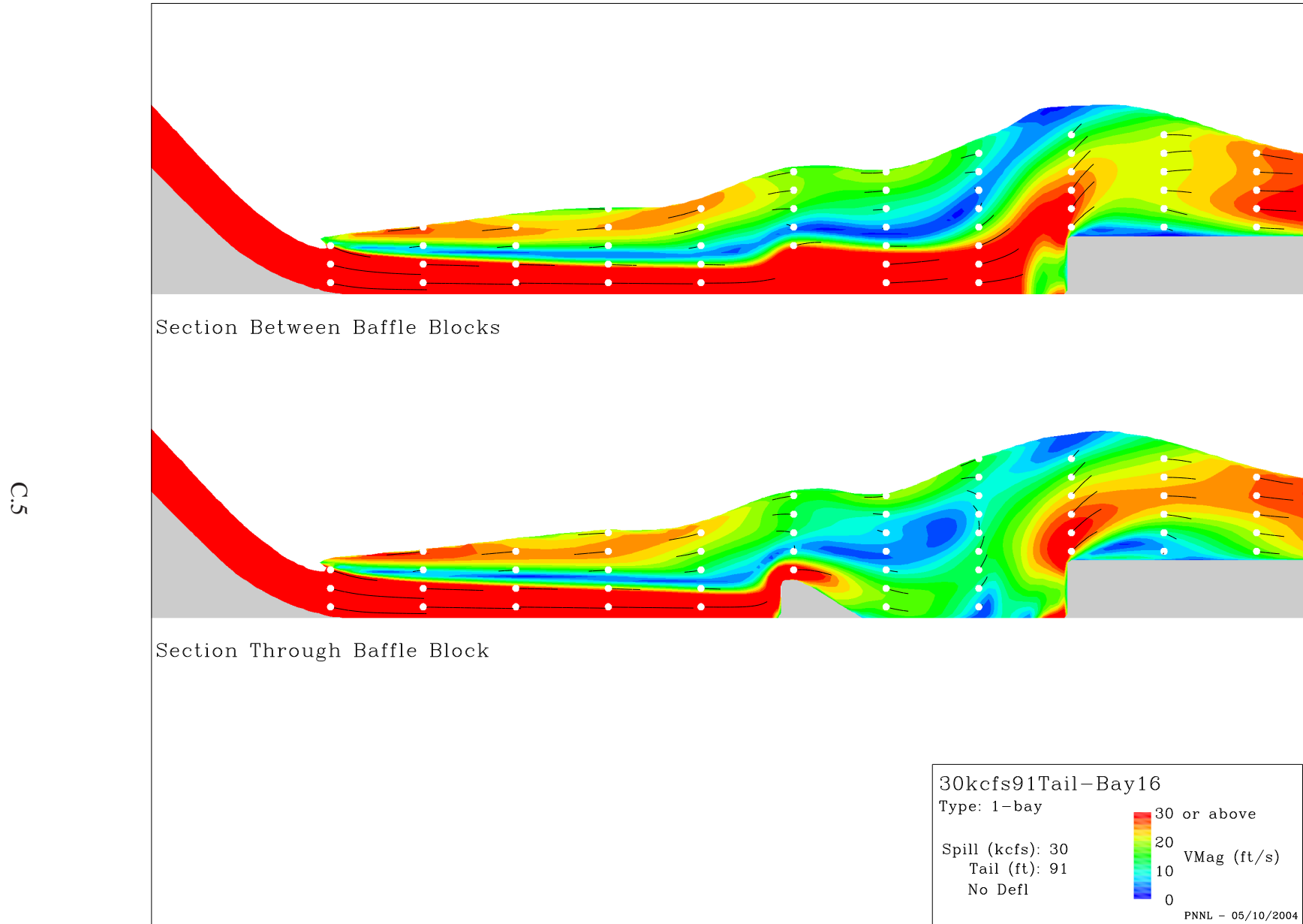


Figure C.4. Results for CFD model of The Dalles Dam tailrace (OneBayB1630kcfs91Tail-Bay16Geom.eps).

C.6

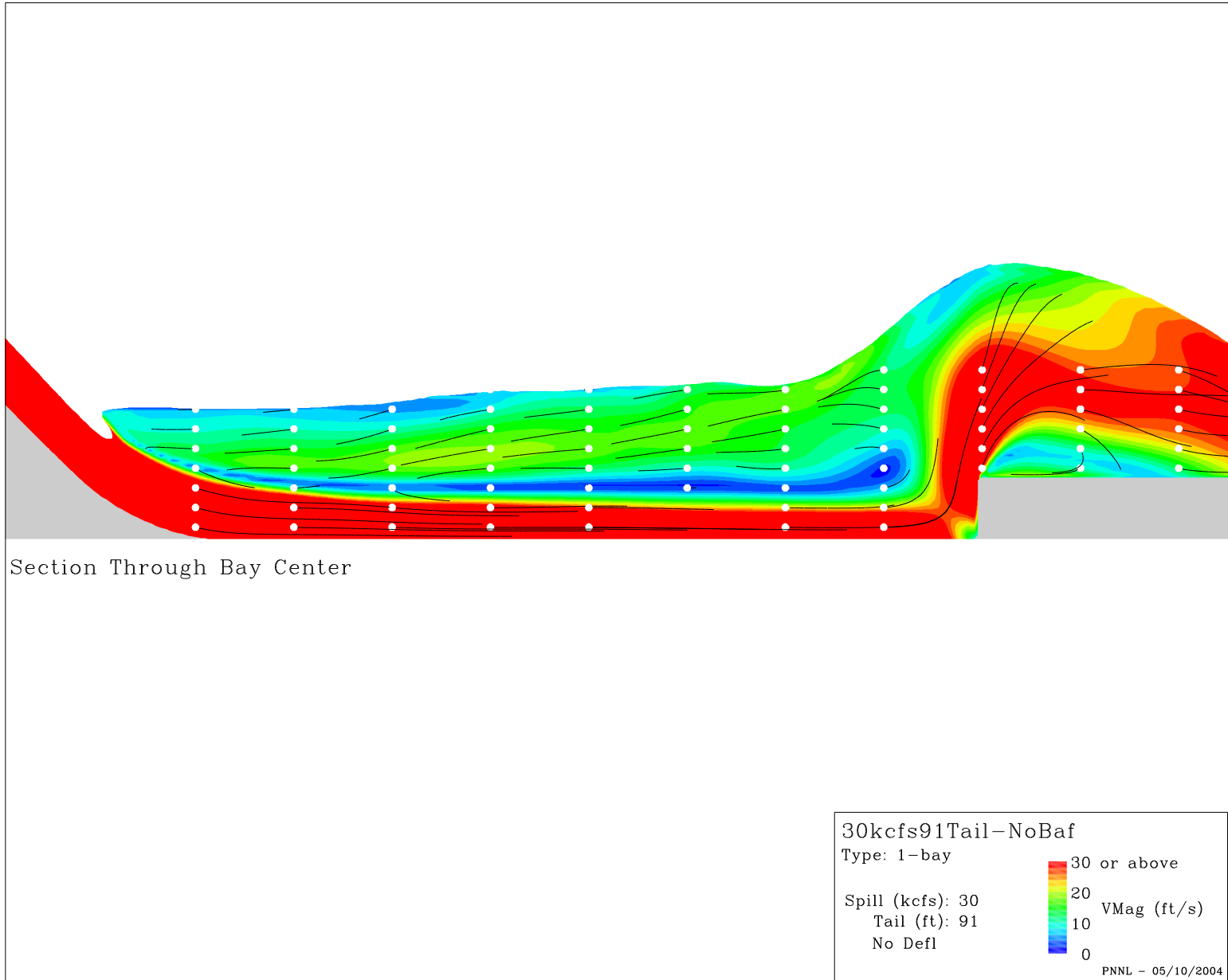


Figure C.5. Results for CFD model of The Dalles Dam tailrace (OneBayNB30kcfs91Tail-NoBaf1.eps).

C.7

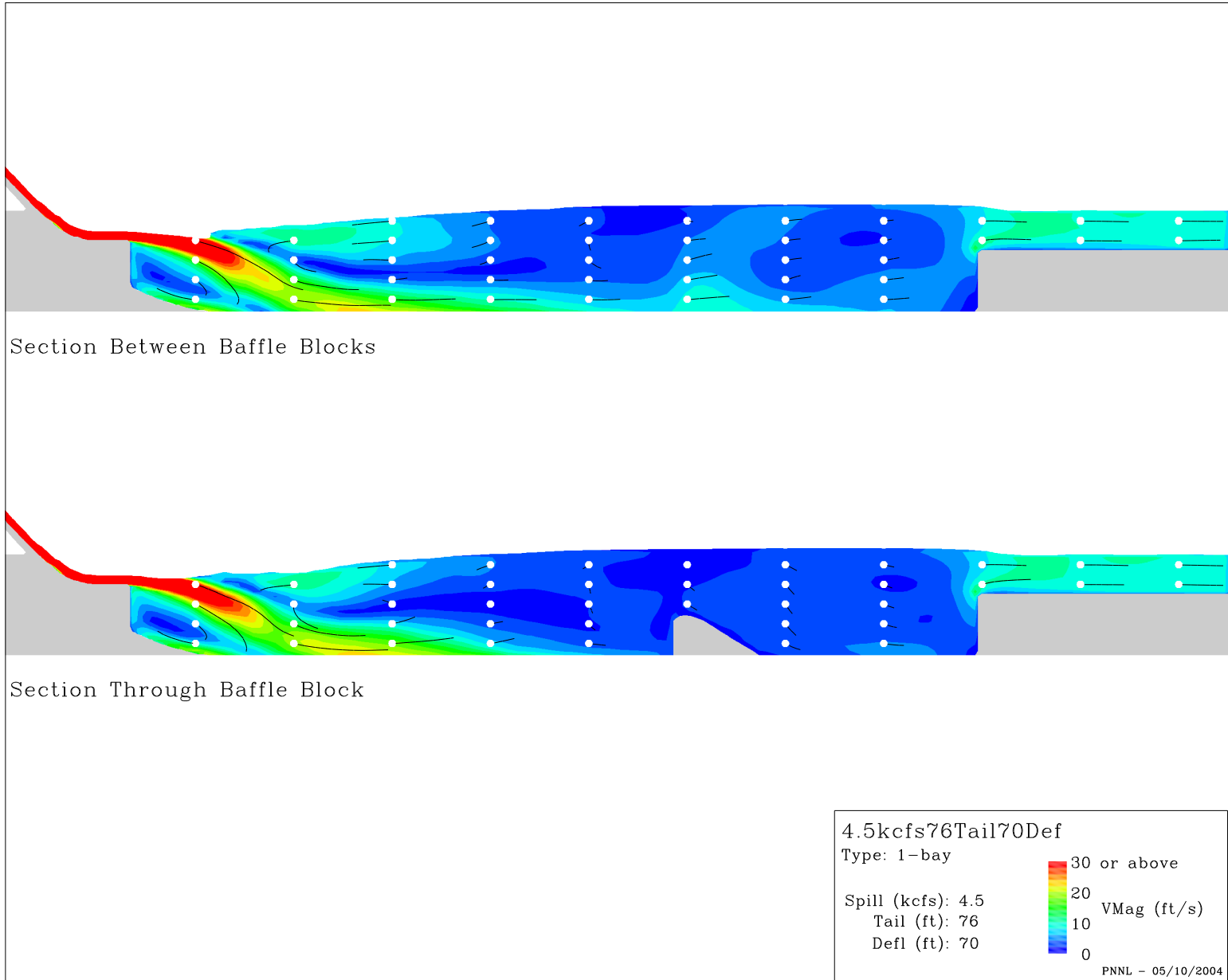


Figure C.6. Results for CFD model of The Dalles Dam tailrace (OneBay4.5kcfs76Tail70Def.eps).

C:8

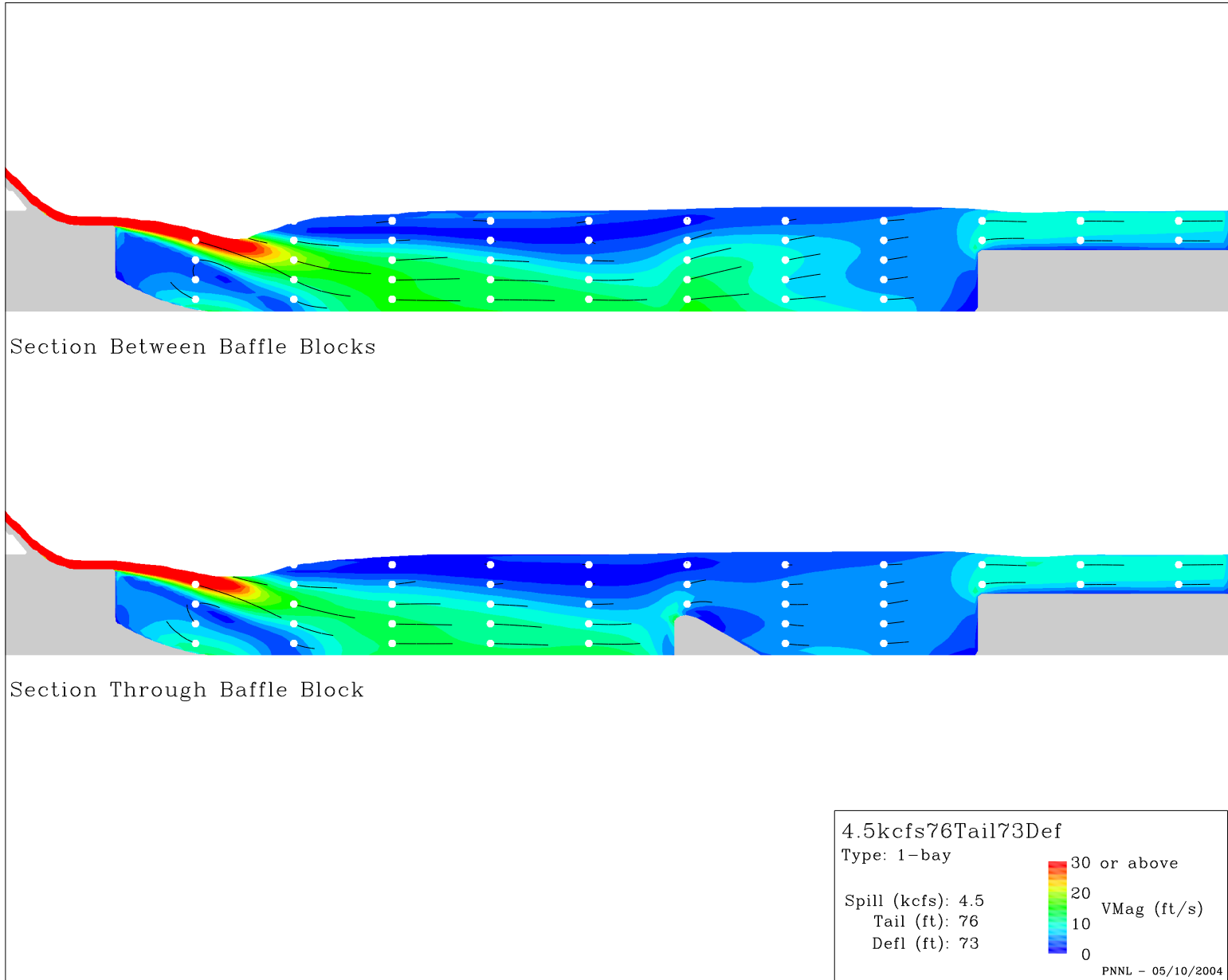


Figure C.7. Results for CFD model of The Dalles Dam tailrace (OneBay4.5kcfs76Tail73Def.eps).

C.9

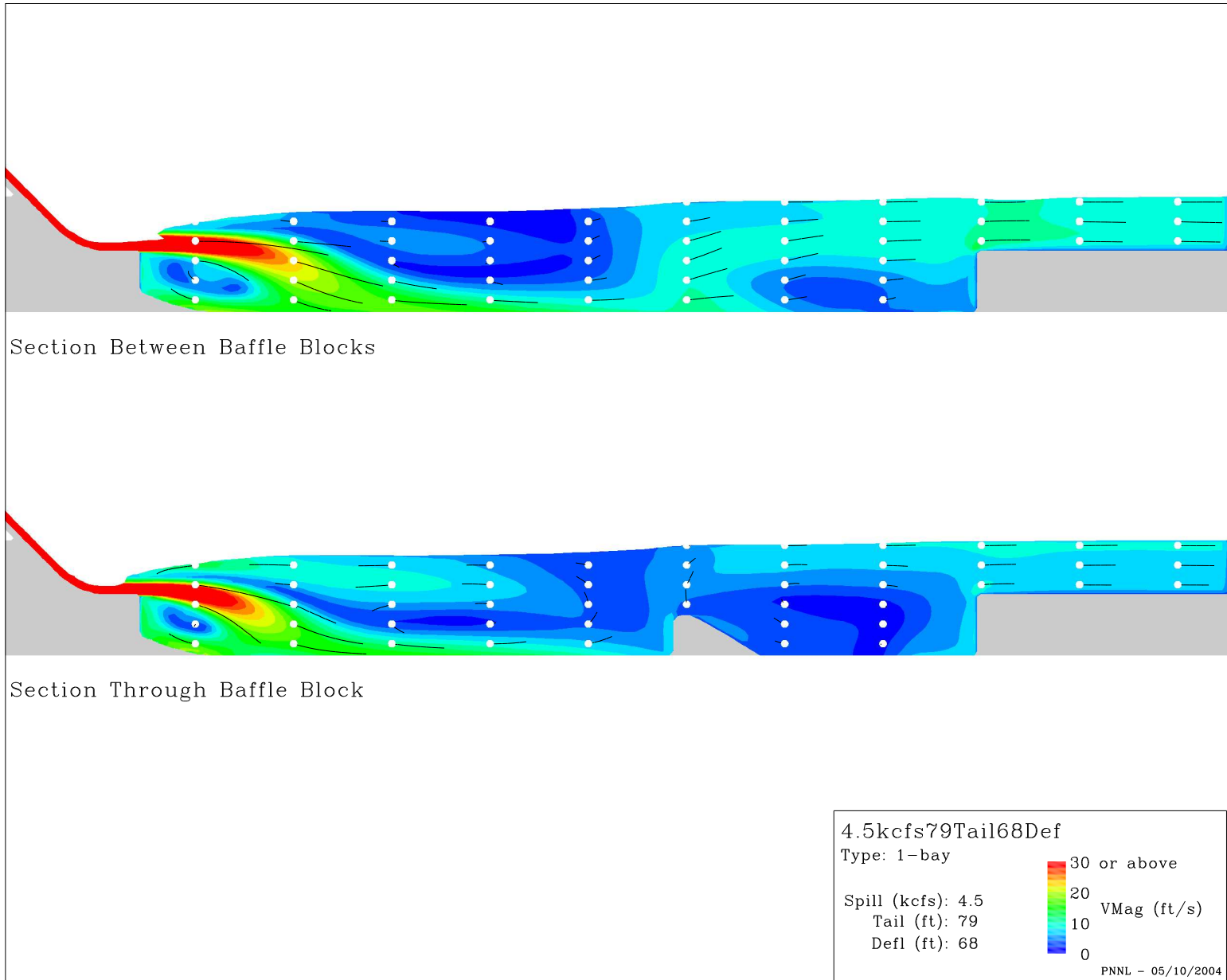


Figure C.8. Results for CFD model of The Dalles Dam tailrace (OneBay4.5kcfs79Tail68Def.eps).

C.10

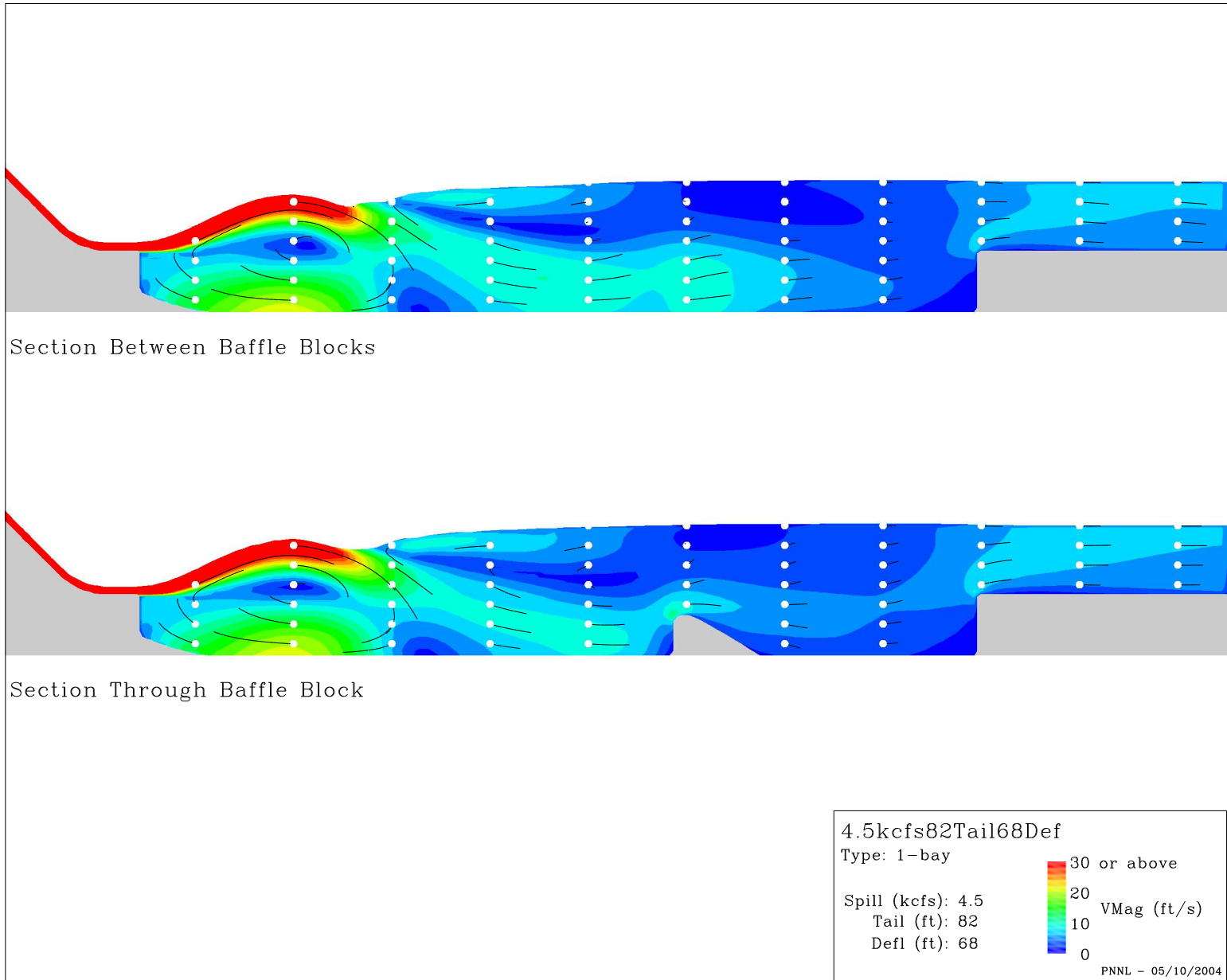


Figure C.9. Results for CFD model of The Dalles Dam tailrace (OneBay4.5kcfs82Tail68Def.eps).

C.11

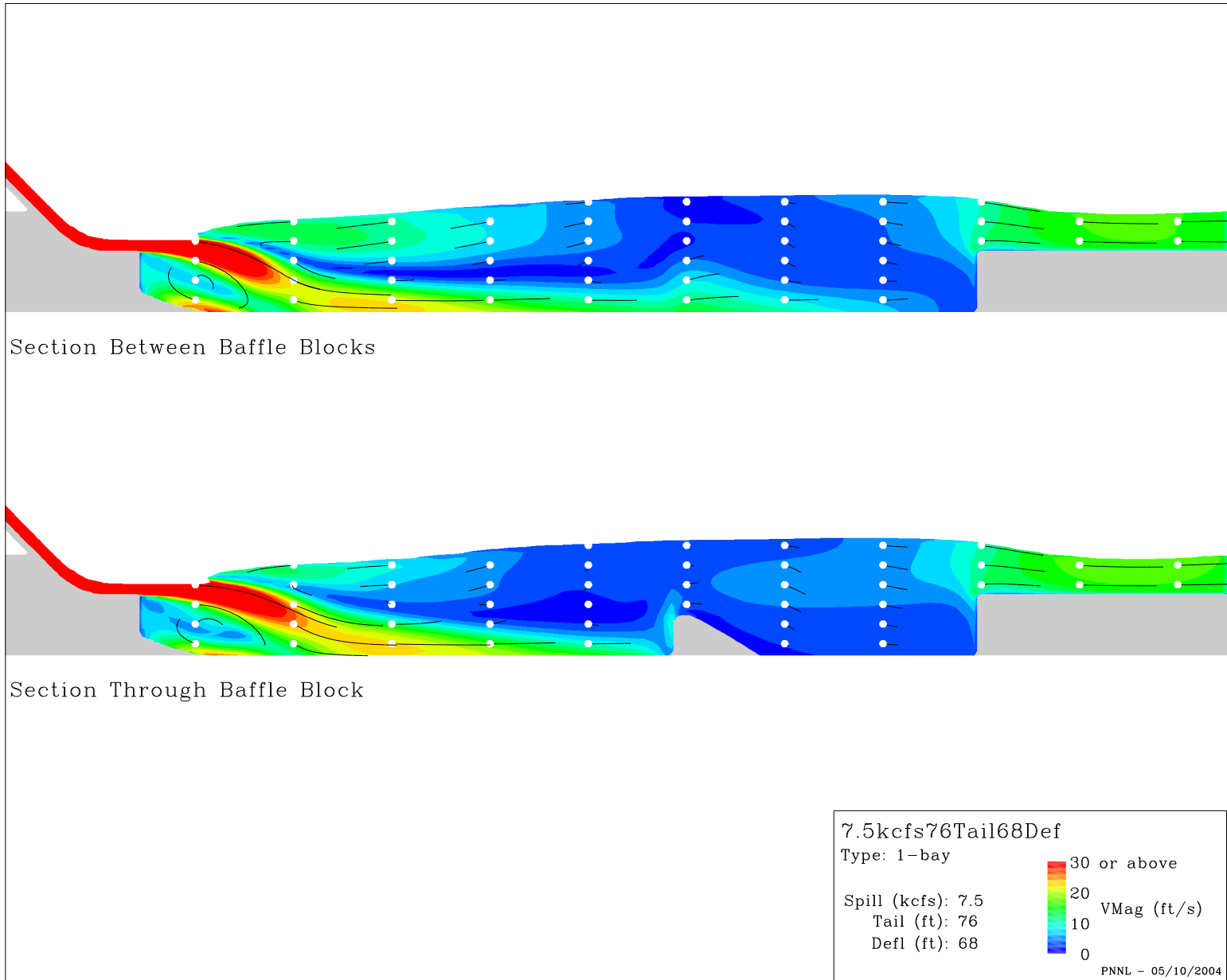


Figure C.10. Results for CFD model of The Dalles Dam tailrace (OneBay7.5kcfs76Tail68Def.eps).

C.12

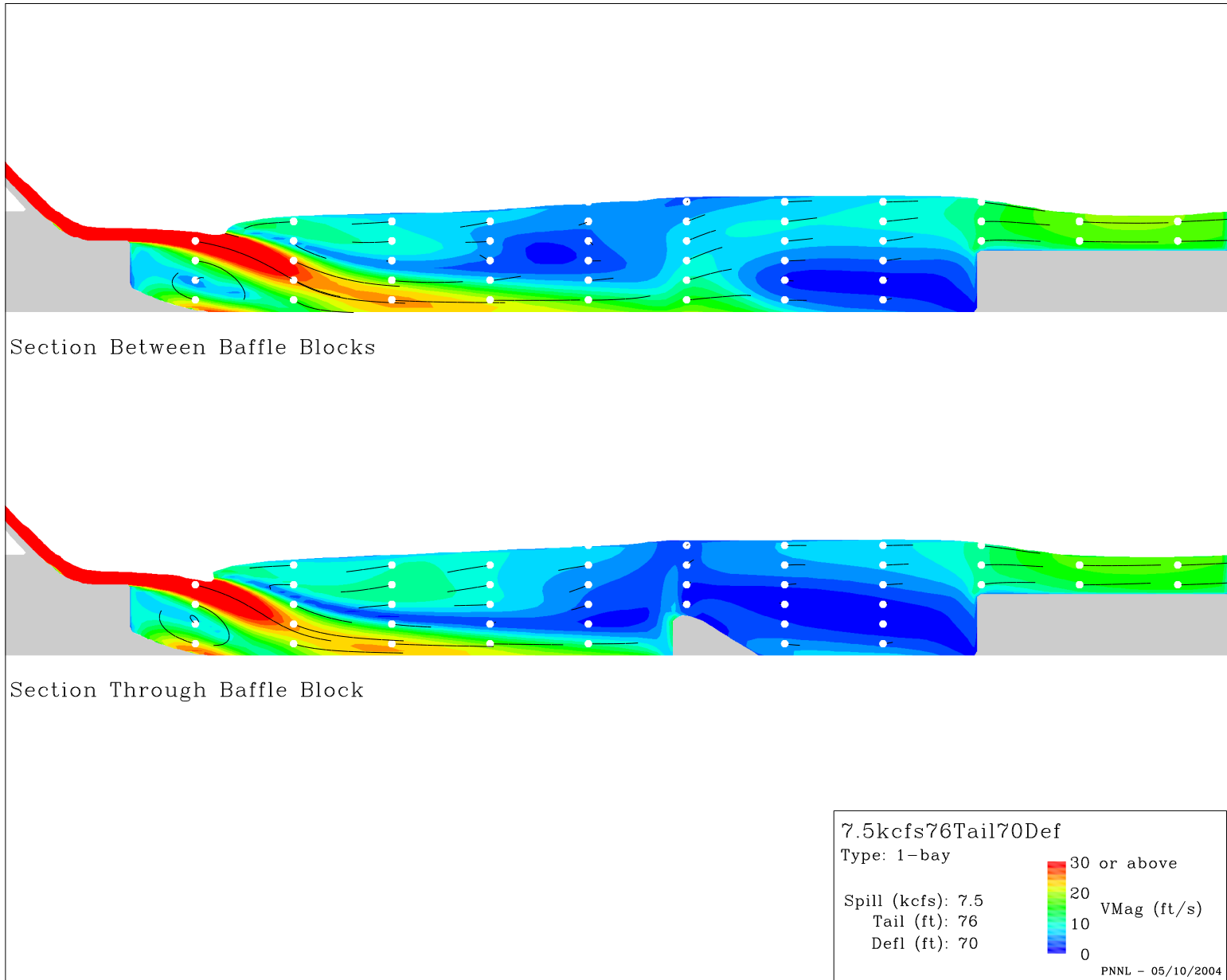


Figure C.11. Results for CFD model of The Dalles Dam tailrace (OneBay7.5kcfs76Tail70Def.eps).

C.13

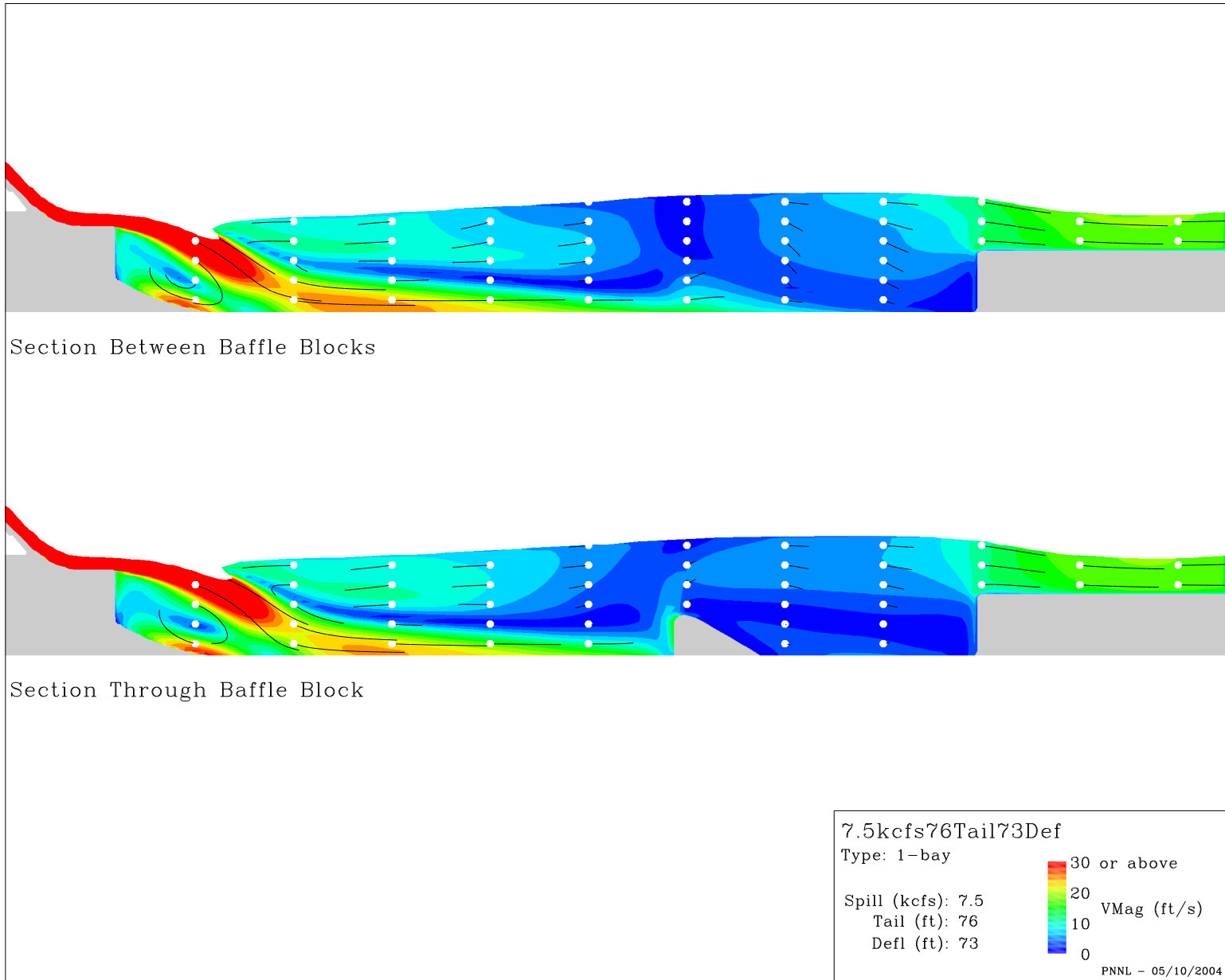


Figure C.12. Results for CFD model of The Dalles Dam tailrace (OneBay7.5kcfs76Tail73Def.eps).

Appendix D

2-Bay Simulations

Appendix D – 2-Bay Simulations

The following appendix summarizes simulation results from a single spillway bay (Figure A.3 displays the domain extent). In all figures particle tracks of equal duration have been added to illustrate the direction of flow. The circles indicate the starting position for each track and the track length is proportional to the velocity magnitude.

D.2

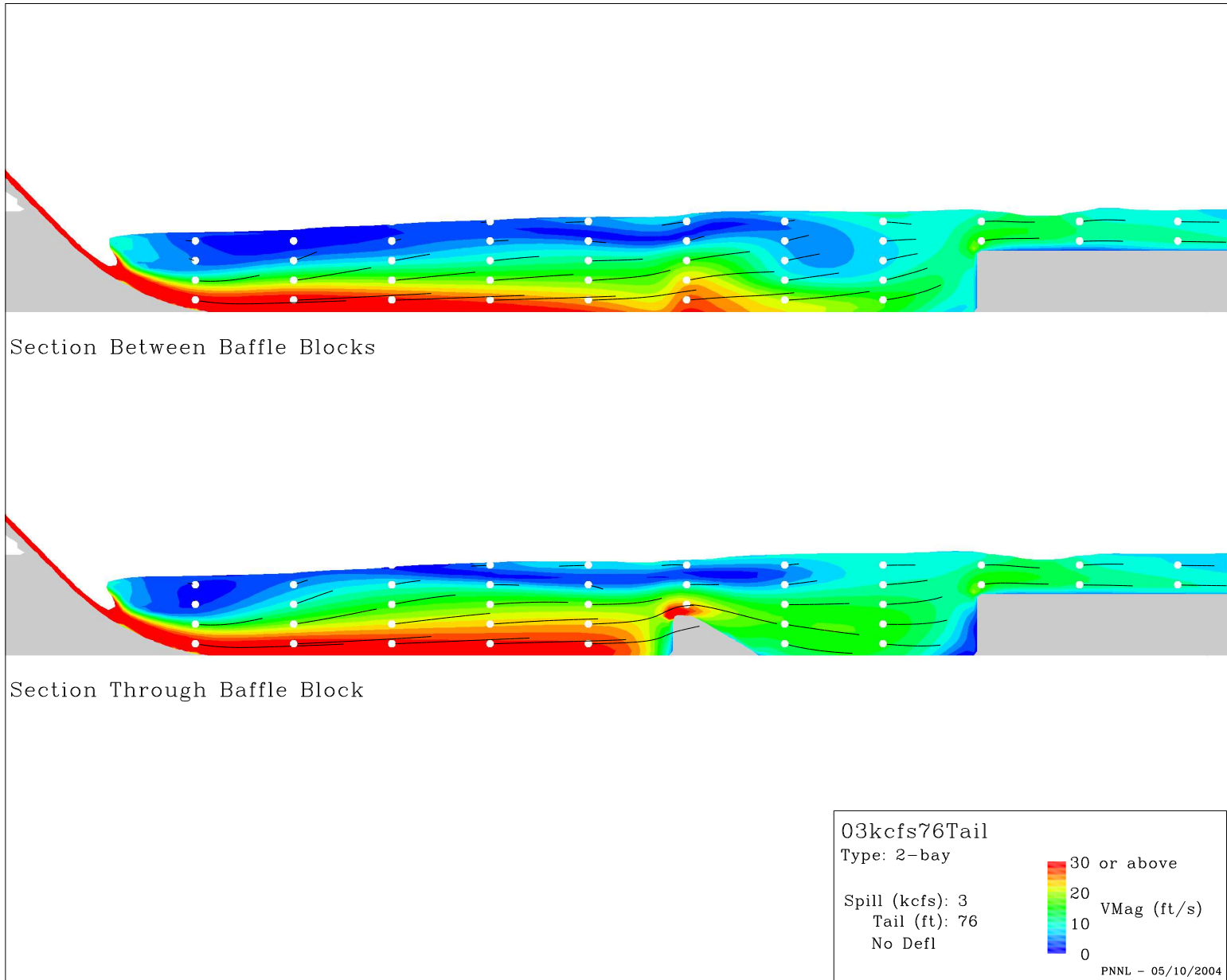


Figure D.1. Results for CFD model of The Dalles Dam tailrace (OneBayFVF03kcfs76Tail.eps).

D.3

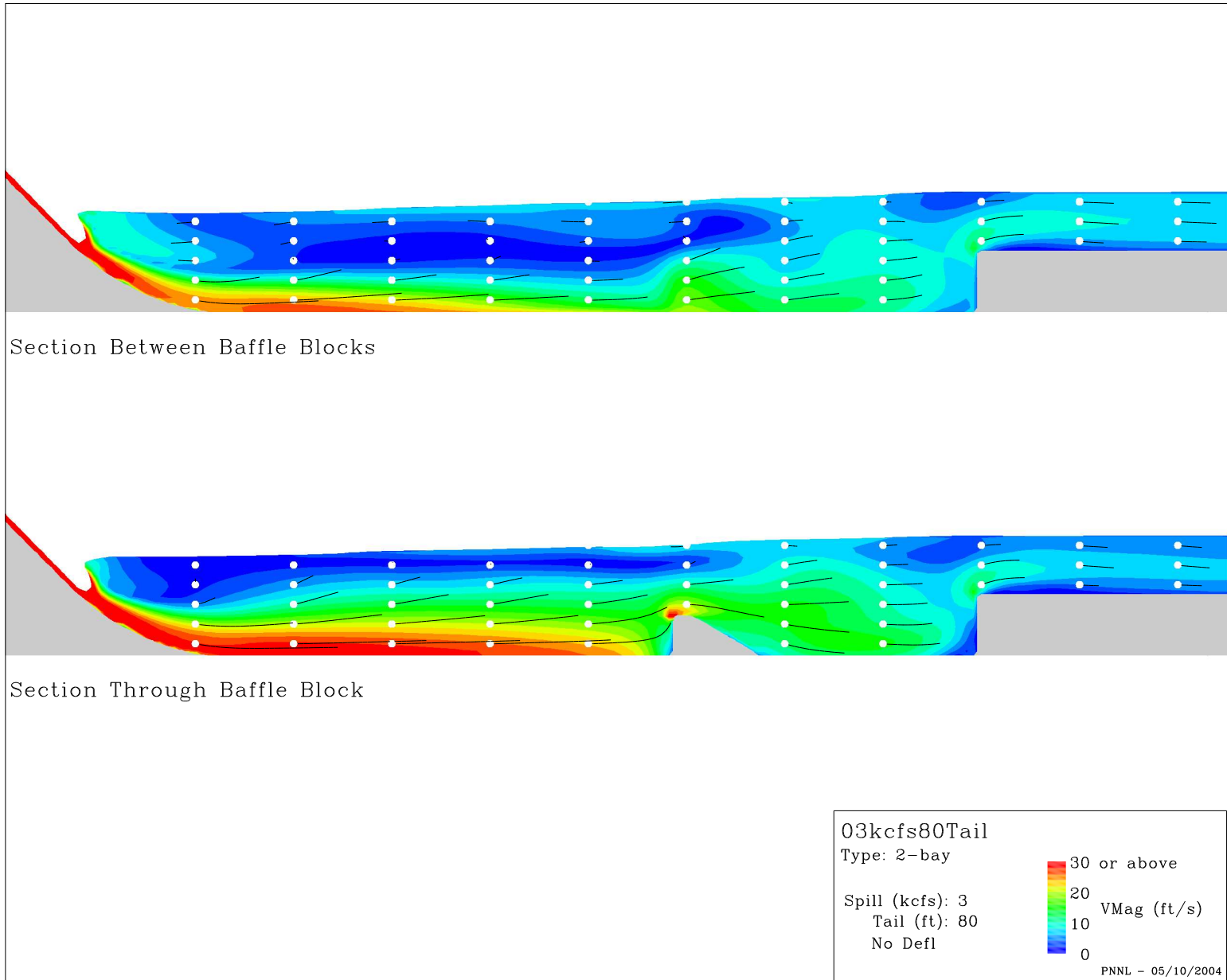


Figure D.2. Results for CFD model of The Dalles Dam tailrace (OneBayFVF03kcfs80Tail.eps).

D.4

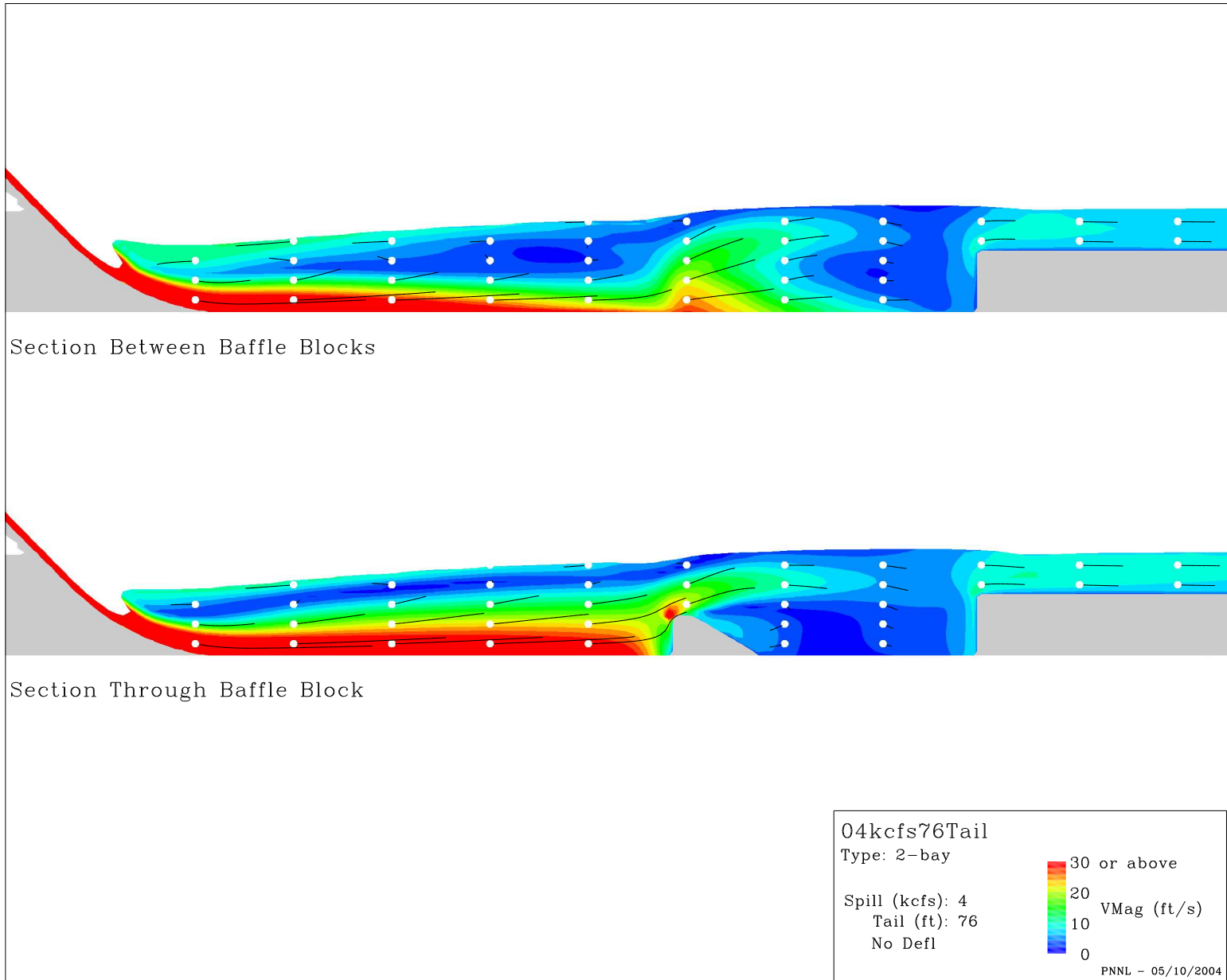


Figure D.3. Results for CFD model of The Dalles Dam tailrace (OneBayFVF04kcfs76Tail.eps).

D.5

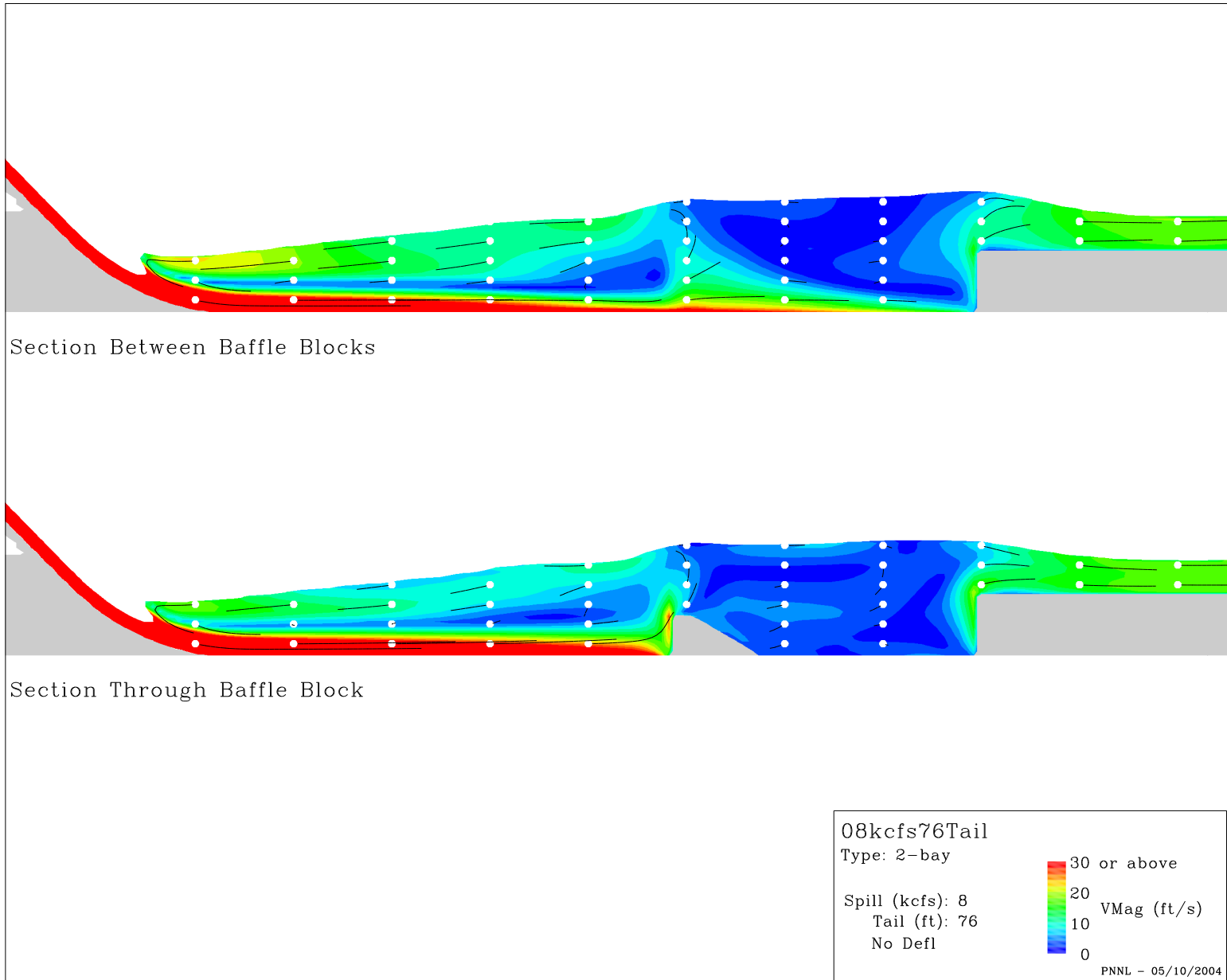


Figure D.4. Results for CFD model of The Dalles Dam tailrace (OneBay08kcfs76Tail.eps).

D.6

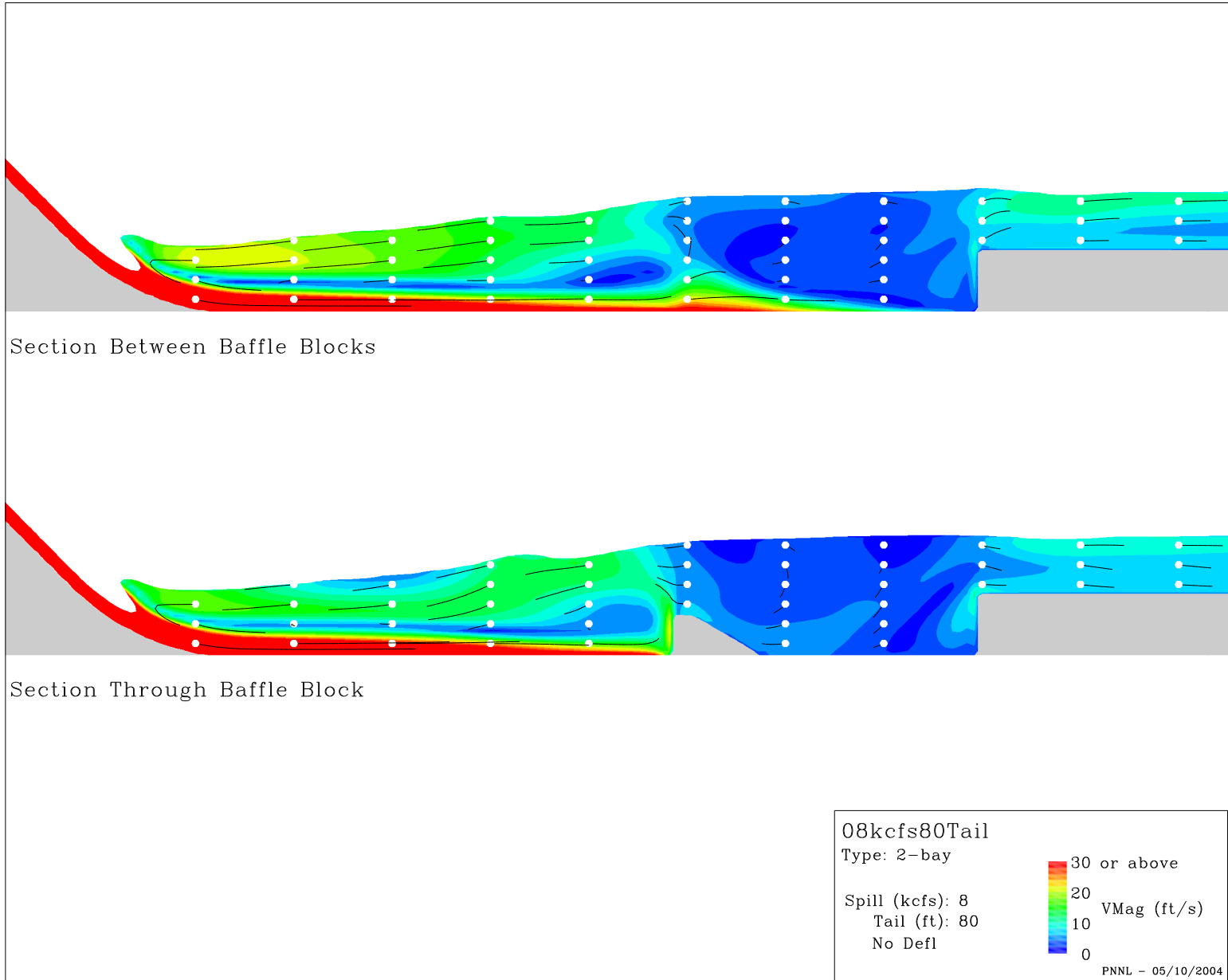


Figure D.5. Results for CFD model of The Dalles Dam tailrace (OneBay08kcfs80Tail.eps).

D.7

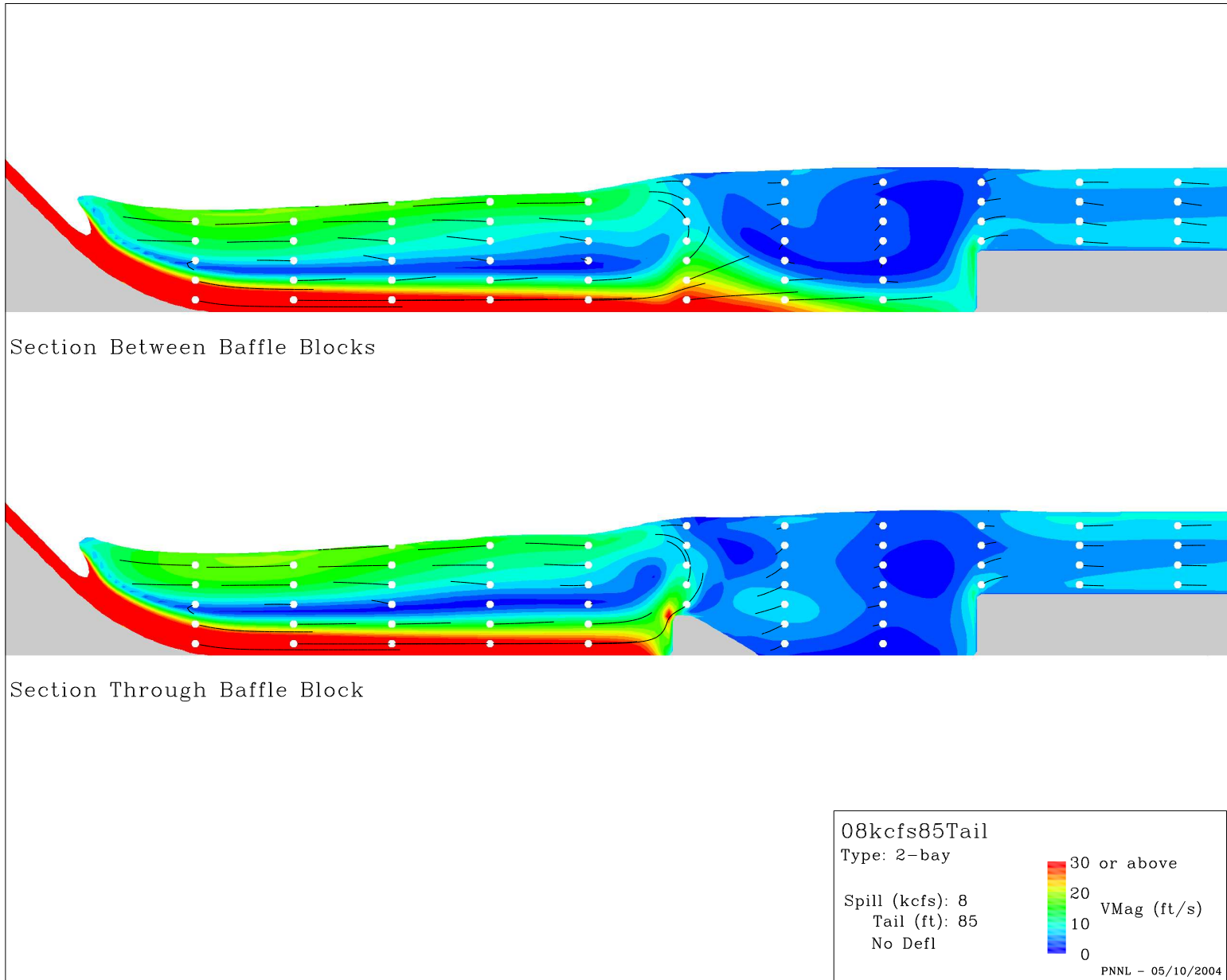


Figure D.6. Results for CFD model of The Dalles Dam tailrace (OneBay08kcfs85Tail.eps).

D.8

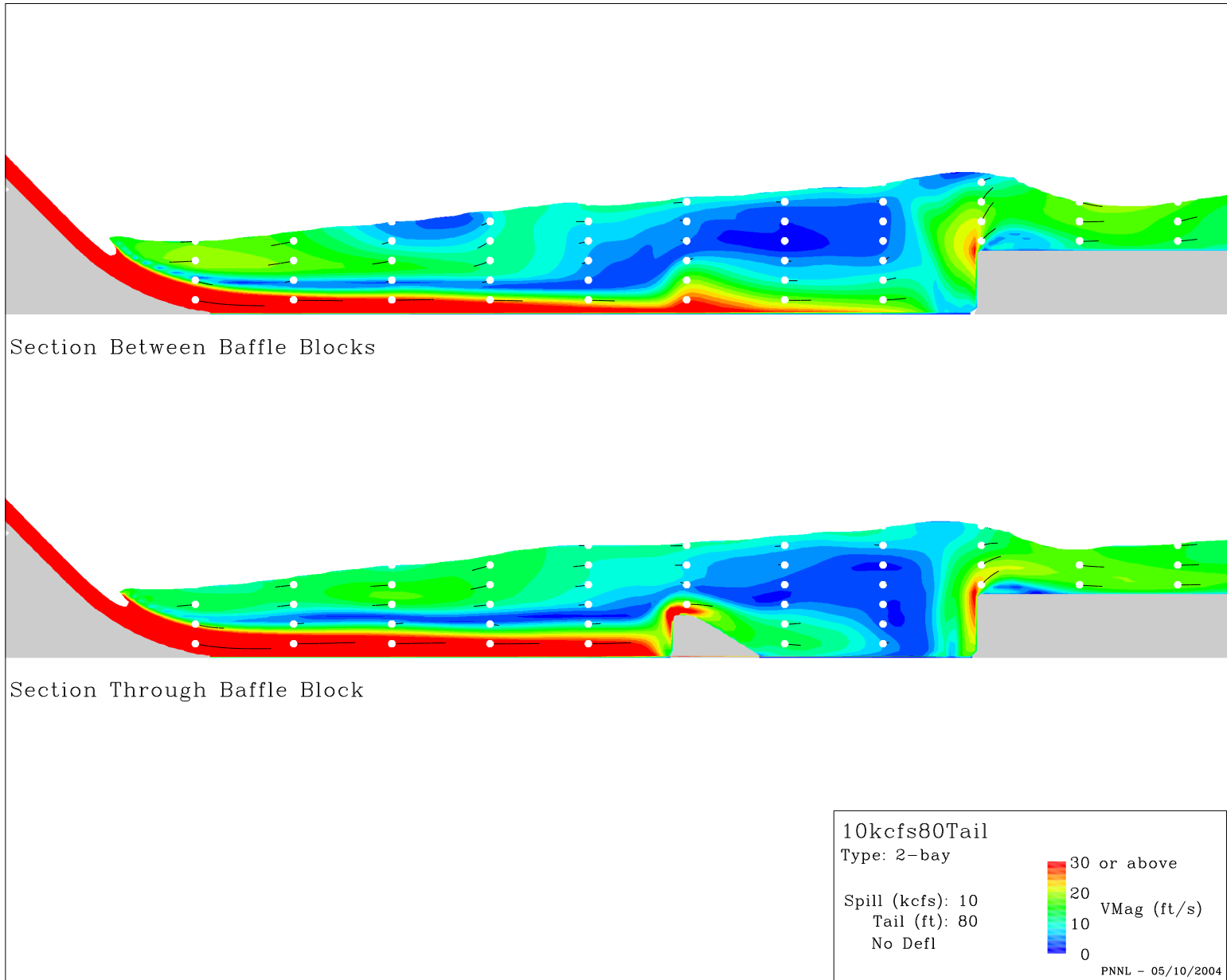


Figure D.7. Results for CFD model of The Dalles Dam tailrace (OneBay10kcfs80Tail.eps).

D.9

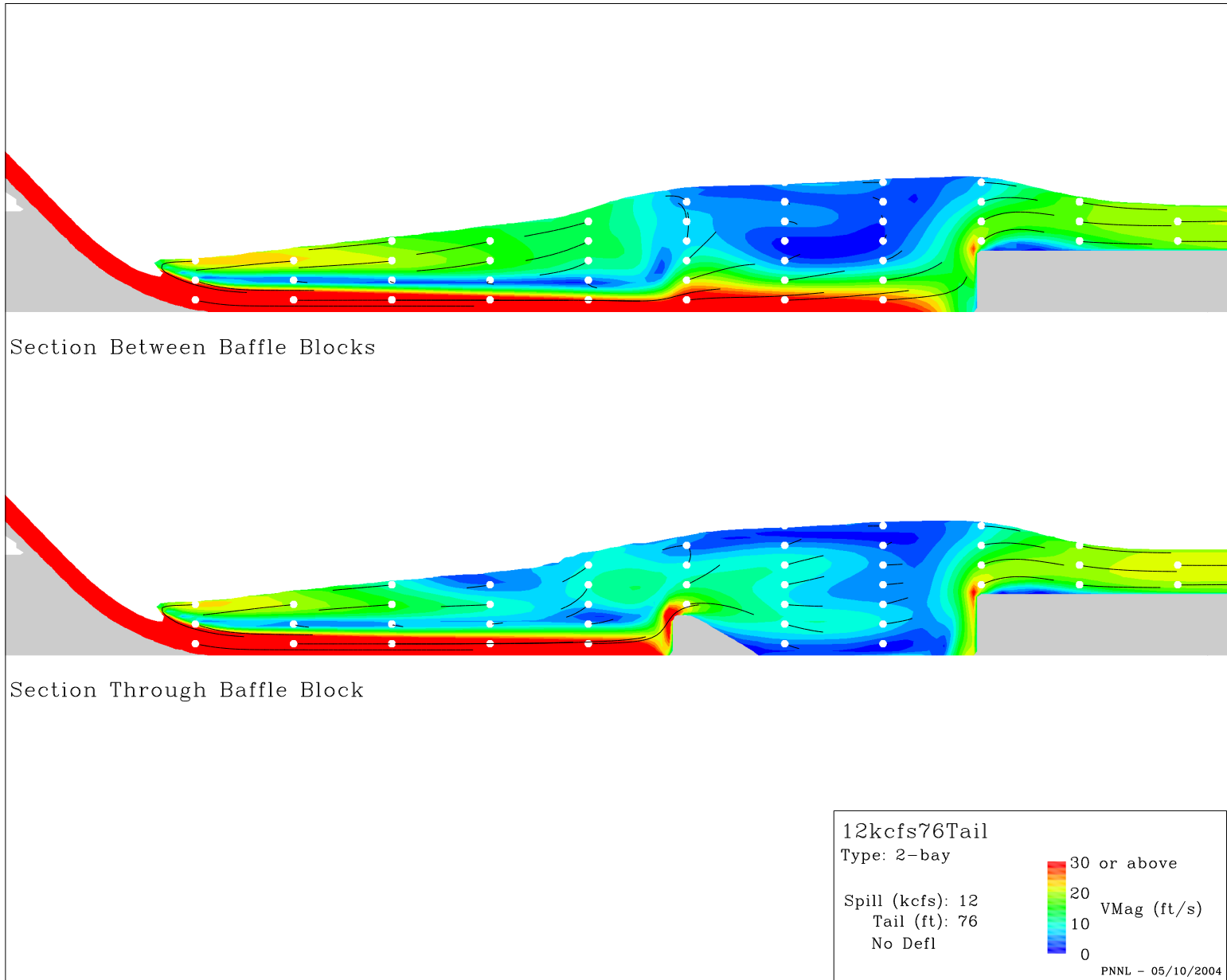


Figure D.8. Results for CFD model of The Dalles Dam tailrace (OneBay12kcfs76Tail.eps).

D.10

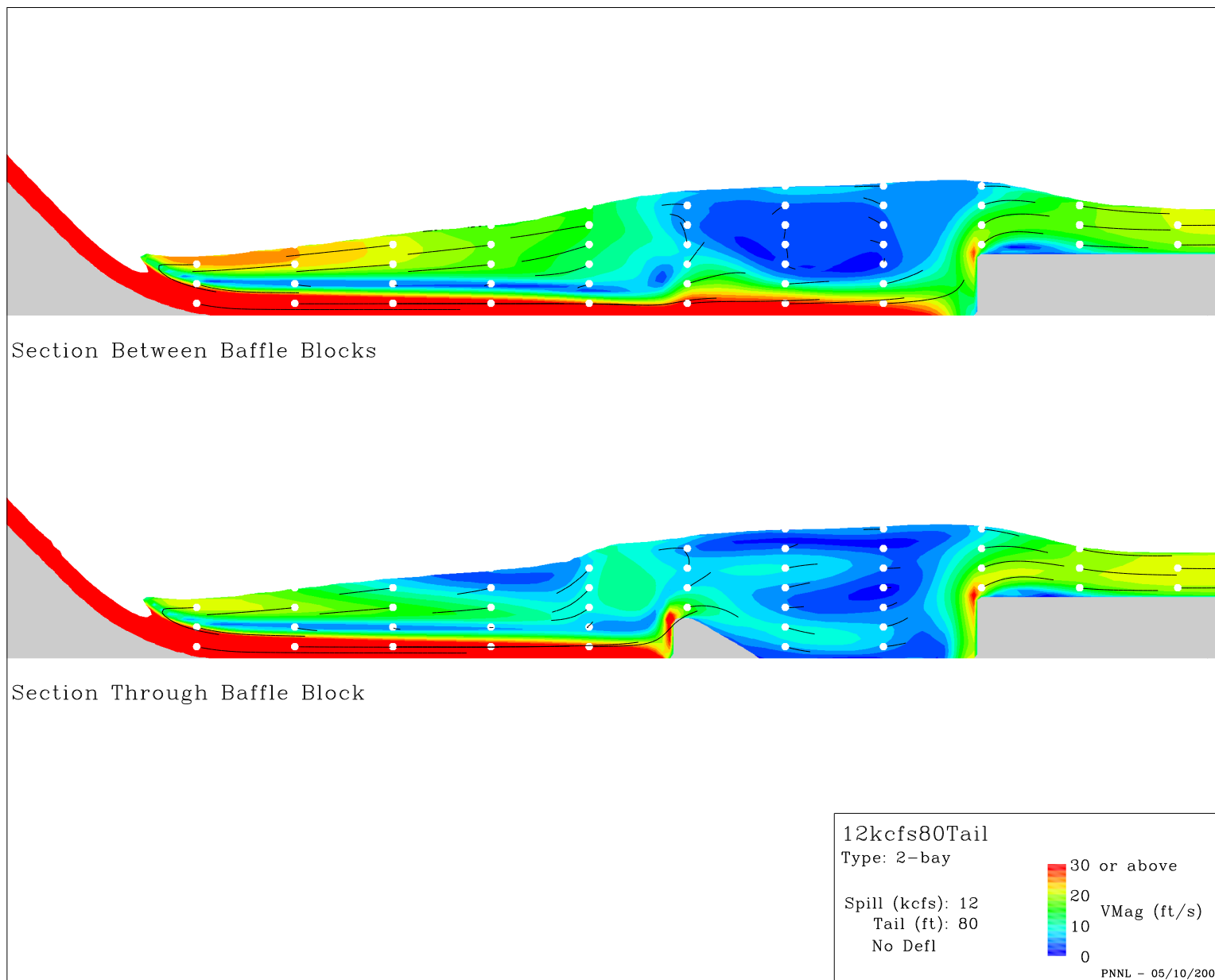


Figure D.9. Results for CFD model of The Dalles Dam tailrace (OneBay12kcfs80Tail.eps).

D.11

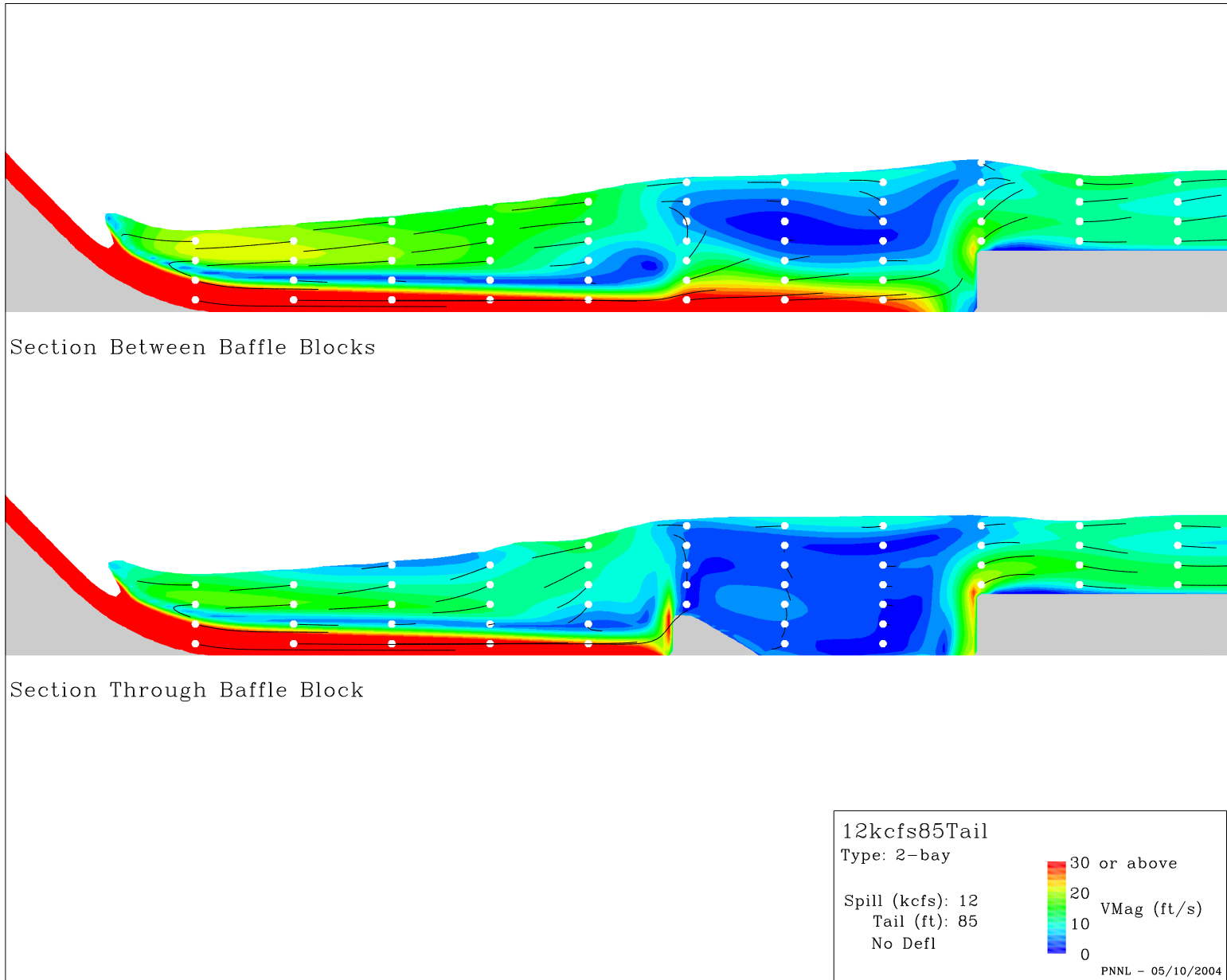


Figure D.10. Results for CFD model of The Dalles Dam tailrace (OneBay12kcfs85Tail.eps).

D.12

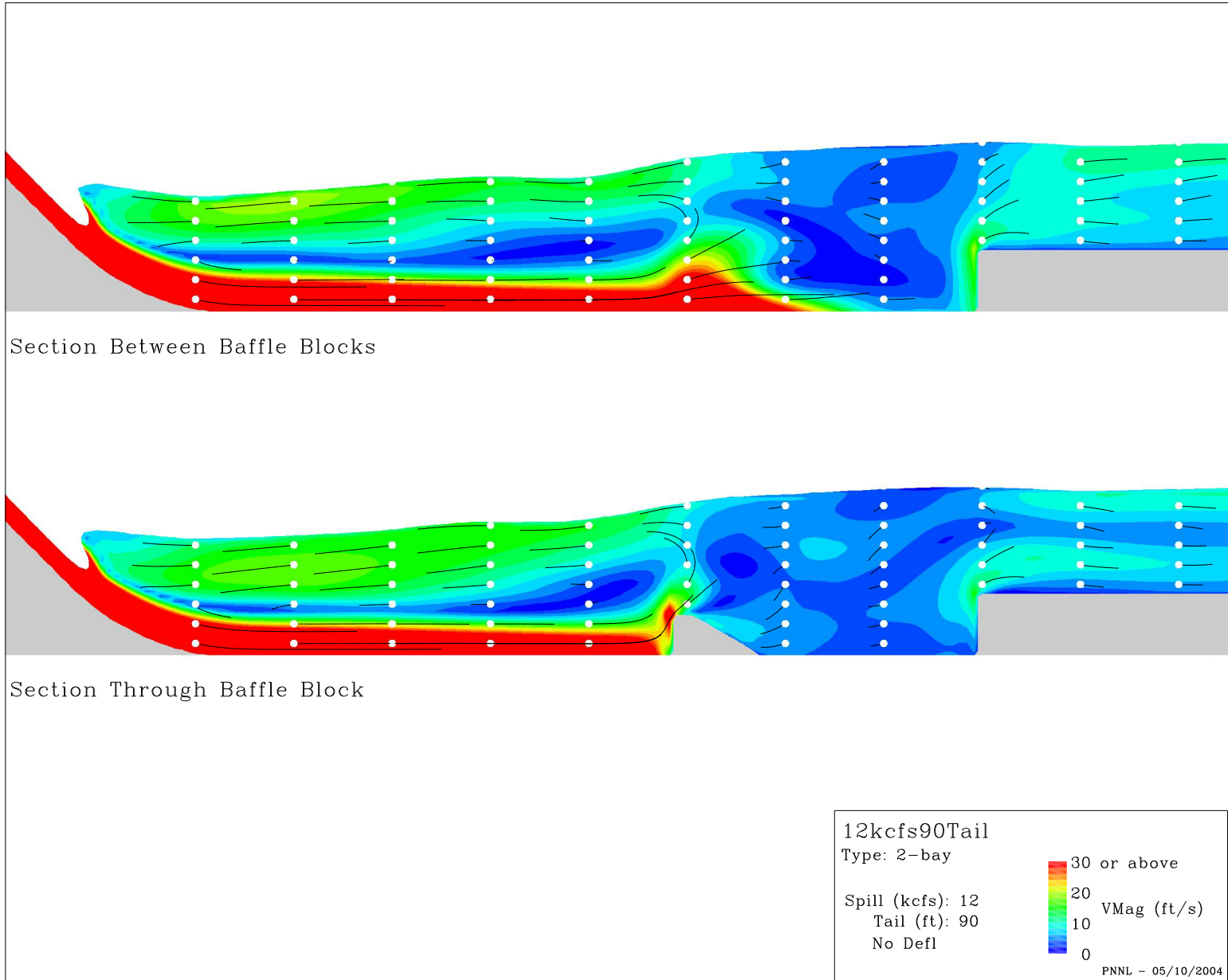


Figure D.11. Results for CFD model of The Dalles Dam tailrace (OneBay12kcfs90Tail.eps).

D.13

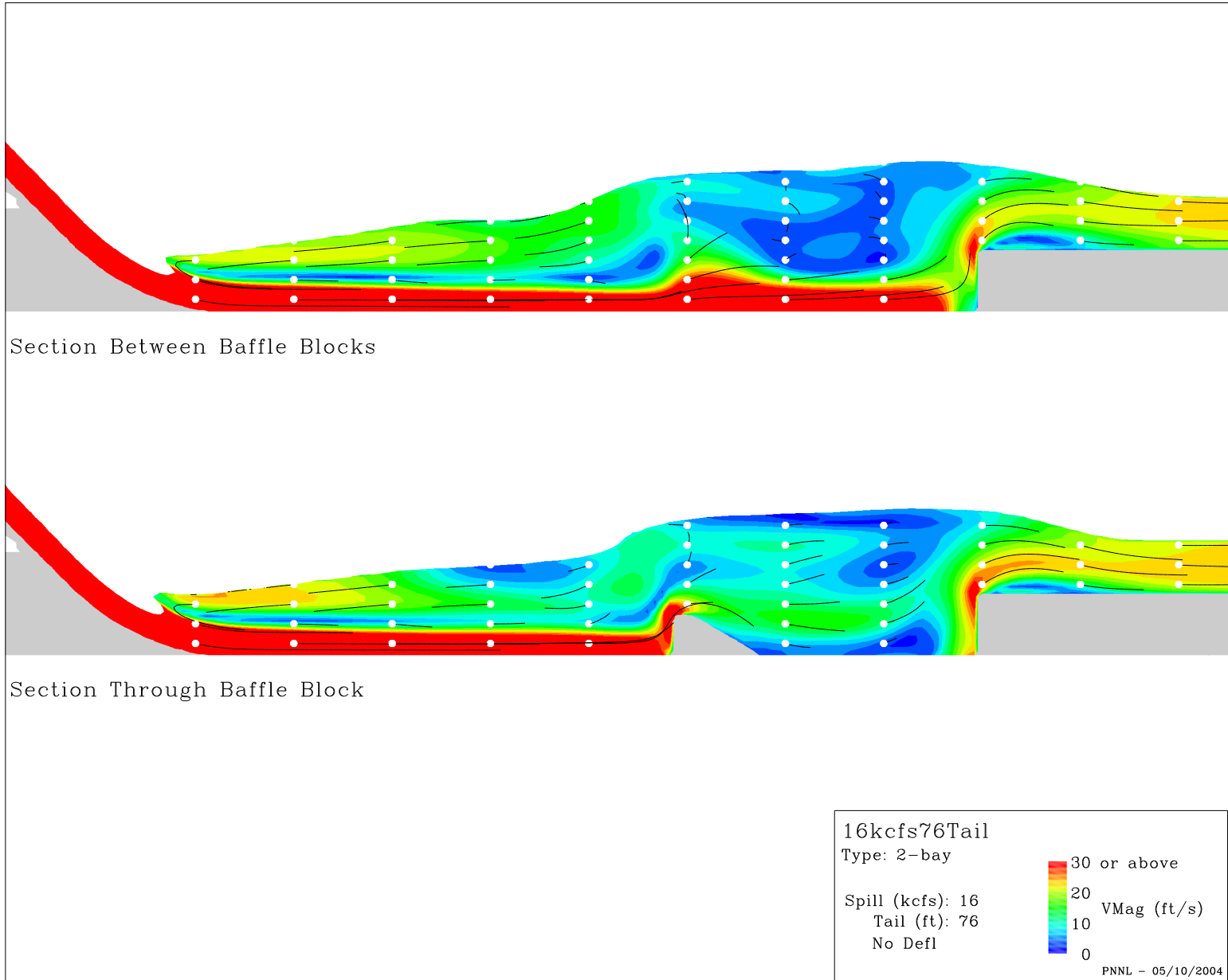


Figure D.12. Results for CFD model of The Dalles Dam tailrace (OneBay16kcfs76Tail.eps).

D.14

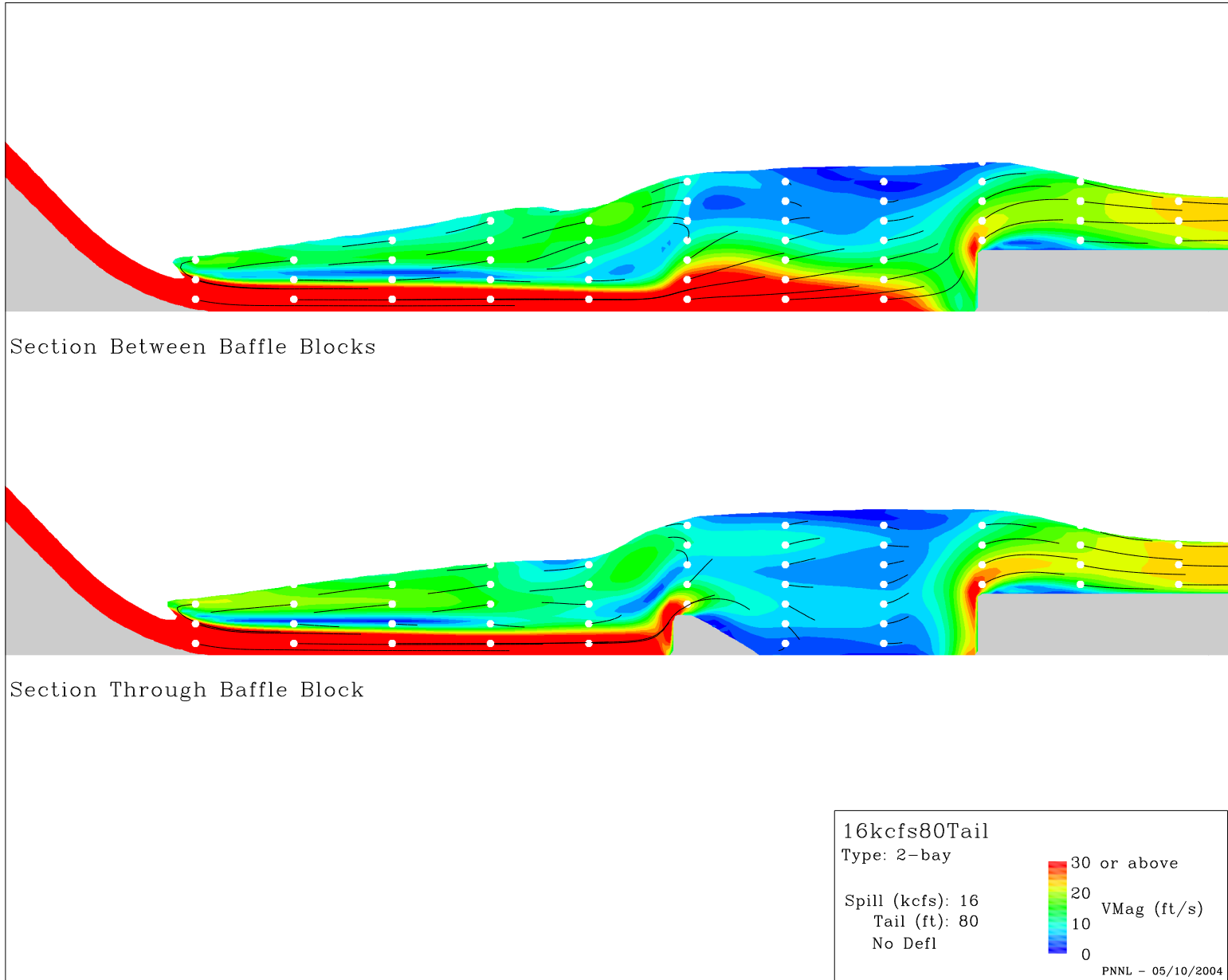


Figure D.13. Results for CFD model of The Dalles Dam tailrace (OneBay16kcfs80Tail.eps).

D.15

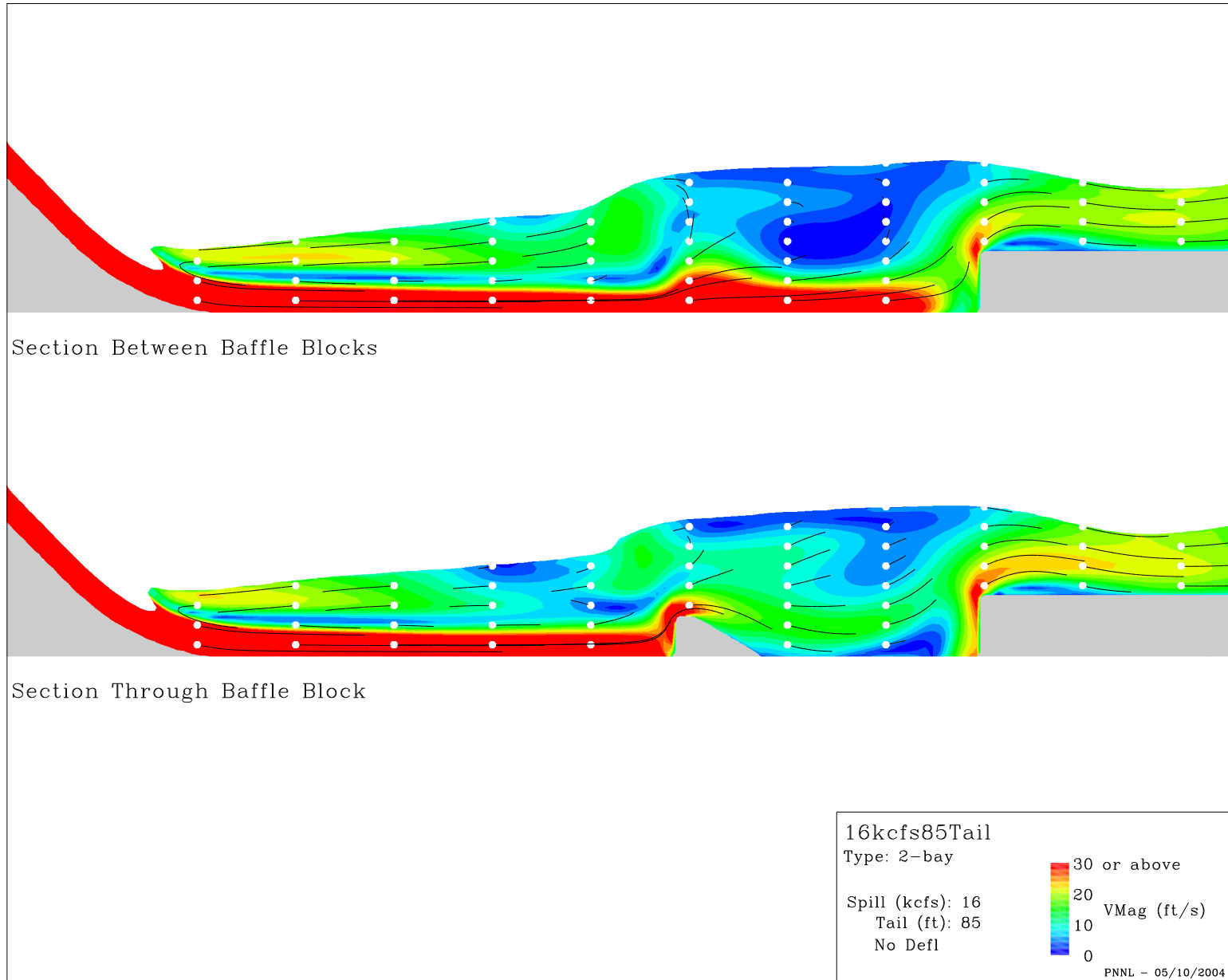


Figure D.14. Results for CFD model of The Dalles Dam tailrace (OneBay16kcfs85Tail.eps).

D.16

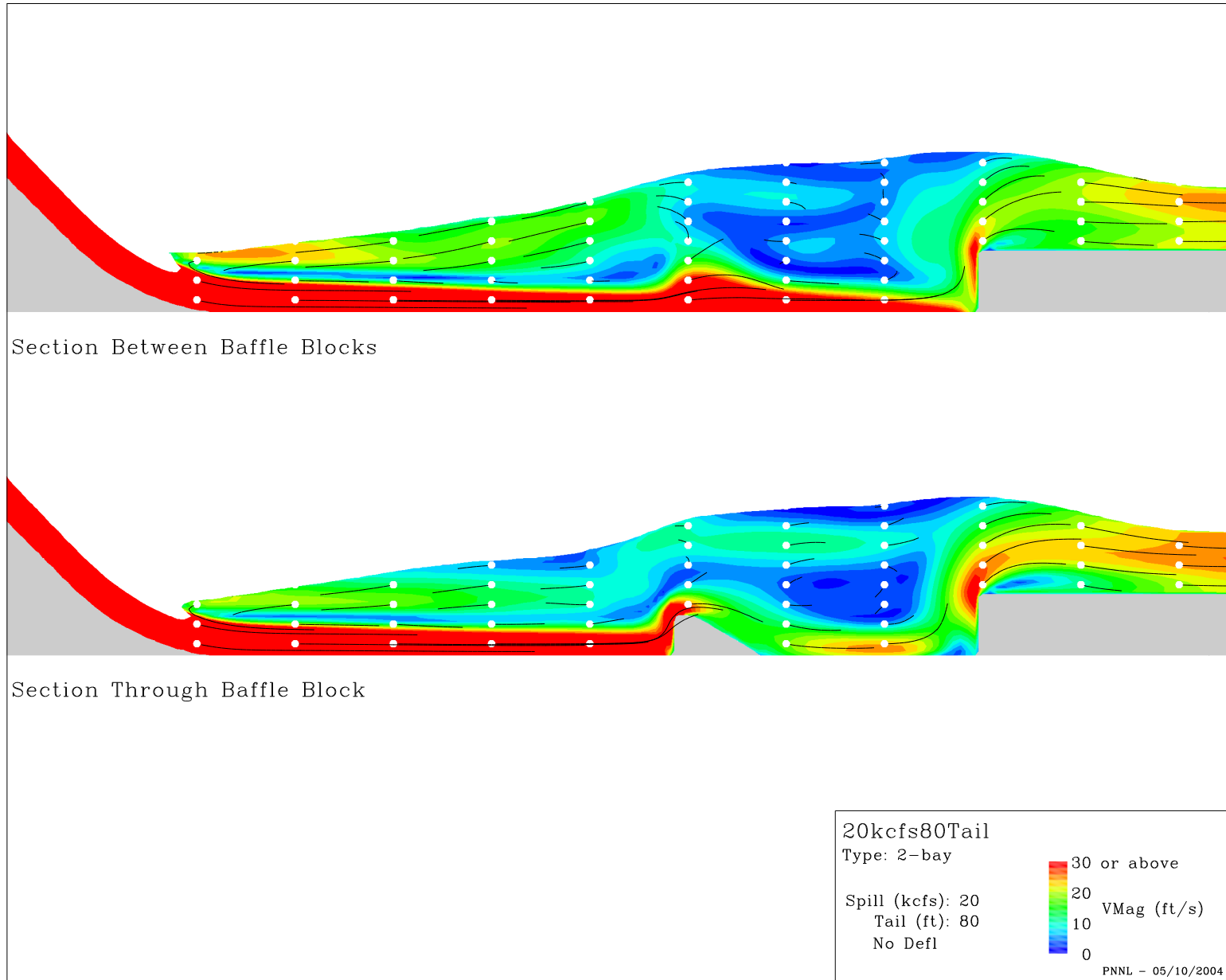


Figure D.15. Results for CFD model of The Dalles Dam tailrace (OneBay20kcfs80Tail.eps).

D.17

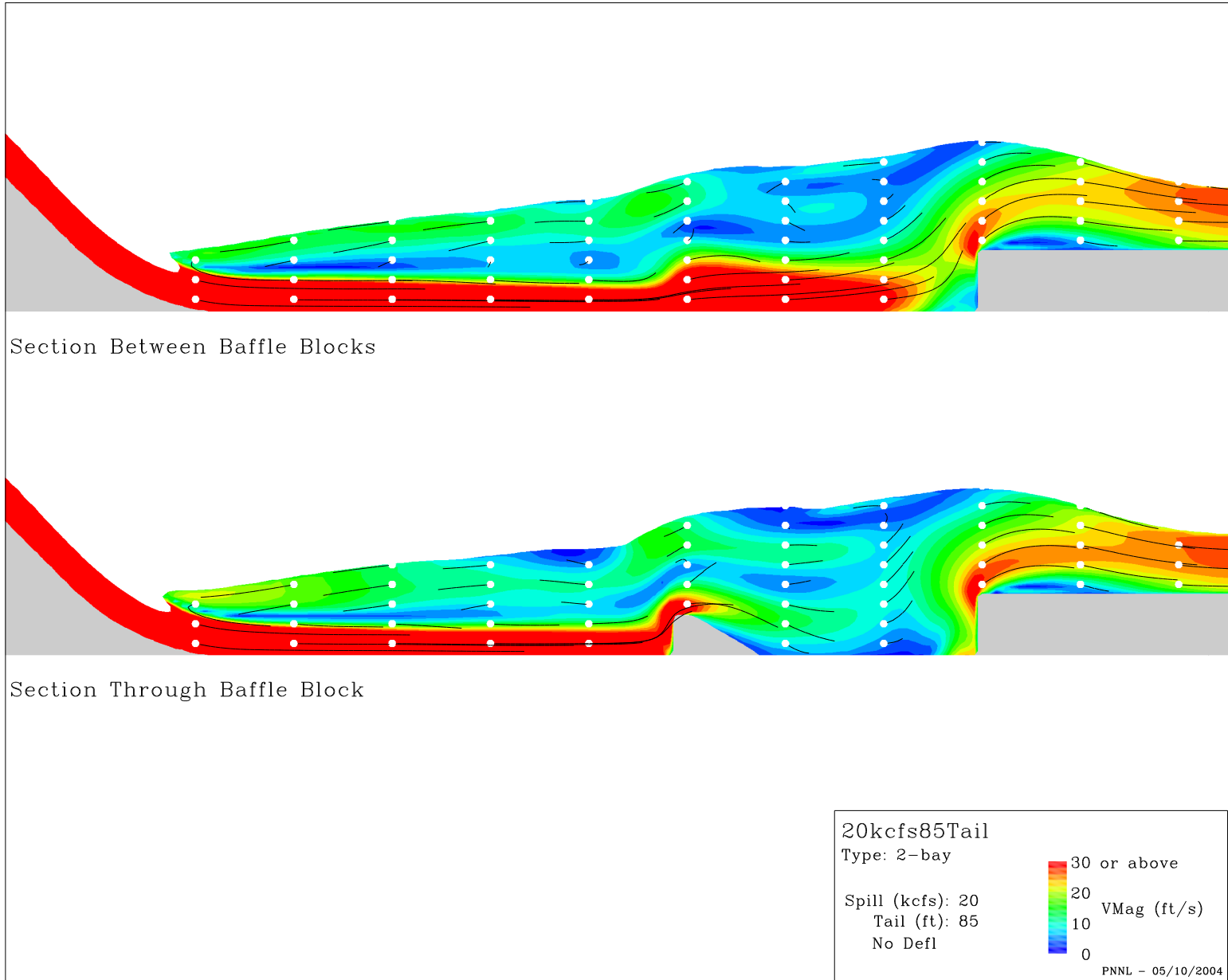


Figure D.16. Results for CFD model of The Dalles Dam tailrace (OneBay20kcfs85Tail.eps).

D.18

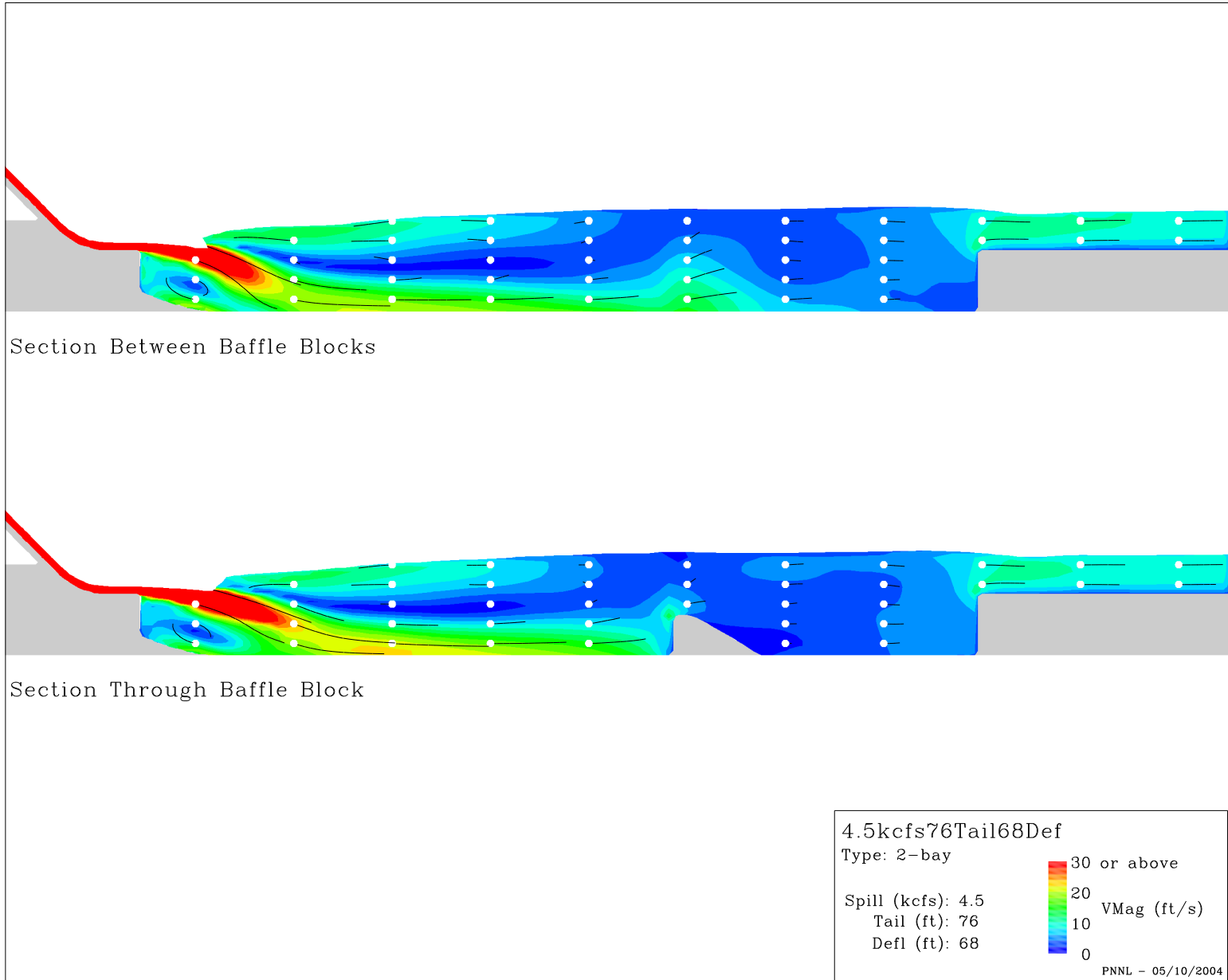


Figure D.17. Results for CFD model of The Dalles Dam tailrace (OneBay4.5kcfs76Tail68Def.eps).

Appendix E

12-Bay Simulations

Appendix E – 12-Bay Simulations

The following appendix summarizes simulation results from a single spillway bay (Figure A.4 displays the domain extent). In all figures particle tracks of equal duration have been added to illustrate the direction of flow. The circles indicate the starting position for each track and the track length is proportional to the velocity magnitude.

E.2

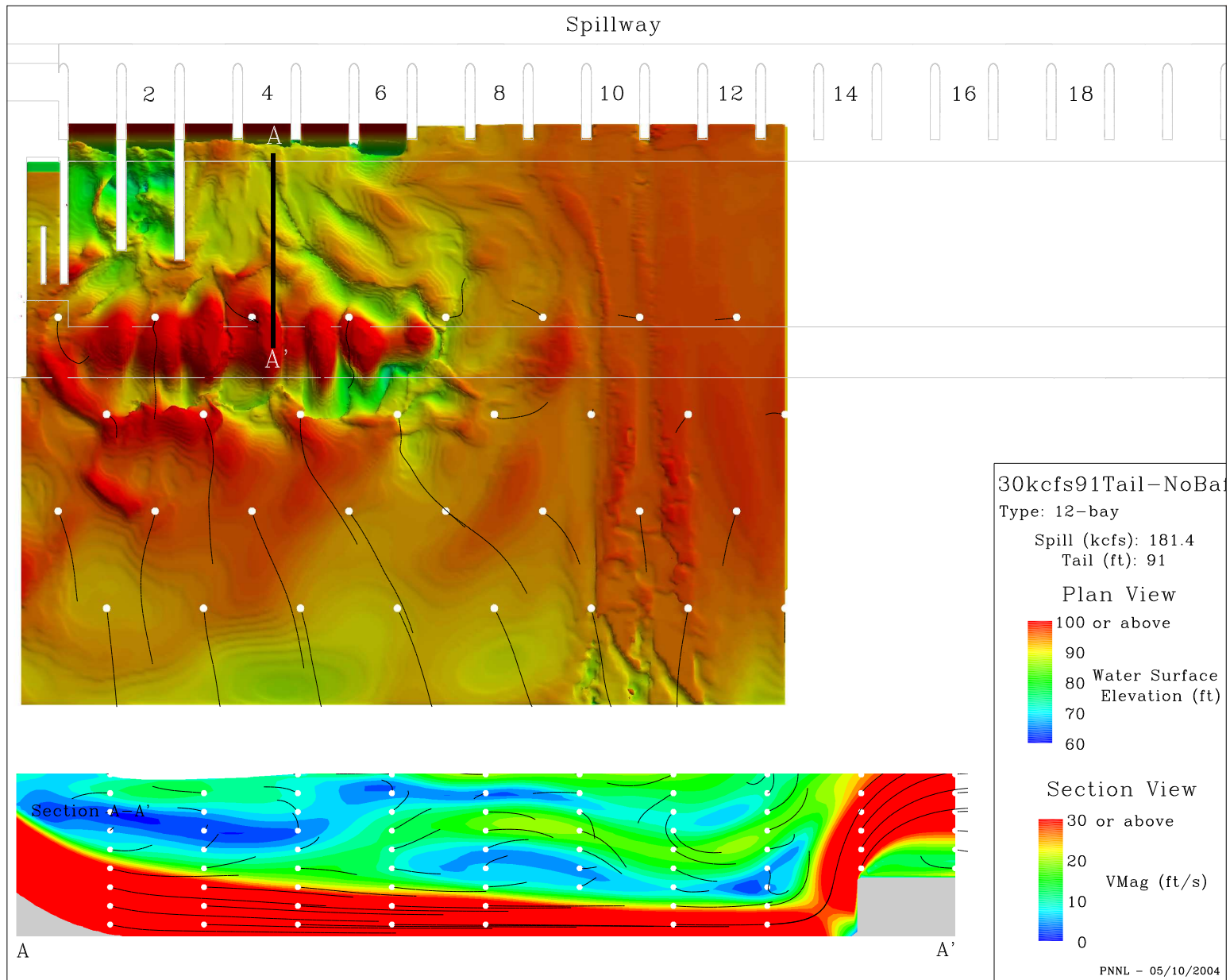


Figure E.1. Results for CFD model of The Dalles Dam tailrace (19Bay30kcfs91Tail-NoBaf.eps).

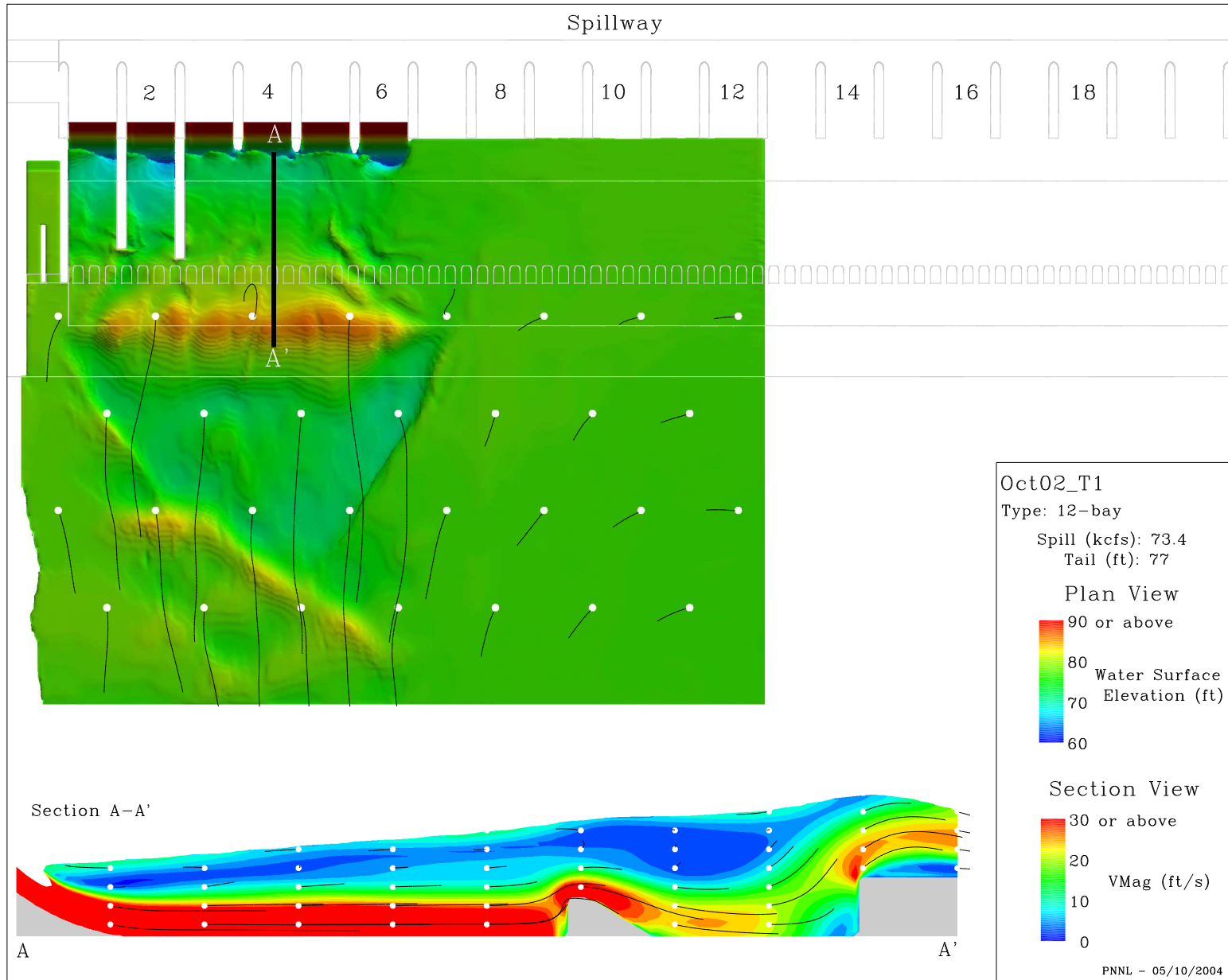


Figure E.2. Results for CFD model of The Dalles Dam tailrace (19BayOct02T1.eps).

E.4

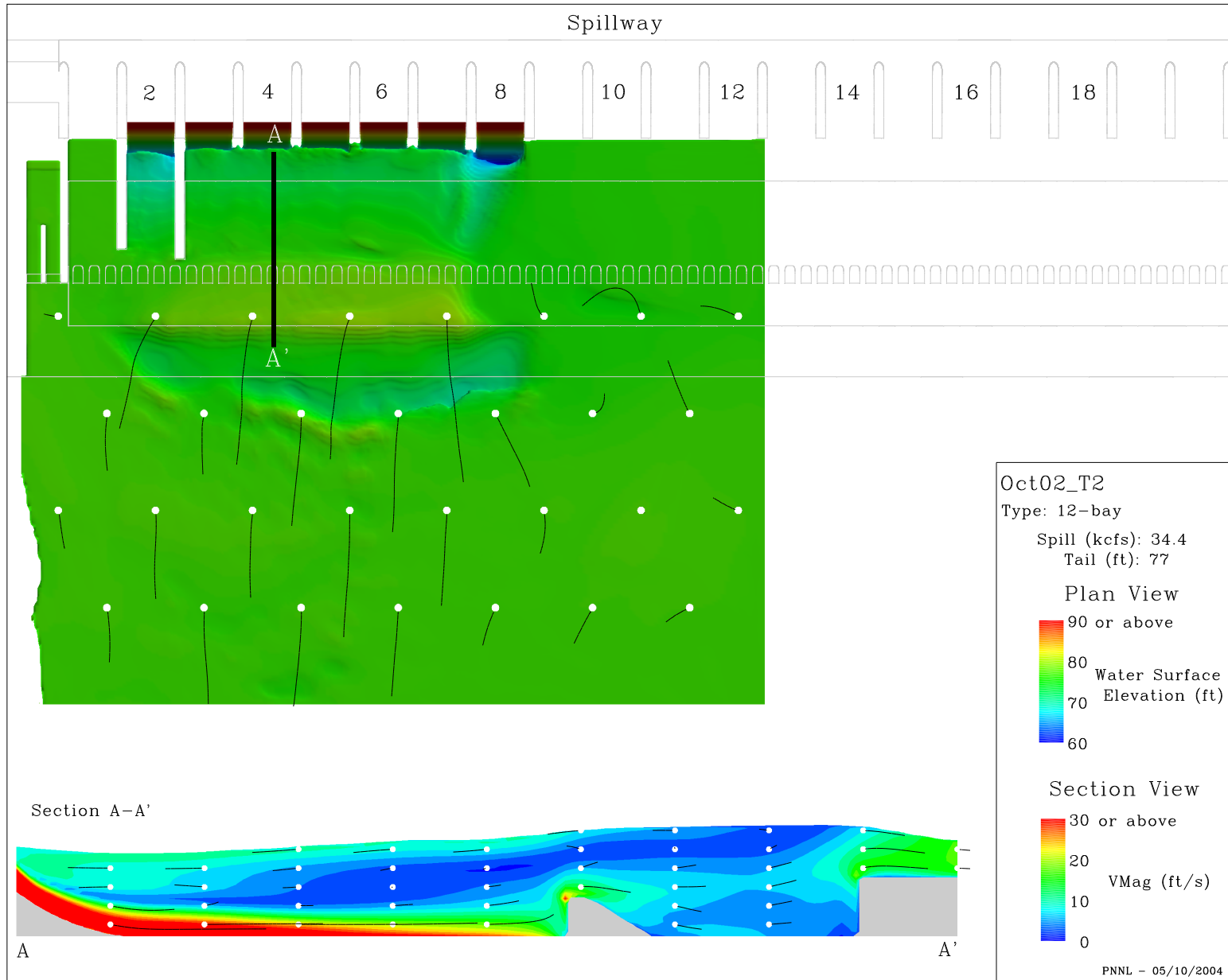


Figure E.3. Results for CFD model of The Dalles Dam tailrace (19BayOct02T2.eps).

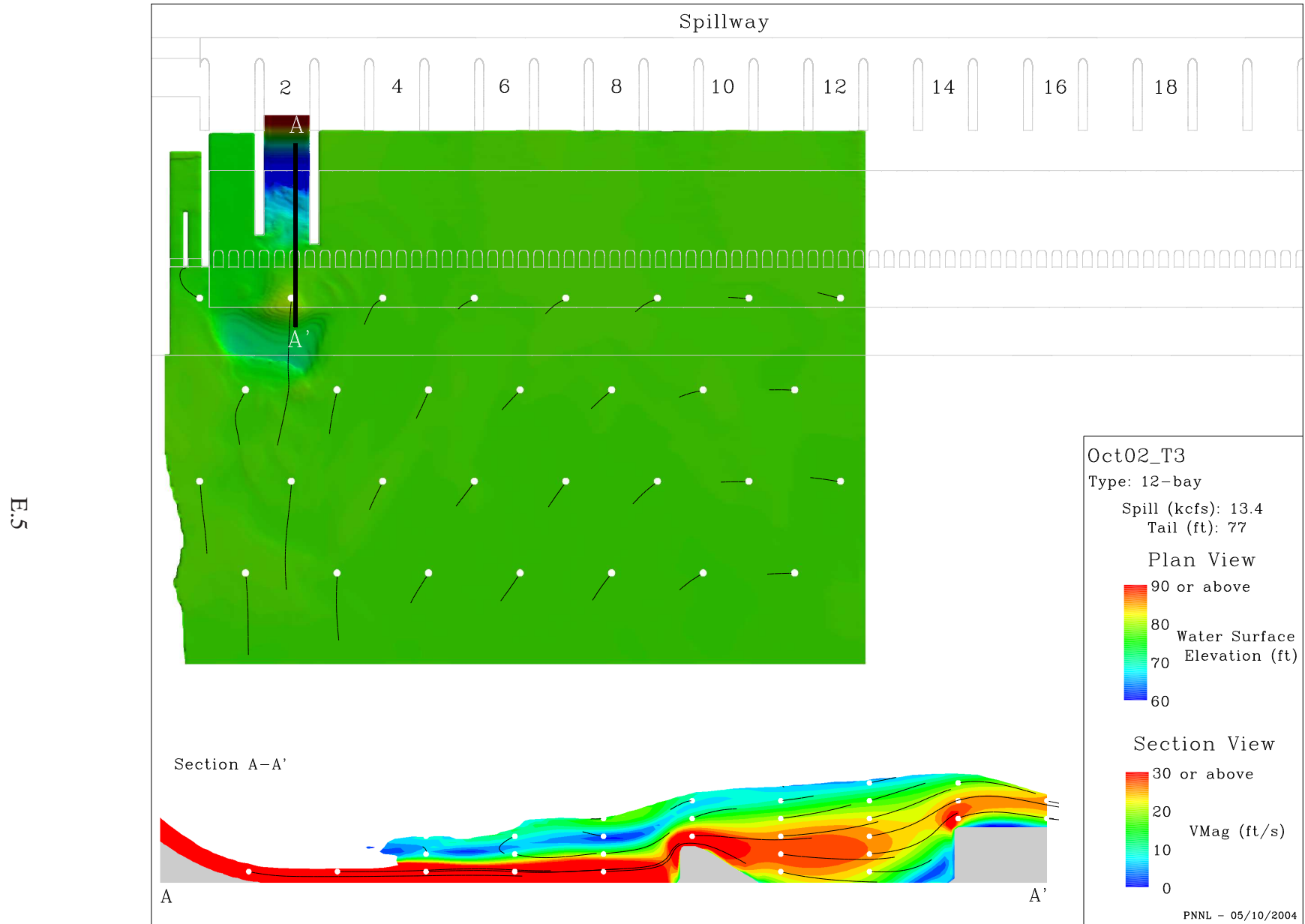


Figure E.4. Results for CFD model of The Dalles Dam tailrace (19BayB2Oct02T3.eps).

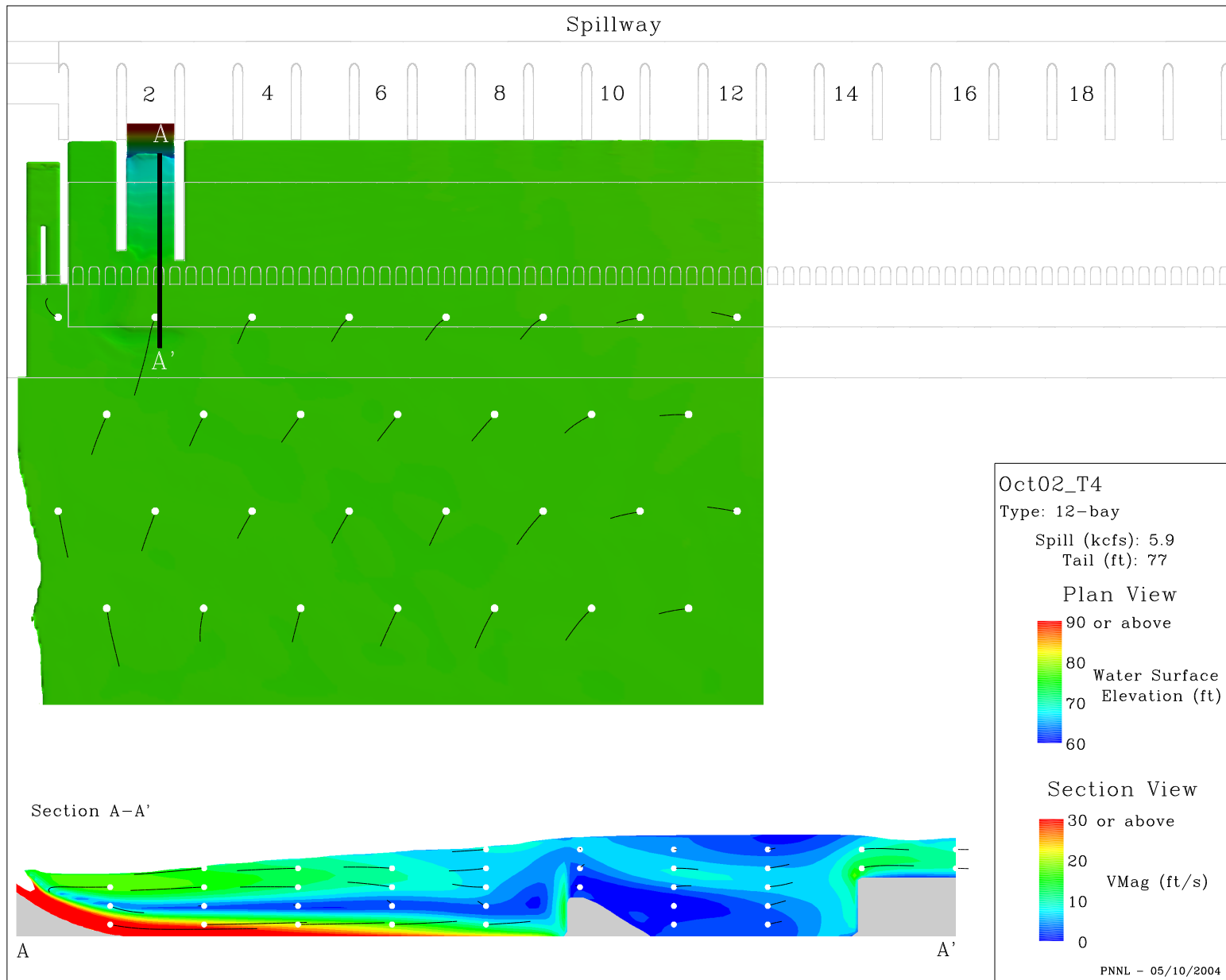


Figure E.5. Results for CFD model of The Dalles Dam tailrace (19BayB2Oct02T4.eps).

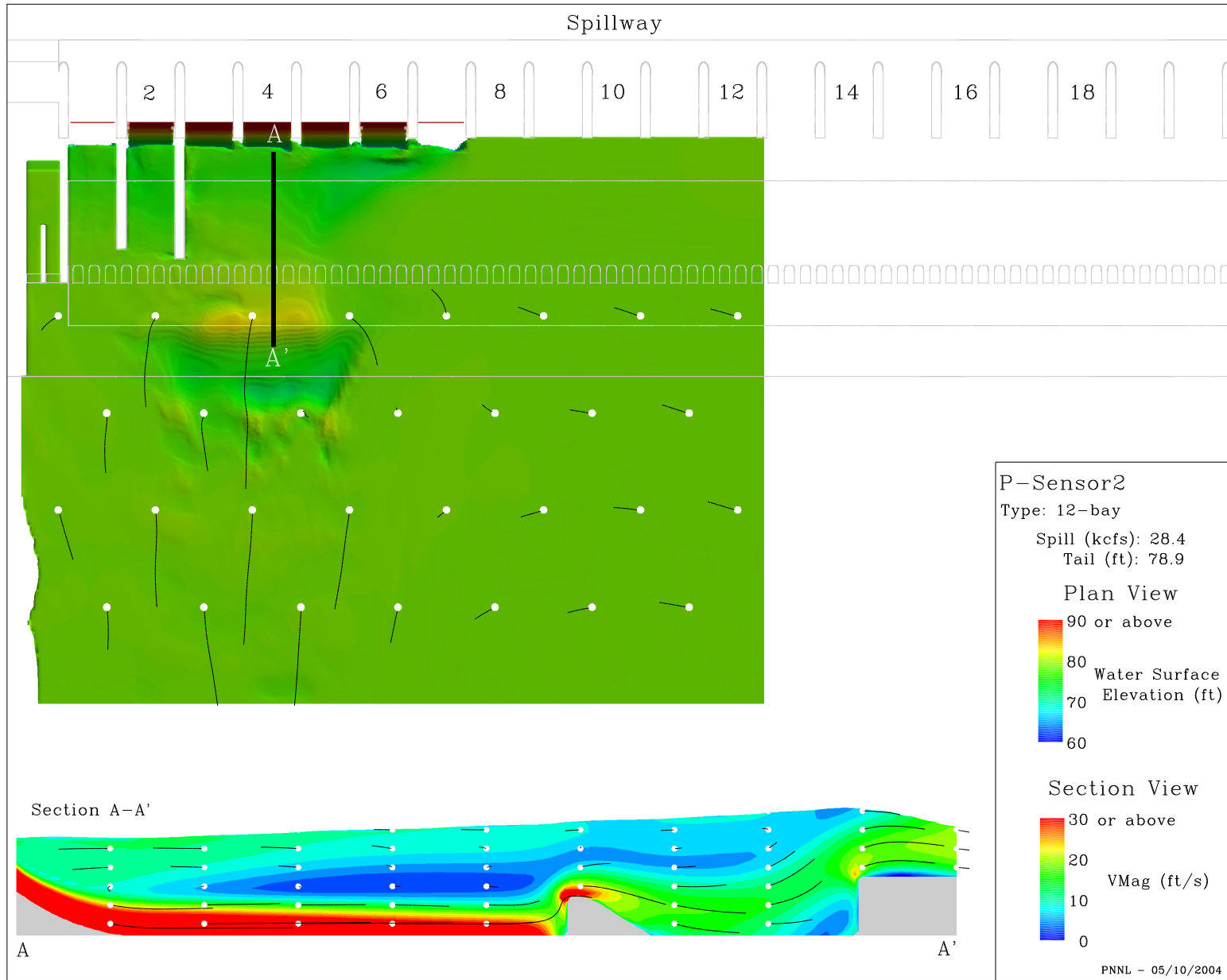


Figure E.6. Results for CFD model of The Dalles Dam tailrace (19BayP-Sensor2.eps).

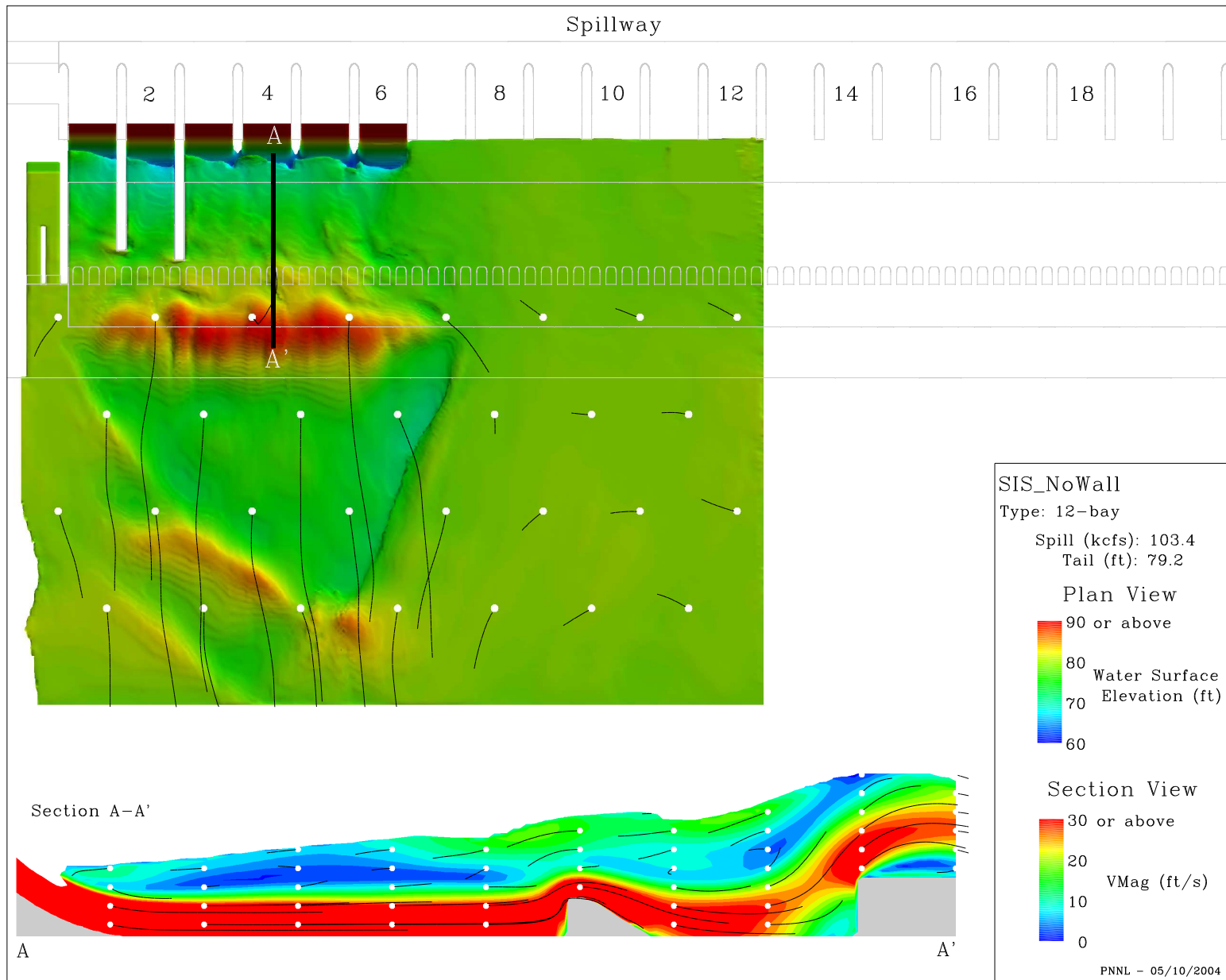


Figure E.7. Results for CFD model of The Dalles Dam tailrace (19BaySISNoWall.eps).

E.9

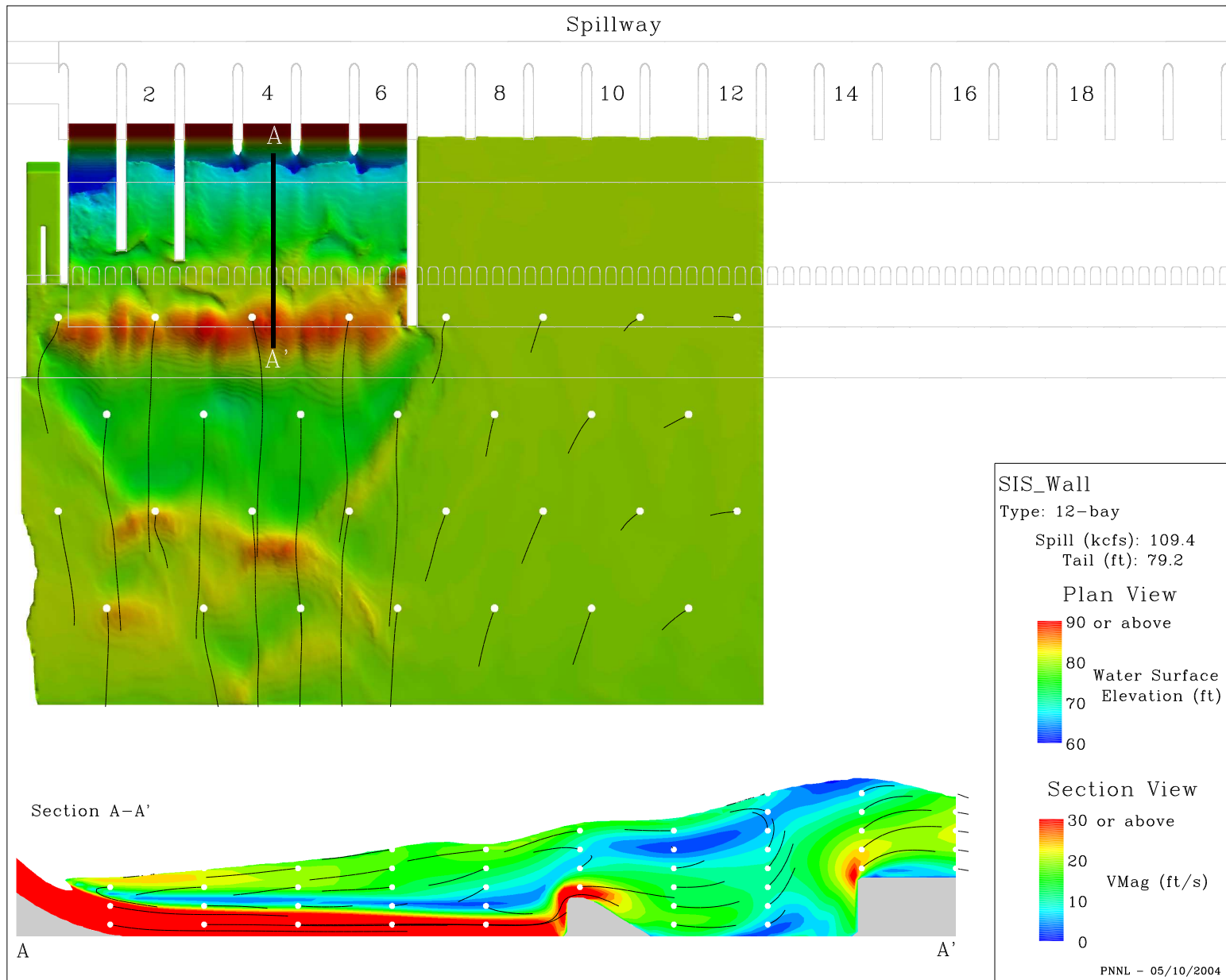


Figure E.8. Results for CFD model of The Dalles Dam tailrace (19BaySISWall.eps).

E.10

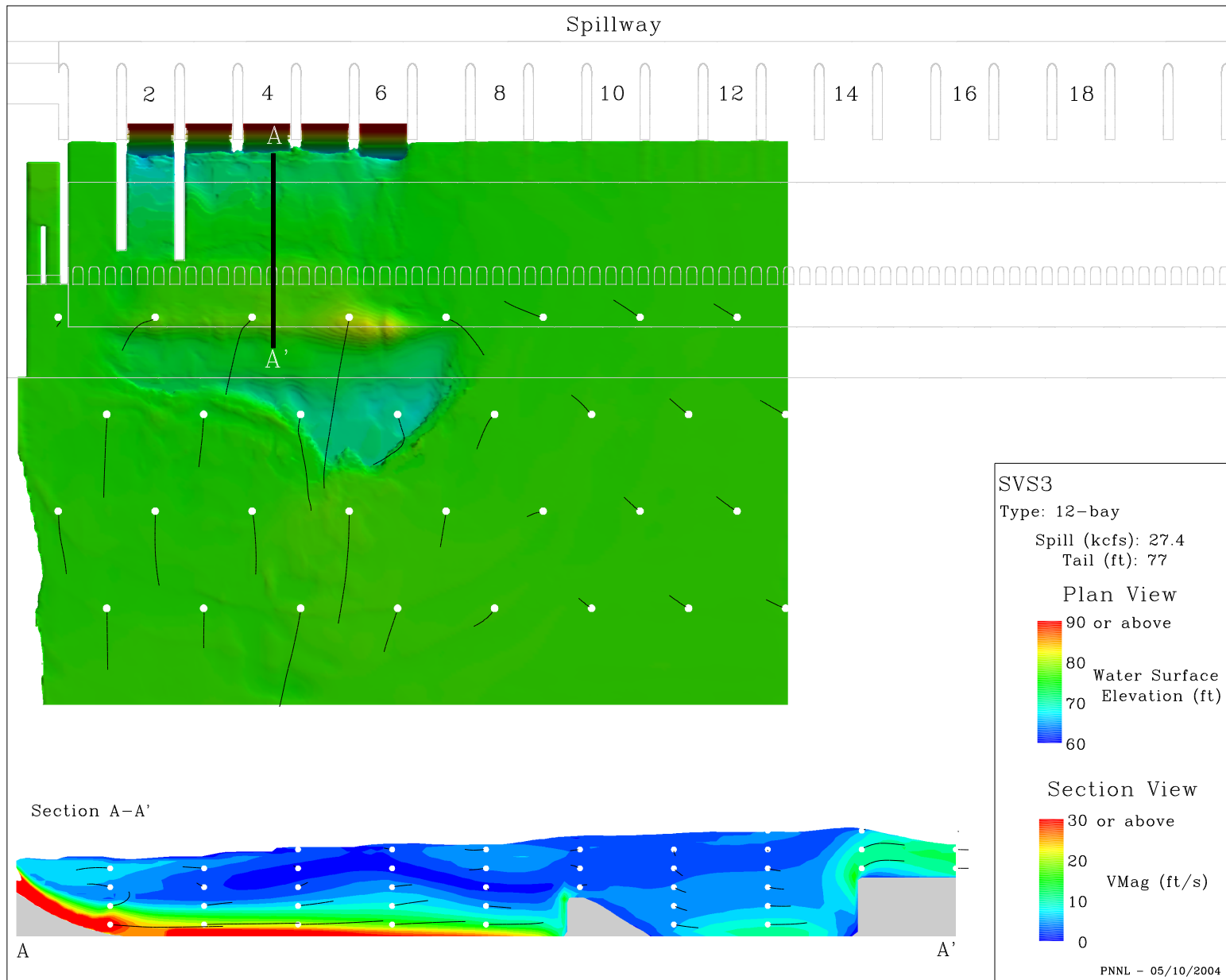


Figure E.9. Results for CFD model of The Dalles Dam tailrace (19BaySVS312.eps).

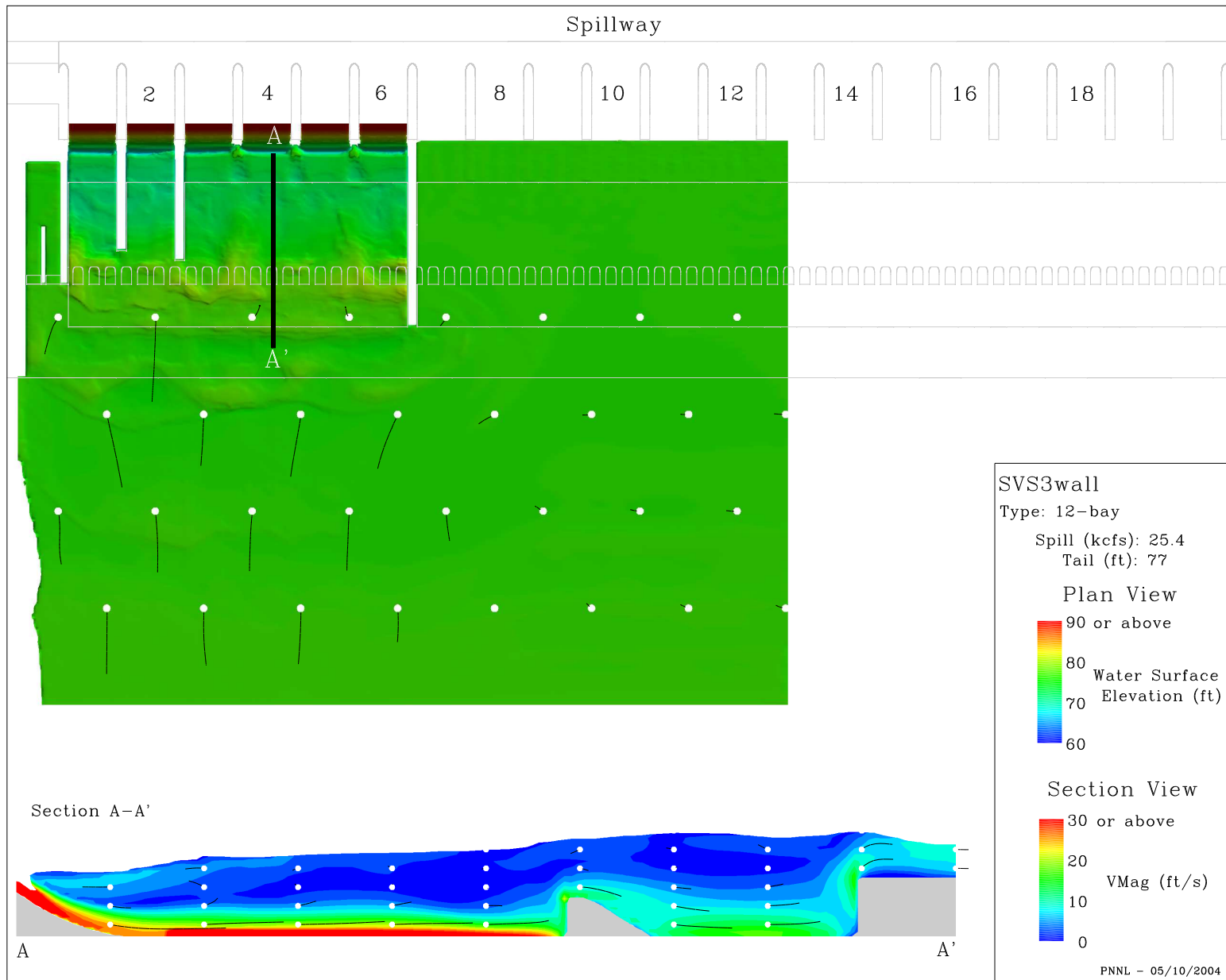


Figure E.10. Results for CFD model of The Dalles Dam tailrace (19BayFVFSVS3wall12.eps).

E.12

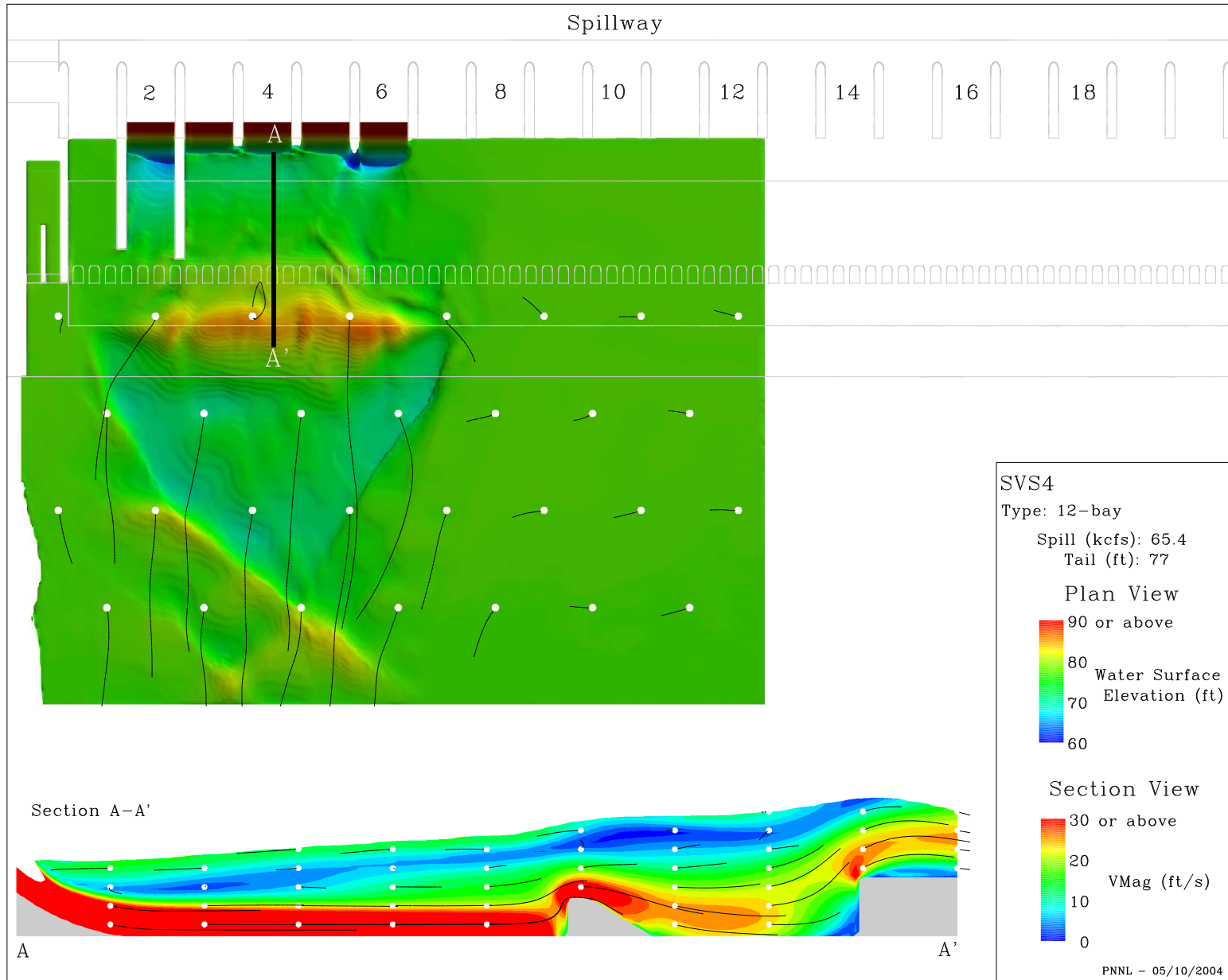


Figure E.11. Results for CFD model of The Dalles Dam tailrace (19BaySVS412.eps).

E.13

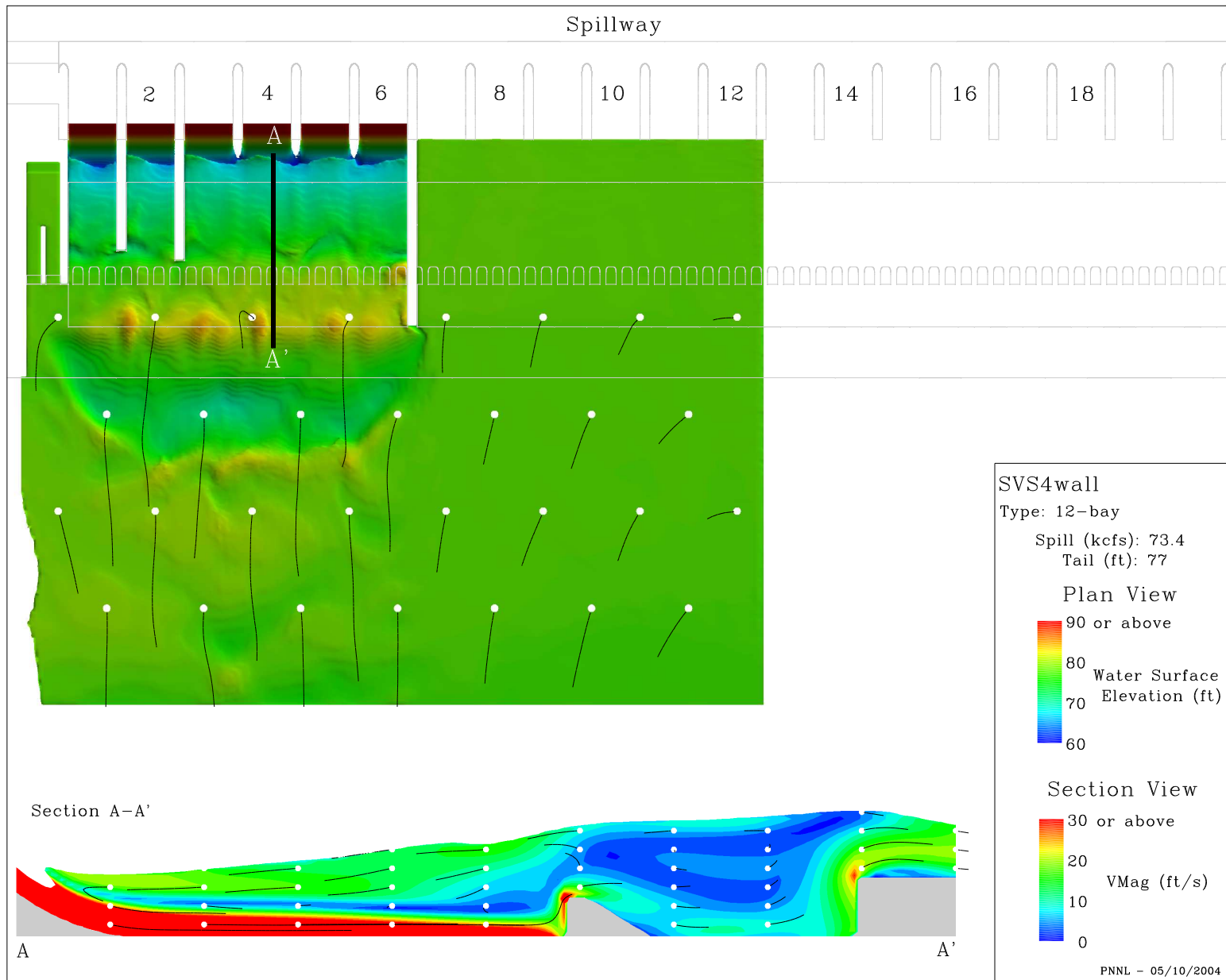


Figure E.12. Results for CFD model of The Dalles Dam tailrace (19BaySVS4wall12.eps).

Appendix F

15-Bay Simulations

Appendix F – 15-Bay Simulations

The following appendix summarizes simulation results from a single spillway bay (Figure A.5 displays the domain extent). In all figures particle tracks of equal duration have been added to illustrate the direction of flow. The circles indicate the starting position for each track and the track length is proportional to the velocity magnitude.

F.2

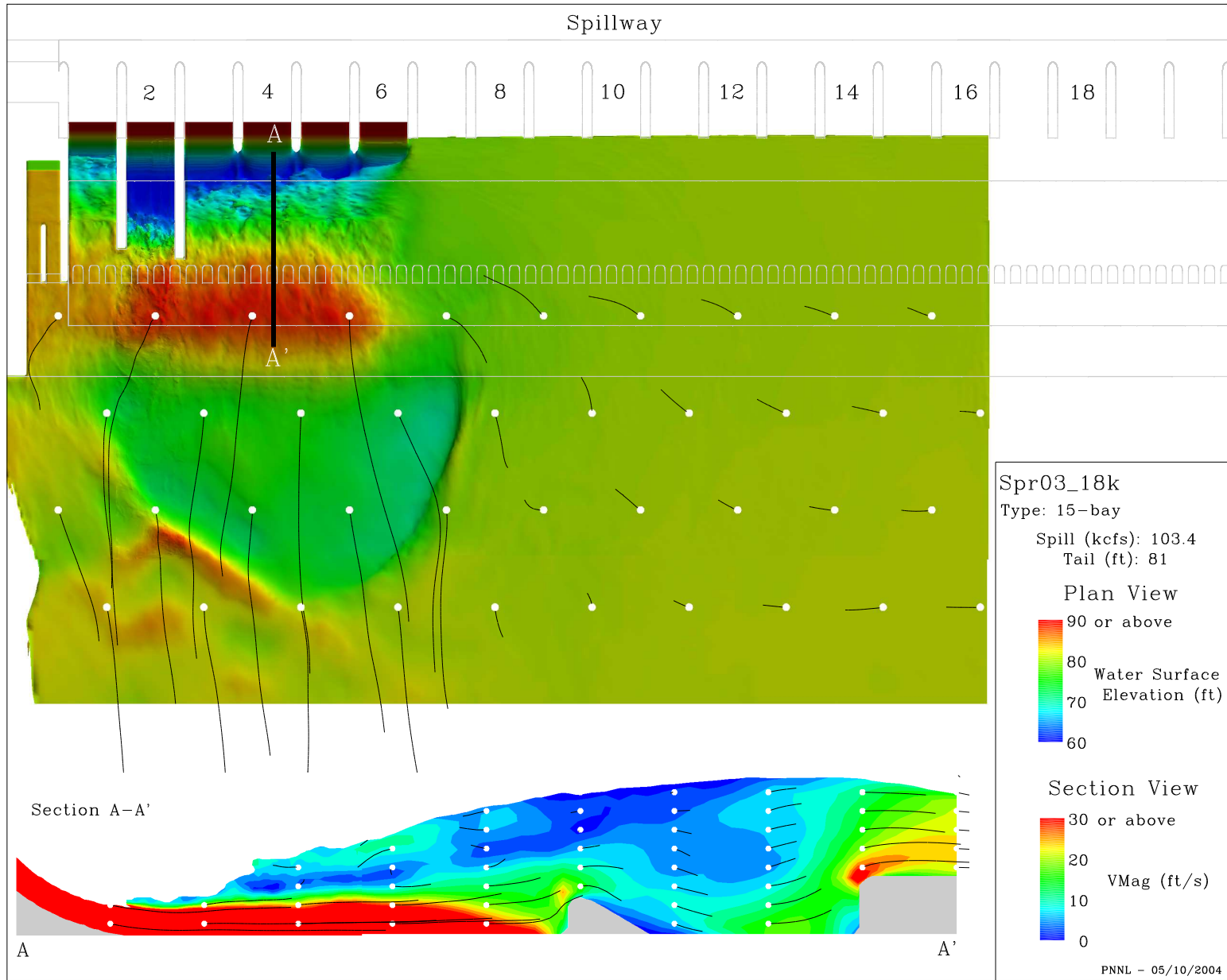


Figure F.1. Results for CFD model of The Dalles Dam tailrace (19BaySpr0318k.eps).

F.3

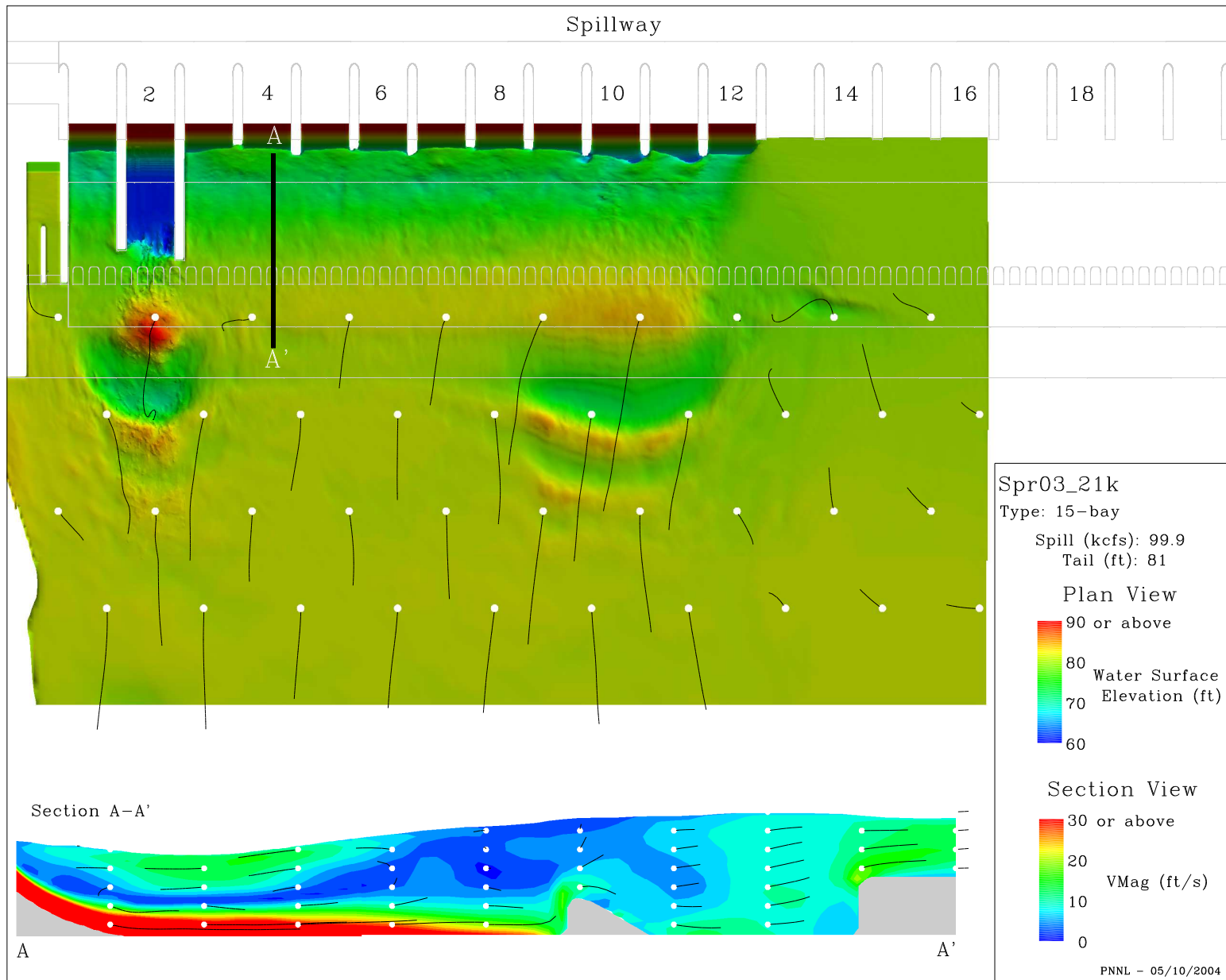


Figure F.2. Results for CFD model of The Dalles Dam tailrace (19BaySpr0321k.eps).

Appendix G

19-Bay Simulations

Appendix G – 19-Bay Simulations

The following appendix summarizes simulation results from a single spillway bay (Figure A.6 displays the domain extent). In all figures particle tracks of equal duration have been added to illustrate the direction of flow. The circles indicate the starting position for each track and the track length is proportional to the velocity magnitude.

G.2

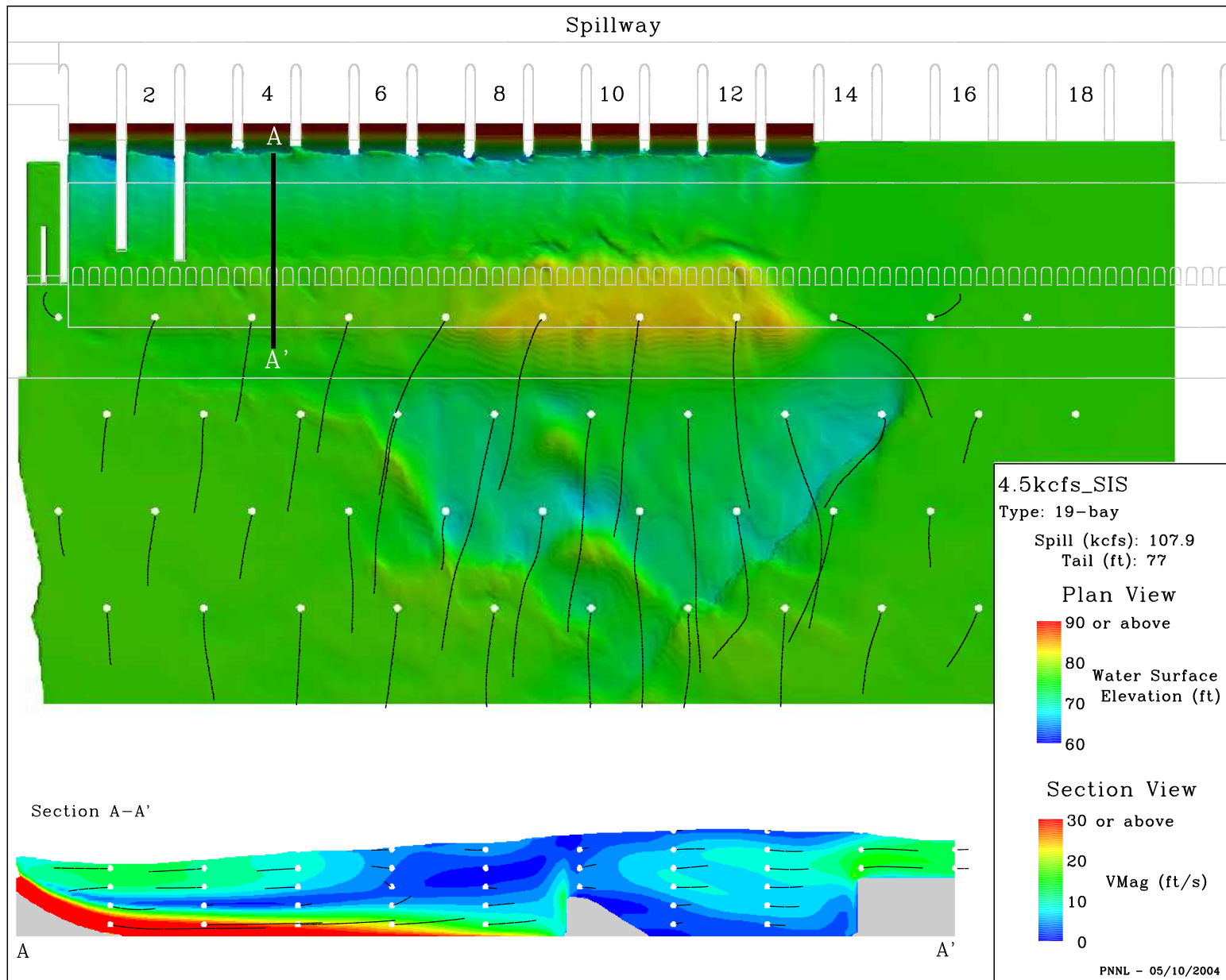


Figure G.1. Results for CFD model of The Dalles Dam tailrace (19Bay4.5kcfsSIS.eps).

G.3

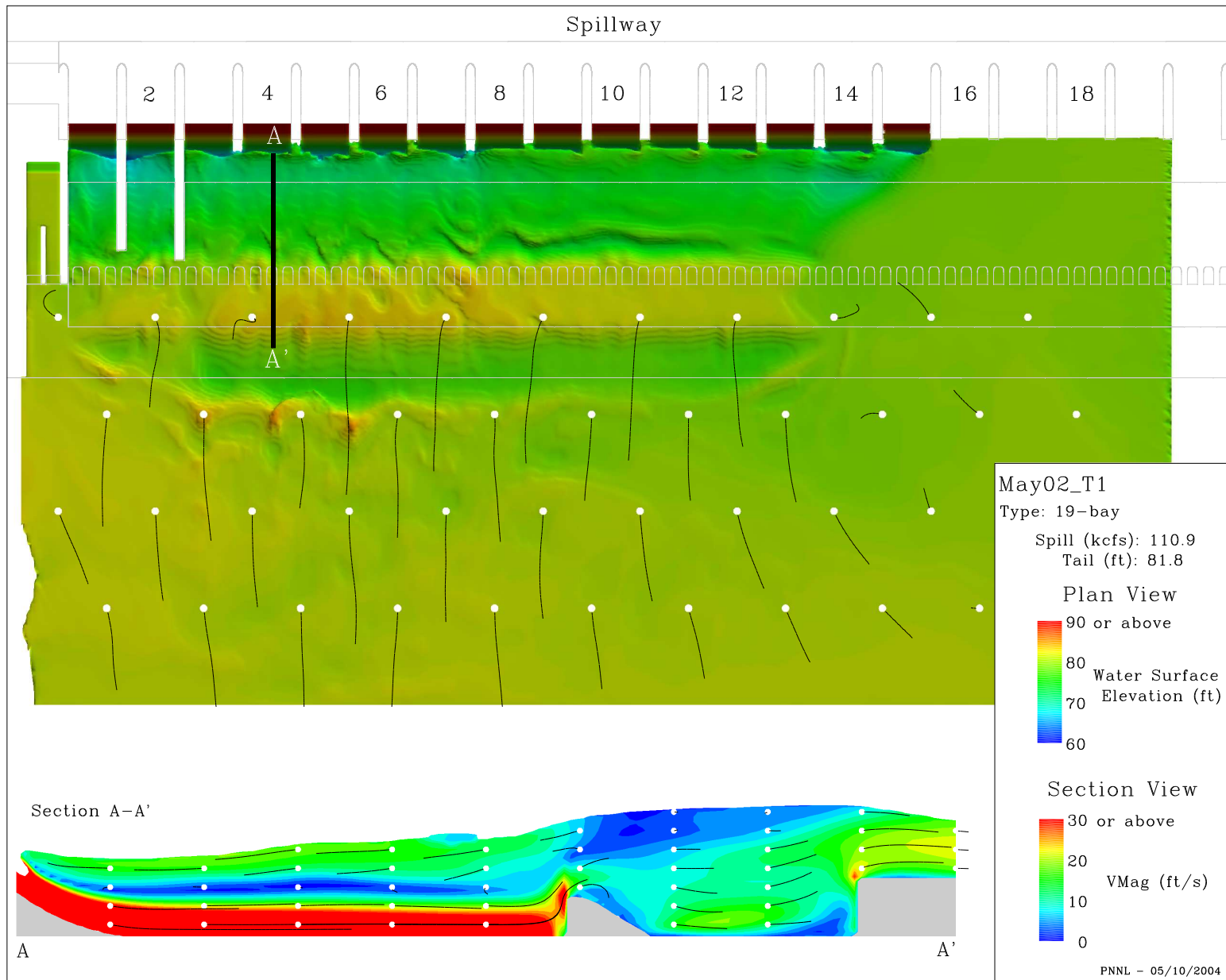


Figure G.2. Results for CFD model of The Dalles Dam tailrace (19BayMay02T1.eps).

G.4

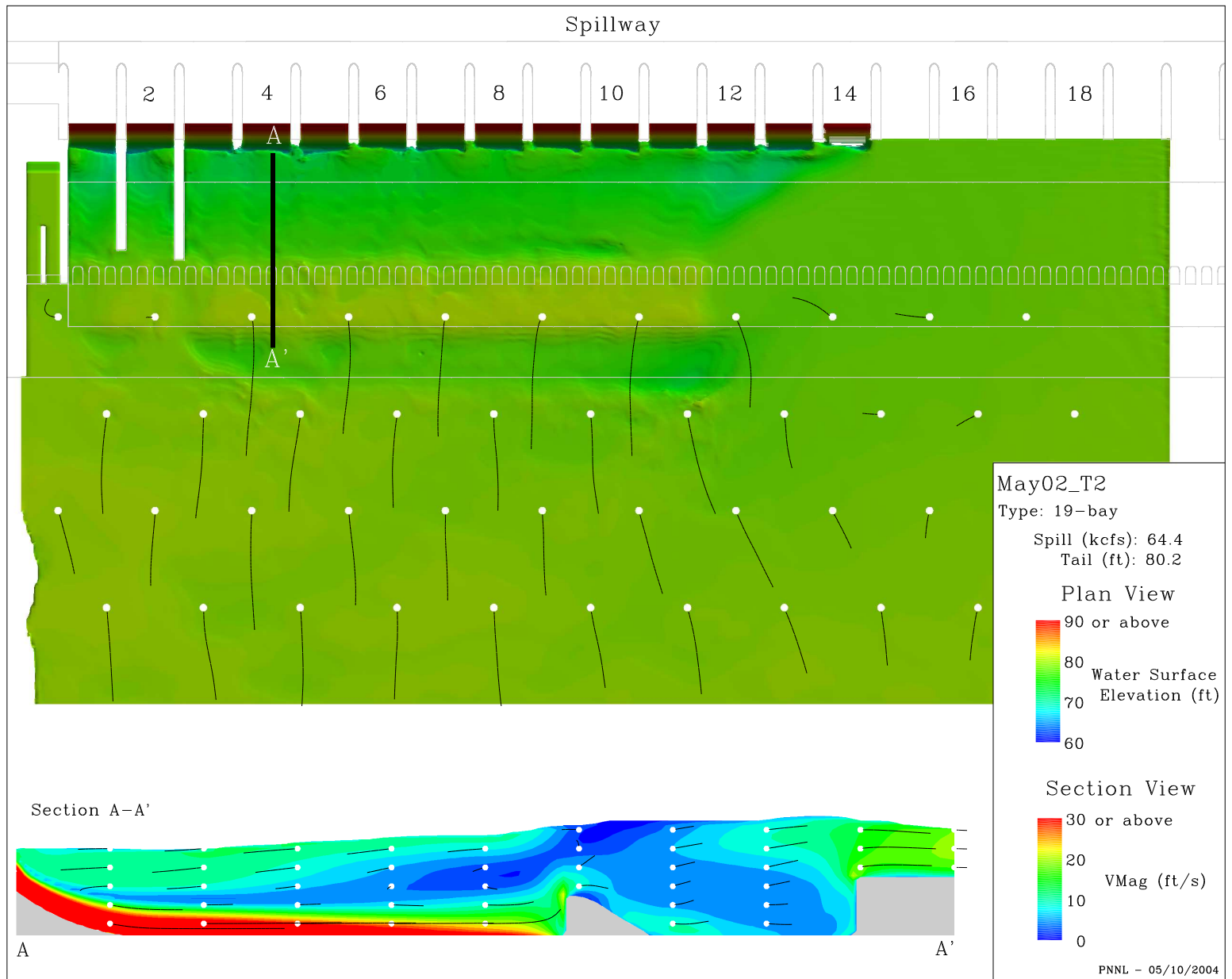


Figure G.3. Results for CFD model of The Dalles Dam tailrace (19BayMay02T2.eps).

G.5

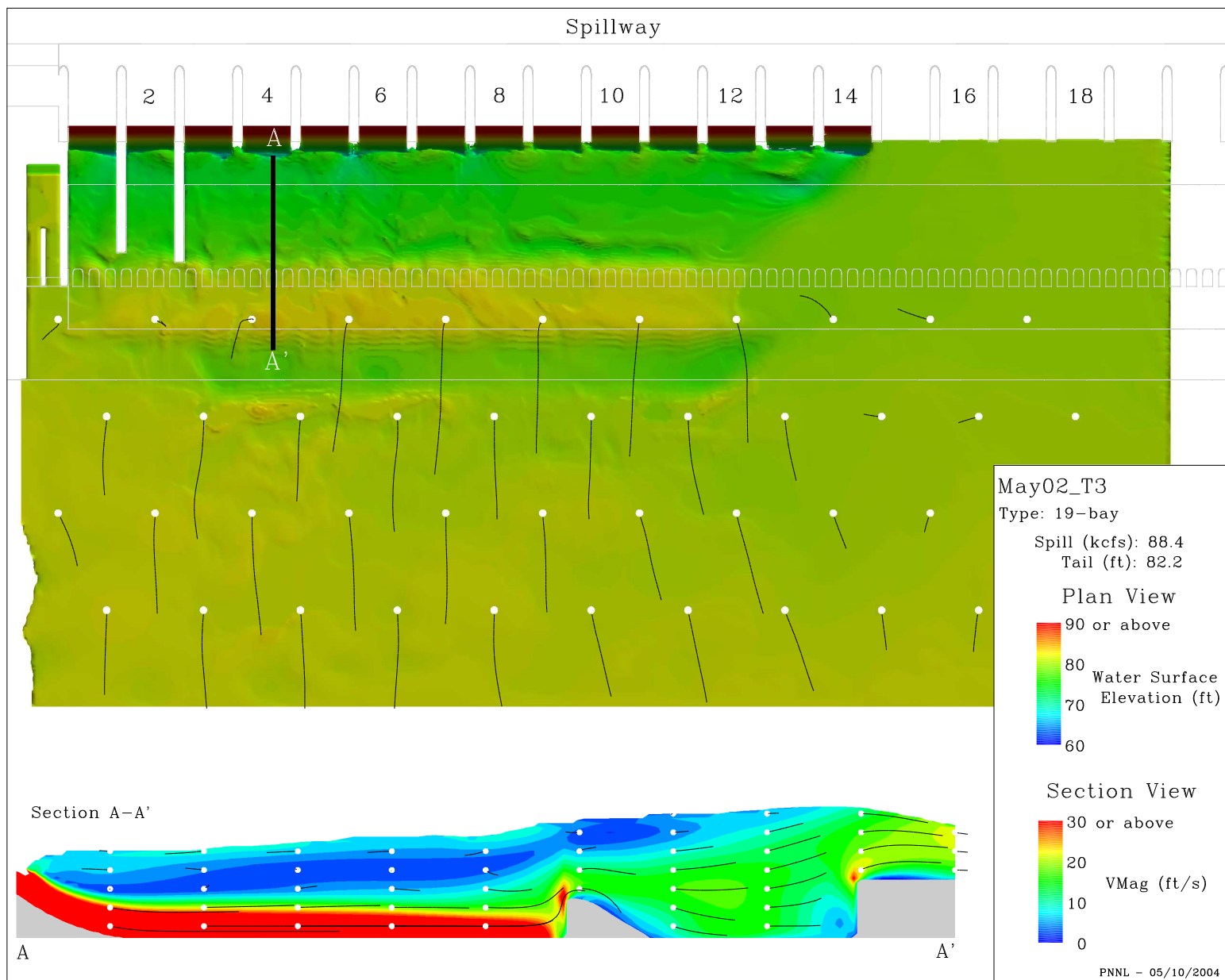


Figure G.4. Results for CFD model of The Dalles Dam tailrace (19BayMay02T3.eps).

G.6

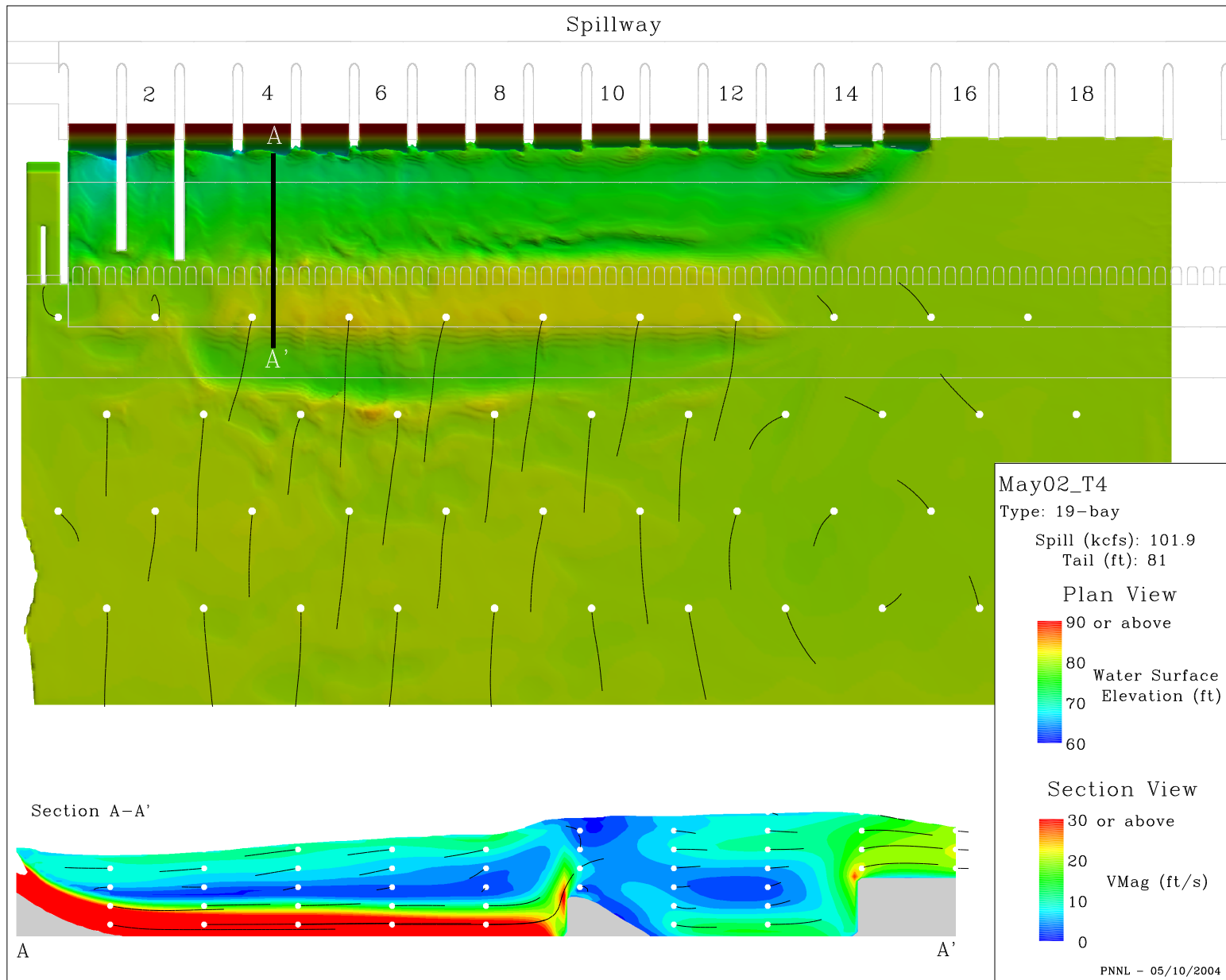


Figure G.5. Results for CFD model of The Dalles Dam tailrace (19BayMay02T4.eps).

G.7

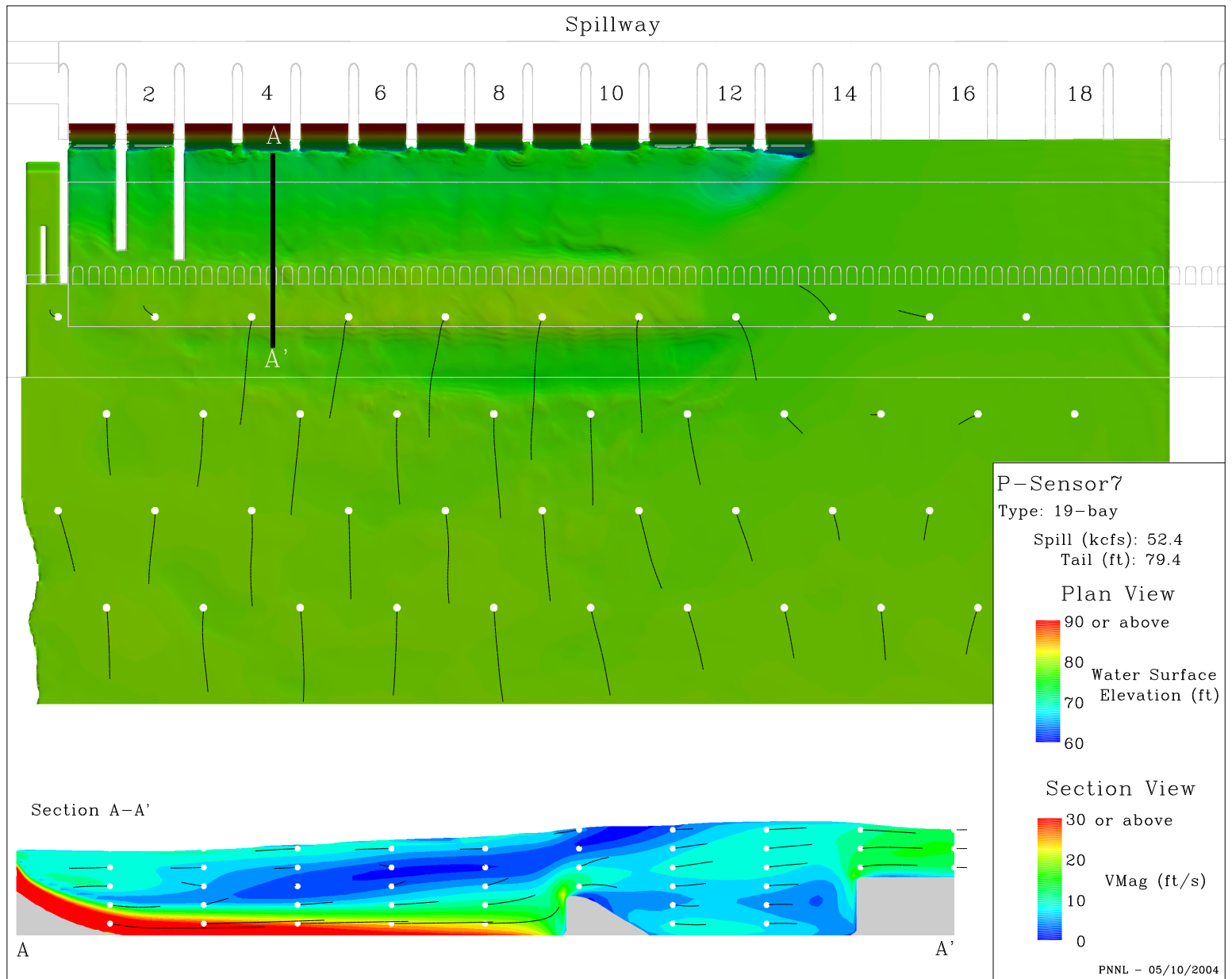


Figure G.6. Results for CFD model of The Dalles Dam tailrace (19BayP-Sensor7.eps).

G.8

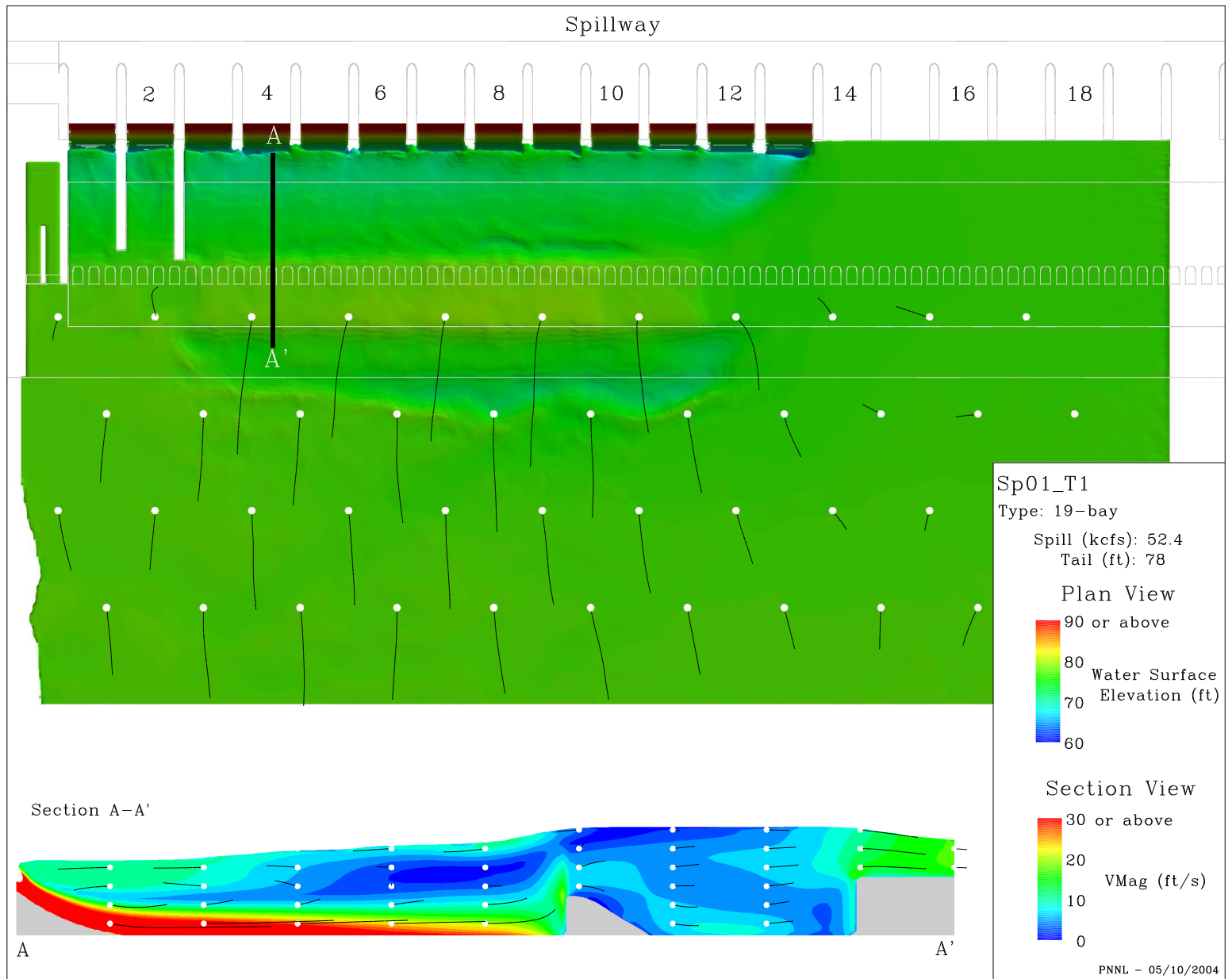


Figure G.7. Results for CFD model of The Dalles Dam tailrace (19BaySp01T1.eps).

G.9

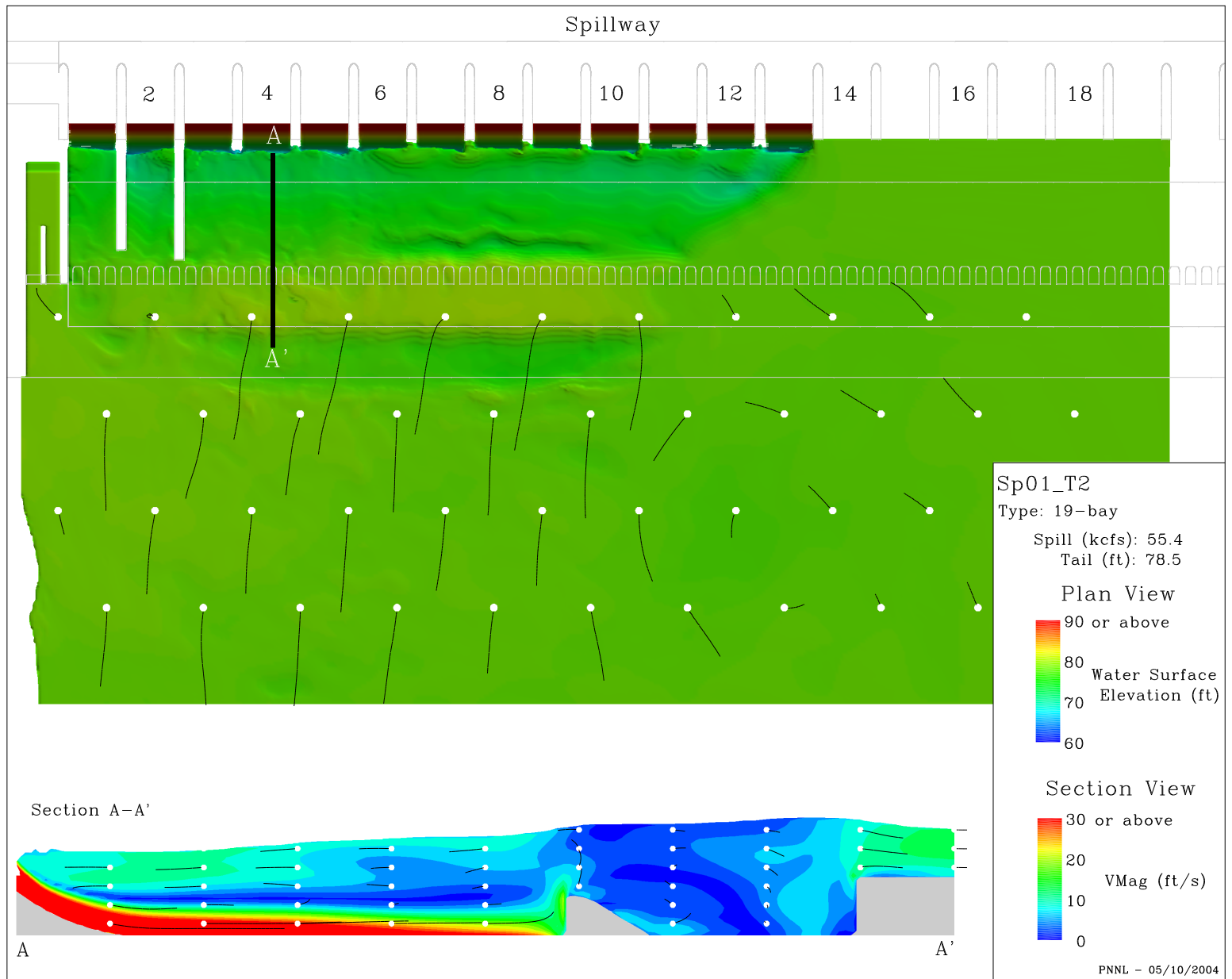


Figure G.8. Results for CFD model of The Dalles Dam tailrace (19BaySp01T2.eps).

G.10

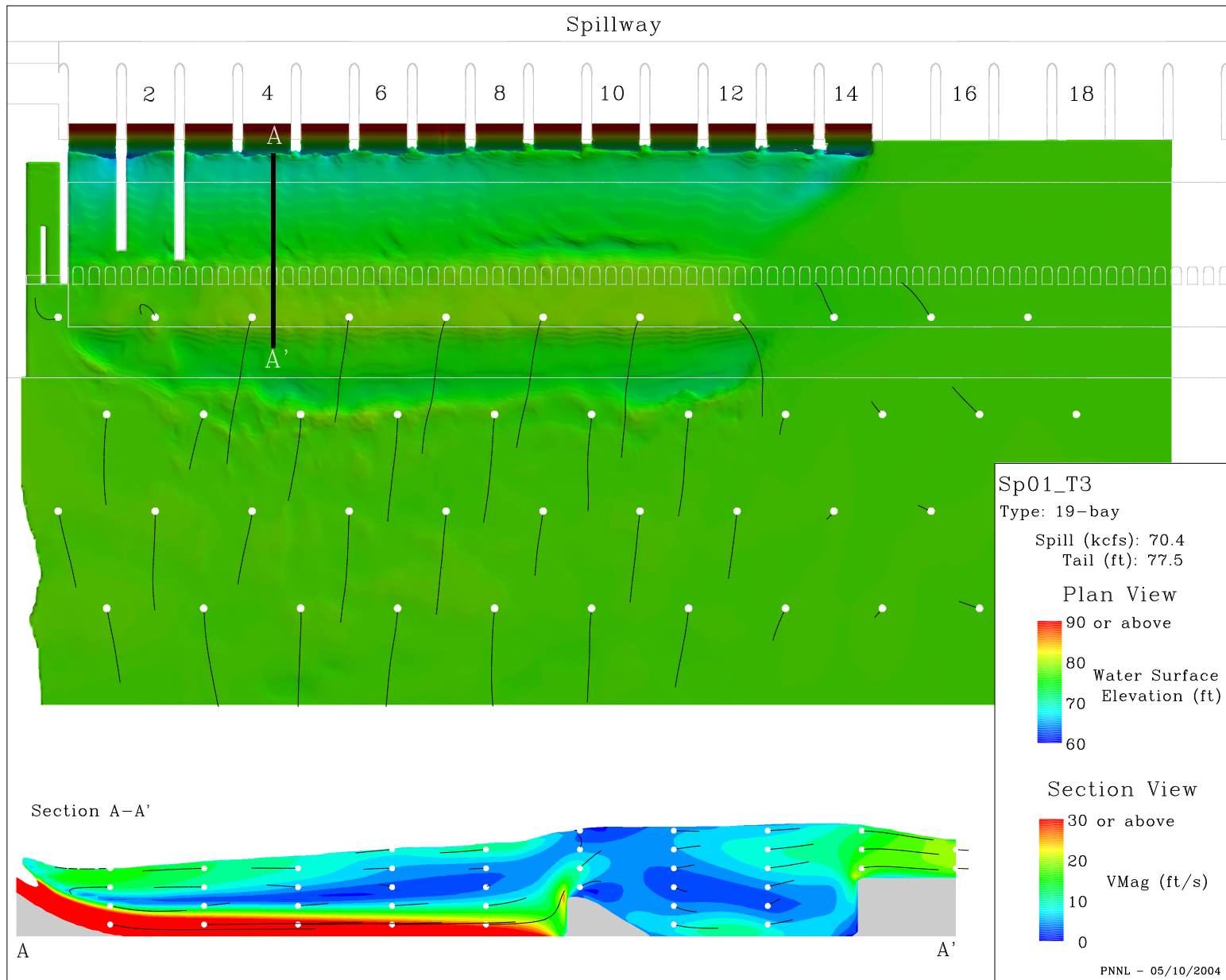


Figure G.9. Results for CFD model of The Dalles Dam tailrace (19BaySp01T3.eps).

G.11

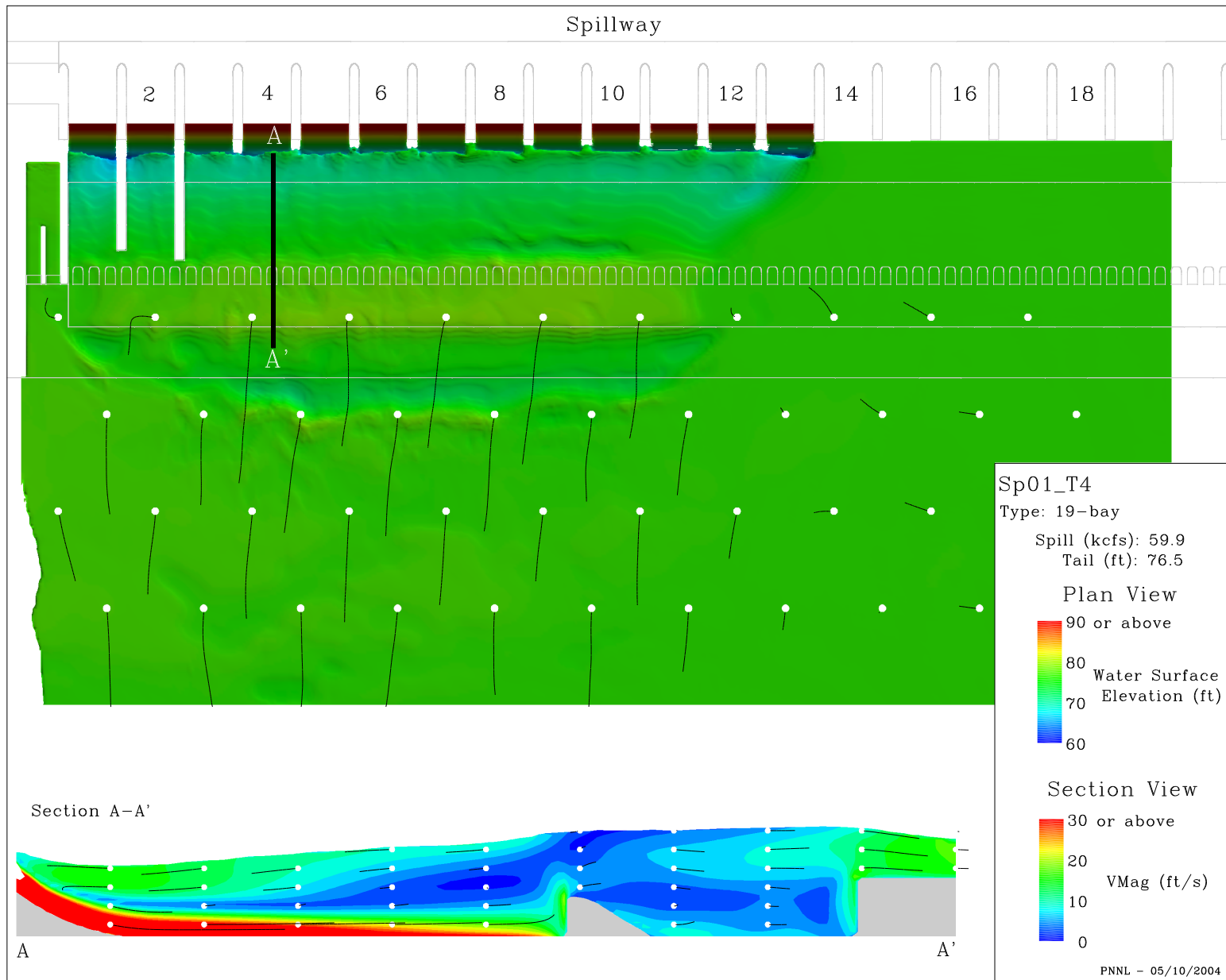


Figure G.10. Results for CFD model of The Dalles Dam tailrace (19BaySp01T4.eps).

Appendix H

Bank-to-Bank 8-Block Simulations

Appendix H – Bank-to-Bank 8-Block Simulations

The following appendix summarizes simulation results from a single spillway bay (Figure A.7 displays the domain extent). In all figures particle tracks of equal duration have been added to illustrate the direction of flow. The circles indicate the starting position for each track and the track length is proportional to the velocity magnitude.

H.2

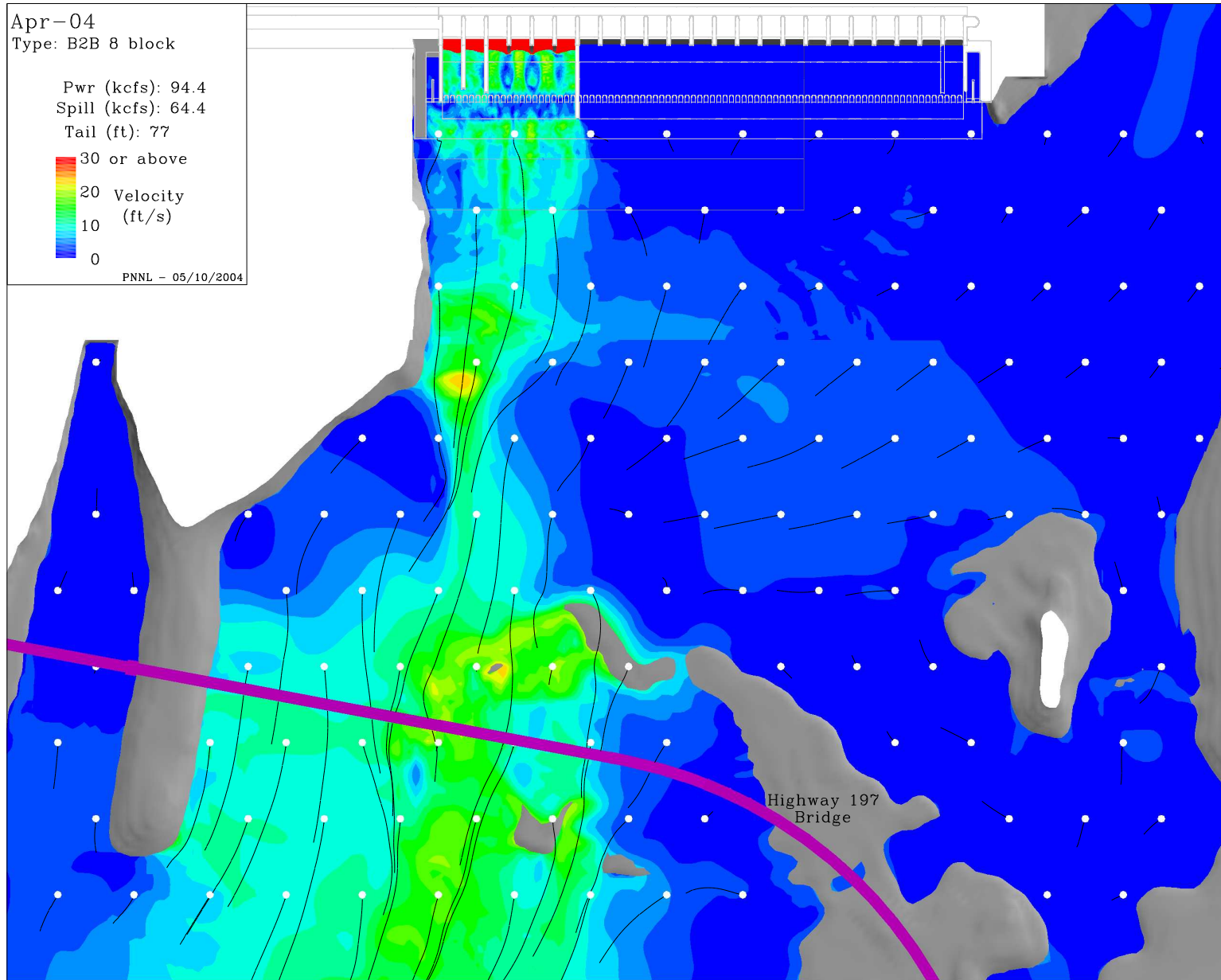


Figure H.1. Results for CFD model of The Dalles Dam tailrace (FullSpillwayApr-04.eps).

H3

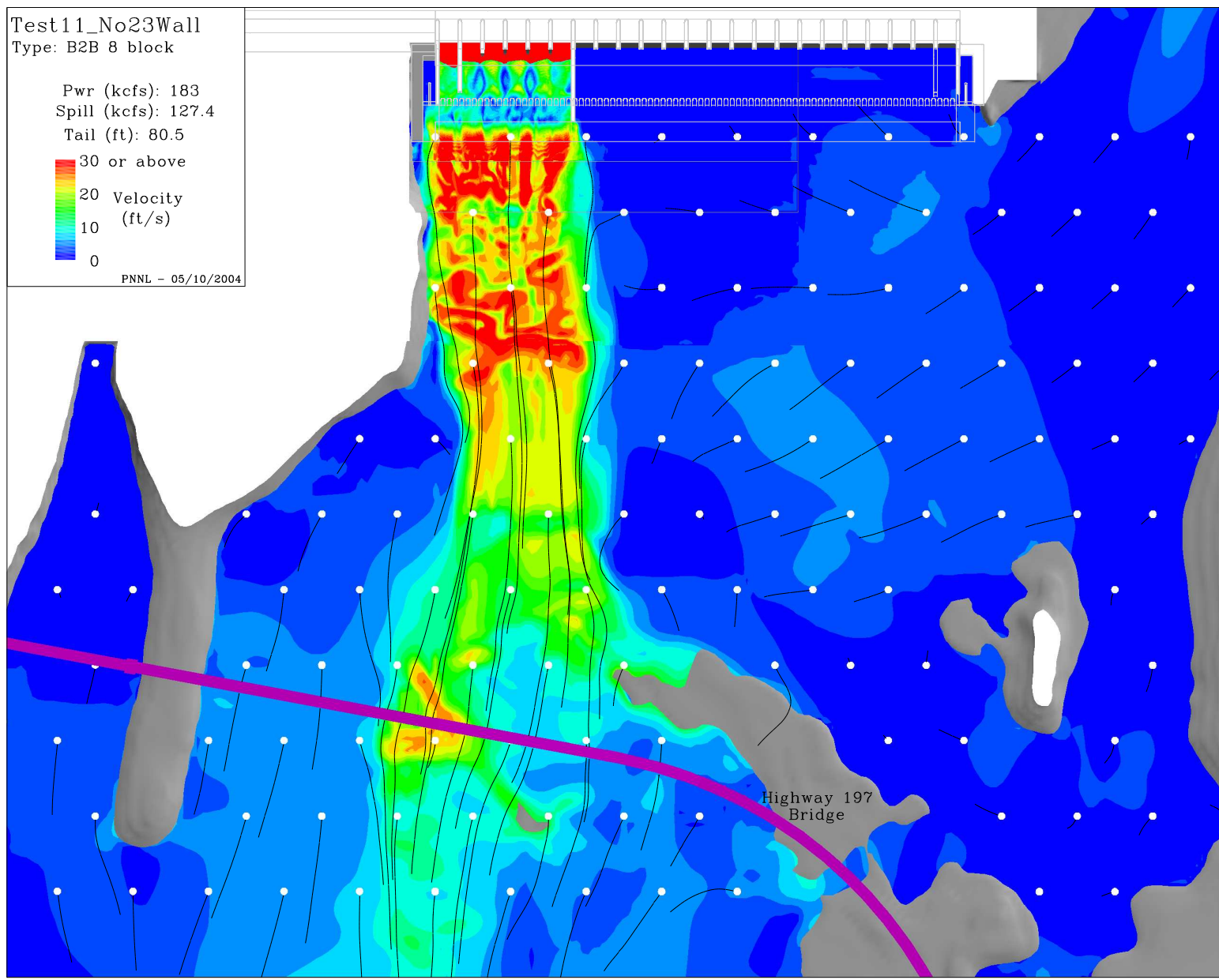


Figure H.2. Results for CFD model of The Dalles Dam tailrace (FullSpillwayTest11No23Wall.eps).

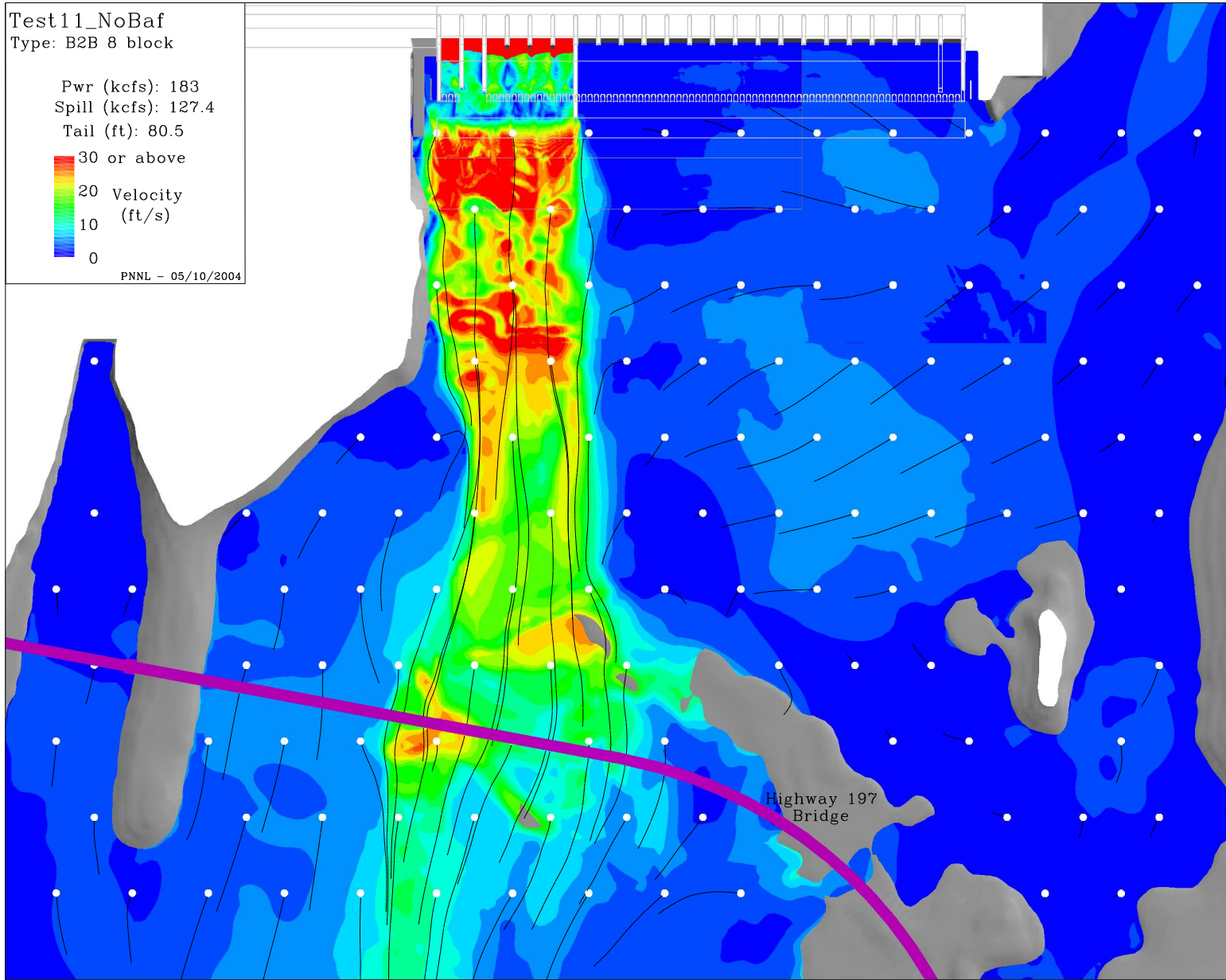


Figure H.3. Results for CFD model of The Dalles Dam tailrace (FullSpillwayTest11NoBaf.eps).

H.5

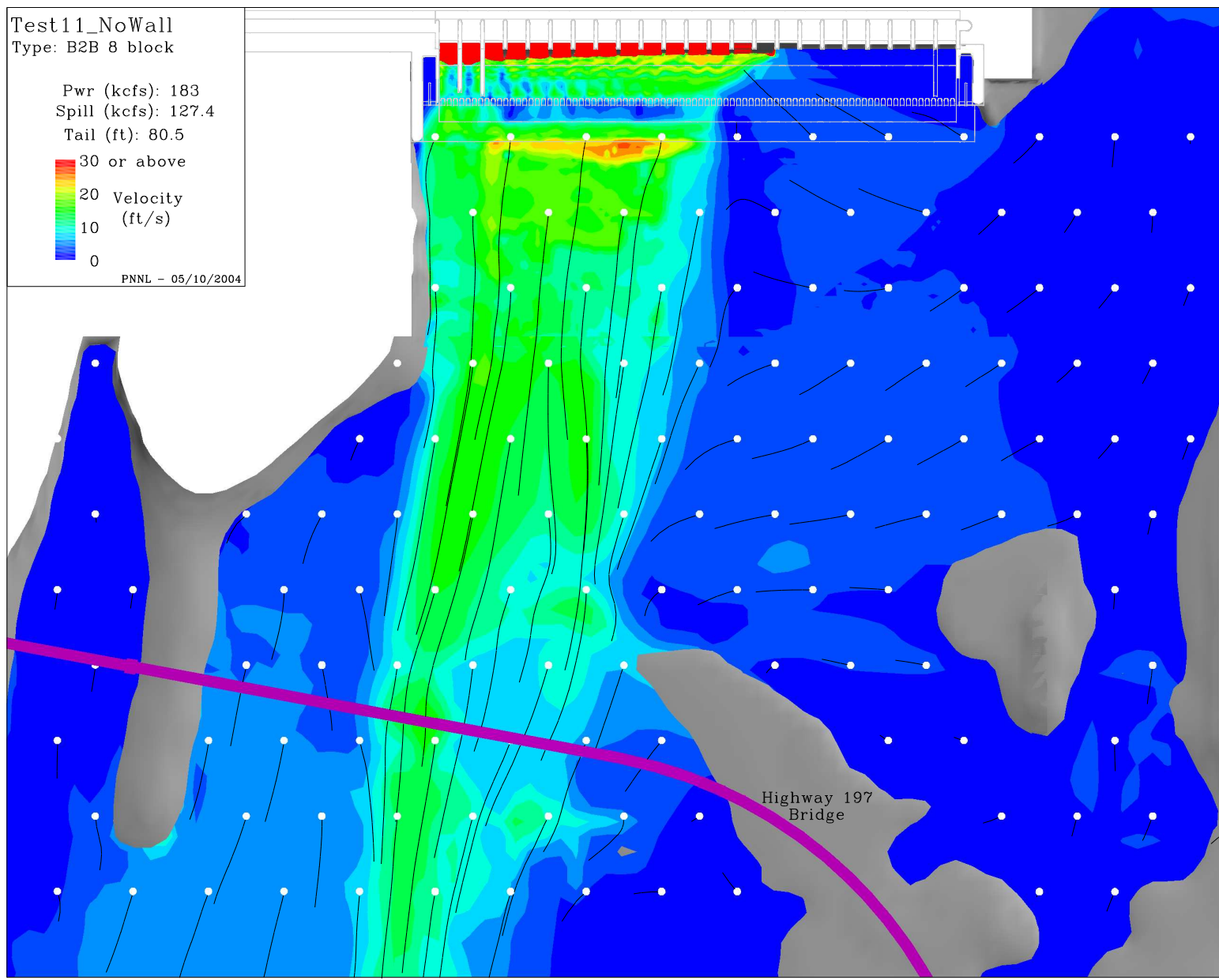


Figure H.4. Results for CFD model of The Dalles Dam tailrace (FullSpillwayTest11NoWall.eps).

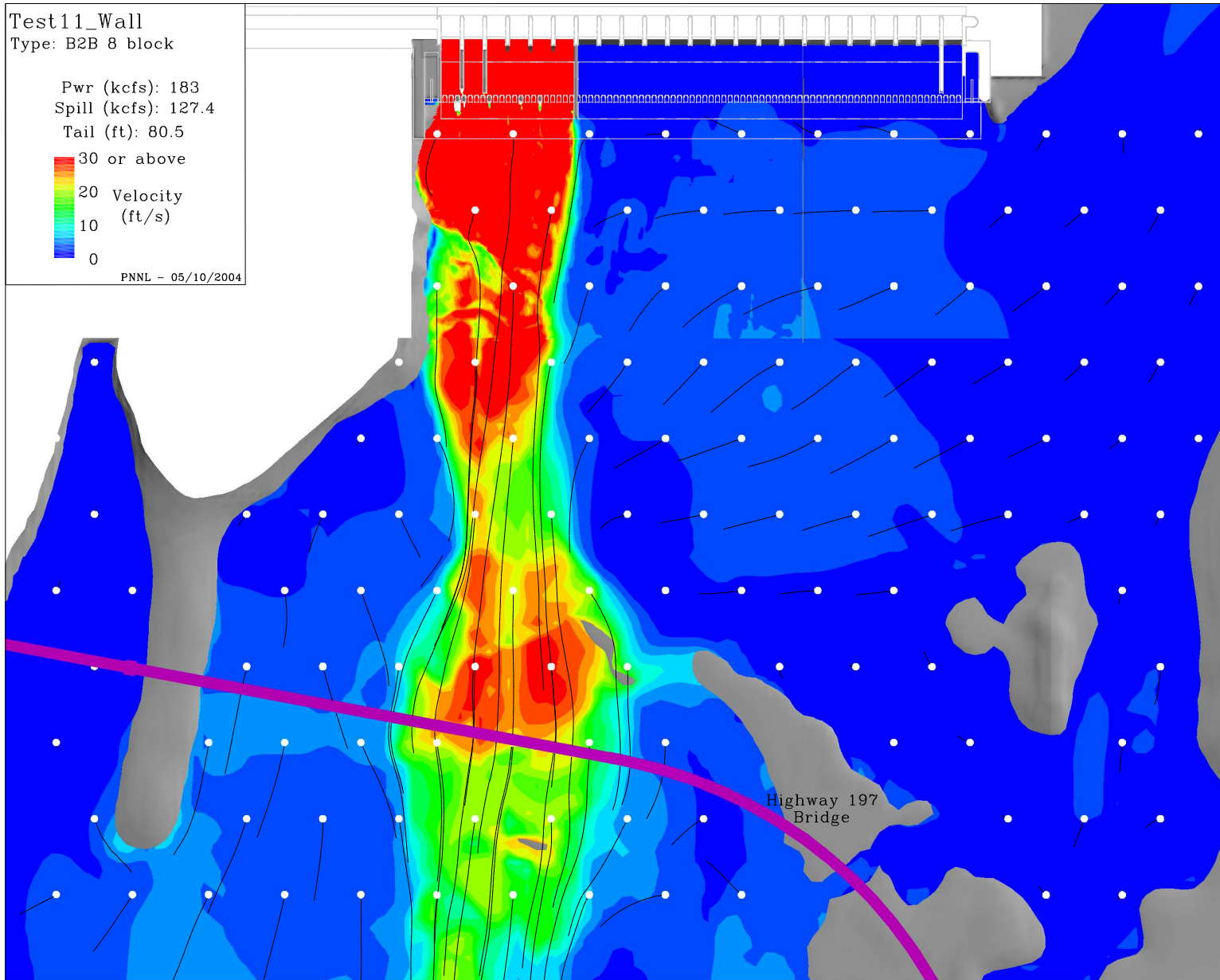


Figure H.5. Results for CFD model of The Dalles Dam tailrace (FullSpillwayTest11Wall.eps).

Appendix I

Bank-to-Bank 4-Block Simulations

Appendix I – Bank-to-Bank 4-Block Simulations

The following appendix summarizes simulation results from a single spillway bay (Figure A.8 displays the domain extent). In all figures particle tracks of equal duration have been added to illustrate the direction of flow. The circles indicate the starting position for each track and the track length is proportional to the velocity magnitude.

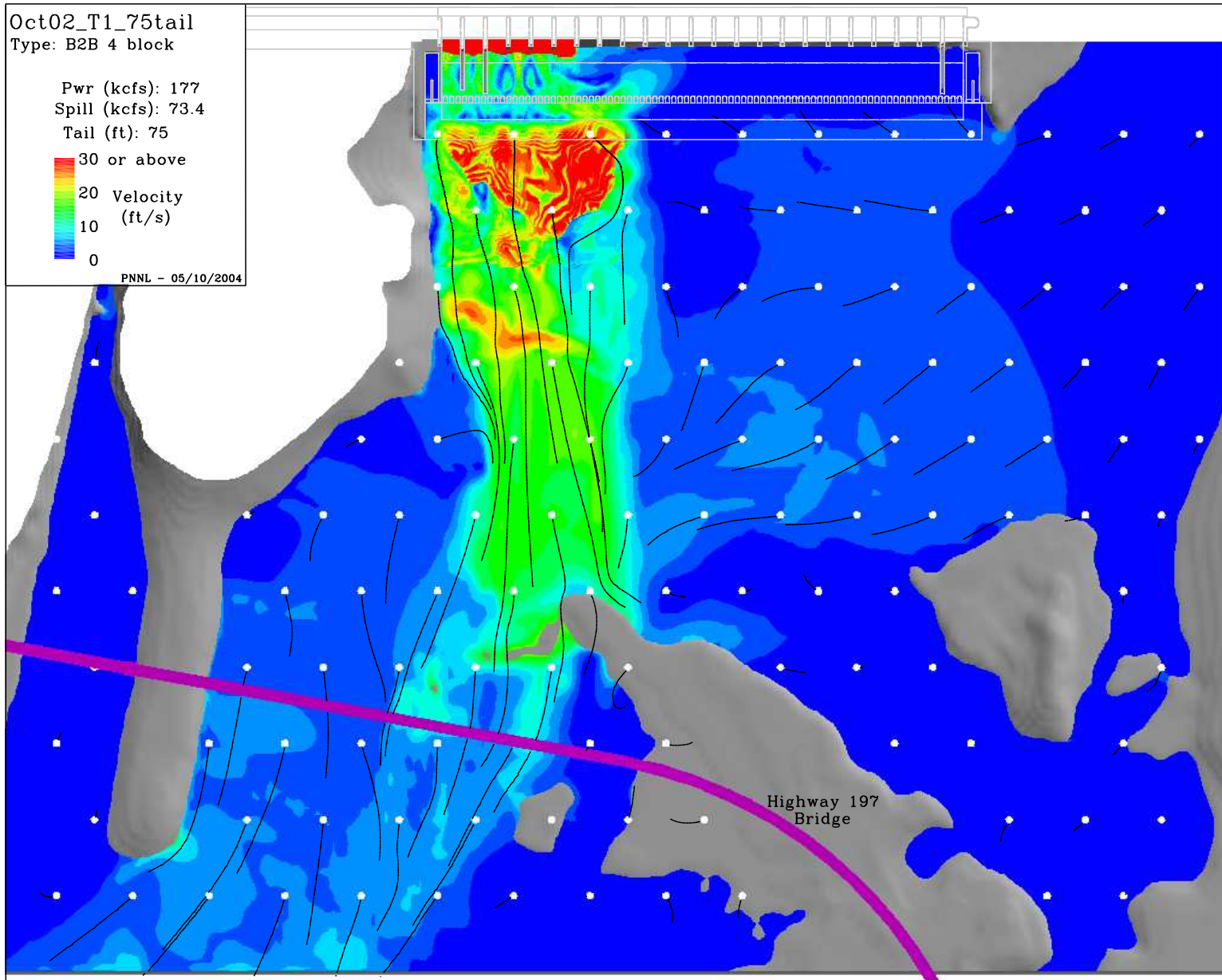


Figure I.1. Results for CFD model of The Dalles Dam tailrace (FullSpillwayOct02T175tail.eps).

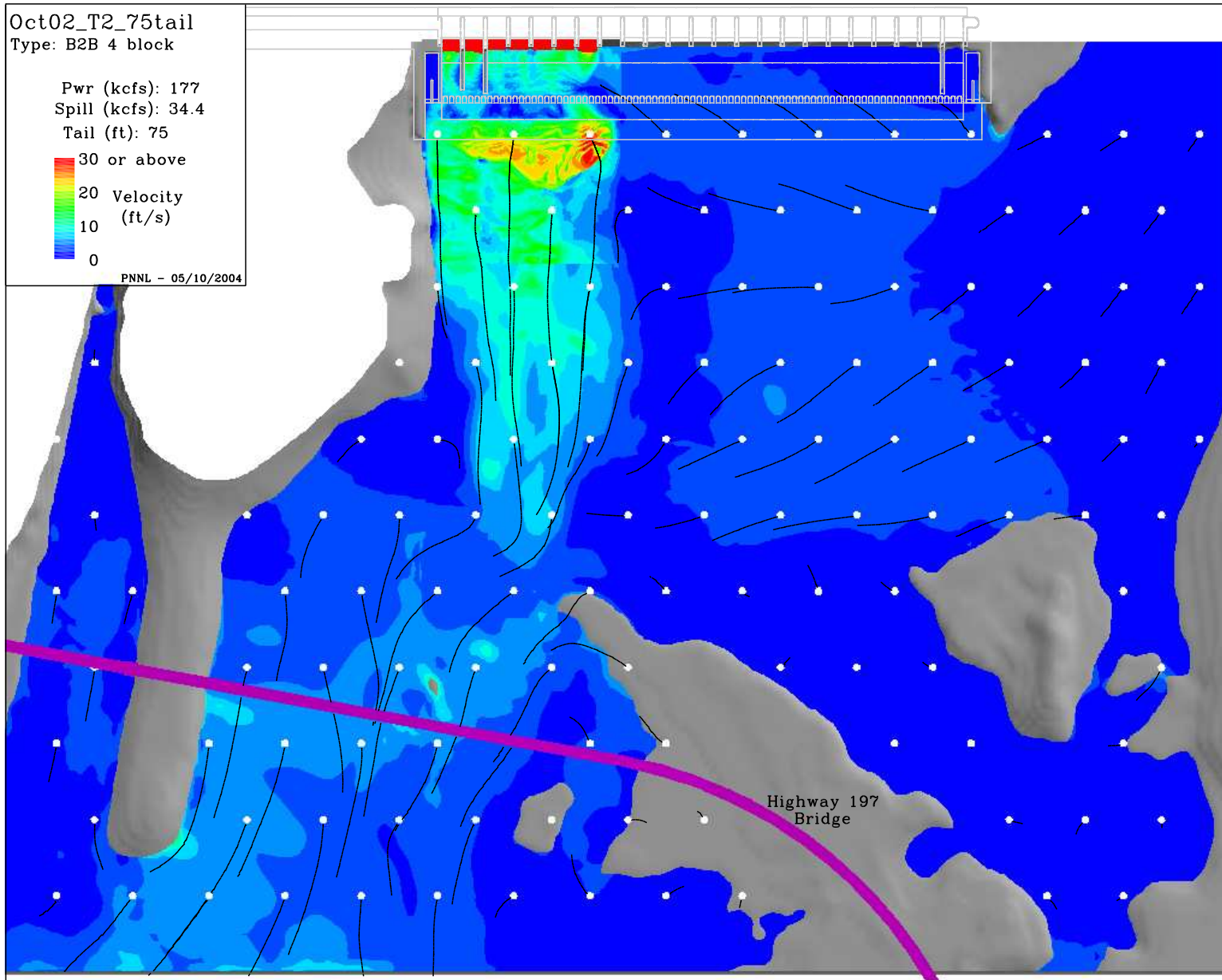


Figure I.2. Results for CFD model of The Dalles Dam tailrace (FullSpillwayOct02T275tail.eps).

Appendix J

Bank-to-Bank 1-Block Simulations

Appendix J – Bank-to-Bank 1-Block Simulations

The following appendix summarizes simulation results from a single spillway bay (Figure A.9 displays the domain extent). In all figures particle tracks of equal duration have been added to illustrate the direction of flow. The circles indicate the starting position for each track and the track length is proportional to the velocity magnitude.

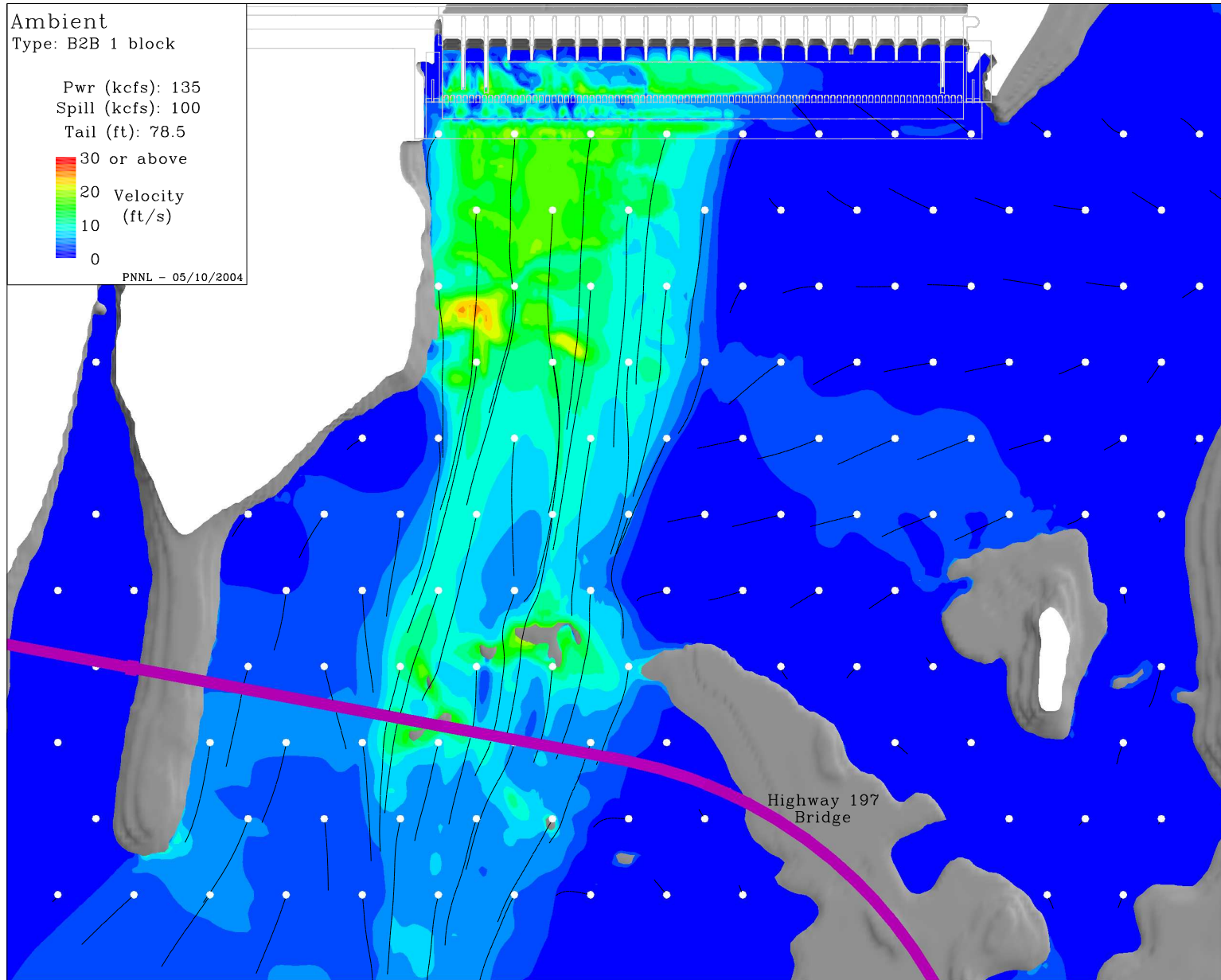


Figure J.1. Results for CFD model of The Dalles Dam tailrace (FullSpillwayAmbient.eps).

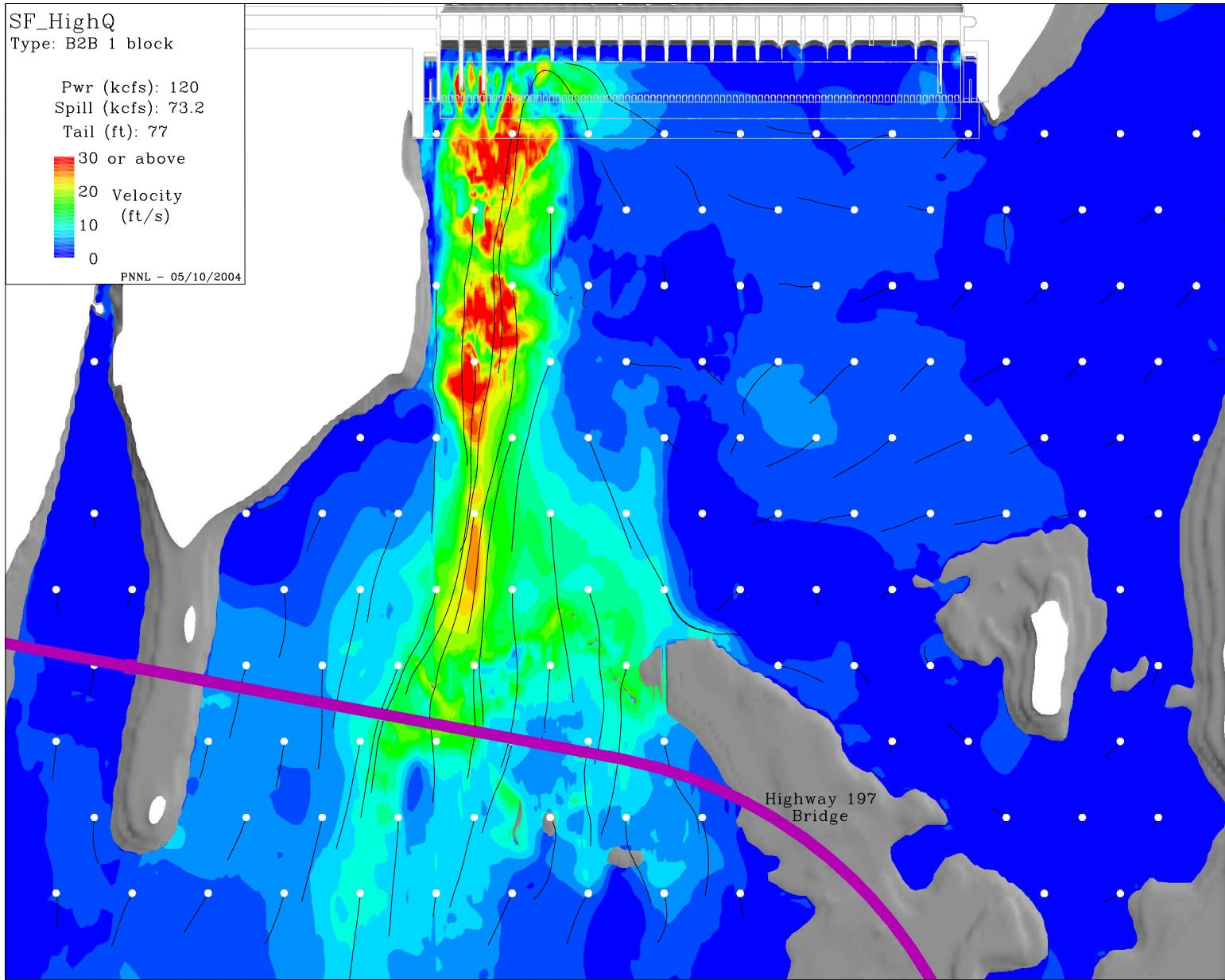


Figure J.2. Results for CFD model of The Dalles Dam tailrace (FullSpillwaySFHighQ.eps).

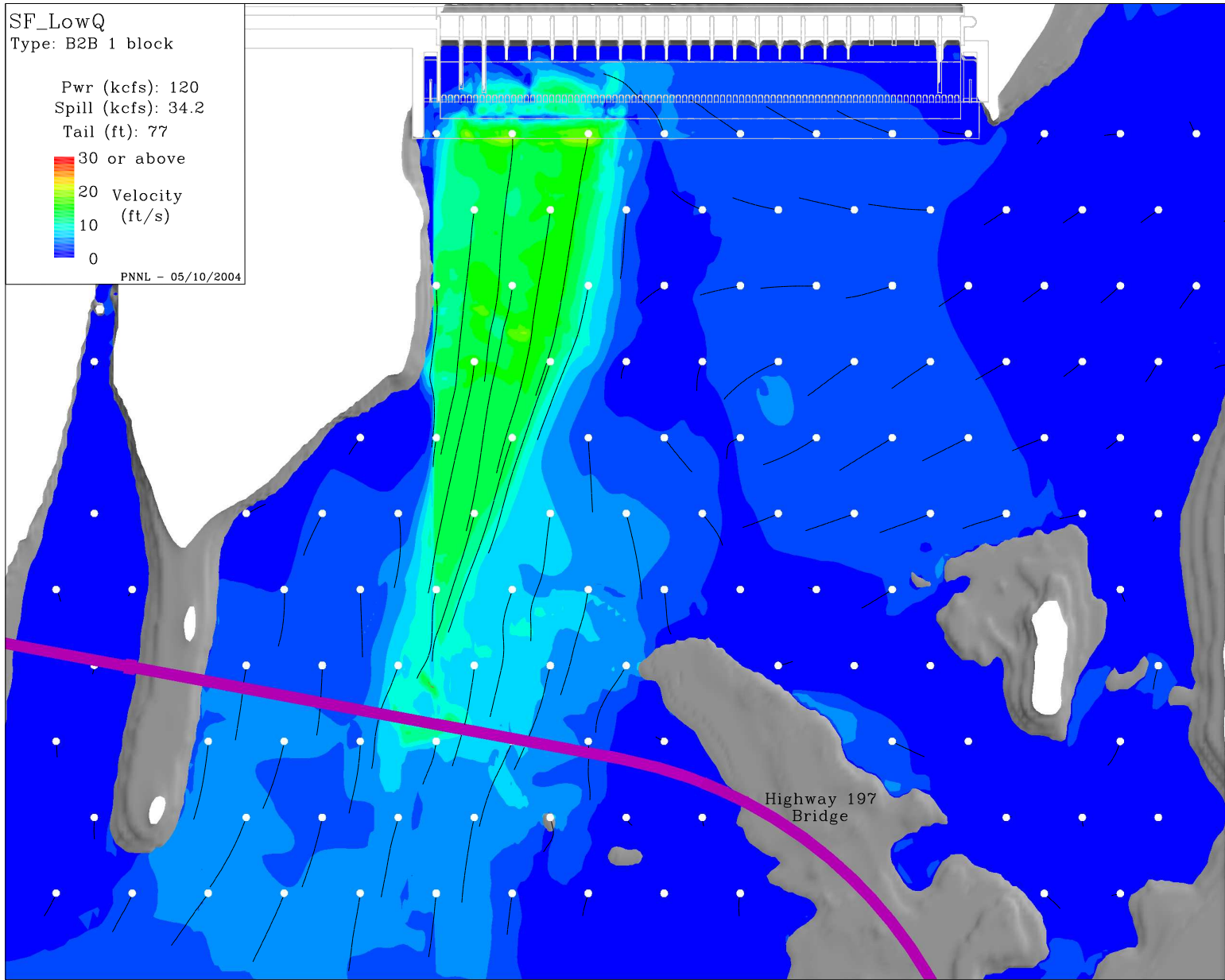


Figure J.3. Results for CFD model of The Dalles Dam tailrace (FullSpillwaySFLowQ.eps).

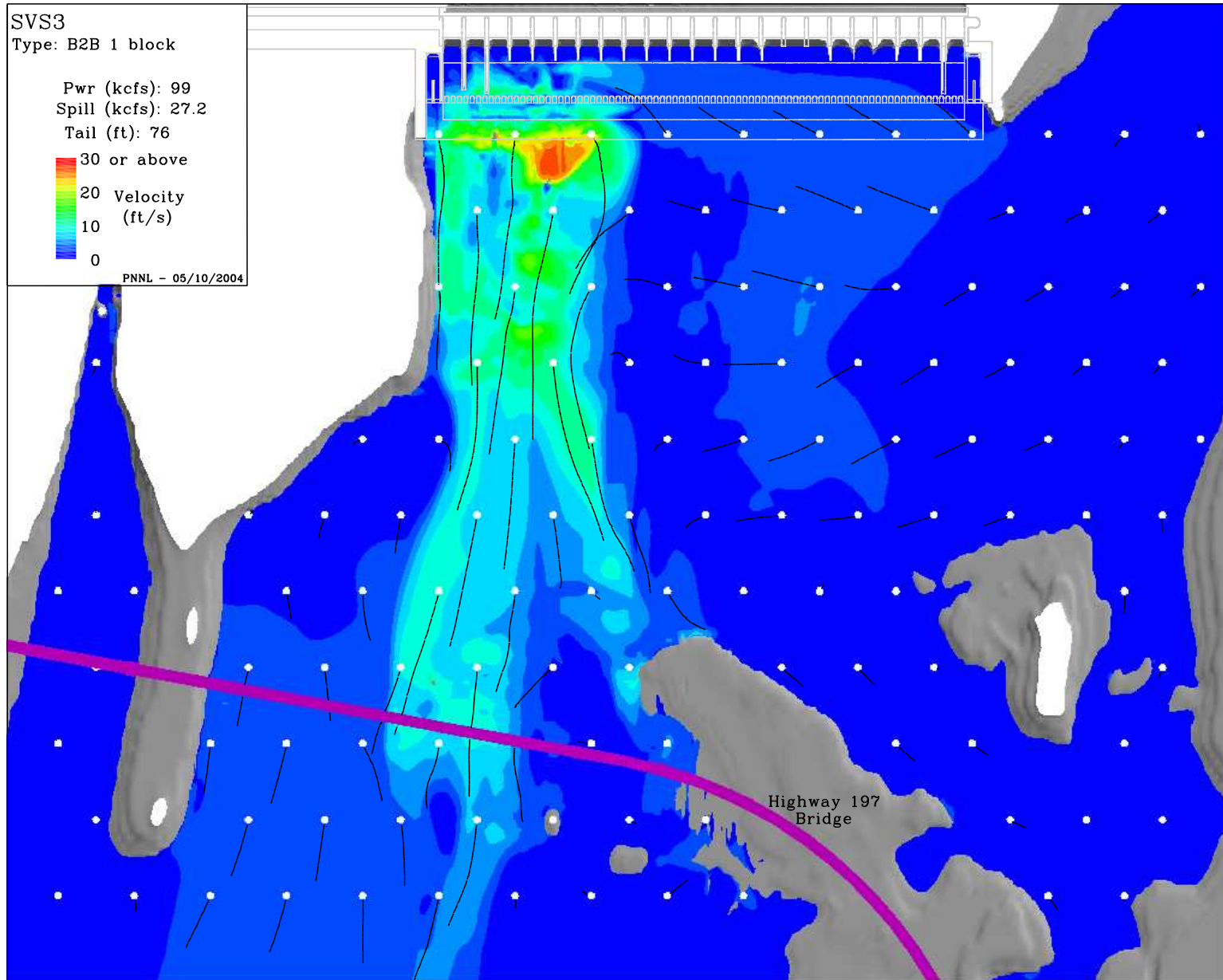


Figure J.4. Results for CFD model of The Dalles Dam tailrace (FullSpillwaySVS3.eps).

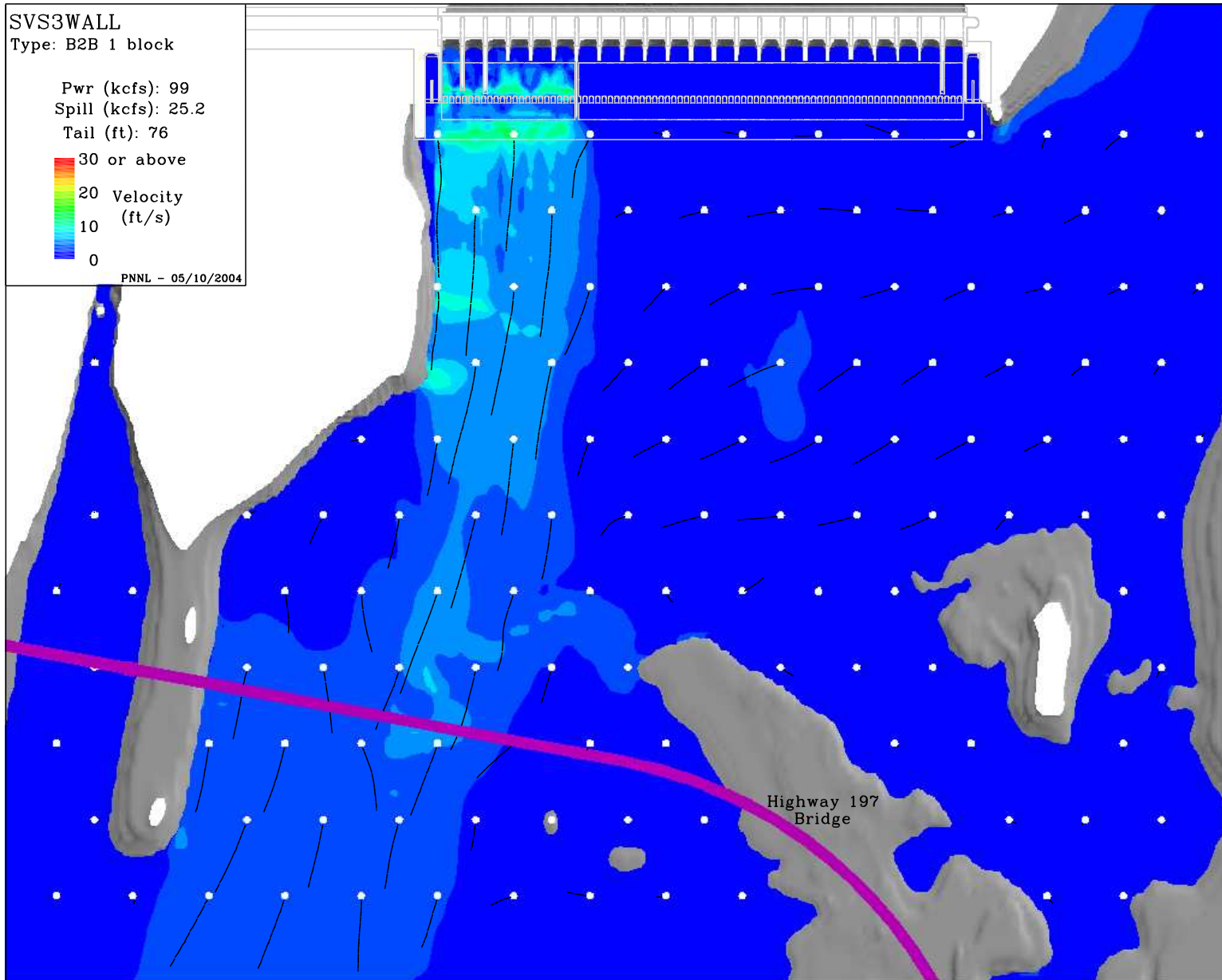


Figure J.5. Results for CFD model of The Dalles Dam tailrace (FullSpillwaySVS3wall.eps).

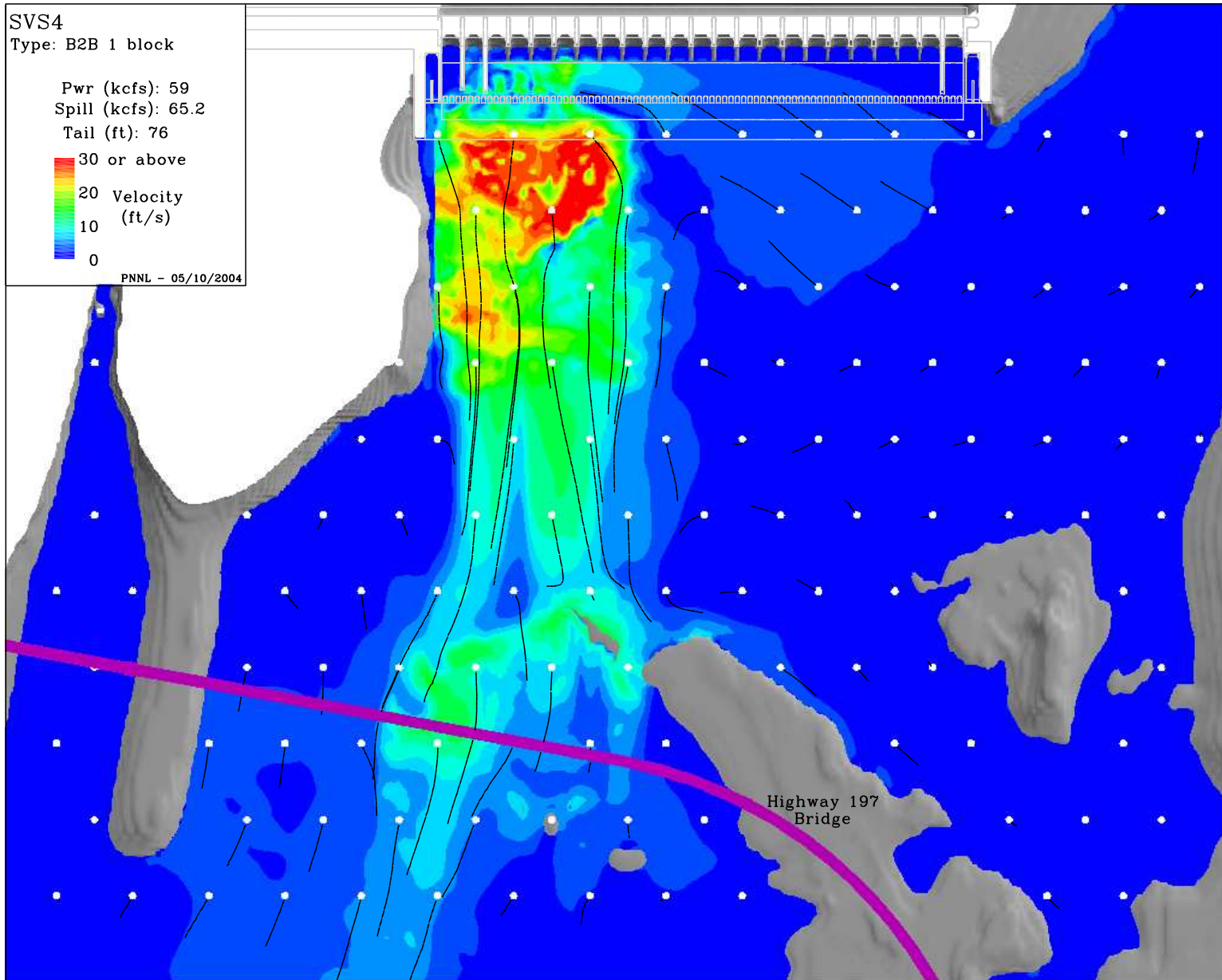


Figure J.6. Results for CFD model of The Dalles Dam tailrace (FullSpillwaySVS4.eps).

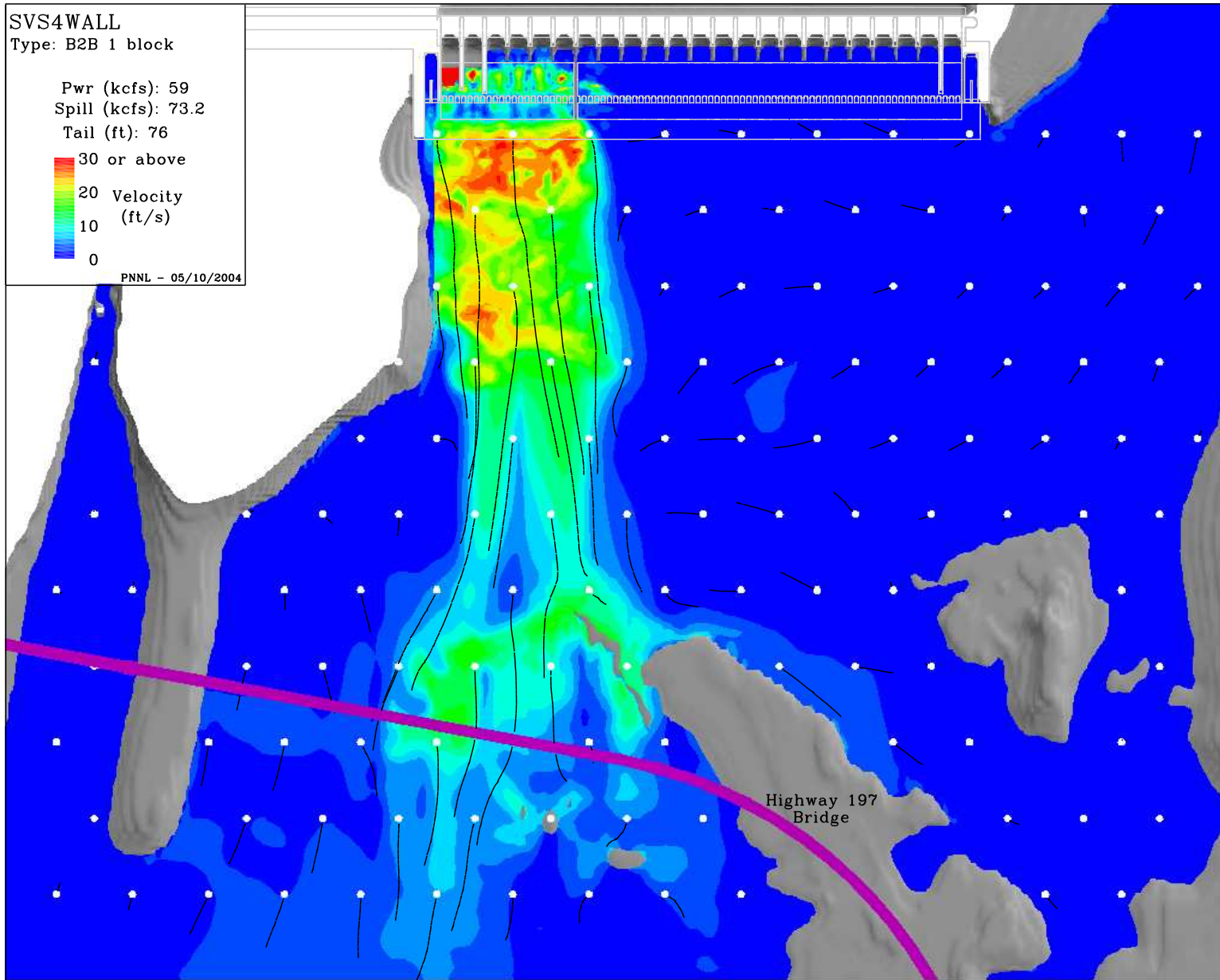


Figure J.7. Results for CFD model of The Dalles Dam tailrace (FullSpillwaySVS4wall.eps).

Appendix K

Powerhouse Tailrace Simulations

Appendix K – Powerhouse Tailrace Simulations

The following appendix summarizes simulation results from a single spillway bay (Figure A.10 displays the domain extent). In all figures particle tracks of equal duration have been added to illustrate the direction of flow. The circles indicate the starting position for each track and the track length is proportional to the velocity magnitude.

K.2

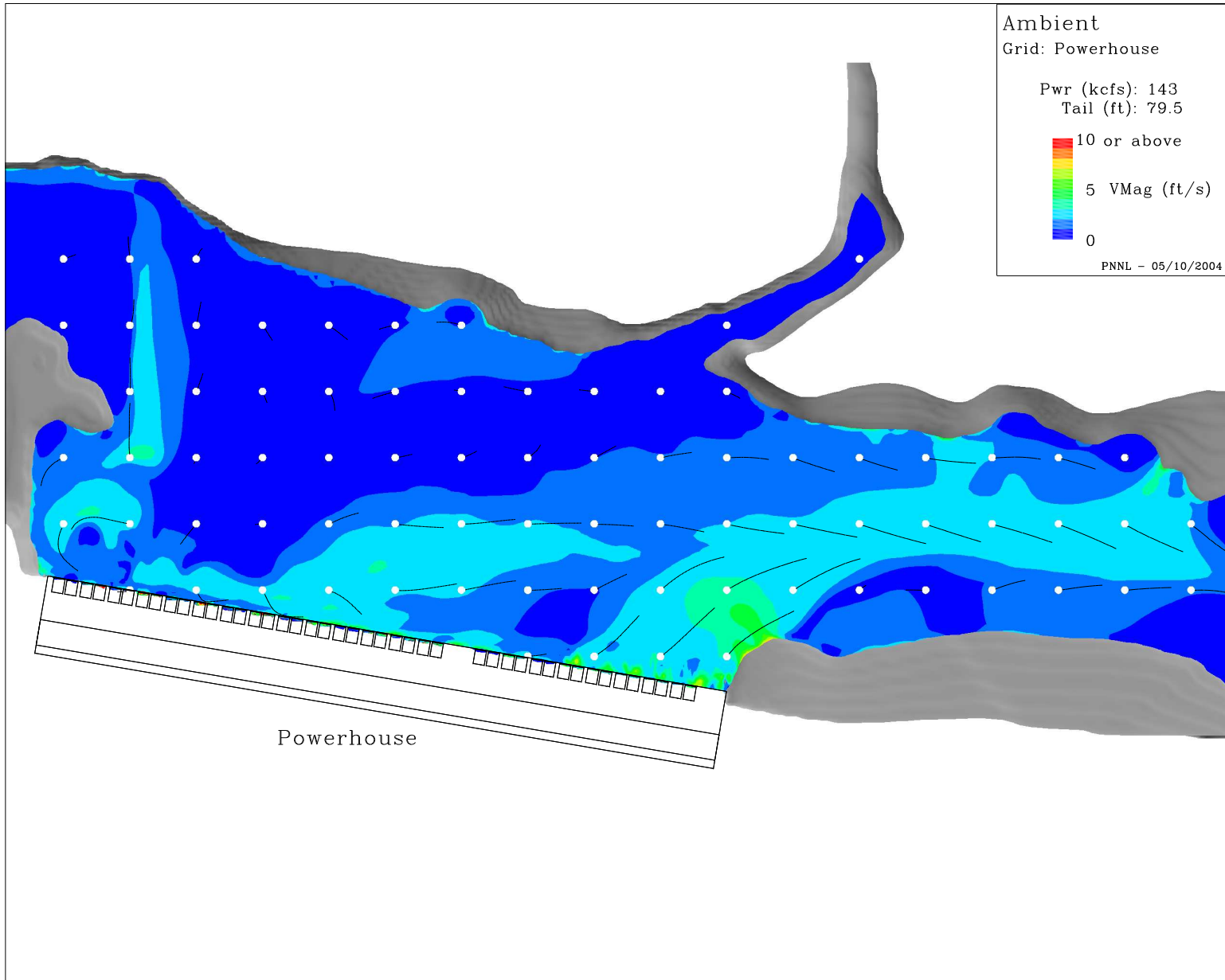


Figure K.1. Results for CFD model of The Dalles Dam tailrace (PowerhouseAmbientP.eps).

K.3

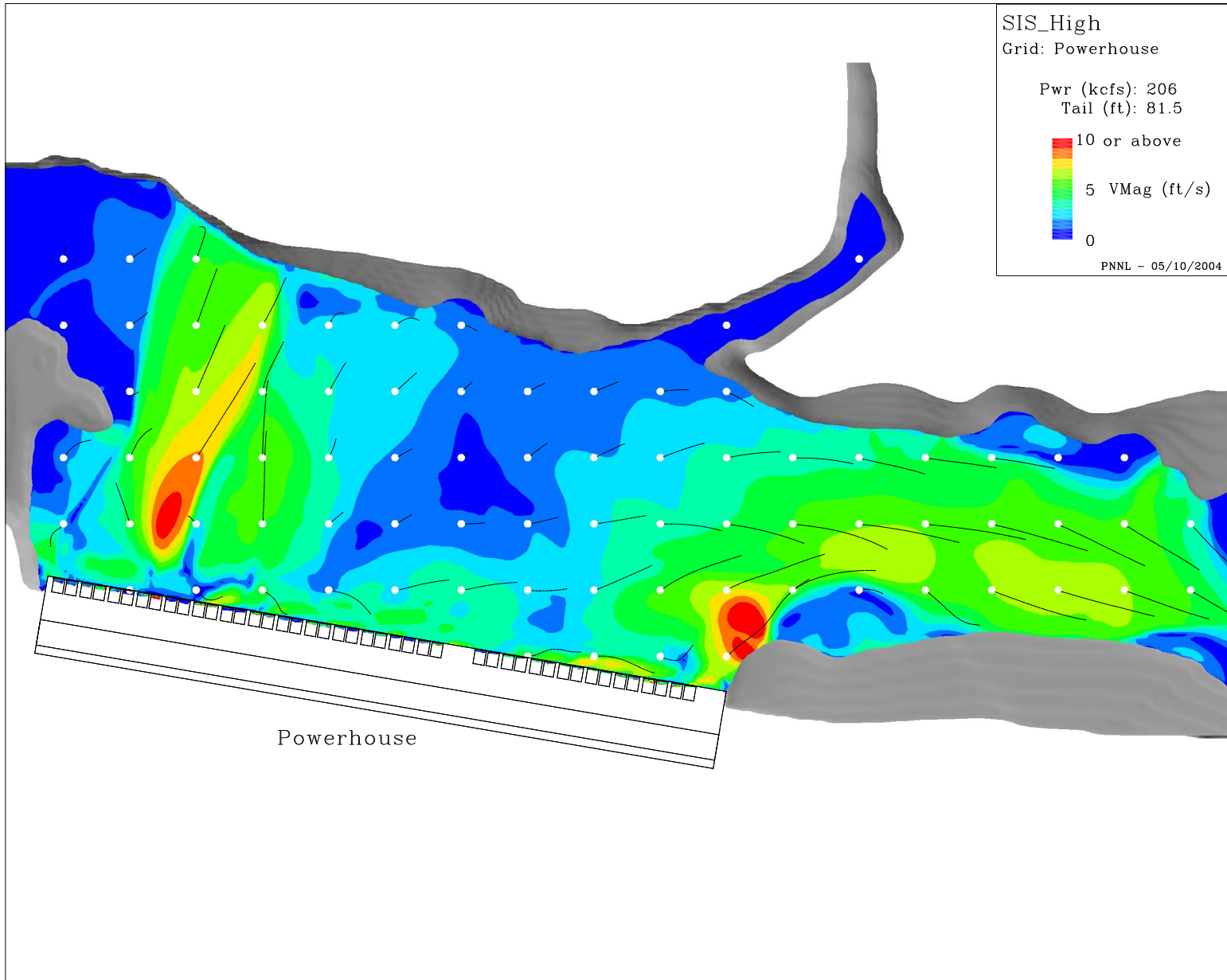


Figure K.2. Results for CFD model of The Dalles Dam tailrace (PowerhouseSISHigh.eps).

K.4

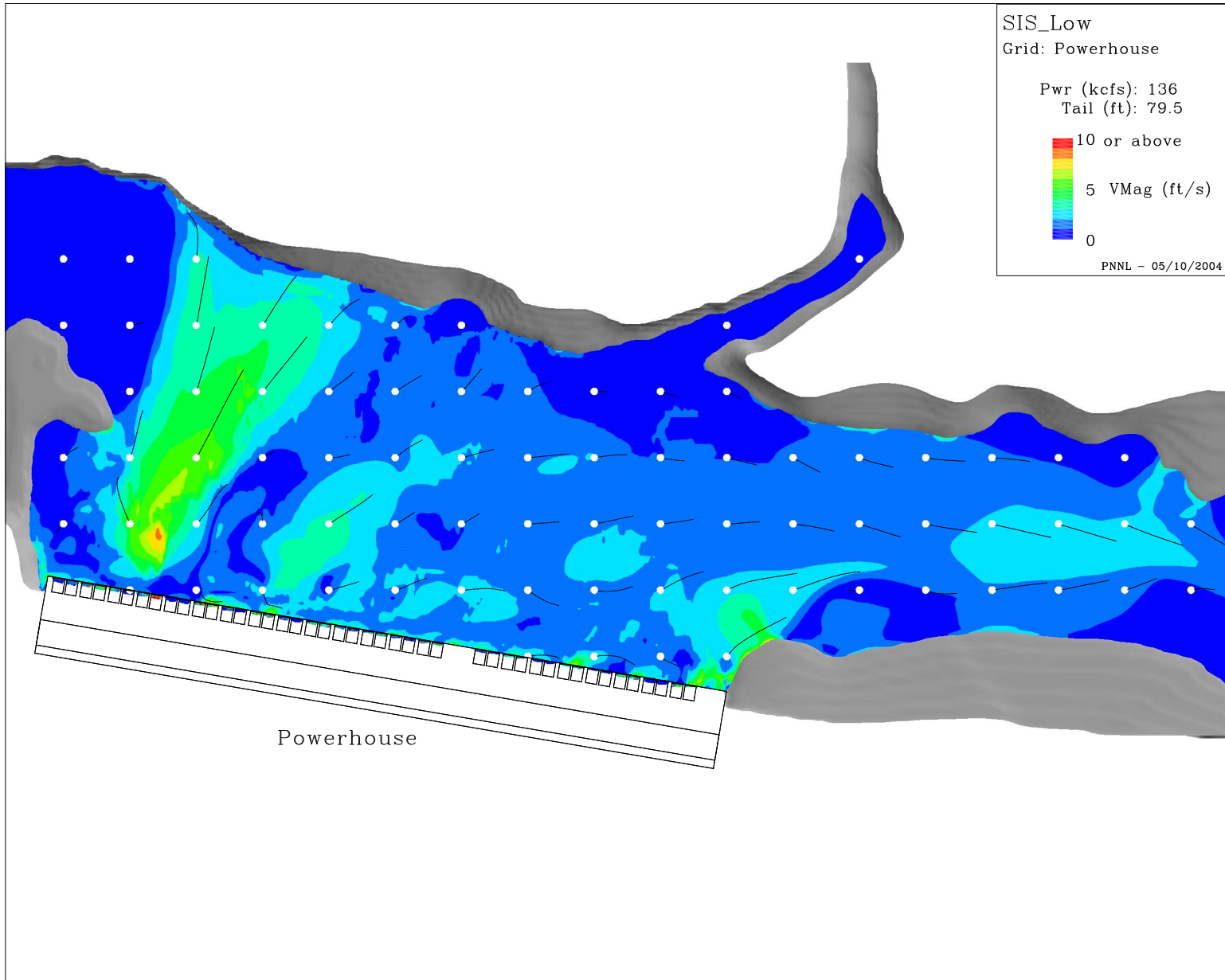


Figure K.3. Results for CFD model of The Dalles Dam tailrace (PowerhouseSISLow.eps).

K.5

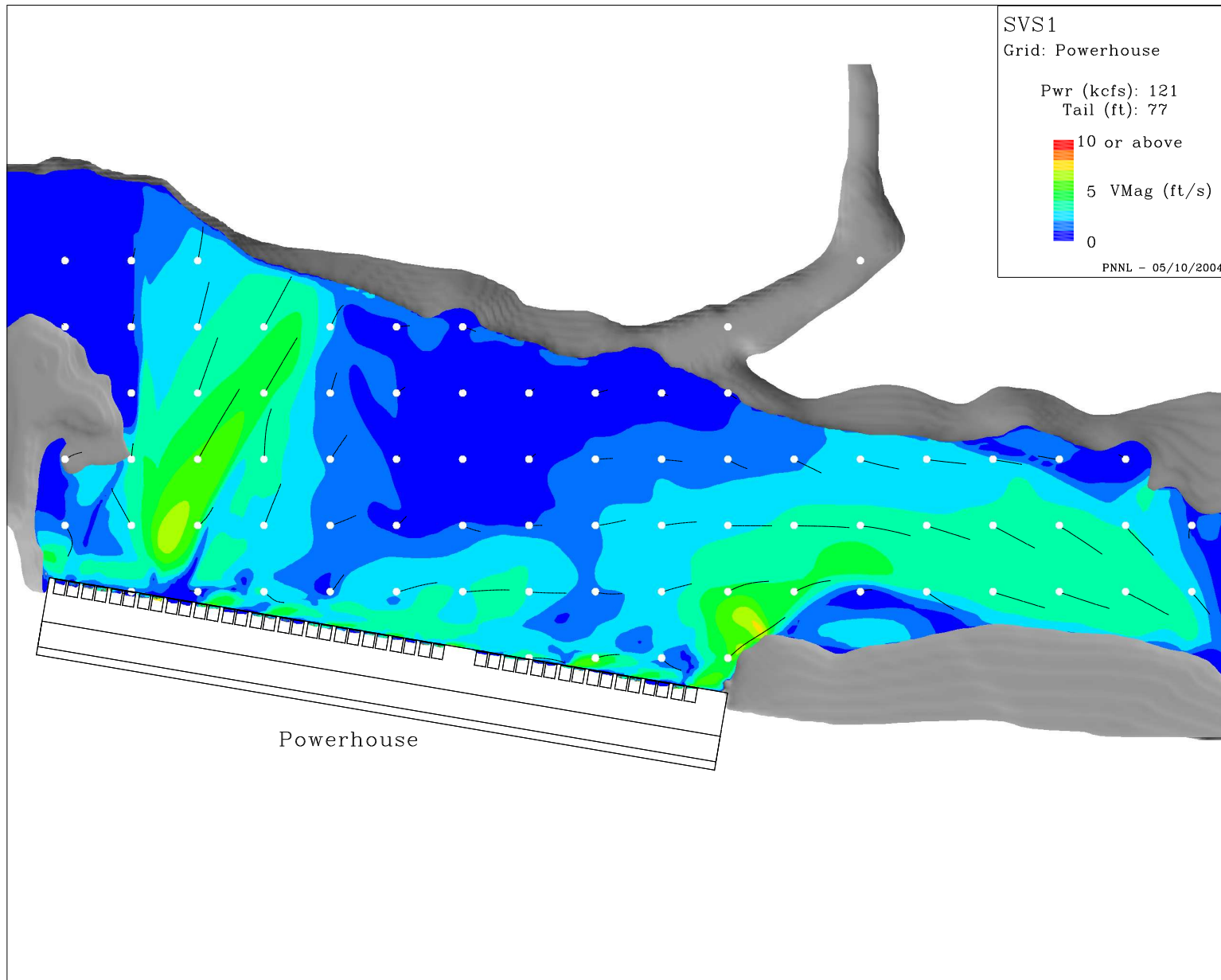


Figure K.4. Results for CFD model of The Dalles Dam tailrace (PowerhouseSVS1.eps).

K.6

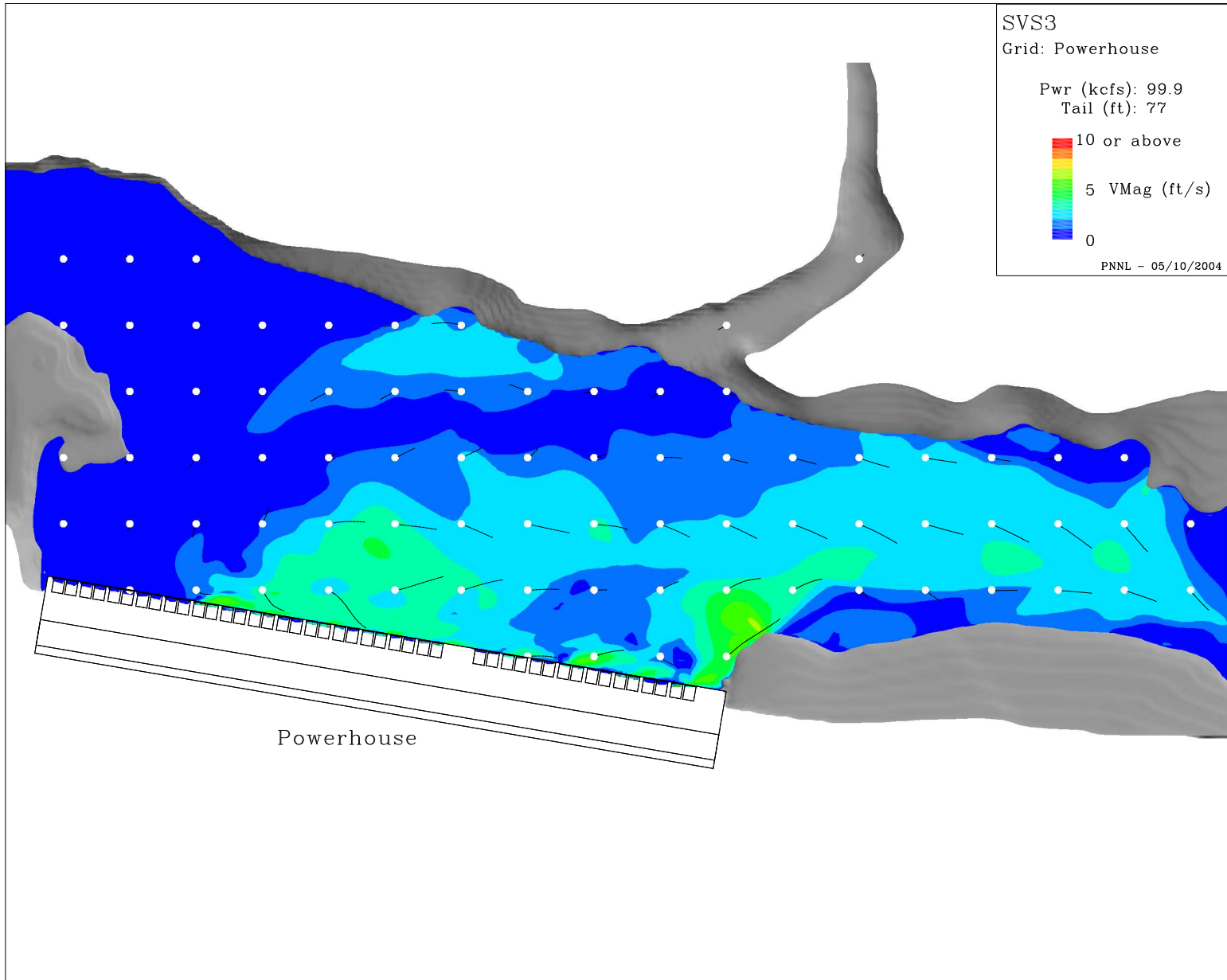


Figure K.5. Results for CFD model of The Dalles Dam tailrace (PowerhouseSVS3P.eps).

K.7

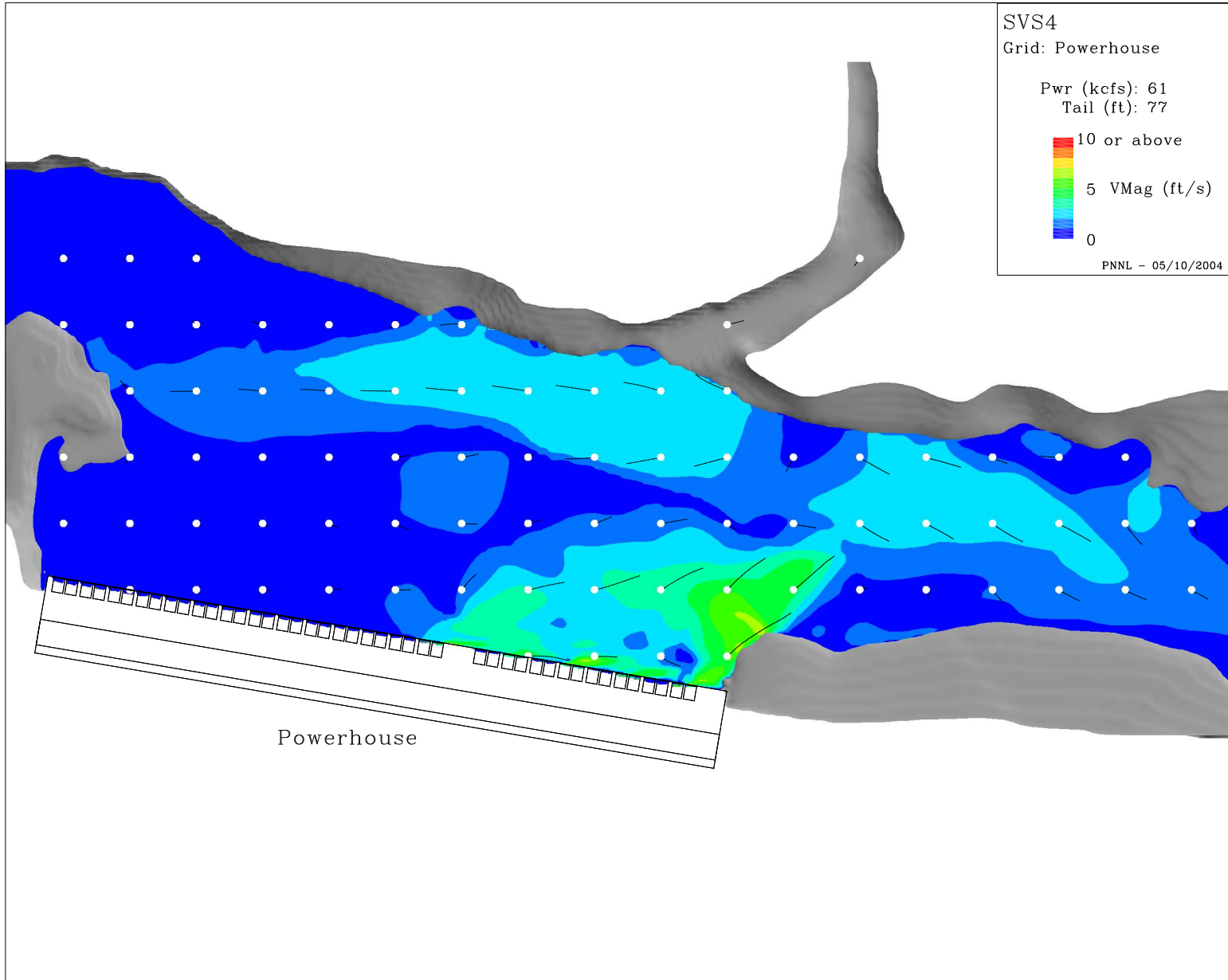


Figure K.6. Results for CFD model of The Dalles Dam tailrace (PowerhouseSVS4P.eps).

Appendix L

1:80 scale Powerhouse and Spillway Tailrace Simulations

Appendix L – 1:80 scale Powerhouse and Spillway Tailrace Simulations

The following appendix summarizes simulation results from a single spillway bay (Figure A.11 displays the domain extent). In all figures particle tracks of equal duration have been added to illustrate the direction of flow. The circles indicate the starting position for each track and the track length is proportional to the velocity magnitude.

L.2

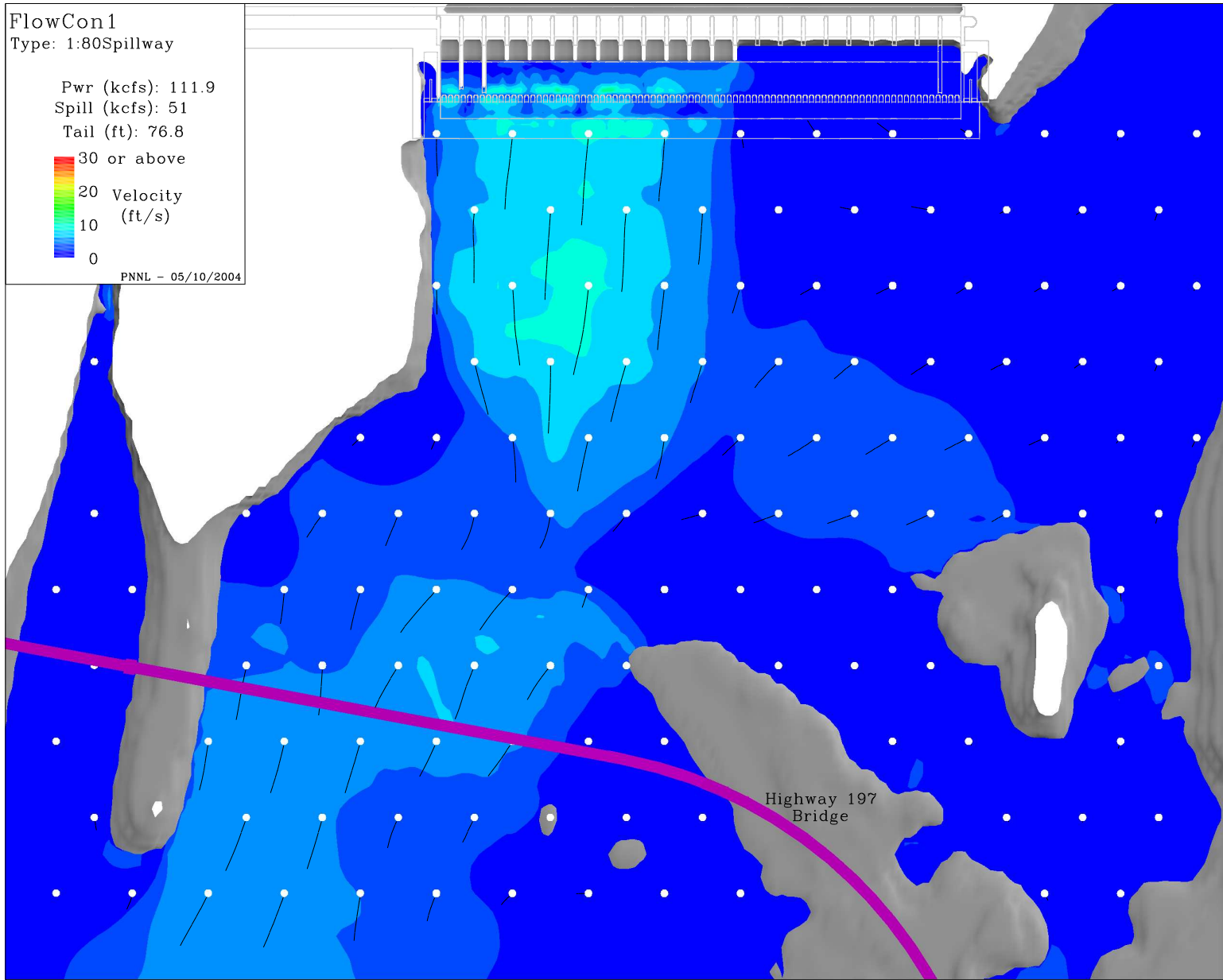


Figure L.1. Results for CFD model of The Dalles Dam tailrace (FullSpillway1to80FlowCon1.eps).

L.3

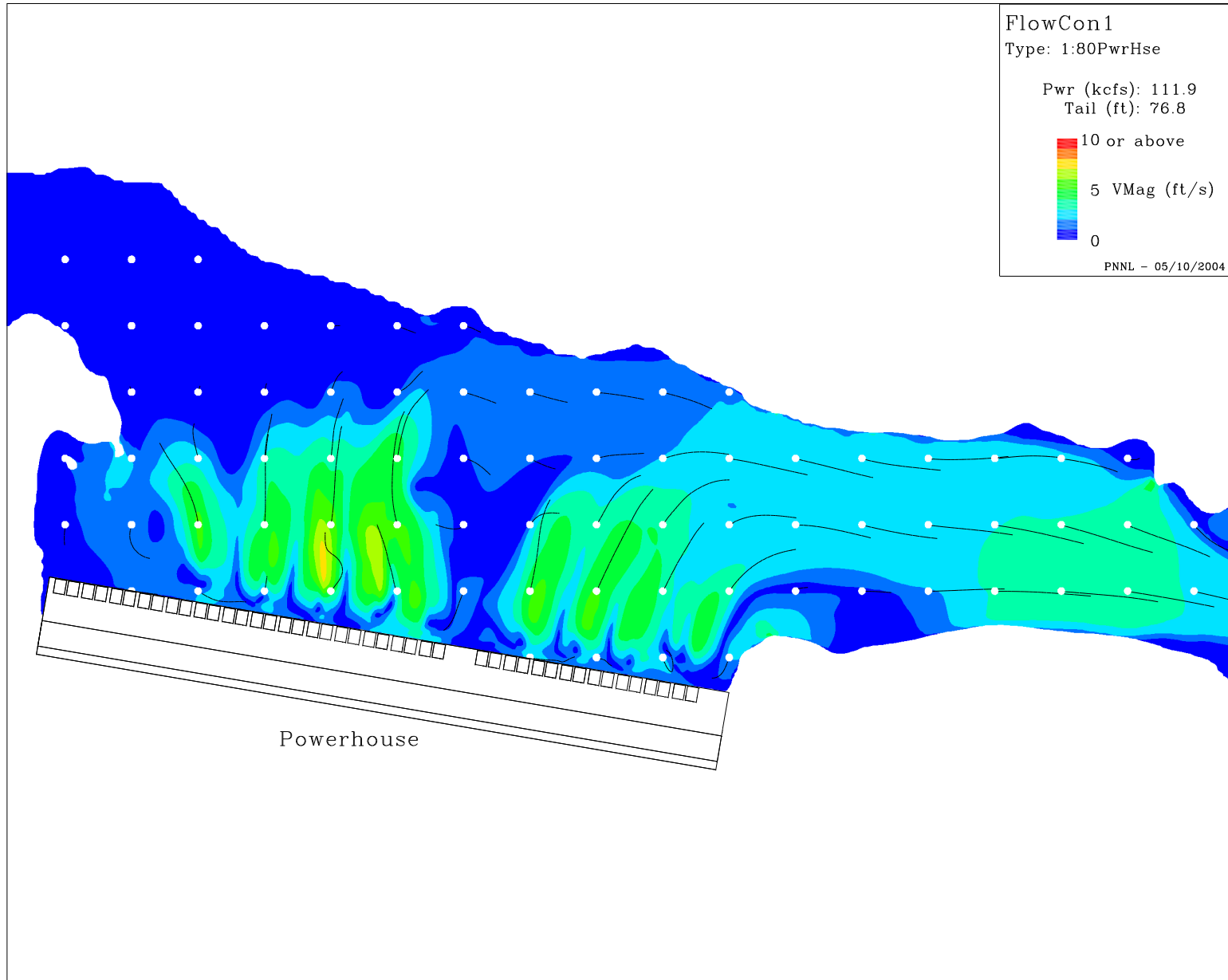


Figure L.2. Results for CFD model of The Dalles Dam tailrace (Powerhouse1to80FlowCon1P.eps).

L.4

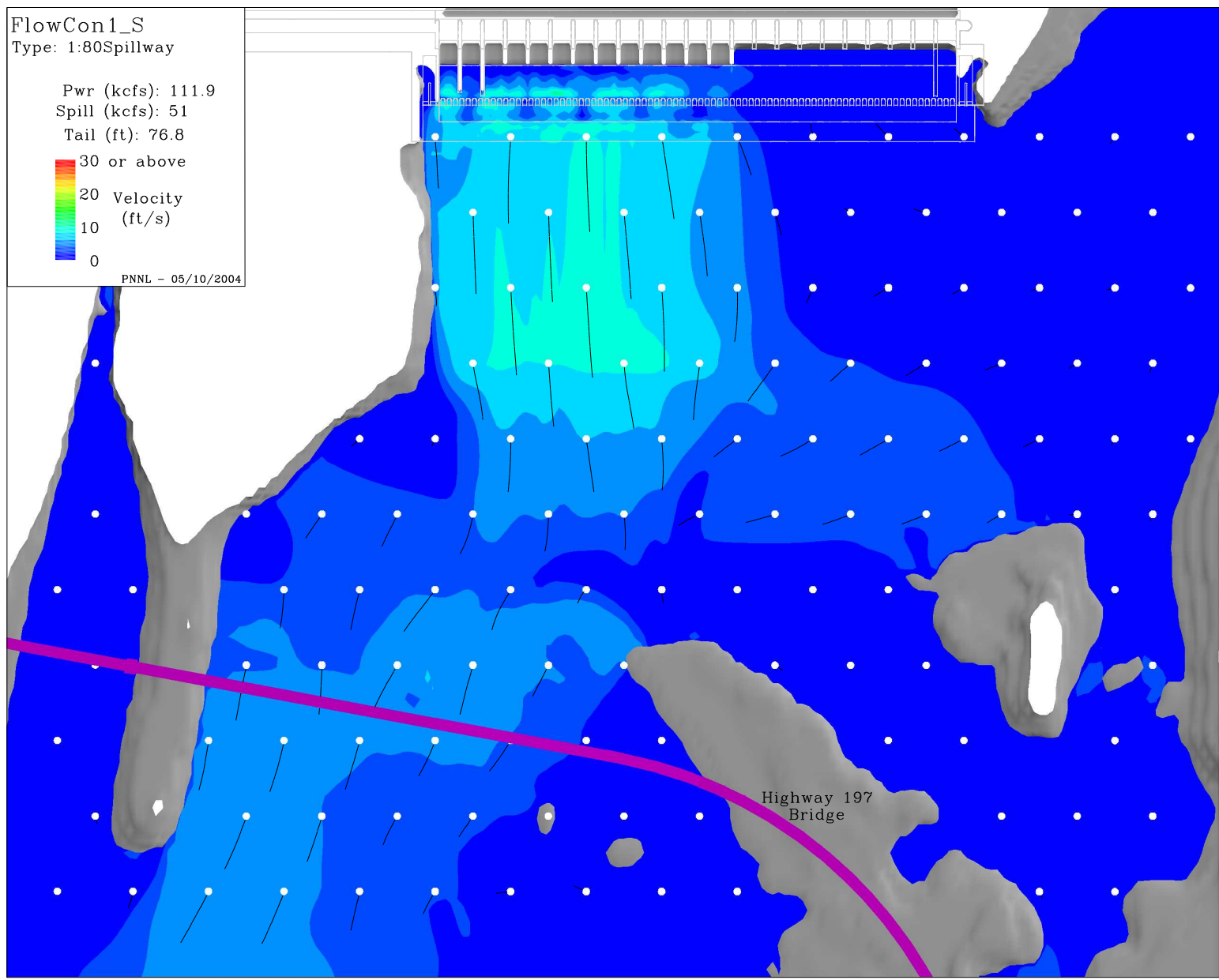


Figure L.3. Results for CFD model of The Dalles Dam tailrace (FullSpillway1to80FlowCon1Smooth.eps).

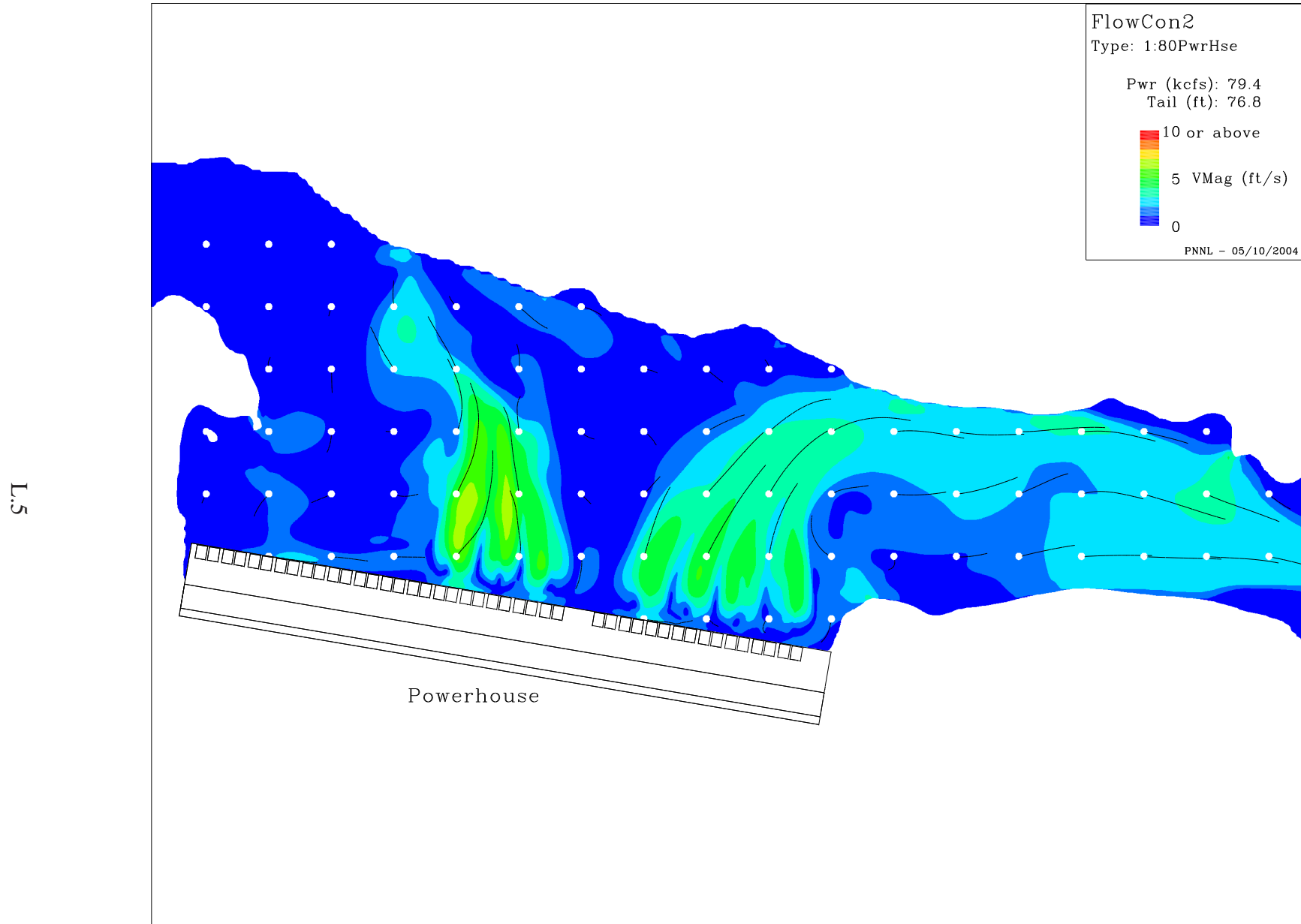


Figure L.4. Results for CFD model of The Dalles Dam tailrace (Powerhouse1to80FlowCon2.eps).

Appendix M

1:36 and 1:40 scale Simulations

Appendix M – 1:36 and 1:40 scale Simulations

The following appendix summarizes simulation results from a single spillway bay (Figure A.12 displays the domain extent). In all figures particle tracks of equal duration have been added to illustrate the direction of flow. The circles indicate the starting position for each track and the track length is proportional to the velocity magnitude.

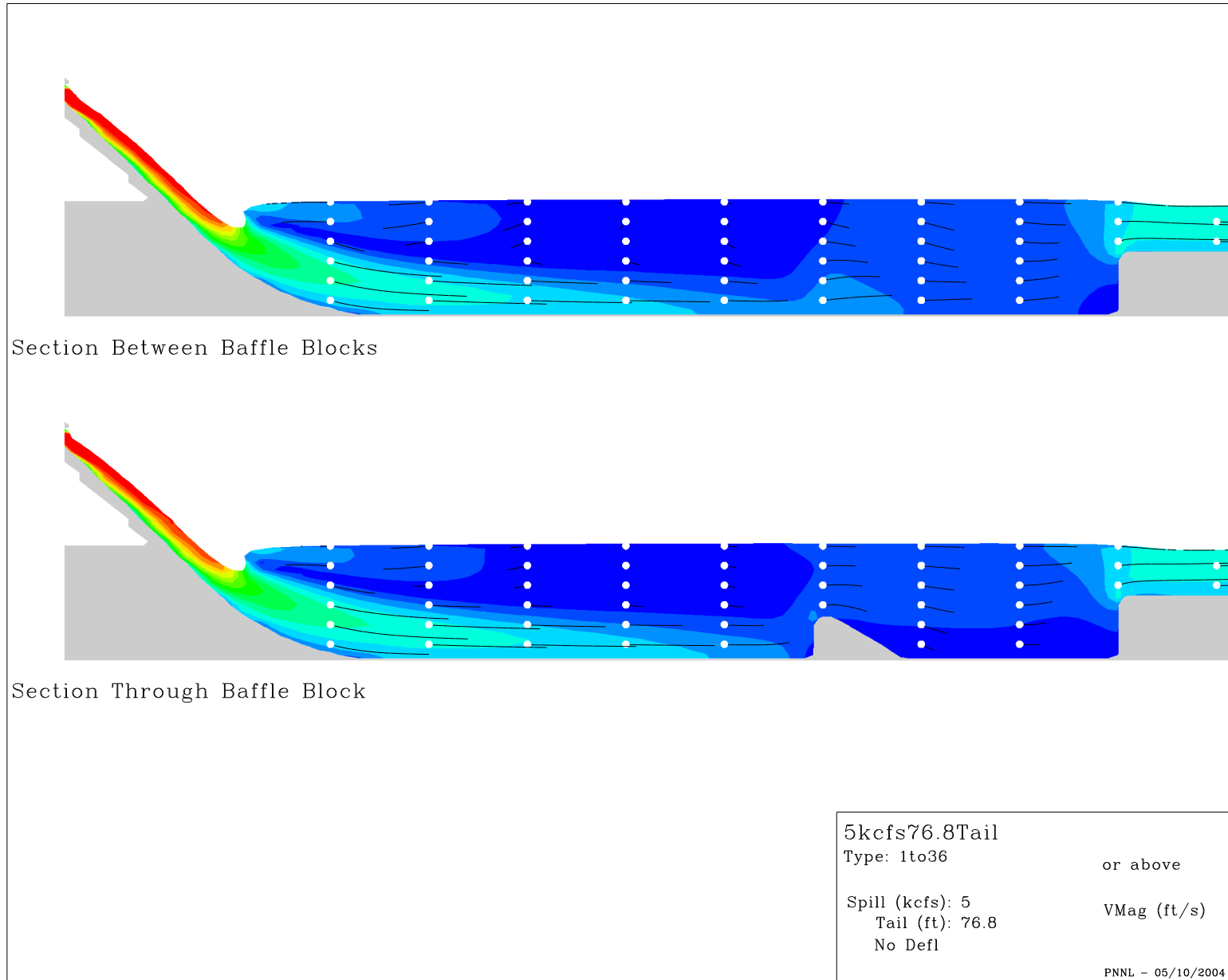


Figure M.1. Results for CFD model of The Dalles Dam tailrace (OneBay1to365kcfs76.8Tail.eps).

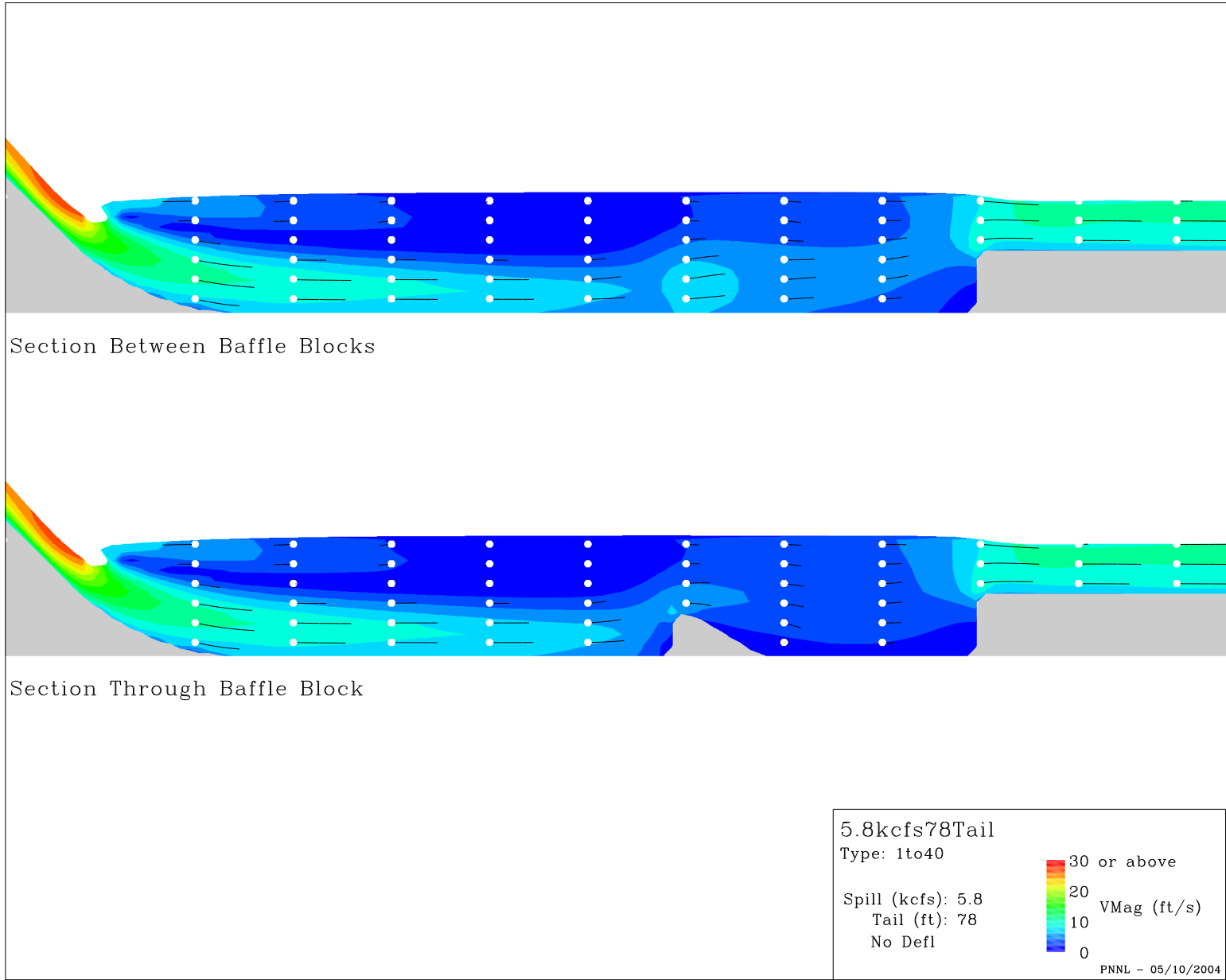


Figure M.2. Results for CFD model of The Dalles Dam tailrace (OneBay1to405.8kcfs78Tail.eps).

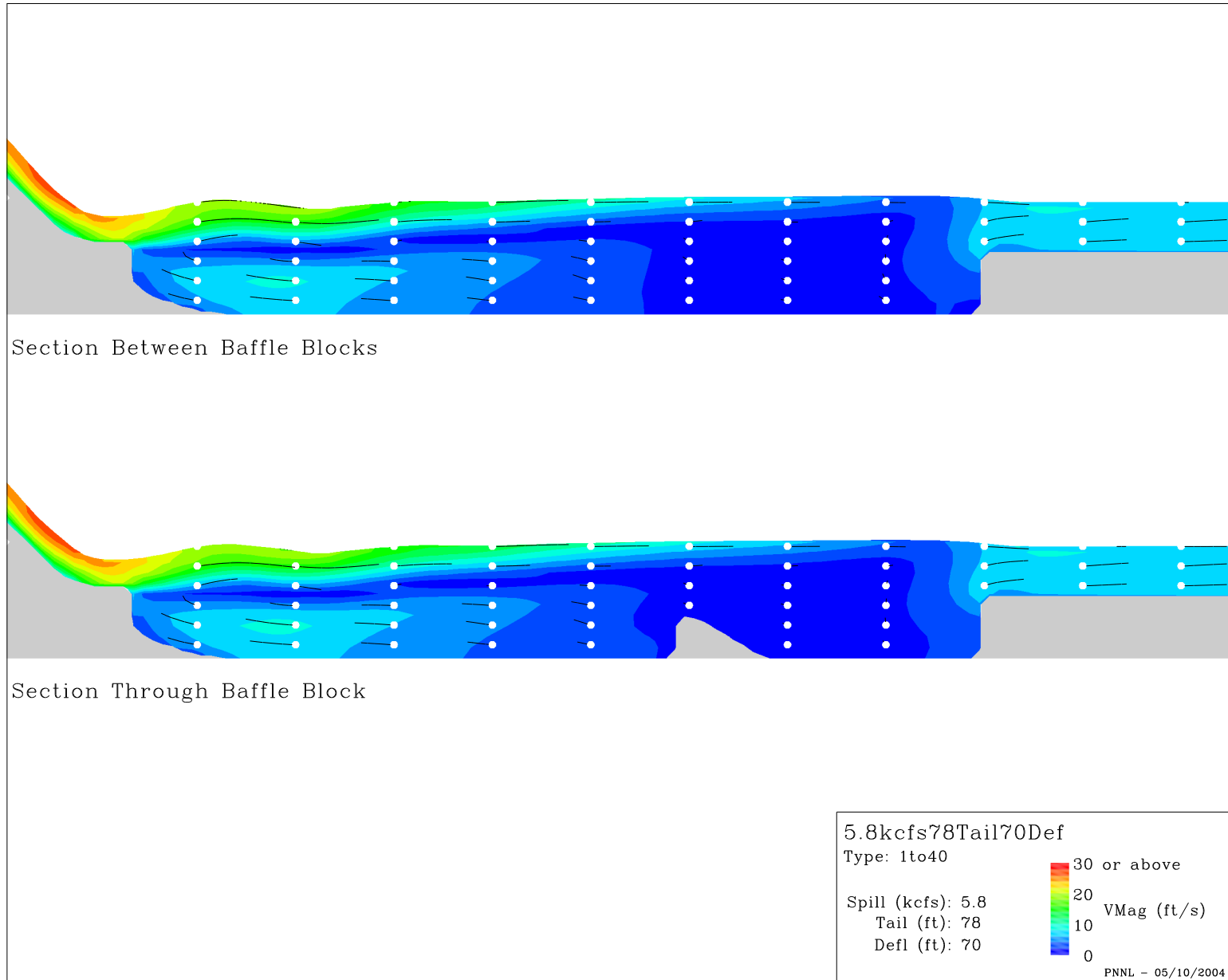


Figure M.3. Results for CFD model of The Dalles Dam tailrace (OneBay1to405.8kcfs78Tail70Def.eps).

6.5

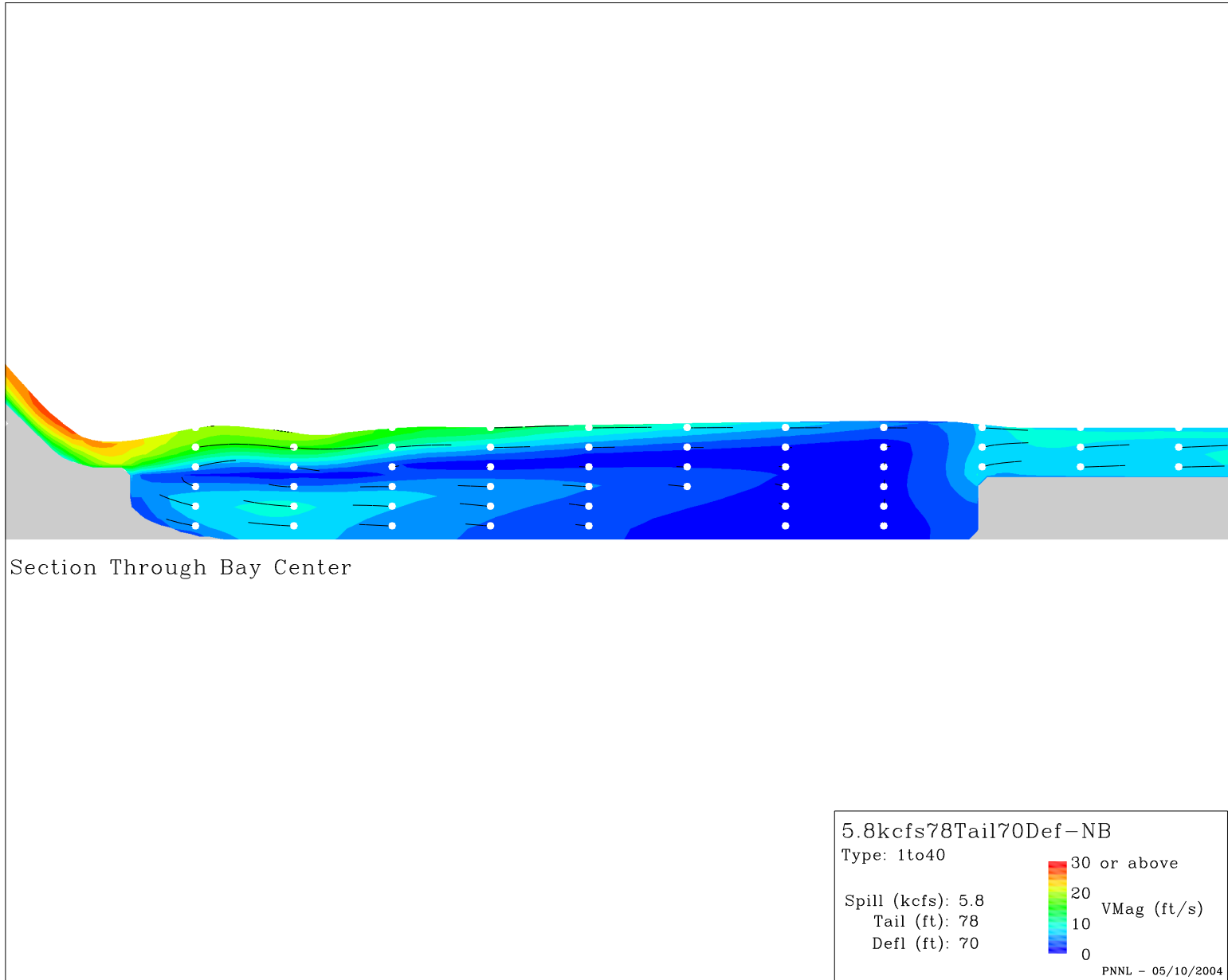


Figure M.4. Results for CFD model of The Dalles Dam tailrace (OneBay1to40NB5.8kcfs78Tail70Def-NoBaf.eps).

9.9

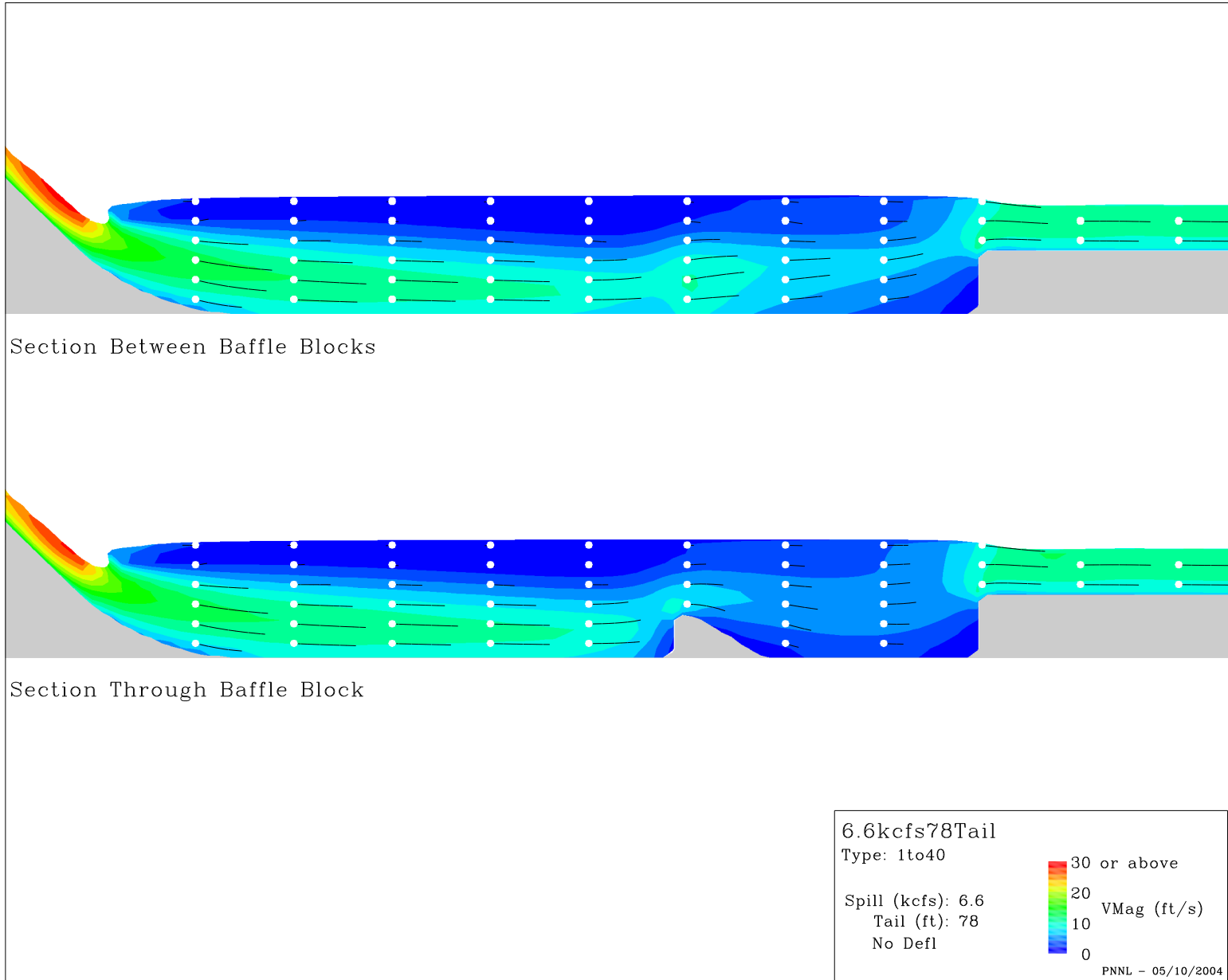


Figure M.5. Results for CFD model of The Dalles Dam tailrace (OneBay1to406.6kcfs78Tail.eps).